Synthesis, Crystallography and Spectroscopy of dinuclear Gold(I) NHC Macrocycles

Dissertation

zur

Erlangung des Doktorgrades (Dr. rer. nat.)

der

Mathematisch-Naturwissenschaftlichen Fakultät

der

Rheinischen Friedrich-Wilhelms-Universität Bonn

vorgelegt von

Stefanie Kobialka

aus

Bad Neuenahr-Ahrweiler

Bonn 2014

Angefertigt mit Genehmigung der Mathematisch-Naturwissenschaftlichen Fakultät der Rheinischen Friedrich-Wilhelms-Universität Bonn

1. Gutachter: Prof. Dr. Sigurd Höger

2. Gutachter: Prof. Dr. Arne Lützen

Tag der Promotion:13.04.2015

Erscheinungsjahr: 2015

Zusammenfassung

Die Synthese, spektroskopischen Eigenschaften und Röntgenkristallstrukruren von sieben systematischen Serien dinuklearer Münzmetall(I)-NHC-Komplexe werden hier gezeigt. Als Anionen werden sowohl Bromid als auch Hexafluorophosphat verwendet, bei dem Münzmetallzentrum handelt es sich um Gold(I) oder Silber(I). Die NHC Liganden basieren auf Imidazol oder Benzimidazol und besitzen Methyl- oder Ethylseitenketten. Die Länge der flexiblen Alkyllinker variiert von lediglich einer bis zu sechs Methylengruppen. Insgesamt werden 24 Ligandvorläufer und 42 Münzmetall(I)-NHC-Komplexe untersucht.

Die Züchtung von Einkristallen, welche für die Röntgenstrukturanalyse geeignet sind, ist von 32 der Münzmetall(I)-NHC-Komplexen gelungen. Sie bestehen in (fast) allen Fällen aus Makrozyklen der Form $M_2L_2^{2+}$. Diese zeigen eine große Vielfalt von starren, zurückgefalteten oder offenen bis hin zu verdrehten Konformationen der Makrozyklen; sogar eine Polymerstruktur ist zu finden. Als Folge können sich Dimere durch kurze Au(I)-Au(I) Abstände bilden, die zusätzlich durch π-π Wechselwirkungen stabilisiert sein können.

Kurze Gold-Gold-Abstände von <3.5 Å (Summe der van der Waals Radien) werden als aurophile Bindungen bezeichnet. Als Folge können außergewöhnliche Fluoreszenzeigenschaften auftreten, die in der vorliegenden Arbeit in Lösung untersucht werden. Es zeigt sich, dass alle Gold-Komplexe mit Propylenlinker, unabhängig von der Wahl des Lösemittels, des Anions und sogar der Wahl des NHC Liganden, eine außergewöhnlich starke Emissionsbande bei 375 nm aufweisen. Diese spricht für eine stabile, formale Gold-Gold-Einfachbindung und damit für die Bildung eines angeregten Triplettkomplexes der Form $^3[d\sigma^*p\sigma]$. Die Komplexe mit kurzen Linkerlängen zeigen zudem ein erstaunlich dynamisches Verhalten in Lösung, welches NMR-spektroskopisch bei verschiedenen Temperaturen untersucht wird. Mit diesen Untersuchungen soll ein Beitrag zum besseren Verständnis der Dynamik von dinuklearen Gold(I)-NHC-Komplexen in Lösung geleistet werden.

Contents

1. Introduction

In recent years, there has been an increasing interest in gold complexes with N-heterocyclic carbene (NHC) ligands[1,2] as a consequence of their promising applications in fields like catalysis[3-5], nanotechnology[6,7] and medicine[8-11]. Given the usual linear coordination mode of Au[I], mononuclear gold(I) NHC compounds[1-9] often posses two different ligands (typically a neutral carbene and a coordinating anion)[1,2,12,13]. The respective homoleptic derivatives bearing two identical NHC ligands are usually cationic bis(NHC) gold(I) complexes[1,2,7,13-22]. The two NHC ligands can be connected with a long linker[23,24].With shorter linkers, dinuclear macrocycles are formed that consist of two gold(I) atoms and two bridging bis(NHC) ligands[24-44]. A growing number of such homoleptic dinuclear gold(I) tetra(NHC) macrocycles have been reported in recent years, including compounds with very rigid[31,42,44] and very flexible[24,30,32-34,36,37] linkers connecting the carbene subunits. A few NHC gold(I) compounds with ligands on the basis of benzimidazole have been studied[1,2,36,45,46]. Even a direct N-N connection of two NHC moieties, leading to an extremely short gold-gold distance, is possible[38,39]. A chiral example[34] as well as neutral macrocycles with anionic linkers[25,26,40] have been synthesized. Some multinuclear complexes with NHC-ligated Au[I] atoms are also known[47-50].

A very intriguing feature of gold(I) complexes is the occurrence of aurophilic interactions, often recognized in the solid state by an intermetallic distance shorter than the sum of the van der Waals radii (3.5 Å)[51,52]. The strength of this unusual bonding type is comparable to hydrogen bonds (5-10 kcal/mol)[51-55]. The phenomenon has been associated with the exceptional photophysical properties of gold compounds[29,52,56-64]. Results obtained by the group of Che assigned the excitation of a dinuclear Au(I) complex with bridging phosphine ligands displaying aurophilic interactions to the $5d\sigma^* \rightarrow 6p\sigma$ transition producing the $^3[d\sigma^*p\sigma]$ excited state. This excited state electron configuration represents a formal Au(I)-Au(I) single bond and the visible emission resulting from exciplexes of the form $[Au_2(dcpm)_2]Y_2$ (dcpm = bis(dicyclohexylphosphino)methane, Y = a range of anions, including halides) originates from the $^3[d\sigma^*p\sigma]$ excited-state, which is perturbed by anion/solvent association[65-69]. Nevertheless solution based structural studies for dinuclear Au(I) complexes, which display aurophilic interactions, are rare. Mononuclear gold(I) complexes realize short Au-Au spacings by intermolecular aggregation[51,52], whereas dinuclear complexes can also adopt conformations with short intramolecular Au-Au distances[1,2,51,52].

The synthesis and spectroscopic characterization of a series of flexible gold(I) NHC macrocycles with methyl substituted carbenes has recently been reported, but only one substance has been structurally characterized so far[24,35]. This member of the series (propylene linker) shows an exceptionally efficient luminescence[35]. Its structure reveals a backfolded conformation with short Au-Au distance irrespective of the anion (triflate[24] and hexafluorophosphate[35]). Furthermore, two publications of Hemmert´s group may be combined to compare the first three members of a similar series with hydroxyl-functionalized side chains[32,33].

Hitherto, there are only very few reports of gold(I) NHC complexes with ligands on the basis of benzimidazole. Özdemir et al. report the synthesis and antimicrobial activities of three mononuclear heteroleptic complexes (NHC-Au-Cl) with sterically demanding side chains[46]. Ghdhayeb et al. showed the syntheses and structural characterization of symmetrical mononuclear gold(I) and silver(I) NHC complexes with symmetrical and unsymmetrical ligands. The side chains were short alkyl chains like methyl or allyl or sterically demanding side chains like cyanobenzyle[45]. Mononuclear complexes with long side chains (twelve to 16 methylene units) were reported to form a lamellar bilayer structure with Au-Au distances of ~3.6 Å[1]. The only dinuclear benzimidazole NHC gold(I) complexes were reported by Baron et al.. They showed a series of complexes with propylene linkers, methyl side chains and hexafluorophosphate as counter ion with ligands on the basis of benzimidazole or a mixed compound with imidazole and benzimidazole in one ligand. This mixed compound showed a backfolded conformation like reported before for the complex bearing only imidazole ligands[24,35] with a very short intramolecular gold-gold distance of 3.1 Å. In contrast, the corresponding complex with only benzimidazole ligands showed an open arrangement, which realized a short Au-Au distance only intermolecularly (3.5 Å)[36].

However, the anions affiliated with the reported molecular structures are not identical, which can have a disturbing impact on the observed conformations. Thus, the spectroscopic characteristics and solid state molecular structures of the complete systematic series with alkyl linker lengths ranging from one to six methylene units will be subject of discussion in this report. Both the counter ions bromide and hexafluorophosphate have been investigated, as the nature of the anion is known to have a severe impact on photoluminescent Au(I) complexes[70,71].

The subtle interplay of weak interactions governing the conformation of gold(I) macrocycles is remarkable. Thus, the syntheses and characterization of several systematic series of new dinuclear gold(I) NHC complexes and their corresponding NHC precursors are reported in this work. All compounds vary in the length of the alkyl chain, respectively linking two NHC units. Flexible alkyl linkers were chosen to systematically study the influence of the linker length on the conformation of the gold macrocycles with special respect to the formation of intramolecular gold-gold bonds. The series are categorized into three types of complexes. The complexes Type 1 consist of gold(I) (and silver(I)) complexes with N-heterocyclic carbene ligands on the basis of imidazole with ethyl side chains. As counter ions, bromide and the bulkier hexafluorophosphate are studied. The complexes Type 2 also consist of gold(I) complexes with N-heterocyclic carbene ligands on the basis of imidazole, but with methyl side chains. As counter ions, bromide and the bulkier hexofluorophosphate are studied here again. The complexes Type 3 consist of gold(I) complexes with N-heterocyclic carbene ligands on the basis of benzimidazole with ethyl and methyl side chains. Here, solely bromide serves as counter ion. The three types of complexes are described in three seperate chapters, which can be read detached and in any order. The conclusion at the end of this report referes to all three types of complexes. A summary of the studied compounds is given in scheme 1.1 and tables 1.1 and 1.2. In our group, the synthesis of eight of these complexes (**1a-4a**, **6a**, **14a-16a**) has already been reported[72]. Additionally, structural characterization was successful for six of these compounds (**2a-4a**, **6a**, **15a**, **16a**)[73] in my diploma thesis. Nonetheless, all these structures are discussed here again for the purpose of comparison.
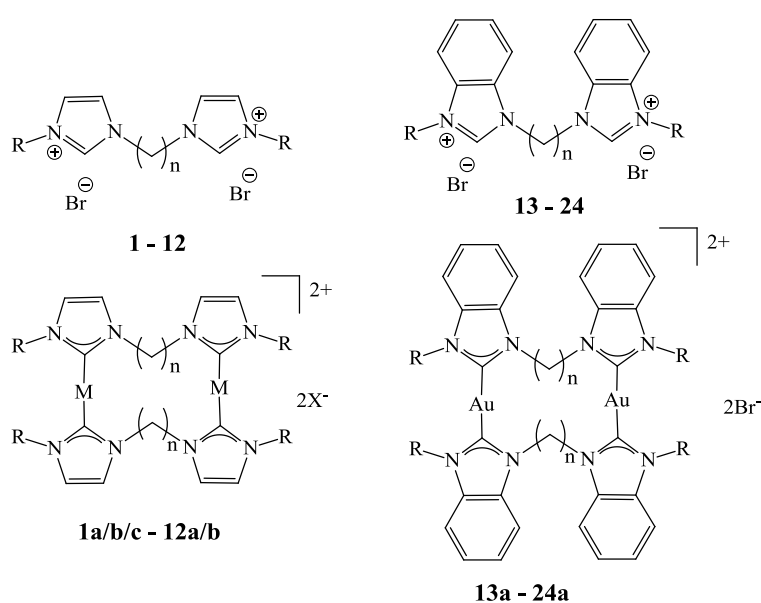
Scheme 1.1. Summary of the studied compounds.

Table 1.1. Summary of the studied ligand precursors and their classification.

	n =	1	2	3	4	5	6
imidazole	R = ethyl	**1**	**2**	**3**	**4**	**5**	**6**
	R = methyl	**7**	**8**	**9**	**10**	**11**	**12**
benzimidazole	R = ethyl	**13***	**14**	**15**	**16**	**17***	**18***
	R = methyl	**19**	**20**	**21**	**22**	**23***	**24**

* Syntheses not known to literature yet

Table 1.2. Summary of the studied complexes and their classification.

	n =	1	2	3	4	5	6	
imidazole	M = Au R = ethyl $X^- = Br^-$	**1a***	**2a***	**3a***	**4a***	**5a***	**6a***	Complexes Type 1
	M = Au R = ethyl $X^- = PF_6^-$	**1b***	**2b***	**3b***	**4b***	**5b***	**6b***	
	M = Ag R = ethyl $X^- = Br^-/$ $AgBr_2^-$	**1c***	**2c***	**3c**	**4c***	**5c***	**6c***	
	M = Au R = methyl $X^- = Br^-$	**7a**	**8a**	**9a**	**10a**	**11a***	**12a***	Complexes Type 2
	M = Au R = methyl $X^- = PF_6^-$	**7b**	**8b**	**9b**	**10b**	**11b***	**12b***	
benzimidazole	M = Au R = ethyl $X^- = Br^-$	**13a***	**14a***	**15a***	**16a***	**17a***	**18a***	Complexes Type 3
	M = Au R = methyl $X^- = Br^-$	**19a***	**20a***	**21a***	**22a***	**23a***	**24a***	

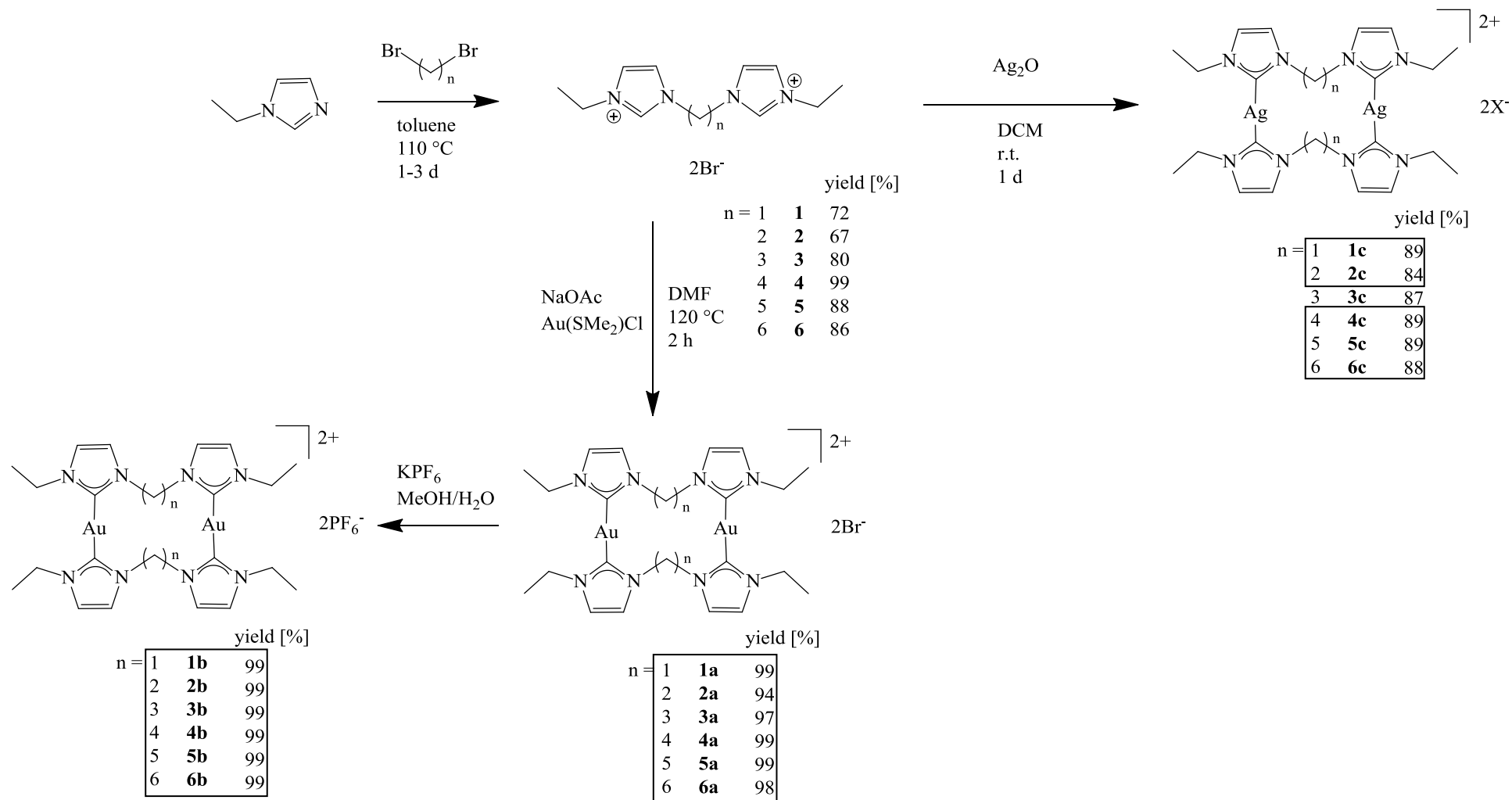* Syntheses not known to literature yet

2. Complexes Type 1 based on Ethylimidazole

The synthesis and characterization of three systematic series of new dinuclear gold(I) (and silver(I)) NHC complexes and their corresponding NHC precursors is reported in this section. One of these compounds (**3c**) has already been structurally characterized by Liu et al.[74] in 2010. Four of the compounds (**2a**-**4a**, **6a**) were structurally characterized in my diploma thesis[73]. Nonetheless, these structures are discussed here again for the purpose of comparison.

2.1 Synthesis

The ethyl imidazolium bromide salts **1-6**[75,76] (Scheme 2.1) were obtained by conversion of N-ethylimidazole with the corresponding alkyldibromide in toluene. The corresponding NHC gold(I) bromide complexes **1a-6a** were synthesized by direct metallation of the respective imidazolium salt in the presence of sodium acetate in DMF according to a well-established procedure[27-29,32,33,35-37]. The complexes were purified by crystallization (slow diffusion of diethylether into a methanol solution). Subsequent anion exchange with KPF_6 in a methanol/water mixture produced the complexes **1b-6b** in excellent yields. The analogous silver(I) complexes **1c**-**6c** were obtained by direct metallation of the ethyl imidazolium bromide salts **1-6** with silver(I)oxide, which is not only the silver source in the reaction, but the base as well[77,78]. The silver complexes were synthesized successfully with the aim of obtaining crystals suitable for X-ray measurements as a means to study the influence of aurophilic and argentophilic interactions, respectively, vs. π-π interactions. Their r.t. solution phase NMR spectroscopic behaviour is in accordance with the expectations for NHC silver(I) complexes[1,2]. Argentophilic interactions are a common phenomenon among NHC silver(I) complexes while considered a weak interaction, even weaker than aurophilicity[51,79]. The compounds **1a/b/c**-**6a/b/c** were readily characterized by electrospray mass spectra showing intense signals for the intact dicationic macrocycle M^{2+}, except for the silver(I) compound **4c** (vide infra). Indications for the presence of mononuclear complexes with a chelating bis-NHC-ligand known for longer linkers were not found[23,24].

Scheme 2.1. Syntheses of the NHC precursors **1-6** and the gold(I) NHC complexes **1a/b/c-6a/b/c** (X^- = Br^- or $AgBr_2^-$). Syntheses not kown to literature yet are indicated by black boxes.

2.2 NMR Spectroscopy

The room temperature ^{1}H and ^{13}C NMR spectra for the complexes **1a/b-6a/b** confirm the expected highly symmetrical structures. The formation of gold(I)-carbene complexes is accompanied by a vanished acidic imidazolium proton signal at $\delta \sim 9.50$ ppm in the ^{1}H NMR spectrum and a typical shift of the $C_{carbene}$ signal from <140 ppm in the NHC precursor to >180 ppm in the gold(I) complex in the ^{13}C NMR spectrum[1,2]. In accordance to previously reported similar findings[24,27,32,33,35], neither the exocyclic NHC side chain nor the counter anion induce significant changes in the macrocycle resonances at room temperature, whereas an upfield shift in acetonitrile solution is more pronounced. The compounds **1c-6c** undergo the same changes to the NMR spectra with respect to the vanishing acidic imidazolium proton signal and the $C_{carbene}$ signal[1,2], while all signals are shifted downfield in the ^{1}H NMR spectra and upfield for the ^{13}C NMR spectra compared to those of the gold compounds.

The protons of the methylene linkers in compounds **1a/b** are not equivalent and appear as two separated doublets at room temperature[27,32,33,35]. They reversibly coalesce upon heating to $100 - 105\,°C$ (Figure 6.1.1, Appendix). As a result the free activation enthalphy at 298 K of $\Delta G_{298}^{\neq} = 74 \pm 11$ kJ/mol is extracted from an Eyring plot of exchange rates (Figure 6.1.2 and Table 6.1.1, Appendix) obtained by line shape analysis using the programme gNMR[80]. A similar behaviour has been reported for the congener with methyl side chains and has been attributed to an interconversion of exo- and endo hydrogens by a kind of ring inversion[27] (Scheme 2.2).
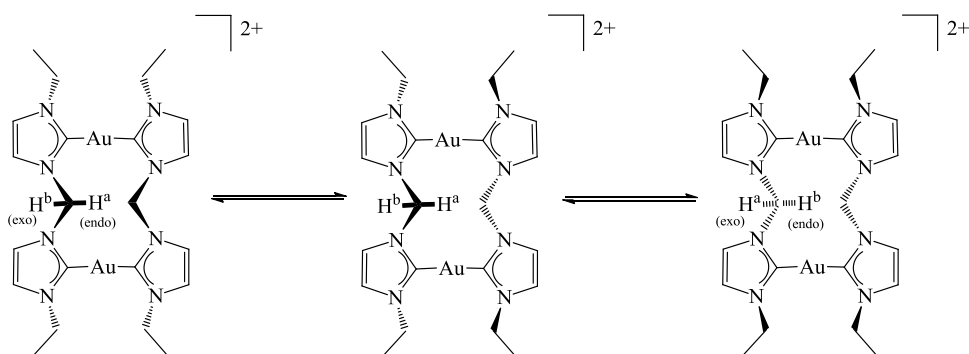
Scheme 2.2. Proposed ring inversion of compounds **1a/b**.

Some more reversible spectral changes occur during heating: The methylene protons of the ethyl side groups seem to be diastereotopic and appear as two multiplets when measured with

500 MHz at room temperature in DMSO-d$_6$ (Figure 6.1.1). Heating the sample leads to coalescence into the quartet signal expected for freely rotating ethyl groups. The signal for the pending methyl protons appears as triplet, which shifts very slightly downfield by 0.05 ppm at higher temperatures. A parallel dynamic behaviour is observable with respect to the signal of the imidazolium proton next to the ethyl side chain. It broadens and resharpens again, similar to the findings reported for the methyl derivative[27]. In summary, all these additional observations are in accordance with a free rotation around the C-CH$_3$ bond, while the rotation around the N-CH$_2$ bond is frozen at room temperature with activation parameters of $\Delta H = 43 \pm 3$ kJ/mol and $\Delta S = -87 \pm 9$ Jmol^{-1}K^{-1} and, thus, a free activation enthalpy of $\Delta G_{298}^{\neq} = 69 \pm 4$ kJ/mol (Figure 6.1.2 and Table 6.1.1). This value is unexpectedly high (and ΔS very low) for a simple ethyl rotation at the periphery of the molecule. An effect of a potentially coordinating anion can be ruled out as similar activation parameters are obtained for the bromide (**1a**) and hexafluorophosphate (**1b**) salt. Inspection of the molecular structure in the solid state in a spacefilled view (vide infra, Figure 6.1.6) might lead to an explanation. The ethyl side chains of the two NHCs coordinating a gold atom come rather close (distance between the methylene carbon atoms $d = 4.350$ Å). Thus, the ethyl groups are jammed and their independant rotation is hindered.

The room temperature ^{1}H NMR spectra for the ethylene-connected macrocycles **2a/b** show a singlet for eight equivalent linker hydrogens and a well-defined quartet for the side chain methylene groups. Thus, chain elongation expectedly enhances the flexibility of the macrocycles. Lowering the temperature reveals a partial freezing of the conformational flexibility: In the ^{1}H NMR spectra of **2a**, a broadening and finally splitting of the linker CH$_2$ signal into two broad singlets at -80 °C is visible with coalescence around -60 °C (Figure 2.1). Line shape analysis (Figure 6.1.2 and Table 6.1.1) yields $\Delta G_{298}^{\neq} = 47 \pm 4$ kJ/mol for the frozen process. It could be interpreted as an inversion of the ethylene-bridged macrocycle equilibrating exo and endo protons in analogy to the behaviour of **1a/b** described above. The smaller ΔH and much lower ΔS value are fully consistent with the enhanced flexibility of the elongated linker. In addition, signal broadening during cooling of the sample is visible for the H5 imidazol proton, and, similar to the findings for the smaller macrocycle **1a/b**, for the CH$_2$ groups in the ethyl side chains. Unfortunately, the signals do not yet split into separated ones at the experimental minimum of -80 °C, which impedes a modelling of the kinetic rate constants due to unknown chemical shifts of the system with frozen dynamics. Nevertheless,

a concerted ethyl rotation of partly jammed ethyl side chains again seems plausible (see Figure 6.1.6 for a spacefilled view of the solid state molecular structure).
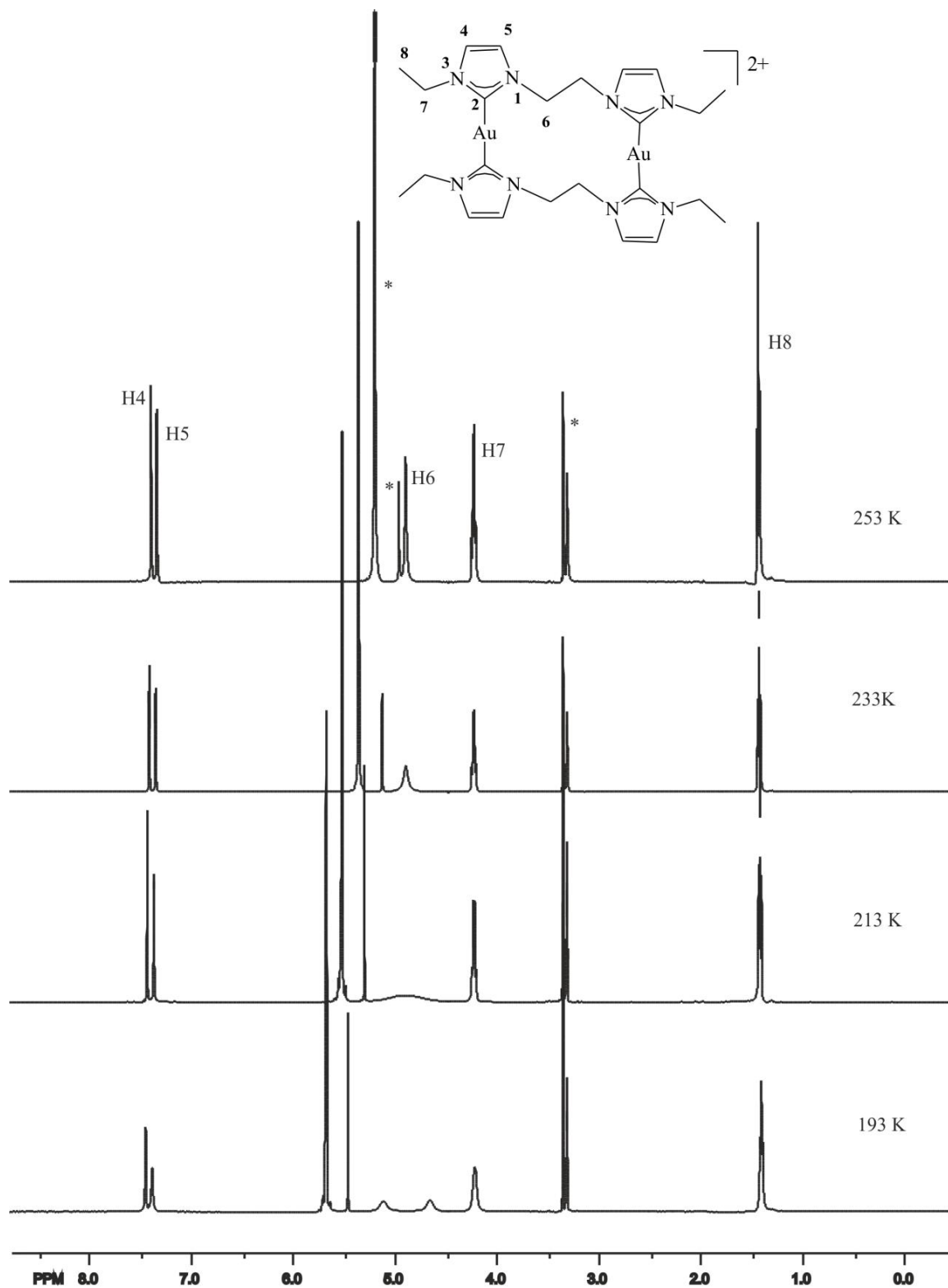
Figure 2.1. Low-temperature ^{1}H NMR spectra (500.13 MHz, CD$_3$OD) of **2a**. *partially deuterated and undeuterated methanol and water, respectively.
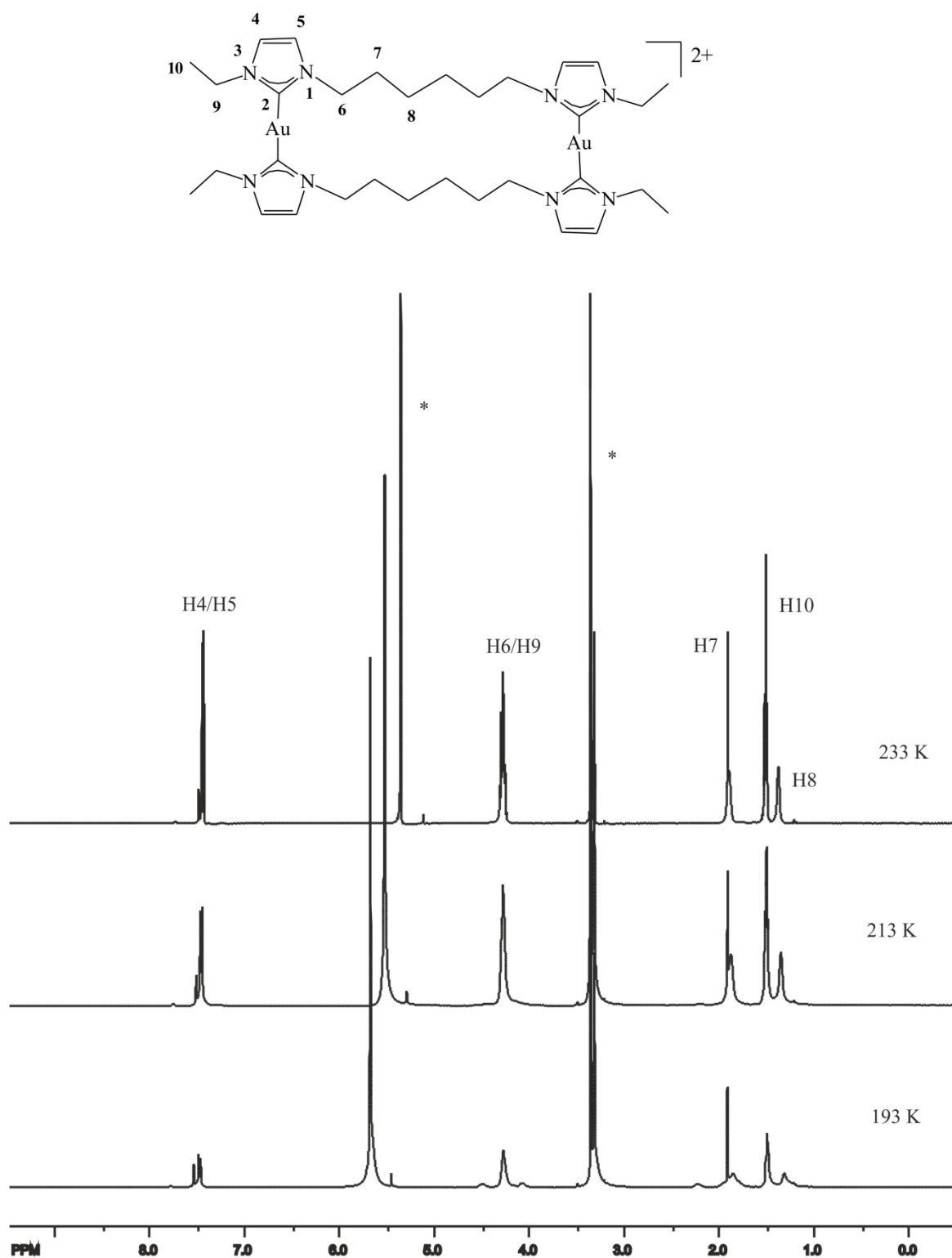
Figure 2.2. Low-temperature ^{1}H NMR spectra (500.13 MHz, CD$_3$OD) of **6a**. *partially deuterated and undeuterated methanol and water, respectively.

The ^{1}H NMR spectra of the macrocycles with three, four and five methylene groups as linkers (**3a**, **4a**, **5a**) show broadening of the methylene signals at lower temperatures, but coalescence could not be reached in the temperature range down to -80 °C (Figures 6.1.3 – 6.1.5,

Appendix). The changes in the NMR spectra for **4a** are rather subtle, whereas broadening of the H8 signal and thus a hindered ethyl side chain rotation is clearly visible for compound **3a**. For compound **5a**, the imidazol protons broaden and shift downfield by 0.1 ppm, and the CH_2 and CH_3 signals of the ethyl groups broaden and shift upfield by 0.3 and 0.15 ppm, respectively.

For substance **6a** with six methylene units in the linker, sample cooling has a different effect on the ^{1}H NMR spectra (Figure 2.2). At -80 °C, additional broad signals are clearly visible, which could be interpreted as signs of a starting aggregation inspired by the solid state packing with dominant π-π interactions arranging the cations in long chains (vide infra).

2.3 X-ray Crystal Structures

Single crystals suitable for X-ray diffraction could be obtained by slow diffusion of diethylether in a methanol solution (**1a**-**4a**, **6a**), an acetonitrile solution (**1b**-**6b**) or a DCM solution (**1c**, **3c**, **4c**). Thus 14 out of 18 complexes were structurally characterized. Selected structural data is summarized in Table 2.1. The compounds containing gold centres consist of dicationic dinuclear complexes $Au_2L_2^{2+}$ with bridging dicarbene ligands L. The basic structural parameters fit the expectations: The gold atoms are doubly coordinated with C-Au-C angles close to linearity and mean C-Au bond lengths of 2.02 Å typical for gold(I) NHC compounds[1,2]. The compounds **1c** and **3c** show similar macrocycles with dicationic dinuclear complexes $Ag_2L_2^{2+}$ containing bridging dicarbene ligands L. The complex **4c** shows a completely different organization with polymer chains instead of macrocycles. Two different ligands connect three instead of two Ag atoms. Nonetheless in all three silver compounds the silver atoms are doubly coordinated with C-Ag-C angles close to linearity and mean C-Ag bond lengths of 2.08 Å typical for silver(I) NHC compounds[74,79].

Owing to the almost linear C-M-C axis, the torsion angles can be measured between N-C-C-N of the two ligands in a dication to describe their position. For all cations studied here, except for the ones with ethylene linkers **2a/b** and the silver compounds **1c** and **3c**, the torsion angle is close to zero and the NHC planes on opposite sides of the metal are coplanar. Each cation is accompanied by two bromide, hexafluorophosphate or $AgBr_2^-$ anions, respectively. In all cases, the complexes are arranged in a way, that layers are formed consisting of organic ligands on the one hand and coin metal atoms with counter ions on the other. NHC ligands of neighboured complexes are interconnected by π-π interactions.

Table 2.1. Selected structural data for complexes **1a/b/c – 6a/b**.

	n	Crystal symmetry	M-C/ Å	C-M-C/°	N-C-C-N/° (a)	dihedral angle of NHC planes/° (b); *(c)*	Confor-mation next to NHC	M • M/Å intra-molecular (d)	M • M/Å inter-molecular (d)	π • π/ Å inter-molecular (d)
1a	1	$P\,2_1/n$	2.015(12) 2.018(13) 2.026(12) 2.031(12)	170.0 174.5	-4.6 -1.4	0.8 28.1 109.0 107.9	-	3.6633(1)	3.57866(16)	3.48279(16)
1b	1	$C\,2/m$	2.017(5) 2.022(5)	172.6 174.3	0.0	11.4 14.5 106.2	-	3.6475(5)	5.2346(8)	3.6386(5)
1c	1	$P\,2_1/c$	2.100(5) 2.103(5)	164.8	-87.0	109.5	-	3.4707(1)	9.2156(3)	3.5851(2)
2a	2	$P\,2_1/n$	2.018(5) 2.021(5) 2.023(5) 2.025(5)	173.8 177.4	-42.8 -56.9	43.3 55.8 51.9 38.8	gauche	3.3988(1)	7.2397(3)	3.91031(16)
2b	**2**	$P\,2_1/c$	2.025(3) 2.027(3) 2.032(3) 2.032(3)	175.3 176.2	-49.4 -55.5	47.0 49.7 *39.1* *41.9*	gauche	3.2328(2)	6.2975(2)	3.49732(15)
3a	3	$Pmmn$	2.012(5)	178.6	0.0	6.0 126.3	trans	6.7918(3)	7.1092(4)	3.6215(3)
3b	3	$P\,\text{-}1$	2.0069(3) 2.0151(3) 2.0261(3) 2.0333(3)	175.6 176.6	1.5 1.6	11.4 7.9 103.4 104.8	trans	6.4190(9)	3.2916(4)	3.5878(4)
3c	3	$P\,\text{-}1$	2.088(6)	176.1	-70.1	66.0	gauche/ trans	5.7454(5)	7.1354(6) 4.7244(4)*	3.7113(2)
4a	4	$P\,\text{-}1$	2.01734(14) 2.01675(13)	175.7	3.5	3.2	gauche	6.7729(4)	3.69214(15)	3.59182(14)
4b	4	$P\,\text{-}1$	2.057(2) 2.061(2)	176.5	2.4	3.3	gauche	6.972(6)	3.5818(25)	3.607(3)
4c	4	$P\,\text{-}1$	2.089(9)	180.0	0.0	0.0	gauche	7.472(3)		7.472(3)
5b	5	$C\,2/c$	2.01847(6) 2.02094(6)	176.7	2.5	3.7	gauche	4.9425(2)	3.5478(1)	3.74249(12)
6a	6	$P\,\text{-}1$	1.99590(16) 2.02309(16)	178.8	2.2	6.0	gauche	8.7084(7)	3.8164(3)	3.6865(3)
6b	6	$P\,\text{-}1$	2.036(15) 2.046(14)	177.3	-7.3	4.4	gauche	8.8268(7)	3.3582(2)	3.5897(2)

(a) torsion angle between the two NHC rings (EtN-$C_{carbene}$-$C_{carbene}$-NEt) coordinating a metal atom; (b) dihedral angle of the two NHC planes coordinating an M atom; (c) dihedral angle of the two NHC planes in the linker; (d) the shortest value is given. * Ag • AgBr$_2$ [Å]

Further, all solid state structures of the gold compounds, except for **3a**, reveal a relatively short Au-Au distance, either intra- or intermolecularly; in one case (**1a**) even both is realized.

The silver compound **1c** is the only one shown here with a short Ag-Ag distance (3.47 Å). The space groups and crystal packing of the two complexes with the same cation typically differ due to the size difference of the two anions studied. The same applies to two complexes with different coin metals. However, the influence of the counter ion on the conformation of the cation is unexpectedly small (Figures 2.3 – 2.15 and 6.1.7-6.1.9, Table 2.1) compared to similar examples in literature[24,35-37].

One of the more obvious conformational differences is observed for the smallest cation bearing only methylene linkers. Here, all ethyl side chains point inwards for the bromide salt **1a** (Figure 2.3), but show an in/out conformation for **1b** with PF_6^- (Figure 2.4). In both cases, the ethyl side groups of the two NHC rings coordinating an Au atom come rather close, which renders an independant rotation of the two groups impossible (Figure 6.1.6). The angles of the NHC substituents at the methylene group are identical (111.8° and 111.1°, respectively) and the intramolecular Au-Au distance (3.663 Å vs. 3.648 Å) is only 0.016 Å shorter for **1b**. The crystal structure of both **1a/b** consists of pairs of macrocycles with parallel arrangement of a whole NHC-Au-NHC unit. The dimers of macrocycles are further connected by head-to-tail $\pi-\pi$ interactions with neighbouring NHC units (Figure 2.3 and 2.4). The intermolecular distance between the gold atoms of a dimer of macrocycles is much shorter in **1a** (3.579 Å) than in **1b** (5.235 Å) due to the different orientation of the ethyl side chains. In contrast, the corresponding silver structure **1c** shows an outward orientation of the ethyl side chains leading to a zig-zag pattern for the ligands. However, this zig-zag pattern is shifted for the ligands on opposite sides of the silver atoms (ligand planes are not coplanar) (Figure 2.5). Nonetheless the angle of the NHC substituents at the methylene group is identical (111.6°) to the one in the corresponding gold complexes **1a/b**. The intramolecular Ag-Ag distance is by ~0.2Å shorter (3.471Å) than the Au-Au distances found in the gold complexes, which confirms similar published findings[1,12,81-85]. The dimers of macrocycles are further connected by head-to-tail $\pi-\pi$ interactions with neighbouring NHC units (Figure 2.6).

A similar complex published by Barnard et al. has methyl side groups and I$^-$ as counter ion[27]. The shape of the cation is comparable to **1a/b**, but the intramolecular Au-Au distance is shorter (3.5425(6) Å). Further, Hemmert and coworkers structurally characterized two methylene-bridged gold-NHC complexes with alcohol- or carboxylate-functionalized side chains (Au-Au 3.514 Å and 3.589 Å, respectively)[32,33]. An even shorter distance (3.3610(7) Å) could be realized by Fränkel et al.[25] in a neutral complex containing a BH_2-unit

instead of a methylene linker and by the group of Hahn via incorporation into a large macrocycle (3.0737(3) Å)[43]. A short Ag-Ag distance (3.318 Å) was found in a similar complex with methyl side chains and chloride as counter ion by Wang et al.[86]. In contrast, the NHCs on both sides of one Ag atom are coplanar.
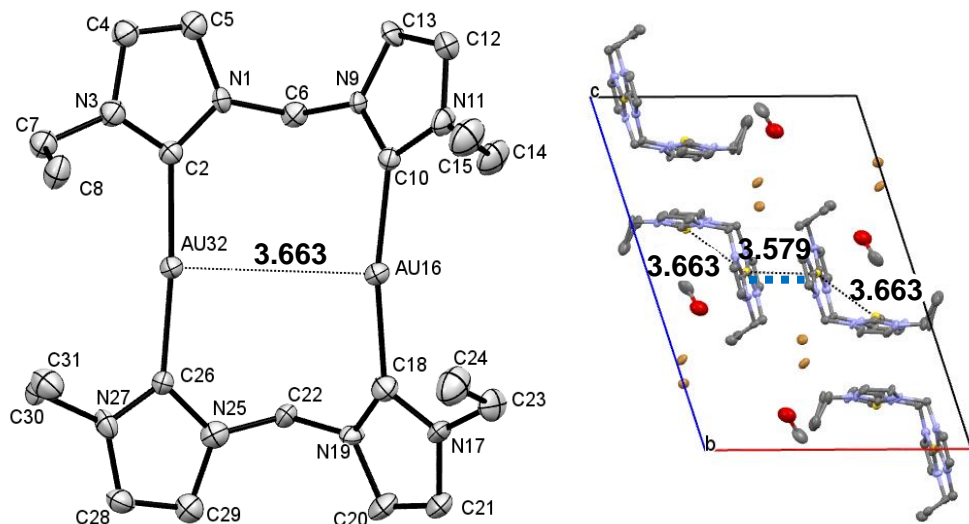

Figure 2.3. ORTEP drawing (left) and crystal packing (view along b axis, right) of complex **1a** (50% probability level for the thermal ellipsoids). Au-Au bound dimers of macrocycles are connected by intermolecular π−π interactions indicated by dotted blue lines. Hydrogen atoms have been omitted for clarity.
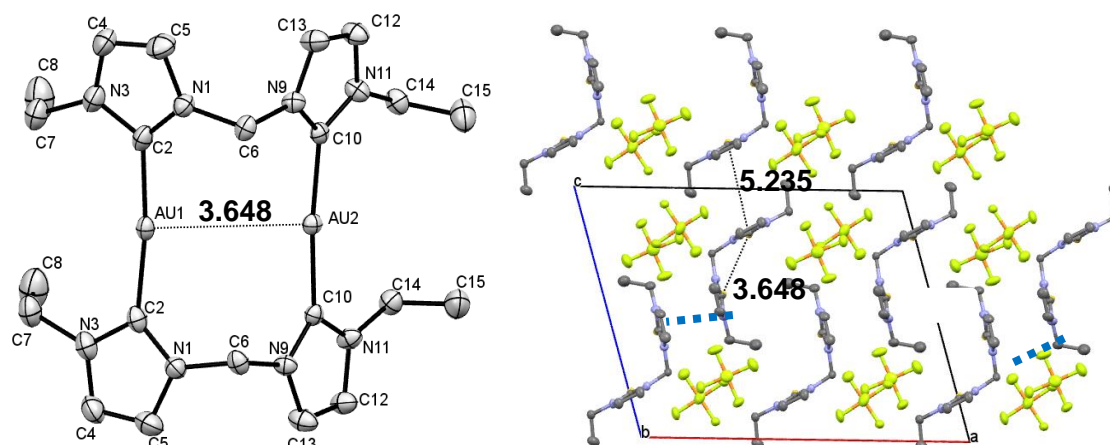

Figure 2.4. ORTEP drawing (left) and crystal packing (view along b axis, right) of complex **1b** (50% probability level for the thermal ellipsoids). Intermolecular π−π interactions are indicated by dotted blue lines. Hydrogen atoms have been omitted for clarity.
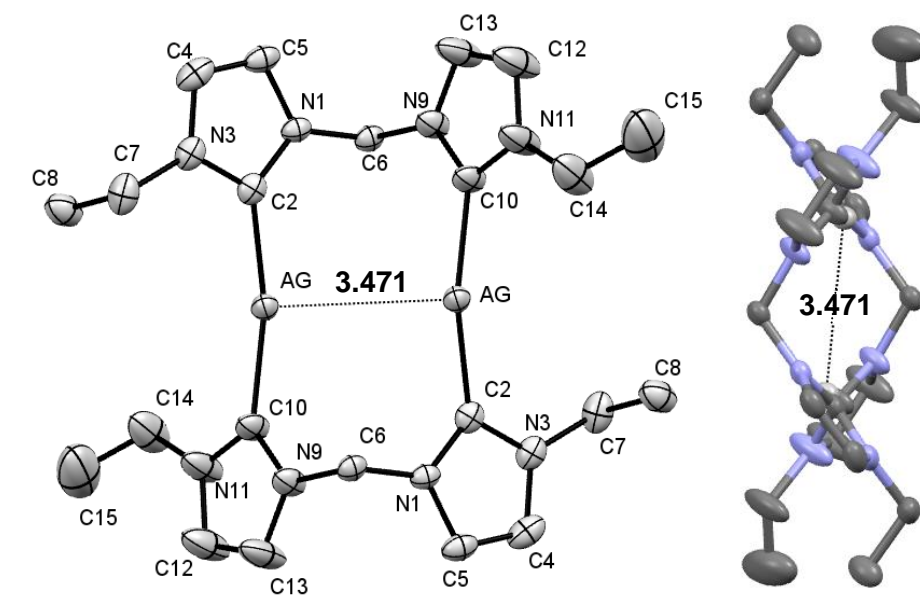
Figure 2.5. ORTEP drawing (left) and top view (right) of complex **1c** (50% probability level for the thermal ellipsoids). Br⁻ anions and hydrogen atoms have been omitted for clarity.
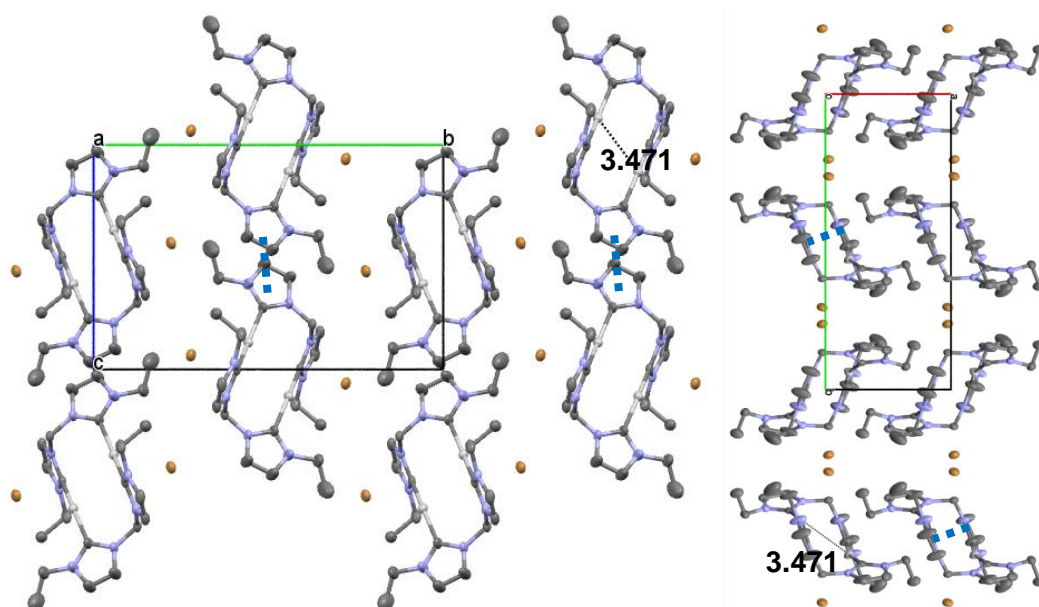
Figure 2.6. Crystal packing (right: view along a axis, left: view along c axis) of complex **1c** (50% probability level for the thermal ellipsoids). Intermolecular $\pi-\pi$ interactions are indicated by dotted blue lines. Hydrogen atoms have been omitted for clarity.

The complexes **2a/b** both form monoclinic space groups as well (**2a**: $P2_1/n$, **2b**: $P2_1/c$). The overall conformation of the dicationic macrocycle is unusual, but rather similar for both anion types (Firgure 2.7), apart from the relative position of the ethyl side groups. A backfolded twisted geometry with gauche conformation in the ethylene linkers leads to a short intramolecular Au-Au distance (**2a**: 3.3988(1) Å, **2b**: 3.2328(2) Å). The Au-Au bond is

significantly ($\Delta d = 0.167$ Å) shorter for the bigger hexafluorophosphate salt. This cation is the only one of the whole series of gold complexes, for which the two NHC planes bound to a gold atom are not coplanar, but twisted by approx. 50°, respectively, - probably to avoid steric repulsion of the ethylene linkers, while retaining the short Au-Au distance.
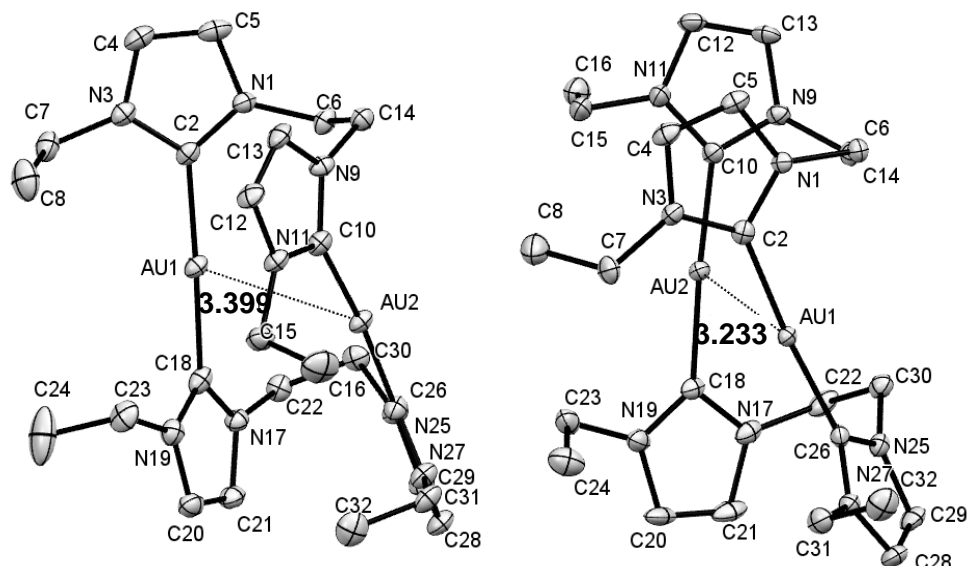
Figure 2.7. ORTEP drawing of complex **2a** (left) and **2b** (right) (50% probability level for the thermal ellipsoids). Counter ions (Br⁻ and PF₆⁻, repectively), hydrogen atoms and cocrystallized water and methanol (for **2a**) have been omitted for clarity.

The conformational folding of the dication **2a** is so compact and twisted, that close arrangement with neighbouring macrocycles is restricted to a single π−π interaction per molecule, while the hexafluorophosphate congener **2b** can perform two π−π interactions per molecule (Figure 2.8).
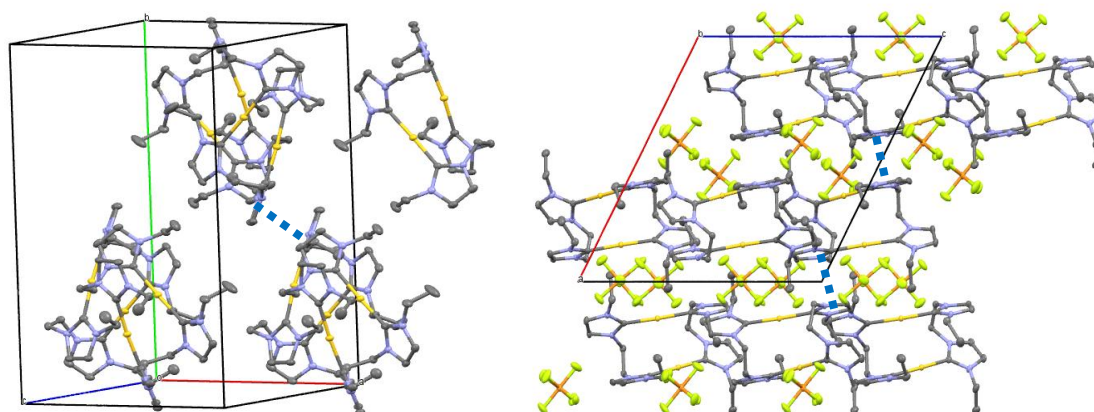

Figure 2.8. Crystal packing of complex **2a** (view along no axis, left) and **2b** (view along b axis, right) (50% probability level for the thermal ellipsoids). Intermolecular π−π interactions are indicated by dotted blue lines. Bromide anions and hydrogen atoms have been omitted for clarity.

The only published ethylene-linked NHC-Au complex structurally characterized by X-ray bears a bulky alcohol-functionalized side group and PF_6^- anions[33]. Its conformation is backfolded with 50° twisted NHC planes and an intramolecular Au-Au bond in the range of 3.3 Å. It strongly resembles the conformations of the ethyl derivatives described here. The fact, that all side chains point to the same side of the molecule thus is not enforced by hydrogen bonds between OH groups, because a similar conformation is retained by simple ethyl groups as well. In sight of the absence of strong intra- or intermolecular $\pi-\pi$ interactions, the backfolded conformation should have an attractive aurophilic origin even though the two gold atoms are cationic.
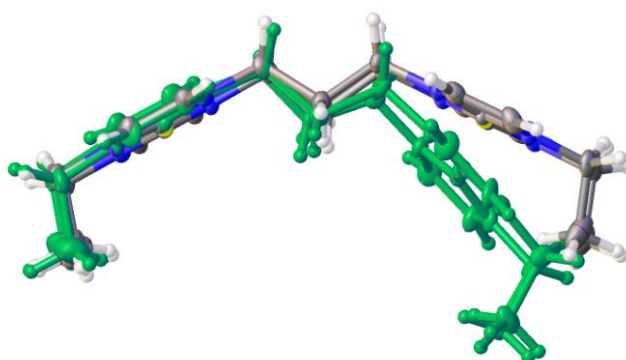
Figure 2.9. Top view of the overlay of complexes **3a** and **3b** (green) (50% probability level for the thermal ellipsoids). The difference in the angle of the linker results in a shorter Au-Au distance in **3b**.

Figure 2.10. Crystal packing of complex **3a** (view along b (left) and c (right) axis, 50% probability level for the thermal ellipsoids). The macrocycles form double-layers connected by intermolecular $\pi-\pi$ interactions indicated by dotted blue lines. Hydrogen atoms have been omitted for clarity.
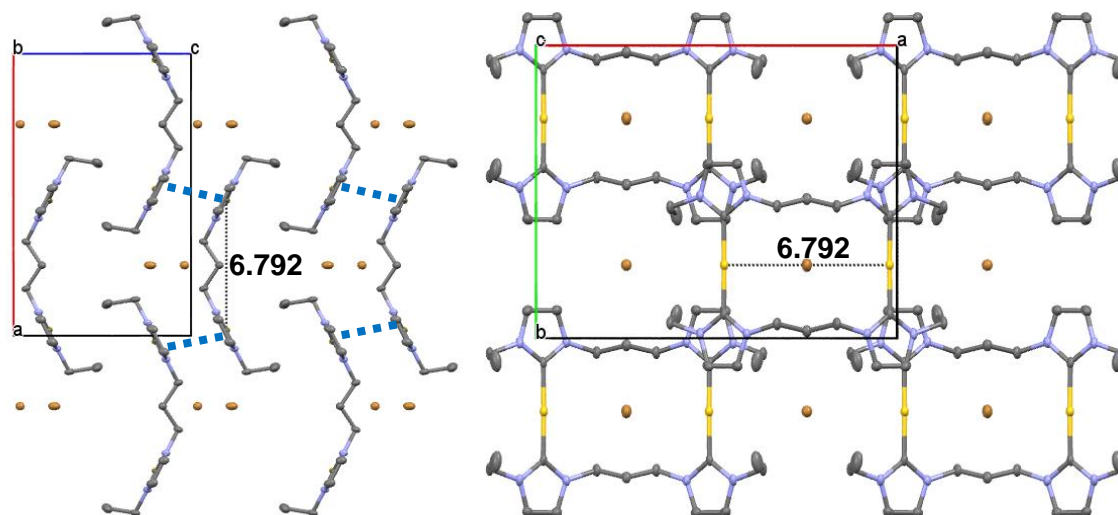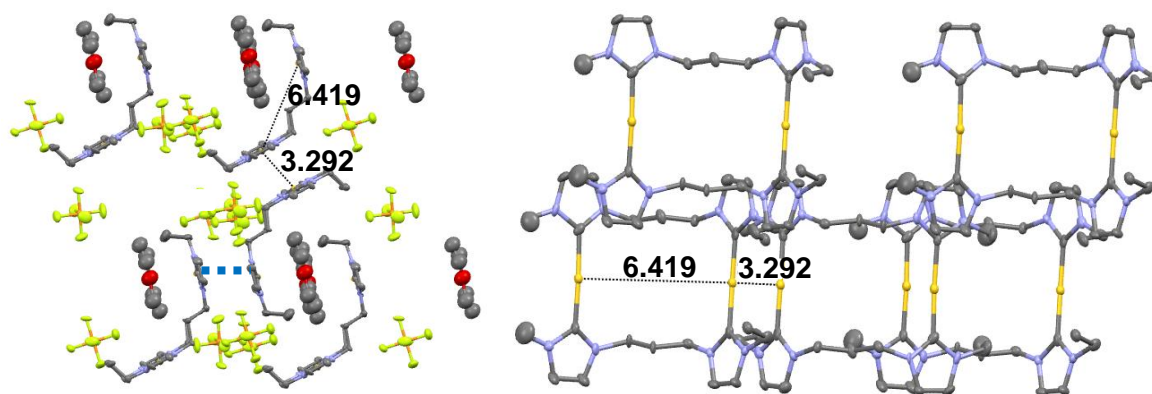
Figure 2.11. Two views of the crystal packing of complex **3b** (50% probability level for the thermal ellipsoids). Au-Au bound dimers of macrocycles are connected by intermolecular π−π interactions indicated by dotted blue lines. Hydrogen atoms and in the right view also PF_6^- anions and cocrystallized Et_2O and have been omitted for clarity.

Both dications **3a/b** with propylene-linked NHC ligands show an open, W-like conformation with an all-*trans* propylene linker (Figures 2.10 and 2.11). The intramolecular Au-Au distance is very long for both structures, but for **3a** even 0.373 Å longer than for **3b** (see Figure 2.9). This is the result of a flattened conformation as the dihedral angle of 103° - 105° between the two NHC planes of a ligand in the PF_6^- structure **3b** is widened to 126° when crystallized as the bromide salt **3a** (Figure 2.9). The reason probably is a packing effect: The crystal packing of **3b** closely resembles the one of methylene-linked **1a**. Dimers of macrocycles are formed by a short intermolecular Au-Au distance of 3.292 Å, stabilized by π−π interactions (Figure 2.11). In contrast, the bromide derivative **3a** appears in extended π−π bound double-layers (Figure 2.10), which should be easier to form with flattened macrocycles. It is the only structure of the series that does not show any kind of intra- or intermolecular Au-Au interaction.

Much like **1c**, **3c** has a twisted conformation, where the NHC planes are not coplanar (Figure 2.12., left). The linker is unlike in **3a/b** not all *trans*, but rather a mixture of *trans* and *gauche* on both sides of the Ag atoms. Though close π-π interaction (3.71 Å) is still possible (Figure 2.12, right). The compound **3c** was already structurally characterized by the group of Wang[74].
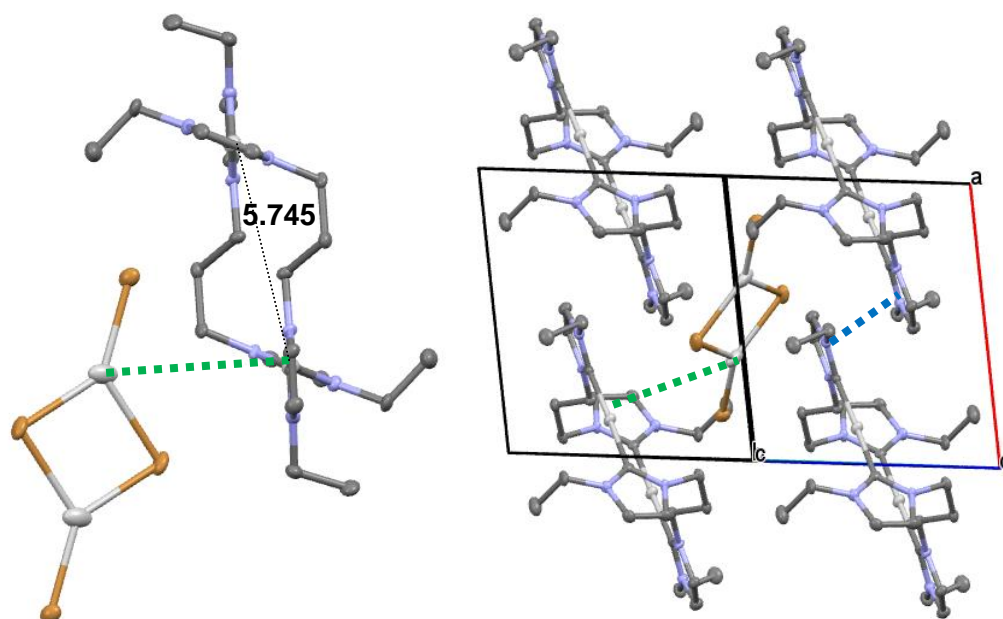
Figure 2.12. Top view (left) and crystal packing (right) of complex **3c** (50% probability level for the thermal ellipsoids). Dimers of macrocycles are connected by intermolecular π–π interactions indicated by dotted blue lines. Ag • AgBr$_2$ contact is indicated by dotted green lines. Hydrogen atoms have been omitted for clarity.

Baron et al. reported the crystal structure of a related propylene bridged Au(I) NHC complex with methyl side chains and PF$_6^-$ as counter ion in 2012[35]. Unlike the situation shown here, the alkyl chains fold in two *gauche* conformations resulting in a U-shaped macrocycle with parallel NHC-Au-NHC subunits and a short intramolecular gold(I)-gold(I) distance of 3.272 Å. Gil-Rubio et al.[24] crystallized the same cation with triflate anions in 2013. This time, a helical conformation with orthogonal NHC-Au-NHC bonds and a very small Au-Au distance of 3.032 Å is realized. In both structures, the backfolded macrocycles form C3- and C2-symmetric columnar aggregates, respectively, with intermolecular Au-Au and π–π interactions of about $d = 3.7$ Å. In contrast, the last structurally characterized propylene-bridged complex of this type crystallizes in an open conformation and a double-layer packing without Au-Au interactions[32], which strongly resembles the findings reported above for the propylene derivative **3a**. It comes from the Hemmert group and possesses PF$_6^-$ anions and bulky side groups with hydroxyl functions. Thus, counter ion as well as the type of side group have an extreme effect on the molecular conformation of propylene-linked dinuclear NHC complexes of gold(I). In particular, the steric increase from methyl to ethyl is sufficient to open the conformation and suppress the formation of an intramolecular Au-Au bond.
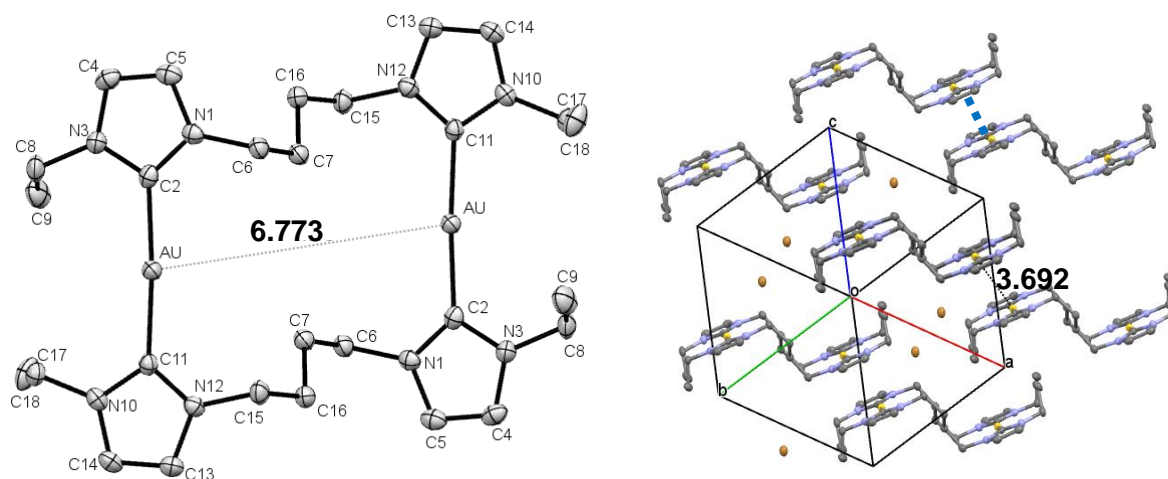
Figure 2.13. ORTEP drawing (left) and crystal packing (right) of complex **4a** (50% probability level for the thermal ellipsoids). Au-Au bound dimers of macrocycles are connected by intermolecular $\pi-\pi$ interactions indicated by dotted blue lines. Cocrystallized methanol and hydrogen atoms have been omitted for clarity.

The complexes **4a/b** both form the triclinic space group *P-1*. The orientation of the cations is similar (Figure 2.13, left). Therefore both cations cannot, due to the open S-arrangement of the cation, realize a short intramolecular Au-Au distance (Figure 2.13, right). Conformation next to the NHC is *gauche* for both cations enabling coplanarity for all NHCs. Complexes **6a/b** are conformationally comparable to **4a/b** (Figure 6.1.7 – 6.1.9, Appendix).
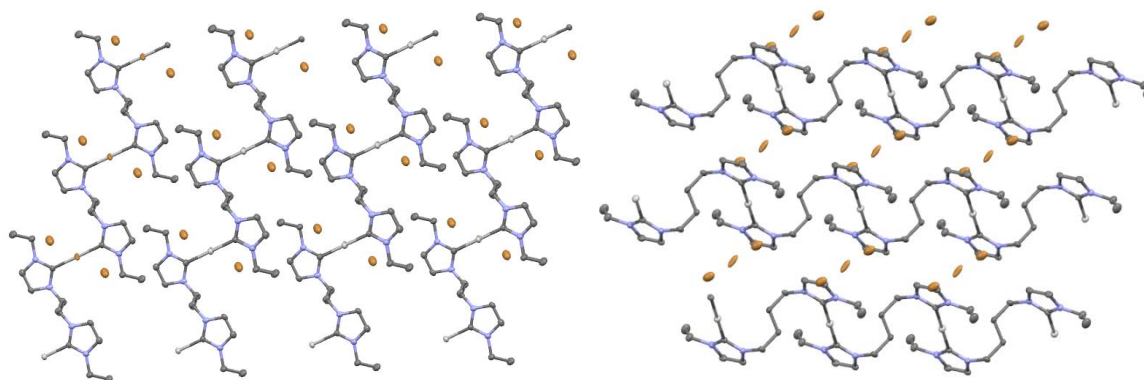
Figure 2.14. Two views of the crystal packing of complex **4c** (50% probability level for the thermal ellipsoids). Hydrogen atoms have been omitted for clarity.

In contrast, **4c** shows a very unusual conformation: the $M_2L_2^{2+}$ macrocycles are replaced by a polymer structure with AgL^+ subunits forming long chains (Figure 2.14). Conformation next to the NHC is *gauche* for **4a/b/c** and **6a/b**, but due to the polymerisation and separation of the

layers by counter ions, there is no possibility for short Ag-Ag distances or $\pi-\pi$ interactions in **4c**.

Comparable complexes with butylene or hexylene linkers are unkown so far. Berners-Price et al.[27] showed a structure with an *o*-phenyl cycle as linker, but the NHCs are connected on both sides, which results in parallel NHC-Au-NHC units in the gold(I) complex and flexibility is not given. The intramolecular Au-Au distance is short (3.0 Å). The corresponding silver structure of cation **4c** with hexafluorophosphate as counter ion has been published by the group of Wang[74]. Contrary to the unusual polymer structure found here, the hexafluorophoyphate congener shows the common $Ag_2L_2^{2+}$ macrocycles with the same arrangement in the X-ray structure as **4a/b**: a long intramolecular Ag-Ag distance of 6.844 Å with a formation of dimers bound by short intermolecular Ag-Ag distances and stabilized by $\pi-\pi$ interactions.
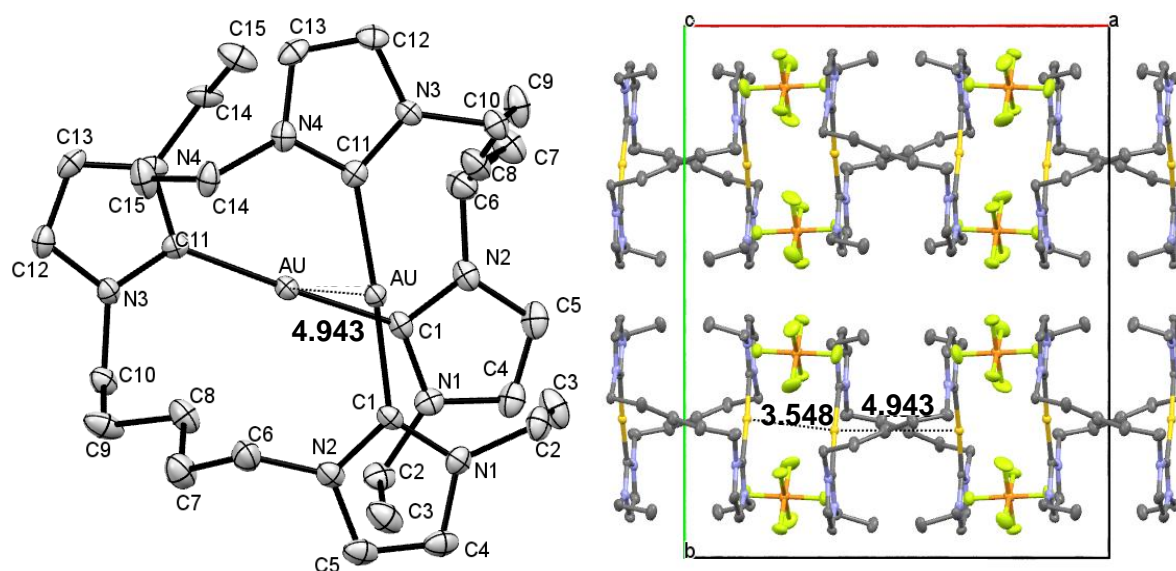
Figure 2.15. ORTEP drawing (left) and crystal packing (view along c axis, right) of complex **5b** (50% probability level for the thermal ellipsoids). Hydrogen atoms have been omitted for clarity.

While purification by crystallization was successful for **5a**, the resulting crystals were not suitable for X-ray diffraction measurements. Yet, **5b** gave good crystals in the monoclinic space group *C*2/*c*. The adjustment of the cation is rather unusual compared to the other complexes of this series (Figure 2.15). The two C-Au-C axes are twisted and not parallel (-64.2°), resulting in a compact cation with a quite long intramolecular Au-Au distance (4.9425(2) Å). Due to the ethyl side chains facing inside, close $\pi-\pi$ stacking and a shorter intermolecular gold-gold distance of 3.548 Å are realized.

Comparable complexes with pentylene linkers are unkown so far. Berners-Price et al.[27] showed structures with a *m*-phenyl and *m*-pyridyl cycle as linker and methyl side chains, but the NHC-Au-NHC units are parallel in the gold(I) complex and flexibility is not given. Zhang et al.[30] showed a structure with an oxydiethyl chain as linker and anthracene side chains. These anthracene units dominate the crystal structure by stacking. Interestingly, the cation is twisted in a similar way (68°), but the intramolecular Au-Au distance is, due to the different angles in the linker, short (3.5 Å).

2.4 UV/Vis and fluorescence studies

Solution based structural studies for dinuclear Au(I) complexes, which display aurophilic interactions, are still rare. To make a contribution to a better understanding of possible triplet state exciplexes and their stability in solution, the ligand precursors **1-6** and the gold complexes **1a/b-6a/b** are studied here both in pure acetonitrile and acetonitrile with 20% water at room temperature. The negliglible role of the counter ion is visible in the X-ray crystal structures, which showed only a minor influence on the formation of Au-Au bonds. In solid state, solely the complexes with the shortest linkers **1a/b** and **2a/b** performed a short intramolecular Au-Au distance, irrespective of the counter ion.

All photophysical measurements were performed with 10^{-5} molar solutions of pure substances (results of the crystallization) in acetonitrile or acetonitrile with 20% water at room temperature. The first measurements in our group were perfomed in DMSO (measurement range <250 nm). To enlarge the measurement range to higher energies (<200 nm) the solvent was changed to ACN. The influence (solvation possibility) of the solvent was insignificant. The results turned out to be hard to reproduce (variability of the absolute intensity), therefore measurements were performed multiple times to eliminate weighing and diluting errors. The results shown here are well-established.

Both the ligand precursors **1-6** and the bromide complexes **1a-6a** show a strong absorption band at 220 nm in acetonitrile, wich disappears by adding 20 % water (Figure 2.16). The complexes **1b-6b** lack the corresponding band. The intensity of the absorption of **3b** is remarkable. All complexes are red shifted compared to the ligand precursors.

ACN

ACN+20 % H₂O

Figure 2.16. Graphics of the absorption measurements of ligand precursors **1**-**6** and complexes **1a**/**b**-**6a**/**b** in pure ACN (left) and ACN with 20% H₂O (right) at room temperature.

ACN   ACN+20% H$_2$O

Figure 2.17. Graphics of the emission measurements of ligand precursors **1**-**6** and complexes **1a/b**-**6a/b** in pure ACN (left) and ACN with 20% H$_2$O (right) at room temperature. The exact excitation wave length used during measurements is 255 nm.

All emission measurements were performed with three different excitation wavelengths (Figure 2.17: λ_{exc} = 255 nm; Figure 6.1.55 - 6.1.56, Appendix: λ_{exc} = 260 nm, 265 nm). The ligand precursors **1-6** are all unremarkable in acetonitrile and show the same strong band at 330 nm. The comparison of the absolute intensities reveals that the addition of water is

quenching this band for ligand precursor **1** and **4**, but increasing the intensity for **2**, **3**, **5** and **6**. The low emission bands at 380 nm of complexes **1b**, **4b-6b** are expected to belong to the naked dication, while blue-shifted emission bands at 330 nm of complexes **1a**, **4a-6a** are expected to belong to the association complex between the corresponding dication and bromide. The bromide counter ion is due to its size capable of arranging around the gold atoms in the macrocycle, possibly related to the corresponding Au(III) NHC halide complexes found in literature[24,35]. The bulky hexafluorophosphate congener has no possibility to form a related association complex. The position of the emission bands and therefore the energy is dependant on the counter ion, which is in agreement with earlier findings[29], but here the low energy emission band is formed by the naked dication in the hexafluorophosphate solution and not by the soft bromide congener. Neither the anion exchange nor the addition of water seems to have any influence on the strongest emitters **2a/b** and **3a/b**, which indicates propably a stable exciplex (^{3}[dσ*pσ] excited state) not influenced by possible anion or solvent association. The addition of 20% water leads to the disappearance of the emission bands at 330 nm of complexes **5a** and **6a**, therefore the decomposition of the suggested dication-bromide complex, possibly because of formation of hydration spheres, while the associated complex of bromide and cation **4a** is stable to the change of the solvent. Interestingly the complex with the shortest linker **1a** seems to form a new kind of associated complex possibly including water with an emission band at 310 nm. The situation of the complex **5b** with a bridging five methylene groups is similar, while the other complexes with the bulky hexafluorophosphate **1b-4b** and **6b** undergo no change in the emission spectra after adding 20% of water to the solution.

The direct comparison of the ligand precursor **1** and the complexes with both bromide (**1a**) and hexafluorophosphate (**1b**) as counter ion in pure ACN and ACN with 20 % water is given in Figure 2.18. Both complexes with a short methylene linker are not influenced by the choice of the counter ion and are hardly emissive compared to the corresponding precursor in ACN. The corresponding solution with the addition of water as solvent shows the increase of the emissive behaviour of **1b**. The excitation measurements confirm the previous observations.

ACN   **ACN+20% H$_2$O**
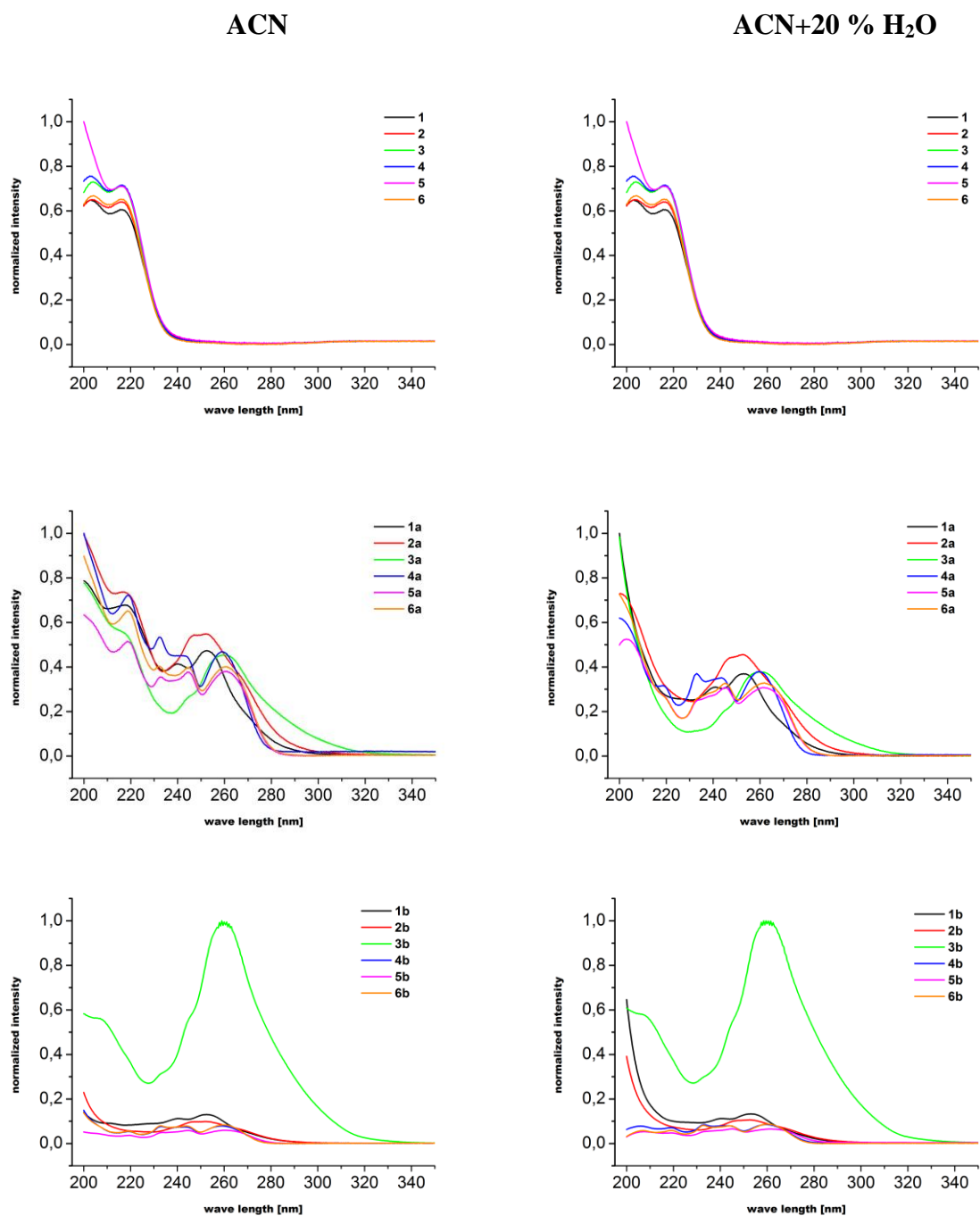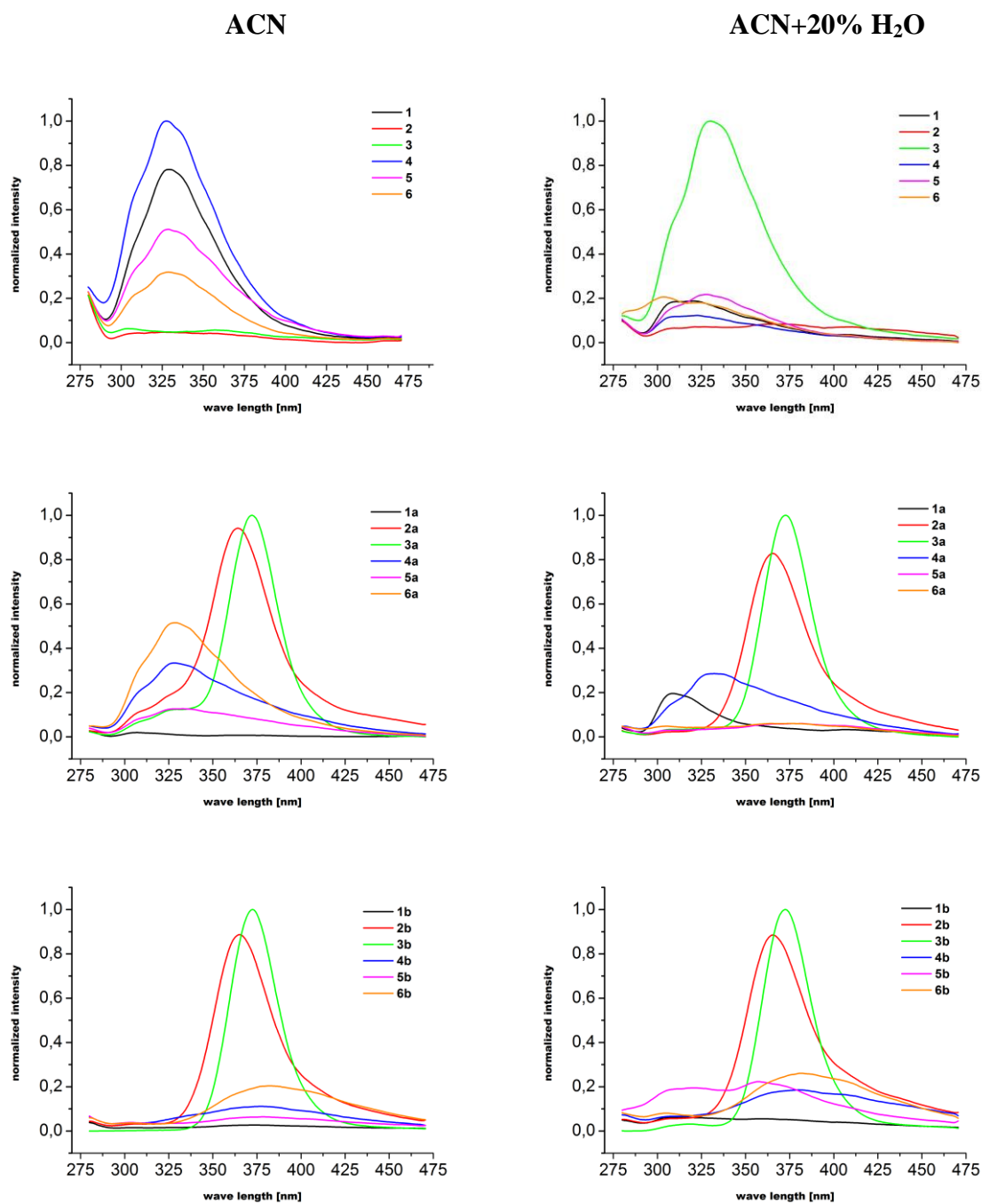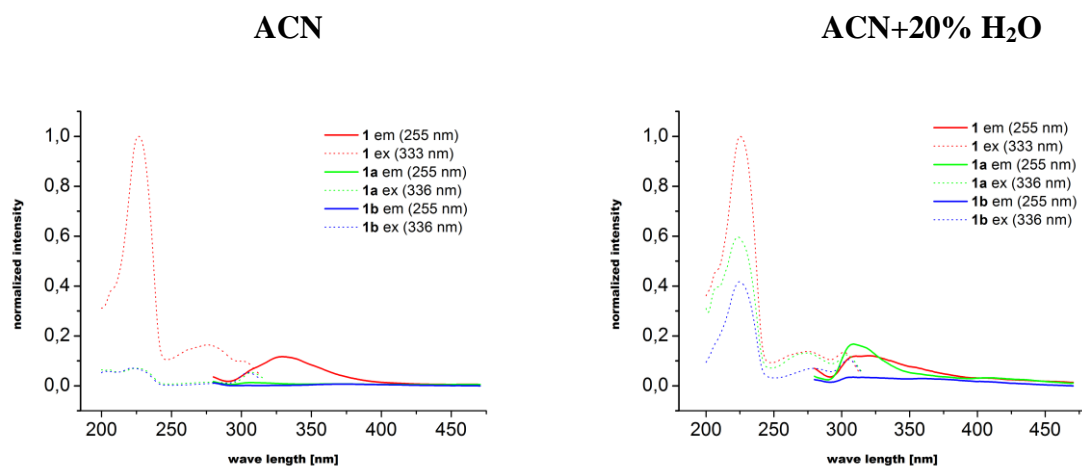

Figure 2.18. Graphics of the emission and excitation measurements of ligand precursor **1** and complexes **1a/b** in pure ACN (left) and ACN with 20% H$_2$O (right) at room temperature. Excitation wave lengths and emission wave lengths respectively used during measurements are given in the legend.
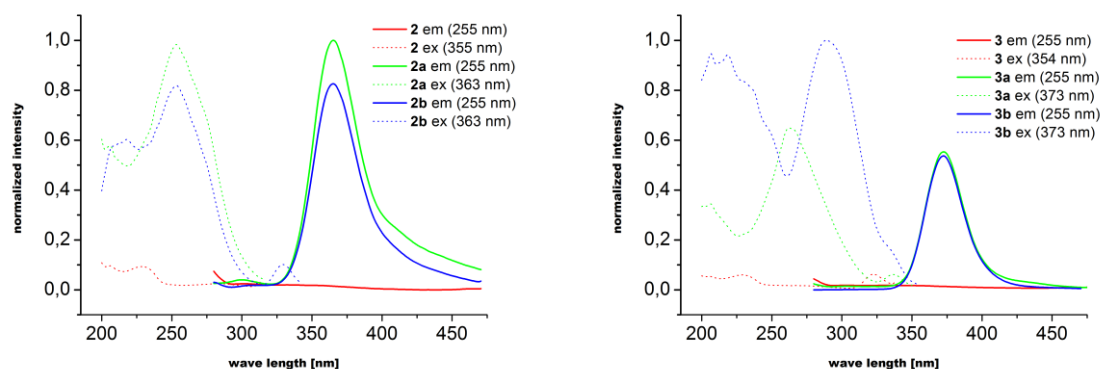
Figure 2.19. Graphics of the emission and excitation measurements of ligand precursor **2** and complexes **2a/b** (left) and of ligand precursor **3** and complexes **3a/b** (right) in pure ACN at room temperature. Excitation wave lengths and emission wave lengths respectively used during measurements are given in the legend.

The direct comparison of the ligand precursors and the complexes with both bromide and hexafluorophosphate as counter ion (Firgure 2.19) confirm the previous observations of stable and highly emissive complexes, possibly stable exciplexes (^{3}[dσ*pσ] excited state), for the complexes with ethylene and propylene linkers **2a/b** and **3a/b**, which are proven before to be able to perform Au-Au bonds in solid state (see above, [35]).

2.5 Summary

Three systematic series of gold(I) (or silver(I)) NHC complexes on the basis of imidazole with ethyl side chains have been shown. The corresponding silver(I) complexes were synthesized successfully with the aim of obtaining crystals suitable for X-ray measurements as a means to study the influence of aurophilic and argentophilic interactions, respectively, vs. π-π interactions.

The VT-NMR spectra reveal interesting dynamic behaviour for the compounds with the shortest linkers **1a/b** and **2a/b** in solution: A kind of ring inversion. The free activation enthalpy for the conversion of the linker conformation could be extracted from an Eyring plot of exchange rates. For substance **6a** with six methylene units in the linker, VT-NMR spectra reveal additional broad signals, which could be interpreted as signs of a starting aggregation.

Altogether, 14 out of 18 complexes were structurally characterized. The compounds containing gold as metal consist of dicationic dinuclear complexes $Au_2L_2^{2+}$ with bridging dicarbene ligands L. The basic structural parameters fit the expectations with doubly coordinated gold (C-Au-C angles close to linearity) and mean C-Au bond lengths of ~2.02 Å[1,2].

The compounds **1c** and **3c** show the same type of macrocycles (dicationic dinuclear complexes $Ag_2L_2^{2+}$). The compound **4c** shows a completely different organization with polymer chains instead of macrocycles. Nonetheless, in all three silver compounds the silver atoms are doubly coordinated with C-Ag-C angles close to linearity and mean C-Ag bond lengths of 2.08 Å[79].

A short M-M distance is realized intramolecularly for the complexes with methylene (**1a/b/c**) and ethylene (**2a/b**) linkers. For the complexes with longer linkers stacking of the cations allows a short intermolecular Au-Au distance stabilized by π-π interactions. Exceptions are the two complexes with propylene linkers **3a/c**, which show head-to-tail π-π interactions and no short metal-metal distance is found intra- or intermolecularly. The exceptional role of the complexes with propylene linkers **3a/b** among the gold compounds is visible in the conformation next to the NHC (*gauche*, while others are *trans*). The polymeric arrangement in complex **4c** allows neither a short intra- or intermolecular Ag-Ag distance nor π-π interactions.

The conformational differences between complexes with varying counter ions are few. The complexes with the bulky hexafluorophosphate counter ions show slightly shorter Au-Au and π-π distances than their bromide congeners. The silver compounds arrange in a different way, where metal-metal interactions seem to have a minor role, which is in accordance with previous publications, which indicate that argentophilicity is a weaker phenomenon than aurophilicity[51,79].

UV/Vis and fluorescence spectra are measured in acetonitrile and a mixture of acetonitrile and water. Neither the anion exchange nor the addition of water seem to impact on the strongest emitters **2a/b** and **3a/b**, which indicates propably a stable exciplex (^{3}[dσ*pσ] excited state) not influenced by possible anion or solvent association. Measurements should be repeated with degassed solvents and additionally solvent-free with pure crystals.

3. Complexes Type 2

The synthesis and characterization of a systematic series of new dinuclear gold(I) NHC complexes and their corresponding NHC precursors will now be reported. The series consists of gold(I) complexes with N-heterocyclic carbene ligands on the basis of imidazole with methyl side chains. The compounds only vary in the length of the alkyl chain linking two NHC units, respectively. One of these compounds (**9b**) was already structurally characterized by Baron et al.[35] in 2012. Nonetheless, the structure is discussed here again for the purpose of comparison.

3.1 Synthesis

The methyl imidazolium bromide salts **7-12**[87] and the gold(I) NHC complexes **7a/b-10a/b**[35] and **11a/b**, **12a/b** were synthesized by well-established procedures (Scheme 3.1). The compounds **7a/b-12a/b** are readily characterized by electrospray mass spectra showing intense signals for the intact dicationic macrocycle $Au_2L_2^{2+}$. Indications for the presence of mononuclear complexes with a chelating bis-NHC-ligand known for longer linkers have not been found[23,24].
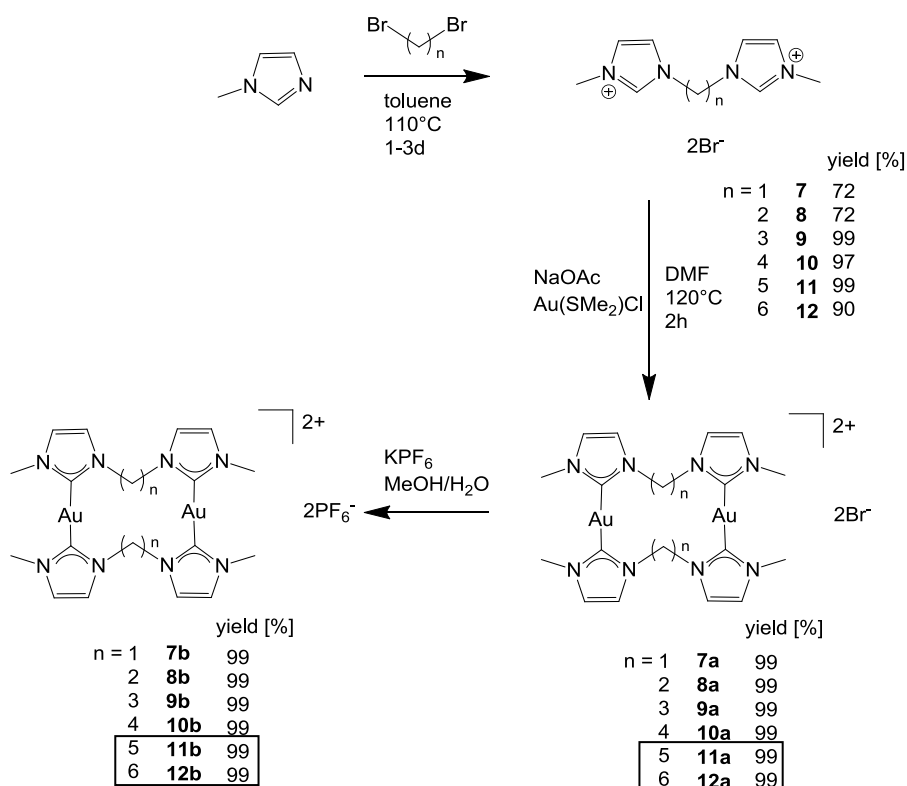

Scheme 3.1. Syntheses of the NHC precursors **7-12** and the gold(I) NHC complexes **7a/b -12a/b.** Syntheses not kown to literature yet are indicated by black boxes.

3.2 NMR Spectroscopy

The room temperature ^{1}H and ^{13}C NMR spectra for the complexes **7a/b-12a/b** confirm the expected highly symmetrical structures. The formation of gold(I)-carbene complexes is accompanied by the disappearance of the acidic imidazolium proton signal at $\delta \sim 9.50$ ppm in the ^{1}H NMR spectrum and a typical shift of the $C_{carbene}$ signal from <140 ppm in the NHC precursor to >180 ppm in the gold(I) complex in the ^{13}C NMR spectrum[1,2]. In accordance to previously reported similar findings[24,27,32,33,35], neither the exocyclic NHC side chain nor the counter anion induce significant changes of the macrocycle resonances at room temperature, whereas an upfield shift in acetonitrile solution is more pronounced.

The protons of the methylene linkers in compounds **7a/b** are not equivalent and appear as two separated doublets at room temperature[27,32,33,35]. They reversibly disappear/coalesce upon heating to 100 - 105 °C (Figure 6.2.1, Appendix). As a result the free activation enthalphy at 298 K of $\Delta G_{298}^{\neq} = 70 \pm 6$ kJ/mol is extracted from an Eyring plot of exchange rates (Figure 6.2.2 and Table 6.2.1, Appendix) obtained by line shape analysis using the programme gNMR[80]. A similar behaviour has already been reported for the identical complex with iodide as counter ion and has been attributed to an interconversion of exo- and endo hydrogens by a kind of ring inversion[27] (Scheme 3.2).
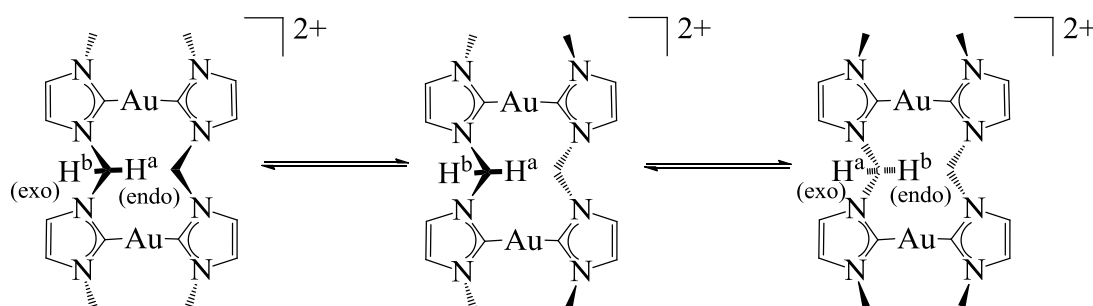
Scheme 3.2. Proposed ring inversion of compounds **7a/b**.

A dynamic behaviour is observable for the signal for the imidazolium proton next to the methyl side chain. It broadens and resharpens again, similar to the findings reported for the iodide derivative[27]. An effect of a potentially coordinating anion can be ruled out as similar activation parameters are obtained for the bromide (**7a**) and hexafluorophosphate (**7b**) salt.
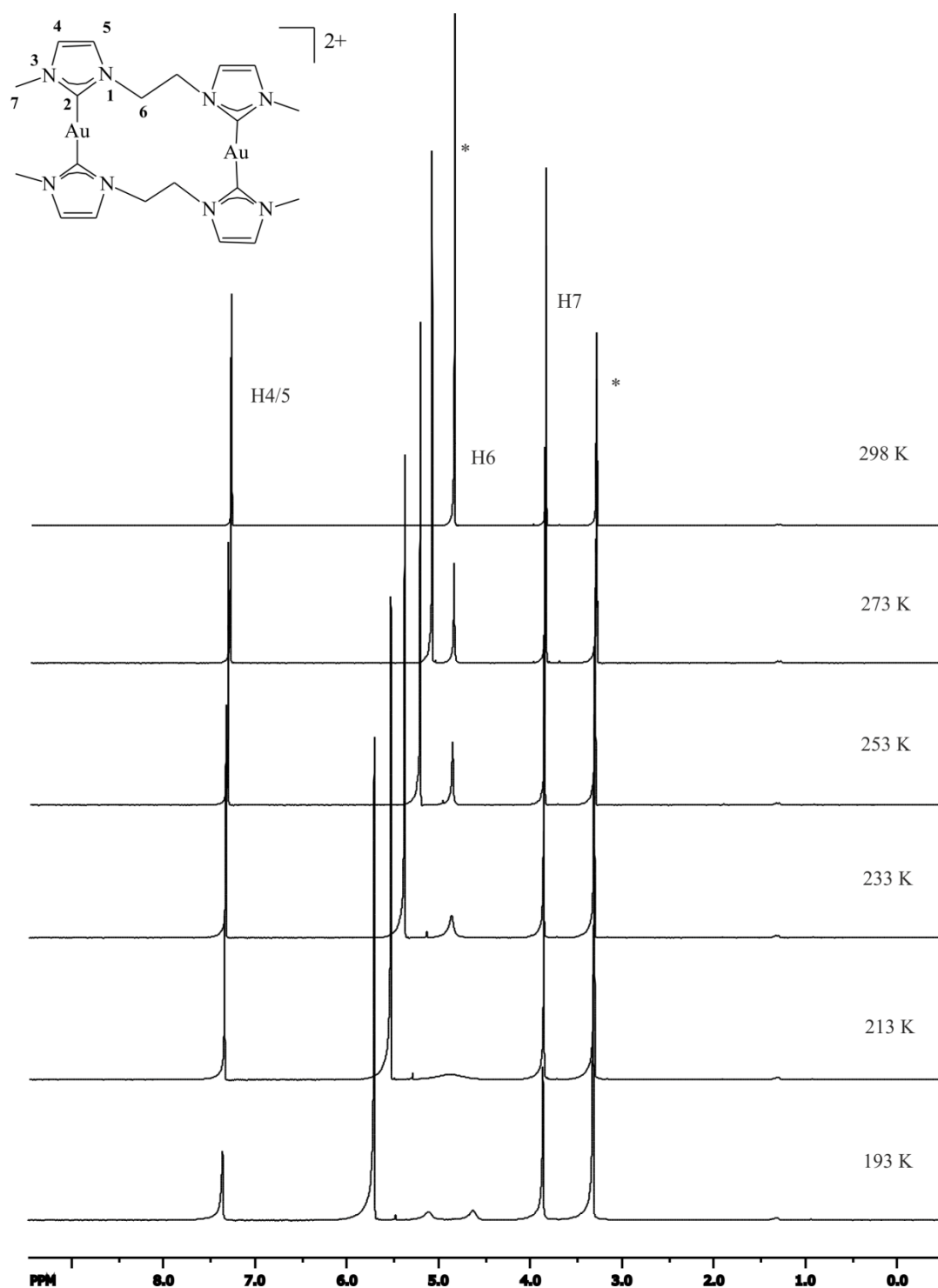
Figure 3.1. Low-temperature ^{1}H NMR spectra (500.13 MHz, CD$_3$OD) of **8a**. *partially deuterated and undeuterated methanol and water, respectively.

The room temperature ^{1}H NMR spectra for the ethylene-connected macrocycles **8a/b** show a singlet for eight equivalent linker hydrogens and for the methyl side chain, respectively (Figure 3.1). Thus, chain elongation expectedly enhances the flexibility of the macrocycles. Lowering the temperature reveals a partial freezing of the conformational flexibility: In the ^{1}H

NMR spectra of **8a**, a broadening and finally splitting of the linker CH_2 signal into two broad singlets at -80 °C is visible with coalescence around -60 °C (Figure 3.1). Line shape analysis (Figure 6.2.2 and Table 6.2.1) yields $\Delta G_{298}^{\neq} = 53 \pm 4$ kJ/mol for the frozen process. It could be interpreted as an inversion of the ethylene-bridged macrocycle equilibrating exo and endo protons in analogy to the behaviour of **7a/b** described above. The smaller ΔH and lower ΔS value are fully consistent with the enhanced flexibility of the elongated linker. In addition, signal broadening during cooling the sample is visible.

The ^{1}H spectra of the macrocycles with C_3, C_4, C_5 and C_6 linkers (**9a**, **10a**, **11a**, **12a**) show broadening of the methylene signals at lower temperatures, but coalescence could not be reached in the temperature range down to -80 °C (Figures 6.2.3 – 6.2.6, Appendix). Especially the H6 signal in the compounds **9a** and **11a** show the same tendencies as **7a** and **8a**, but the signal separation is not distinct and line shape analysis is not possible.

3.3 X-ray Crystal Structures

Single crystals suitable for X-ray diffraction could be obtained by slow diffusion of diethylether in a methanol solution (**7a**-**10a**, **12a**) or an acetonitrile solution (**7b-12b**). Thus, eleven out of twelve complexes were structurally characterized. Selected structural data is summarized in Table 3.1. The compounds consist of dicationic dinuclear complexes $Au_2L_2^{2+}$ with bridging dicarbene ligands L. The basic structural parameters fit the expectations: The gold atoms are doubly coordinated with C-Au-C angles close to linearity and mean C-Au bond lengths of 2.02 Å typical for gold(I) NHC compounds[1,2].

Owing to the almost linear C-M-C axis, the torsion angles can be measured between N-C-C-N of the two ligands in a cation to describe the position of these ligands. For all cations studied here except for one with ethylene linkers **8a**, the ones with the proyplene linkers **9a/b** and the one with the pentylene linker **11b**, the torsion angle is close to zero and the NHC planes on opposite sides of the gold atoms are coplanar. Each cation is accompanied by two bromide or hexafluorophosphate anions, respectively.

Table 3.1. Selected structural data for complexes **7a/b – 12a/b**.

	n	Crystal symmetry	Au-C/ Å	C-Au-C/°	N-C-C-N/ (a)	dihedral angle of NHC planes/° (b); *(c)*	Confor-mation next to NHC	Au • Au/Å intra-molecular (d)	Au • Au/Å inter-molecular (d)	π • π/ Å inter-molecular (d)
7a	1	*P* -1	2.021(8) 2.022(8) 2.023(9) 2.024(8)	169.3 172.3	-0.1 0.8	11.7 28.2 78.4 75.6	-	3.4671(4)	4.4997(5)	3.6191(4)
7b	1	*C* 2/*m*	2.013(4) 2.019(4)	177.9 170.5	0.0	26.5 2.2 108.7	-	3.8842(1)	3.7236(1)	3.7489(1)
8a	2	*P* -1	2.051(11) 2.009(11) 2.028(11) 2.027(11)	177.1 174.0	-3.5 87.9	4.4 93.2 97.3 4.7	gauche/ trans	4.6320(3)	6.8465(3)	3.5726(2)
8b	2	*C* 2/*m*	2.035(5)	177.1	0.0	4.3	trans	5.5492(3)	4.6992(2)	3.7356(2)
9a	3	*C* 2/*c*	2.007(15) 2.045(12)	177.2	160.9	15.6	gauche	3.1153(2)	3.9286(3)	3.4287(2)
9b	3	*P* 3$_1$ 1 2	2.024(6) 2.009(6)	177.6	13.2	10.9 14.7	gauche	3.2283(4)	3.7036(1)	3.45762(7)
10a	4	*P* 2$_1$/*c*	2.027(11) 2.034(12) 2.014(12) 2.004(12)	178.6 176.4	2.0 -1.6	3.1 7.5 8.6 2.4	trans	8.0692(4)	3.5842(2)	3.7420(2)
10b	4	*P* -1	2.032(15) 2.024(15)	176.5	5.6	11.0	gauche	7.0525(5)	4.9587(2)	3.5258(2)
11b	5	*P* 2$_1$	2.017(5) 2.015(5) 2.017(5) 2.029(4)	176.7 176.6	164.8 168.1	9.6 12.0 1.4 7.0	gauche/ trans	4.1307(2)	3.2582(2)	7.3836(4)
12a	6	*P* -1	2.006(12) 2.062(16)	177.2	4.6	6.3	gauche	8.5616(6)	4.9548(3)	3.6847(2)
12b	6	*P* -1	2.008(13) 2.034(13)	177.0	0.1	3.7	gauche	8.8762(8)	3.6224(2)	3.8434(1)

(a) torsion angle between the two NHC rings (MeN-C$_{carbene}$-C$_{carbene}$-NMe) coordinating an Au atom; (b) dihedral angle of the two NHC planes coordinating an Au atom; (c) dihedral angle of the two NHC planes in the linker; (d) the shortest value is given.

In all cases, the complexes are arranged in a way that layers are formed consisting of organic ligands on the one hand and gold atoms with anions on the other. NHC ligands of all neighboured complexes are interconnected by π-π interactions, except the compound with the pentylene linker **11b**. Further, all solid state structures of the gold compounds except for **8a/b**, **10b** and **12a** reveal a relatively short Au-Au distance, either intra- or intermolecularly; in three cases (**7b**, **9a/b**) even both is realized. The space groups and crystal packing of the two complexes with the same cation typically differ due to the size difference of the two anions studied. However, the influence of the counter ion on the conformation of the cation is unexpectedly small (Figures 3.2 – 3.12, Table 3.1) compared to similar examples in literature[24,35-37].
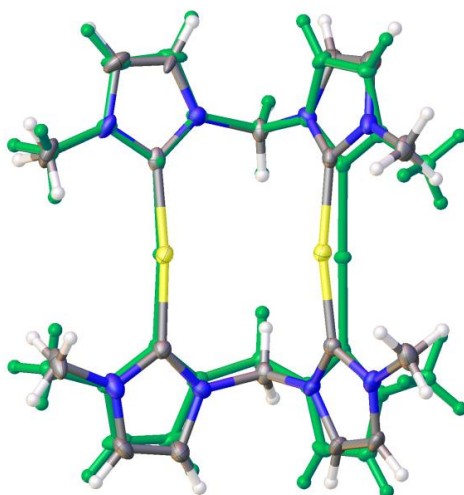

Figure 3.2. Overlay drawing of complex **7a** and **7b** (green) (50% probability level for the thermal ellipsoids). Br⁻ anions and hexafluorophosphate anions have been omitted for clarity.

The smallest cations bearing only methylene linkers are conformationally equal (Figure 3.2). The NHCs on different sides of the gold atoms are coplanar. The angles of the NHC substituents at the methylene group are identical (110.7° and 111.2°, respectively), but the intramolecular Au-Au distance (3.467 Å vs. 3.884 Å) is remarkably shorter for **7a** (0.417 Å). The explanation for this big difference can be found in the angles of the $C_{carbene}$-Au-$C_{carbene}$ axes: While one of the axes has nearly the same amount for both cations (169.3° and 170.5°, respectively), the other axis is more bent for **7a** (172.3°) than for **7b** (177.9°), which leads to the shorter Au-Au distance. The crystal structure of both **7a/b** consists of pairs of macrocycles with parallel arrangement of a whole NHC-Au-NHC unit. The dimers of macrocycles are

further connected by head-to-head and additionally by head-to-tail $\pi-\pi$ interactions with neighbouring NHC units (Figure 3.3). The intermolecular distance between the gold atoms of a dimer of macrocycles is much shorter in **7b** (3.724 Å) than in **7a** (4.500 Å) due to the different arrangement of the anions in the macrocycle layers.
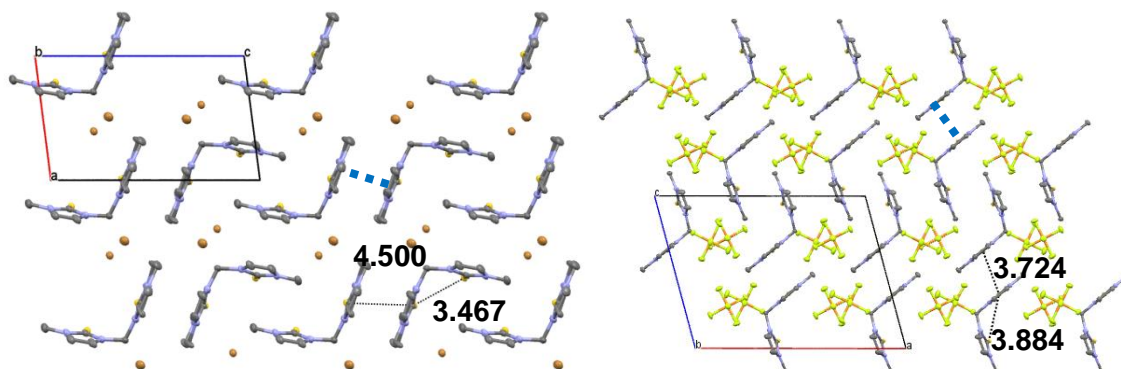

Figure 3.3. Crystal packing of **7a** (view along b axis, left) and of **7b** (view along b axis, right) (50% probability level for the thermal ellipsoids). Intermolecular $\pi-\pi$ interactions are indicated by dotted blue lines. Hydrogen atoms have been omitted for clarity.

A similar complex published by Barnard et al. has a methyl side group as well, but iodide as counter ion[27]. The shape of the cation is identical and the intramolecular Au-Au distance (3.5425(6) Å) is comparable to **7a**. Further, Hemmert and coworkers structurally characterized two methylene-bridged gold-NHC complexes with alcohol- or carboxylate-functionalized side chains (Au-Au 3.514 Å and 3.589 Å, respectively)[32,33]. An even shorter distance (3.3610(7) Å) could be realized by Fränkel et al.[25] in a neutral complex containing a BH$_2$-unit instead of a methylene linker and by the group of Hahn[43] via incorporation into a large macrocycle (3.0737(3) Å).
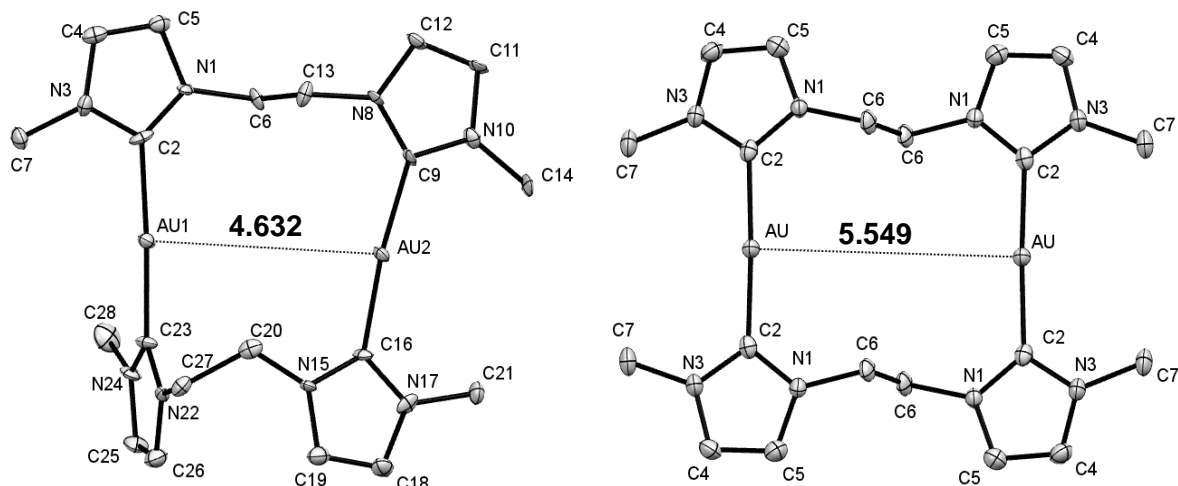
Figure 3.4. ORTEP drawing of complex **8a** (left) and **8b** (right) (50% probability level for the thermal ellipsoids). Anions (Br$^-$ and PF$_6^-$, repectively) and hydrogen atoms have been omitted for clarity.

The macrocycle **8a** crystallizes in the triclinic space group *P -1*. The complex **8b** crystallizes in the monoclinic space group *C 2/m*. It shows an open Z-like conformation with all-*trans* ethylene linker. The resulting intramolecular gold-gold distance is quite long (5.5492(3) Å). In contrast, cation **8a** has one *trans* ethylene linker and one *gauche* ethylene linker, which leads to a shorter Au-Au distance (4.6320(3) Å) (Figure 3.4). Simultaneously, the NHC planes are only coplanar on both sides of one gold atom in the macrocycle, while the other two planes are twisted by approx. 90°. The conformational folding of the dication **8a** is so compact and twisted that a close arrangement with neighbouring macrocycles is restricted to a single π−π interaction per molecule, while **8b** can perform multiple ones (Figure 3.5).
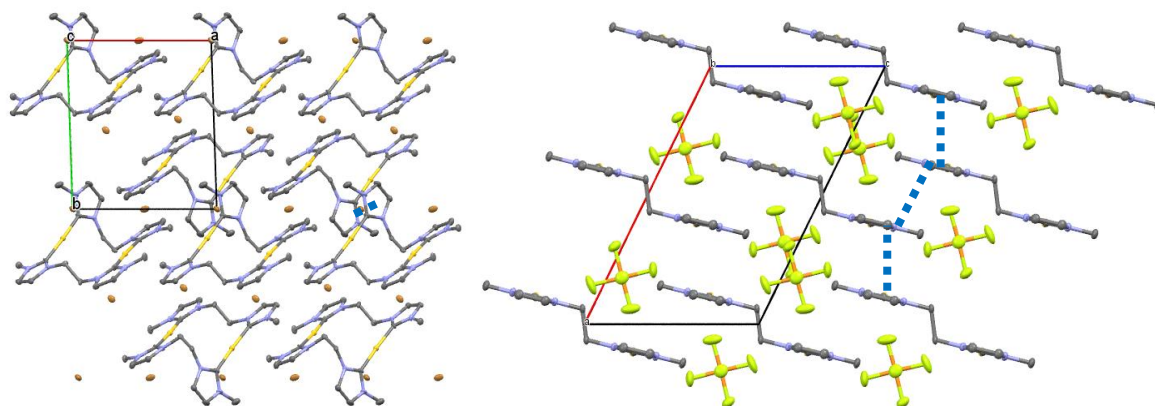

Figure 3.5. Crystal packing (view along c axis, left) of complex **8a** and crystal packing (view along b axis, right) of complex **8b** (50% probability level for the thermal ellipsoids). Intermolecular π−π interactions are indicated by dotted blue lines. Hydrogen atoms have been omitted for clarity.

The only published ethylene-linked NHC-Au complex structurally characterized by X-ray bears a bulky alcohol-functionalized side group and PF_6^- counter ions[33]. Its conformation is backfolded with 50° twisted NHC planes and an intramolecular Au-Au bond in the range of 3.3 Å.

Both dications **9a/b** with C_3-linked NHC ligands show a backfolded conformation with an all-*gauche* propylene linker (Figure 3.6). The intramolecular Au-Au distances are the shortest ones shown here (**9a**: 3.1153(2) Å, **9b**: 3.2283(4) Å). This is the result of a folded conformation as the dihedral angle amounts to 66° - 68° between the N-C-C-C linkers of a ligand. Polymers of macrocycles are formed by a short intermolecular Au-Au distance of 3.7 – 3.9 Å and stabilized by π–π interactions (Figure 3.7).
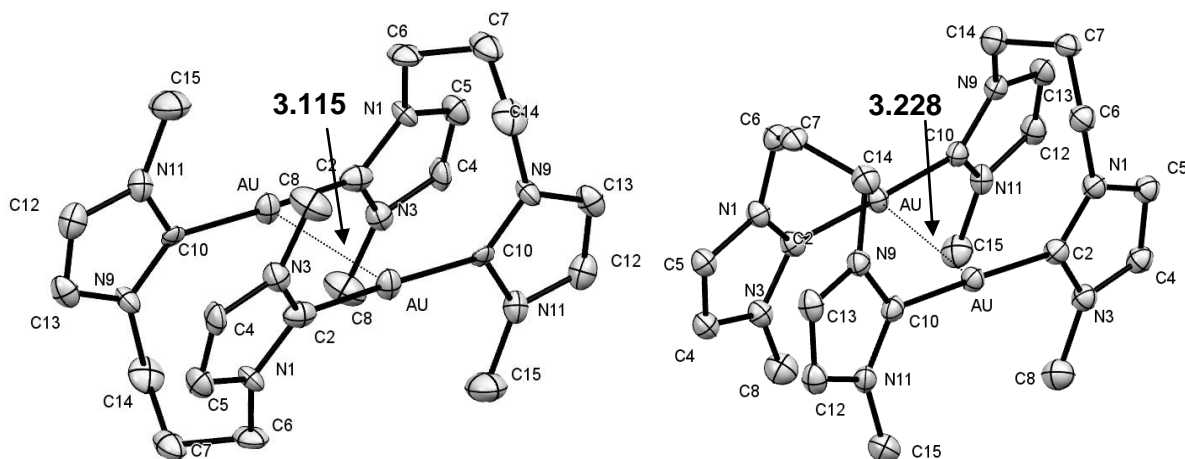
Figure 3.6. ORTEP drawing of complex **9a** (left) and **9b** (right) (50% probability level for the thermal ellipsoids). Anions (Br$^-$ and PF_6^-, repectively), cocrystallized methanol (**9a**) and hydrogen atoms have been omitted for clarity.
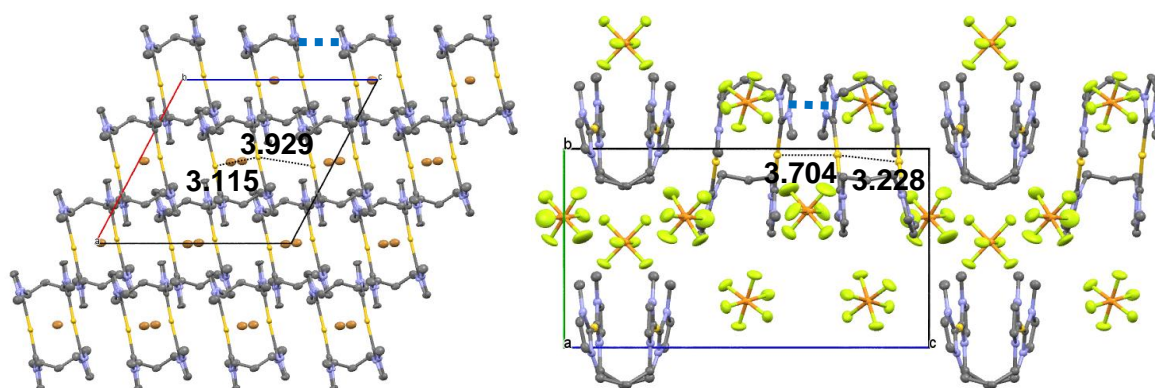
Figure 3.7. Crystal packing of complexes **9a** (view along b axis, left) and **9b** (view along a axis, right) (50% probability level for the thermal ellipsoids). The macrocycles form double layers connected by intermolecular π–π interactions indicated by dotted blue lines. Hydrogen atoms and cocrystallized methanol (**9a**) have been omitted for clarity.

Baron et al.[35] reported the crystal structure of **9b**, a propylene bridged Au(I) NHC complex with methyl side chains and PF_6^- as counter ion in 2012. Gil-Rubio et al.[24] crystallized the same cation with triflate anions in 2013. This time, a helical conformation with orthogonal NHC-Au-NHC bonds and a very short Au-Au-distance of 3.032 Å is realized. In both structures, the backfolded macrocycles form C3- and C2-symmetric columnar aggregates, respectively, with intermolecular Au-Au and $\pi-\pi$ interactions of about $d = 3.7$ Å. In contrast, the last structurally characterized propylene-bridged complex of this type crystallizes in an open conformation and a double-layer packing without Au-Au interactions[32]. It comes from the Hemmert group and possesses PF_6^- anions and bulky side groups with hydroxyl functions. The significant effect of counter ion as well as the type of side group on the molecular conformation of propylene-linked dinuclear NHC complexes of gold(I) is obvious.

Figure 3.8. ORTEP drawing (left) and crystal packing (view along b axis, right) of complex **10a** (50% probability level for the thermal ellipsoids). Au-Au bound dimers of macrocycles are connected by intermolecular $\pi-\pi$ interactions indicated by dotted blue lines. Hydrogen atoms, except the ones belonging to cocrystallized H_2O, have been omitted for clarity.

Figure 3.9. ORTEP drawing (left) and crystal packing (view along a axis, right) of complex **10b** (50% probability level for the thermal ellipsoids). Dimers of macrocycles are connected by intermolecular π−π interactions indicated by dotted blue lines. Hydrogen atoms have been omitted for clarity.

The complex **10a** crystallizes in the monoclinic space group *P 2₁/c*. The cation shows an open conformation, comparable to **8b**, with an all-*trans* butylenes linker (Figure 3.8). Due to this open arrangement, the intramolecular Au-Au distance is very long, but simultaneously the crystal packing allows the formation of columns of NHC-Au-NHC units with close intermolecular gold-gold distances of 3.5842(2) Å. Additionally, these columns are stabilized by intermolecular π−π interactions. In contrast, the complex **10b** crystallizes in the triclinic space group *P -1*. The conformation next to the NHC units is *gauche*, which results in a backfolded conformation comparable to **9b**, but due the additional methylene unit in the linker with a *trans* conformation, the intramolecular gold-gold distance is still very long (7.0525(5) Å) (Figure 3.9). The NHC-Au-NHC units are facing each other and polymers are connected by head-to-tail π-π interactions. The cation **10b** is one out of two examples shown in this series without any close Au-Au contacts.

Comparable complexes with butylene linkers are unkown so far. Barnard et al.[27] showed a structure with a *o*-phenyl cycle as linker, where the NHCs are connected on both sides which results in parallel NHC-Au-NHC units in the gold(I) complex and flexibility is not given. The intramolecular Au-Au distance is short (3.0 Å).
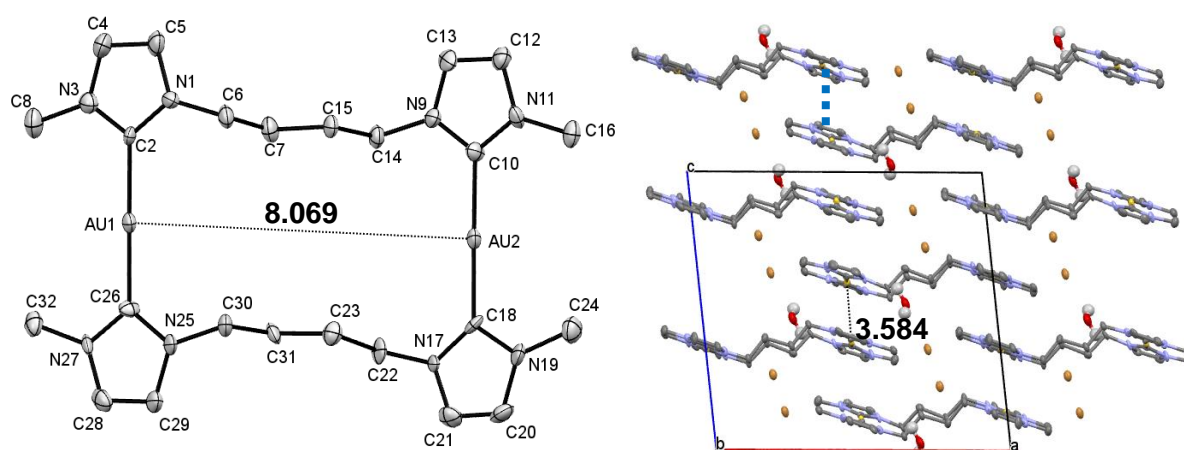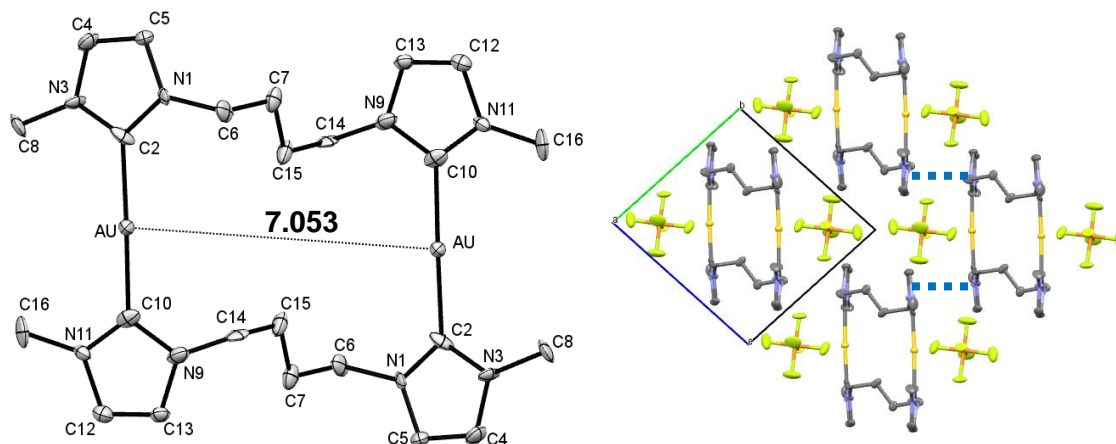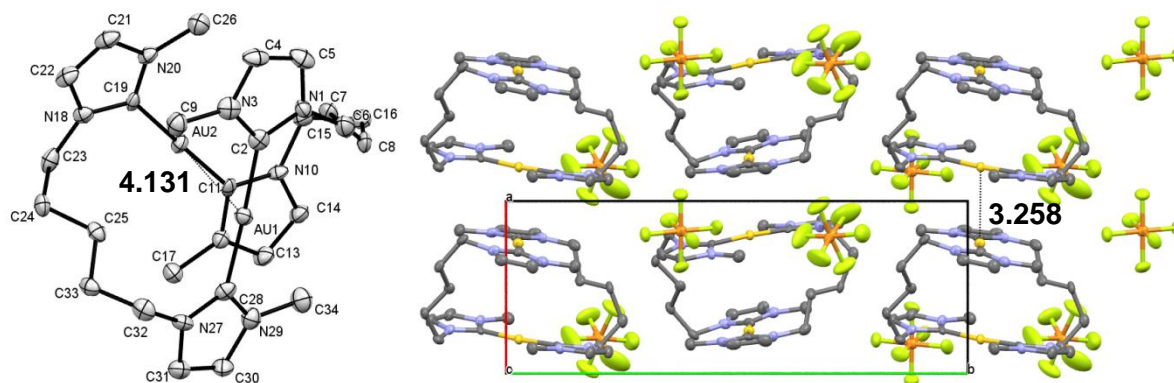
Figure 3.10. ORTEP drawing (left) and crystal packing (view along c axis, right) of complex **11b** (50% probability level for the thermal ellipsoids). Hydrogen atoms have been omitted for clarity.

While purification by crystallization was successful for **11a**, the resulting crystals were not suitable for X-ray diffraction measurements. Yet, **11b** gave good crystals in the monoclinic space group $P\,2_1$. The adjustment of the cation is rather unusual compared to the other complexes of this series. The two C-Au-C axes are twisted and not parallel (-53.2°), resulting in a compact cation with a quite long intramolecular Au-Au distance (4.1307(2) Å) (Figure 3.10). The conformation next to the NHCs is a mixture of three *gauche* and one *trans* arrangement. The C-Au-C axes are forming columns, in which the pentylene linkers are facing each other. A shorter intermolecular gold-gold distance of 3.2582(2) Å is realized, albeit the NHC planes are not parallel. This arrangement is only one in this series, which does not allow intermolecular π–π interactions. The structure determining motif here seems to be the formation of close gold-gold bonds and stabilization through intermolecular π–π interactions is insignificant.

Comparable complexes with pentylene linkers are so far unkown. Barnard et al.[27] showed a structure with a *m*-phenyl and *m*-pyridyl cycle as linker and methyl side chains, but again the NHC-Au-NHC units are parallel in the gold(I) complex and flexibility is not given. Wang et al.[30] showed a structure with an oxydiethyl chain as linker and anthracene side chains. These anthracene side chains dominate the crystal structure by stacking. Interestingly, the cation is twisted in a similar way (68°), but the intramolecular Au-Au distance is short (3.5 Å) due to the different angles in the linker.
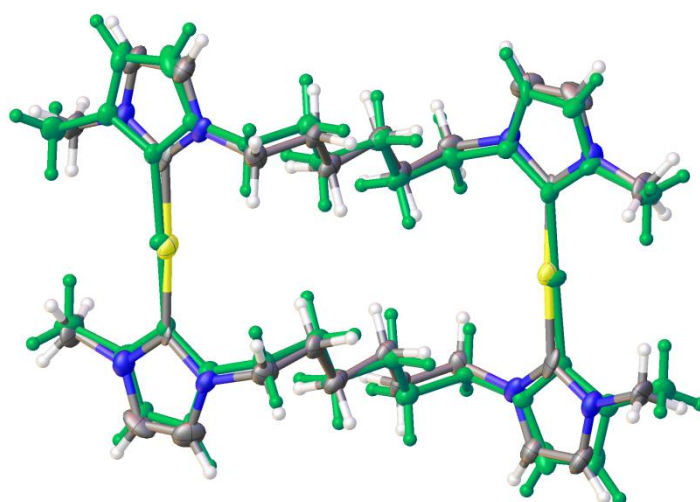
Figure 3.11. Overlay drawing of complex **12a** and **12b** (green) (50% probability level for the thermal ellipsoids). Bromide and hexafluorophosphate anions and methanol molecules (**12a**) have been omitted for clarity.
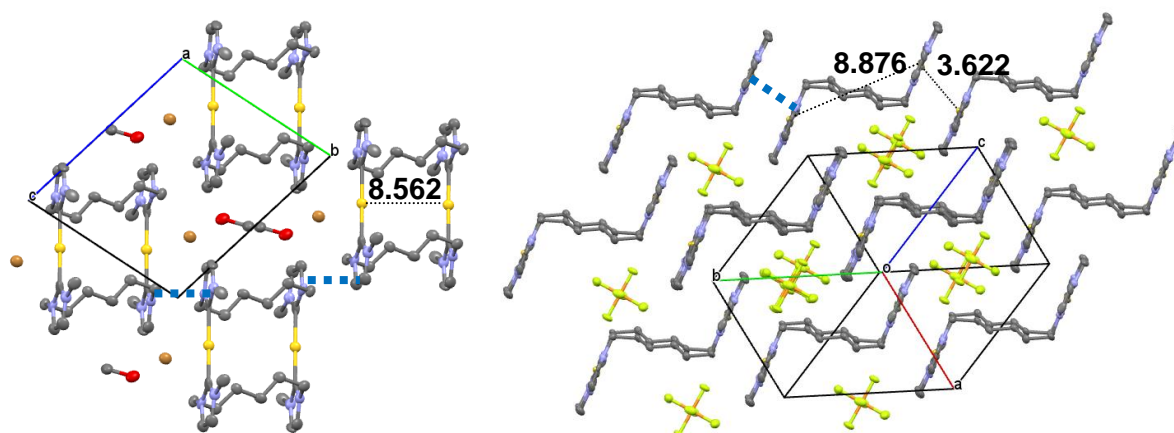
Figure 3.12. Crystal packing (view along a axis, left) of complex **12a** and crystal packing (view along no axis, right) of complex **12b** (50% probability level for the thermal ellipsoids). Au-Au bound dimers of macrocycles are connected by intermolecular π–π interactions indicated by dotted blue lines. Hydrogen atoms have been omitted for clarity.

The complexes **12a/b** crystallize in the triclinic space group *P -1*. The cations show an open conformation, comparable to **9b** and **10b**, with a *gauche* conformation next to the NHC, but *trans* conformation in the hexylene linkers (Figure 3.11). Due to this open arrangement, the intramolecular Au-Au distance is very long for both cations (**12a**: 8.5616(6) Å; **12b**: 8.8762(8) Å). The crystal packing however differs. While the arrangement of the cations in **12a** is comparable to **10b**, dimers are formed by stacking of NHC planes of different cations

stabilized by intermolecular $\pi-\pi$ interactions, the cations of complex **12b** show an arrangement comparable to complex **10a** with close intermolecular Au-Au distances (3.6224(2) Å) stabilized by intermolecular $\pi-\pi$ interactions. The cations **10b** and **12a** are the only ones shown in this series without any close Au-Au contacts.

Comparable complexes with hexylene linkers are unkown so far.

3.4 UV/Vis and fluorescence studies

Solution based structural studies for dinuclear Au(I) complexes which display aurophilic interactions are still rare. To make a contribution to a better understanding of possible triplet state exciplexes and their stability in solution, the ligand precursors **7-12** and the gold complexes **7a/b-12a/b** are studied here in acetonitrile at room temperature. The negliglible role of the counter ion is also visible in the X-ray crystal structures, which showed only a minor influence on the formation of Au-Au bonds. In solid state, solely the complexes with methylene and propylene linkers **7a/b** and **9a/b** performed a short intramolecular Au-Au distance, irrespective of the counter ion.

All photophysical measurements were executed with 10^{-5} (or 10^{-6}) molar solutions of pure substances (results of the crystallization) in acetonitrile at room temperature. The first measurements in our group were perfomed in DMSO (measurement range <250 nm). To enlarge the measurement range to higher energies (<200 nm) the solvent was changed to ACN. The influence (possible solvation effects) of the solvent was insignificant. The results turned out to be hard to reproduce (variability of the absolute intensity); therefore measurements were performed multiple times to eliminate weighing and diluting errors. The results shown here are well-established.

Figure 3.13. Graphics of the absorption measurements of ligand precursors **7**-**12** and complexes **7a**/**b**-**12a**/**b** in ACN at room temperature.

The ligand precursors **7**-**12** show the same absorption band at 220 nm with a prominent shoulder at 210 nm. The complexes **10a/b**, **11a/b** and **12a/b** show the same line shape with several strong maxima below 275 nm. The complexes with the shortest linkers **7a/b** and **8a/b** show a different line shape with a maximum at 255 nm. The complexes with bromide as counter ion (**7a** and **8a**) are clearly less intensive. The complexes with the propylene linker **9a/b** show a strong band at 270 nm. All complexes are red shifted compared to the ligand precursors (Figure 3.13).
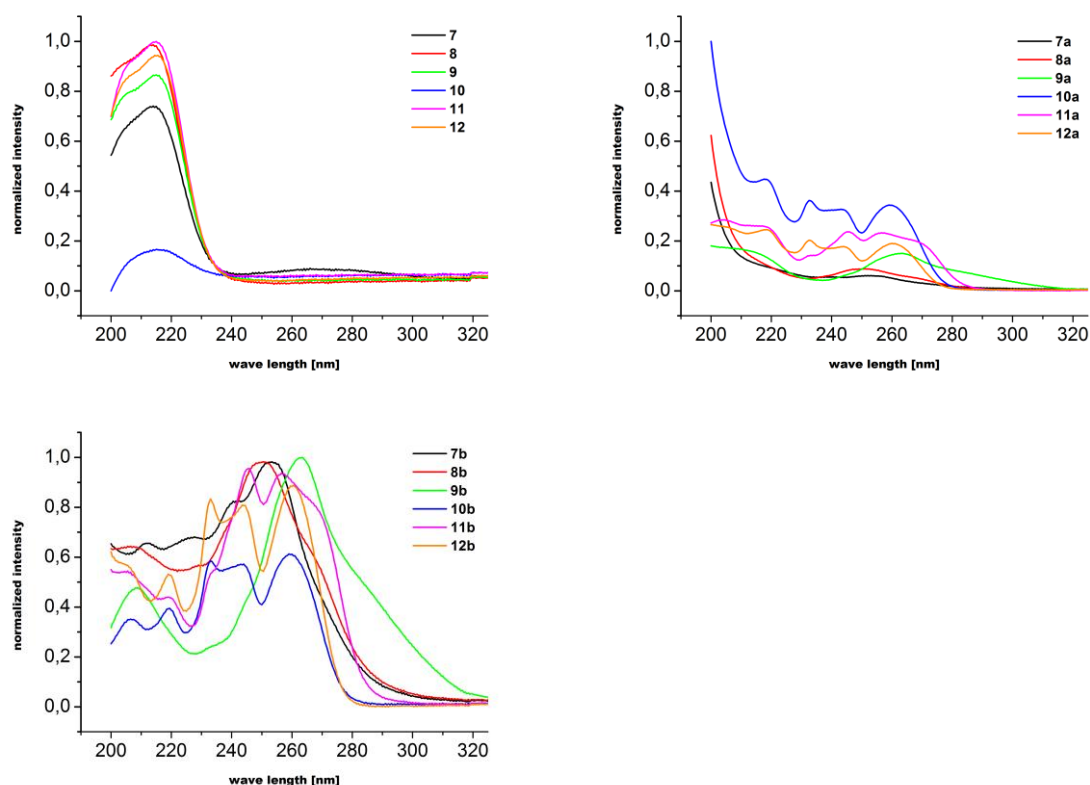
Figure 3.14. Graphics of the emission measurements of ligand precursors **7**-**12** and complexes **7a**/**b**-**12a**/**b** in ACN at room temperature. The exact excitation wave length used during measurements is 215 nm for **7**-**12** and 255 nm for **7a**/**b**-**12a**/**b**.

The ligand precursors **8**-**12** show the exact same line shape with two strong emission bands at 290 nm and 330 nm. Only the ligand precursor with the shortest linker **7** is more intensive than the others and the height of the two bands is inversed. Clearly the strongest emitters are the complexes with the propylene linkers **9a**/**b** with a maximum at 375 nm, which was suggested by Baron et al.[35]. The concentration of the complex **9b** was reduced to a 10^{-6} molar solution to obtain good unaffected spectra. The anion exchange seems to have no influence on the strongest emitters **8a**/**b** and **9a**/**b**, which indicates propably a stable exciplex (^{3}[dσ*pσ] excited state) not influenced by possible anion association. The complexes with the ethylene linkers **8a**/**b** are considerably weaker and blue shifted by 10 nm. These results reflect the X-ray studies found above: the compounds **8a**/**b** seem to be in a transition state between an open and a backfolded arrangement compared to the backfolded macrocyles **9a**/**b** with short Au-Au distances in solid state. In comparison to this, the other complexes are weak emitters. The compounds **7a**, **10a-12a** are expected to form an association complex[24,35] between the macrocycle and bromide, which are hardly emissive here. In contrast, the complexes **7b**,

10b-12b should not be able to form a corresponding association complex with the bulky hexafluoropohosphate and represent therefore the naked dication. Interestingly the complex with the shortest linker **7b** seems to form a new kind of associated complex (possibly including dissolved gases) in the dry solvent with an emission band at 325 nm. The situation of the complex **11b** with a bridging five methylene groups is similar, while the other complexes with the bulky hexafluorophosphate **10b** and **12b** show the same emission band at 375 nm as the strongest emitters **8a/b** and **9a/b**, but the intensity is reduced significantly (Figure 3.14).
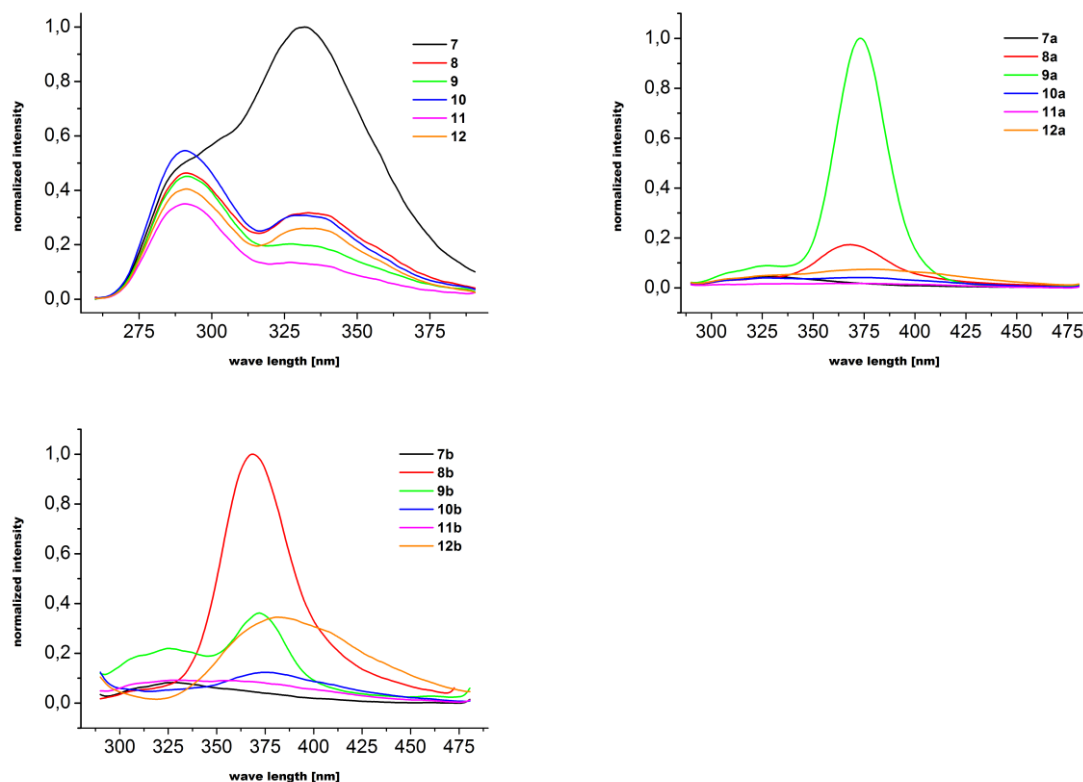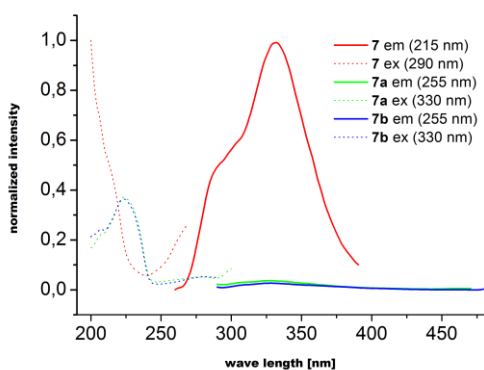

Figure 3.15. Graphics of the emission and excitation measurements of ligand precursor **7** and complexes **7a/b** in ACN at room temperature. Excitation wave lengths and emission wave lengths, respectively, used during measurements are given in the legend.
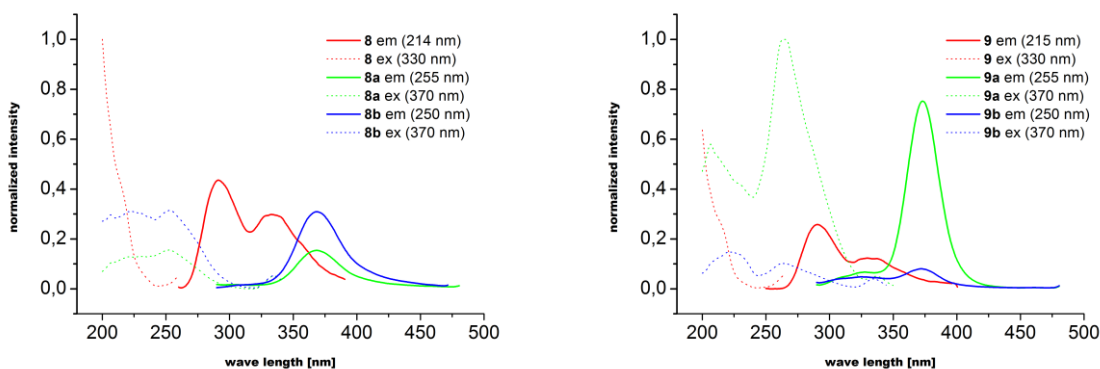

Figure 3.16. Graphics of the emission and excitation measurements of ligand precursor **8** and complexes **8a/b** (left) and of ligand precursor **9** and complexes **9a/b** (right) in ACN at room temperature. Excitation wave lengths and emission wave lengths respectively used during measurements are given in the legend.

The direct comparison of the ligand precursor **7** and the complexes with both bromide (**7a**) and hexafluorophosphate (**7b**) as counter ion in ACN is given in Figure 3.15. Both complexes with a short methylene linker are not influenced by the choice of the counter ion and are hardly emissive compared to the corresponding precursor. The excitation measurements confirm the previous observations.

The direct comparison of the ligand precursors and the complexes with both bromide and hexafluorophosphate as counter ion (Firgure 3.16) confirm the previous observations of stable and highly emissive complexes, possibly stable exciplexes ($^3[d\sigma^*p\sigma]$ excited state), for the complexes with ethylene and propylene linkers **8a/b** and **9a/b**, which are proven before to be able to perform Au-Au bonds in solid state (see above, [35]). The concentration of the intensly emissive complex **9b** was reduced to a 10^{-6} molar solution to to obtain good unaffected spectra.

3.5 Summary

Two systematic series of gold(I) NHC complexes based on imidazole with methyl side chains have been shown here. Bromide or hexafluorophosphate serve as counter ion. The compounds vary in the length of the alkyl chain linking two NHC units, respectively.

The VT-NMR spectra reveal an interesting behaviour for the compounds with short linkers **7a/b** and **8a/b**. The free activation enthalpy for the conversion of the linker conformation could be extracted from an Eyring plot of exchange rates.

Thus eleven out of twelve complexes were structurally characterized. The compounds consist of dicationic dinuclear complexes $Au_2L_2^{2+}$ with bridging dicarbene ligands L. The basic structural parameters fit the expectations: The gold atoms are doubly coordinated with C-Au-C angles close to linearity and mean C-Au bond lengths of 2.02 Å typical for gold(I) NHC compounds[1,2].

A short Au-Au distance is realized intramolecularly for the complexes with methylene (**7a/b**) and propylene (**9a/b**) linkers. For the complexes with longer linkers, stacking of the cations allows a short intermolecular Au-Au distance stabilized by π-π interactions. Exceptions are two complexes with butylenes (**12a**) and hexylene (**10b**) linkers, which show head-to-tail π-π interactions and no short gold-gold distance is found intra- or intermolecularly. The

exceptional role of the complexes with propylene linkers **9a/b** among the gold compounds is visible in the conformation next to the NHC (all-*gauche*, while others are *trans*).

The conformational differences between complexes with varying counter ions are negligible. The complexes with the bulky hexafluorophosphate counter ions show slightly longer Au-Au and π-π distances for short linkers (**7a/b**-**9a/b**) than their bromide congeners. The complex with five methylene units in the linker is the only one in these series without any π-π interactions stabilizing a dimer. The backfolded and twisted arrangement in the cation allows a short gold-gold distance intermolecularly, but the C-Au-C axes are contorted so that π-π stacking is impossible.
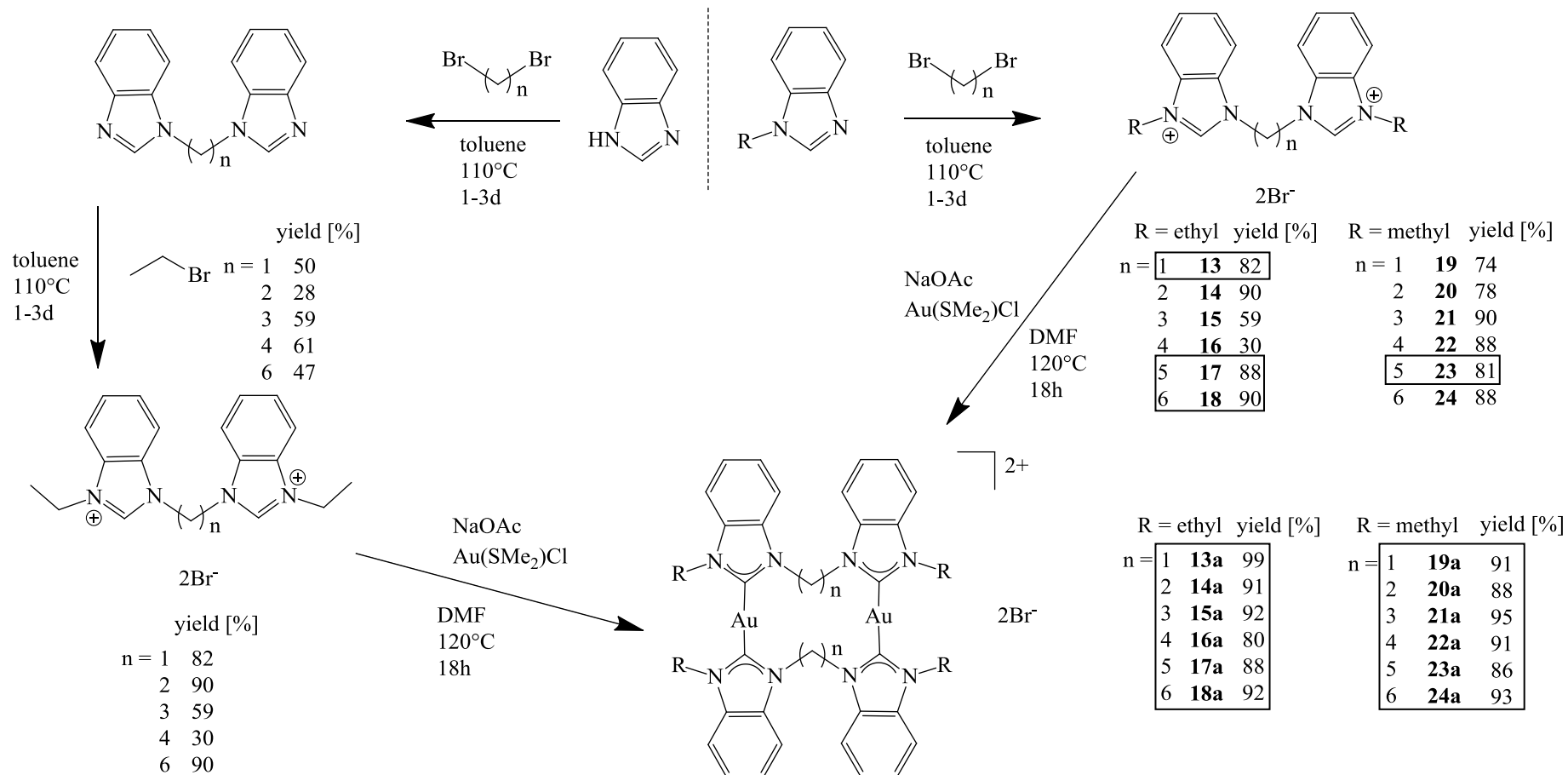
UV/Vis and fluorescence spectra are measured in acetonitrile. The anion exchange doesn´t seem to have any influence on the strongest emitters **8a**/**b** and **9a**/**b**, which indicates propably a stable exciplex (^{3}[dσ*pσ] excited state) not influenced by possible anion association. Measurements should be repeated with degassed solvents and additionally solvent-free with pure crystals.

4. Complexes Type 3

The synthesis and characterization of a systematic series of new dinuclear gold(I) NHC complexes and their corresponding NHC precursors will now be reported. The series consists of gold(I) complexes with N-heterocyclic carbene ligands based on benzimidazole with ethyl or methyl side chains, respectively. The compounds vary in the length of the alkyl chain linking two NHC units, respectively. The conformation of the gold macrocycles with special respect to the formation of intramolecular gold-gold bonds is studied, while the π-π interactions are expected to have a larger influence on the X-ray structures due to the major π-system in the benzimidazole. Two of the compounds were already structurally characterized in my diploma thesis[73] (**15a**, **16a**) Nonetheless, these structures are discussed here again for the purpose of comparison.

4.1 Synthesis

The NHC precursors **13-18** can be obtained by two different synthesis routes, namely the conversion of N-ethylbenzimidazole with the corresponding alkyldibromide in toluene at 110 °C or the conversion of benzimidazole with the corresponding dialkylbromide and subsequent ethylation with ethylbromide (Figure 4.1). Both paths lead to a white powder following purification by washing with toluene/diethylether and drying in vacuo. The syntheses of the ligand precursors **14**, **15** and **16** are already reported, although a different, well-established route is followed here in hope to increase the yield. Nonetheless spectroscopic data is confirmed[88-90]. The NHC precursors **19-24** were obtained by conversion of N-methylbenzimidazole with the corresponding alkyldibromide in toluene at 110 °C giving a white powder following purification by washing with toluene/diethylether and drying in vacuo. The syntheses of the ligand precursors **19**-**22** and **24** are already reported, whereas again the well-established, different route is followed here in hope to increase the yield. Nonetheless, spectroscopic data is confirmed[91-93]. The corresponding NHC gold(I) bromide complexes **13a-24a** were synthesized by direct metallation of the respective imidazolium salt in the presence of sodium acetate in DMF in analogy to the well-established procedure for imidazole congeners[27-29,32,33,35-37]. The complexes were purified by crystallization (slow diffusion of diethylether into a methanol solution) and readily characterized by electrospray mass spectra showing intense signals for the intact dicationic macrocycle $Au_2L_2^{2+}$. Indications for the presence of mononuclear complexes with a chelating bis-NHC-ligands known for longer linkers are not found here[23,24].

yield [%]

n = 1   50
2   28
3   59
4   61
6   47

2Br⁻

yield [%]

n = 1   82
2   90
3   59
4   30
6   90

R = ethyl		yield [%]		R = methyl	yield [%]
n =	1	**13**	82	n = 1	**19**	74
	2	**14**	90	2	**20**	78
	3	**15**	59	3	**21**	90
	4	**16**	30	4	**22**	88
	5	**17**	88	5	**23**	81
	6	**18**	90	6	**24**	88

| R = ethyl		yield [%]		R = methyl		yield [%]
n =	1	**13a**	99	n =	1	**19a**	91
	2	**14a**	91		2	**20a**	88
	3	**15a**	92		3	**21a**	95
	4	**16a**	80		4	**22a**	91
	5	**17a**	88		5	**23a**	86
	6	**18a**	92		6	**24a**	93

Scheme 4.1. Syntheses of the NHC precursors **13-24** and the gold(I) NHC complexes **13a-24a**. Syntheses not kown to literature yet are indicated by black boxes.

4.2 NMR Spectroscopy

The room temperature ^{1}H and ^{13}C NMR spectra for the complexes **13a-24a** confirm the expected highly symmetrical structures. The formation of gold(I)-carbene complexes is accompanied by the disappearance of the acidic benzimidazolium proton signal at δ ~9.50 ppm in the ^{1}H NMR spectrum and a typical shift of the $C_{carbene}$ signal from <140 ppm in the NHC precursor to >180 ppm in the gold(I) complex in the ^{13}C NMR spectrum[1,2]. In accordance to previously reported similar findings[24,27,32,33,35], the exocyclic NHC side chain does not induce significant changes of the macrocycle resonances at room temperature.

The protons of the methylene linkers in compound **13a** are not equivalent and appear as two separated doublets at room temperature[27,32,33,35]. They reversibly disappear/coalesce upon heating to 100 °C (Figure 6.3.1, Appendix). As a result the free activation enthalphy at 298 K of $\Delta G_{298}^{\neq} = 70 \pm 8$ kJ/mol is extracted from an Eyring plot of exchange rates (Figure 6.3.2 and Table 6.3.1, Appendix) obtained by line shape analysis using the programme gNMR[80]. A similar behaviour has been reported for a complex with NHC on the basis of imidazole, methyl side chains and iodide as counter ion and has been attributed to an interconversion of exo- and endo-hydrogens by a kind of ring inversion[27] (Scheme 4.2). The methylene group of the exocyclic side chain appears as a sharp quartet, as expected for a freely-rotating group.
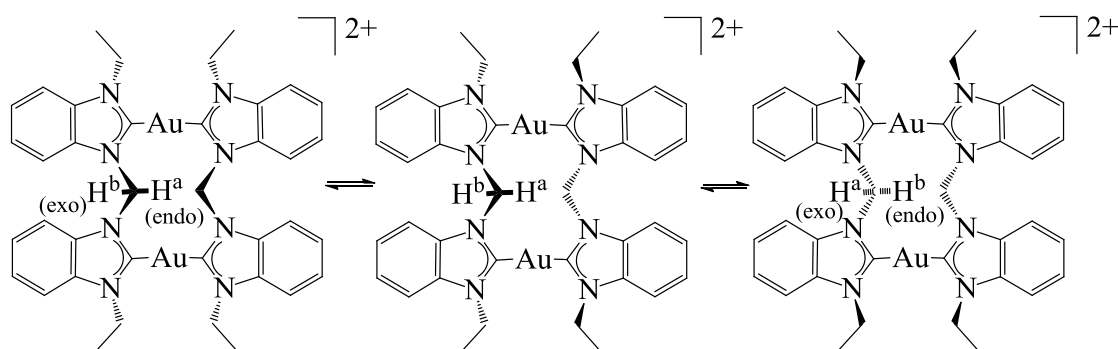
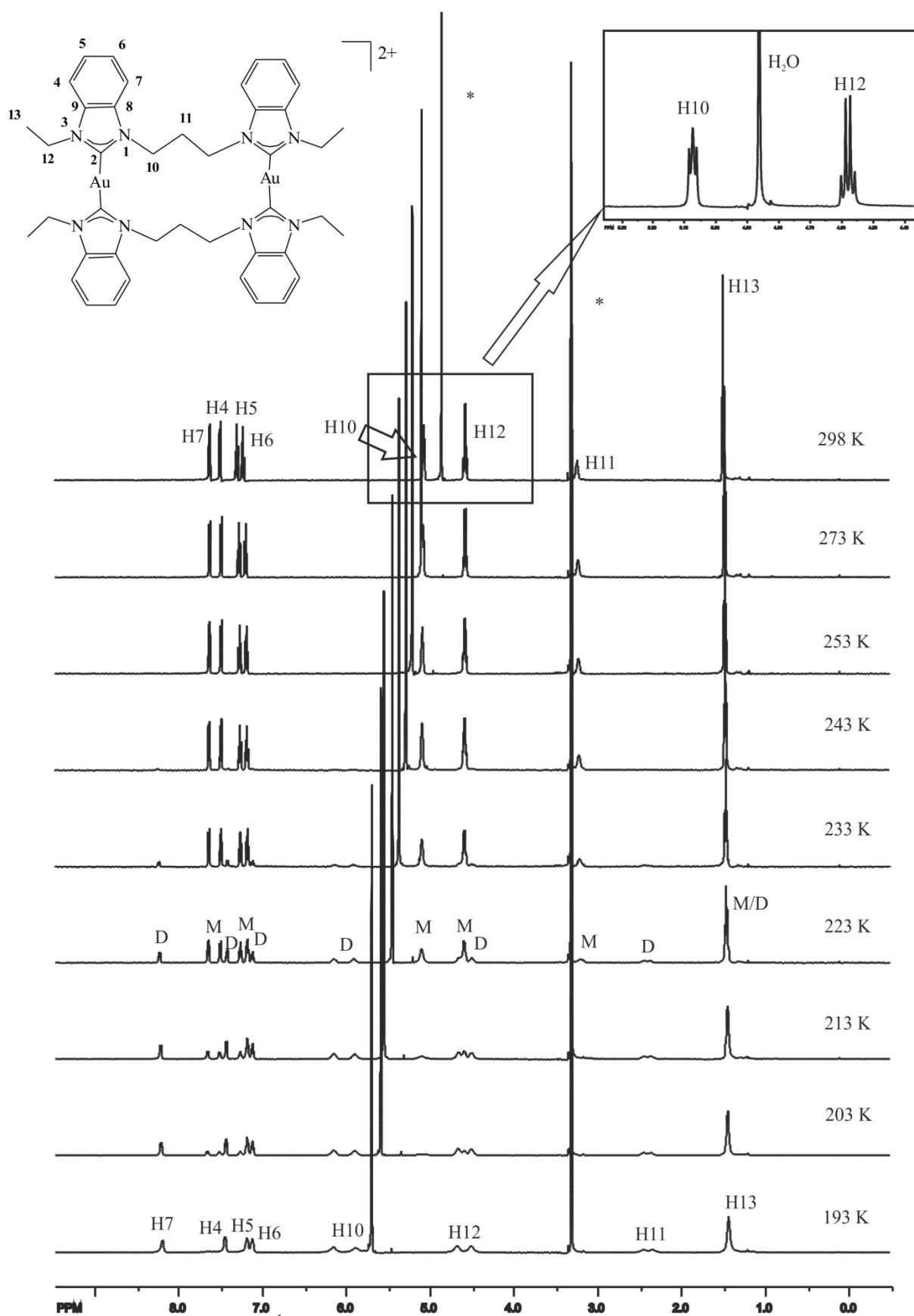**Scheme 4.2.** Proposed ring inversion of compounds **13a**.

Figure 4.1. Low-temperature ^{1}H NMR spectra (500.13 MHz, CD$_3$OD) of **15a**. *partially deuterated and undeuterated methanol and water, respectively.

The room temperature ^{1}H NMR spectra of the complexes **14a-18a** show the expected sharp signals for the linker hydrogens (Figures 6.3.3 – 6.3.6). Cooling leads to broadening of the methylene signals at lower temperatures, but coalescence could not be reached in the temperature range down to -80 °C. Nonetheless, the cation **15a** undergoes some interesting changes: At -40 °C, a complete new set of signals begins to appear, which has about the same intensity as the original signals at -50 °C (Figure 4.1). H,H-COSY NMR measurements at -50°C show no bonding between the two sets of signals. Further cooling to -80 °C leads to the complete disappearance of the original signal set and shows only the new one with two separated broad singlets for the methylene protons next to the NHC (H10 and H12). The new set of signals can be explained by the aggregation of two cations, possibly stabilized by intermolecular Au-Au bonds and/or π-π interactions.

4.3 X-ray Crystal Structures

Single crystals suitable for X-ray diffraction could be obtained by slow diffusion of diethylether in a methanol solution (**13a**-**16a**, **21a**, **22a**, **24a**). Thus, seven out of twelve complexes were structurally characterized. Selected structural data is summarized in Table 4.1. The compounds consist of dicationic dinuclear complexes $Au_2L_2^{2+}$ with bridging dicarbene ligands L. The basic structural parameters fit the expectations: The gold atoms are doubly coordinated with C-Au-C angles close to linearity and mean C-Au bond lengths of 2.02 Å typical for gold(I) NHC compounds[1,2].

Owing to the almost linear C-M-C axis, the torsion angles can be measured between N-C-C-N of the two ligands in a cation to describe the position of these ligands. For the cations with the long butylene (**16a**, **22a**) and hexylene (**24a**) linkers the torsion angle is close to zero and the NHC planes on opposite sides of the gold are coplanar, which is contrary for the complexes with the short methylene (**13a**), ethylene (**14a**) and propylene (**15a**, **21a**) linkers. Each cation is accompanied by two bromide anions. In all cases, the complexes are arranged in a way that layers are formed consisting of organic ligands on the one hand and gold atoms with anions on the other. All NHC ligands of neighboured complexes are interconnected by π-π interactions. Further, all solid state structures of the gold compounds, except for the propylene-linked compounds **15a** and **21a**, reveal a relatively short Au-Au distance, either intra- or intermolecularly. The space groups and crystal packing of the two complexes with the same linker length typically differ due to the size difference of the two side chains studied.

Table 4.1. Selected structural data for complexes **13a** – **24a**.

	n	Crystal symmetry	Au-C/ Å	C-Au-C/°	N-C-C-N/ (a)	dihedral angle of NHC planes/° (b); (c)	Confor-mation next to NHC	Au • Au/Å intra-molecular (d)	Au • Au/Å inter-molecular (d)	π • π/ Å inter-molecular (d)
13a	1	C 2/c	2.032(5) 2.017(5) 2.017(5) 2.022(5)	174.5 175.9	-65.1 -59.6	66.4 65.4 99.7 87.6	-	3.1700(3)	7.8570(2)	3.5369(7)
14a	2	C 2/c	2.023(9) 2.011(9)	175.6	52.8	50.9 43.6	gauche	3.5194(2)	8.1412(4)	3.6578(1)
15a	3	P -1	2.021(4) 2.018(4)	175.3	76. 0	105.6	trans	6.6437(2)	7.1395(2)	3.5227(1)
16a	4	P -1	1.997(9) 2.005(9)	176.6	-1.6	4.7	trans	8.2281(7)	3.2990(3)	3.5992 (3)
21a	3	C 2/c	2.029(15)	175.0	140.3	51.5 66.1	gauche/ trans	4.7375(6)	7.4740(1)	3.6264(4)
22a	4	C 2/c	2.062(10) 2.016(8)	175.3	3.1	1.6 0.2 2.9	trans	7.9193(14)	3.6216(6)	3.7080(6)
24a	6	P 2₁/n	2.021(8) 2.018(7)	175.8	3.4	4.0	gauche/ trans	9.4918(5)	3.5005(2)	3.8593(2)

(a) torsion angle between the two NHC rings (RN-$C_{carbene}$-$C_{carbene}$-NR) coordinating an Au atom; (b) dihedral angle of the two NHC planes coordinating an Au atom; (c) dihedral angle of the two NHC planes in the linker; (d) the shortest value is given.

The smallest cation bearing only methylene linkers **13a** crystallizes in the monoclinic space group *C 2/c*. The NHCs on different sides of the gold atom are not coplanar and the N-C-C-N dihedral angles are comparable (-65.1° and -59.6°, respectively). Nonetheless, the angles of the NHC substituents at the methylene group are identical (110.0° and 111.2°, respectively) and the intramolecular Au-Au distance (3.1700(3) Å) is short. The ethyl side chains on both sides of the gold atoms are conformationally different; they are facing each other on one side of the gold atoms and pointing in the same direction on the other side. The dimers of macrocycles are connected by head-to-tail π−π interactions with neighbouring NHC units, but not by intermolecular close Au-Au distances (Figure 4.2).

A similar complex published by Barnard et al. consists of ligands on the basis of imidazole, a methyl side group and iodide as counter ion[27]. The shape of the cation is quite different

(NHCs are coplanar), with an intramolecular Au-Au distance of 3.5425(6) Å. Further, Hemmert and coworkers structurally characterized two methylene-bridged gold-NHC complexes with alcohol- or carboxylate-functionalized side chains (Au-Au 3.514 Å and 3.589 Å, respectively)[32,33]. An even shorter distance (3.3610(7) Å) could be realized by Fränkel et al.[25] in a neutral complex containing a BH$_2$-unit instead of a methylene linker and by the group of Hahn[43] via incorporation into a large macrocycle (3.0737(3) Å).
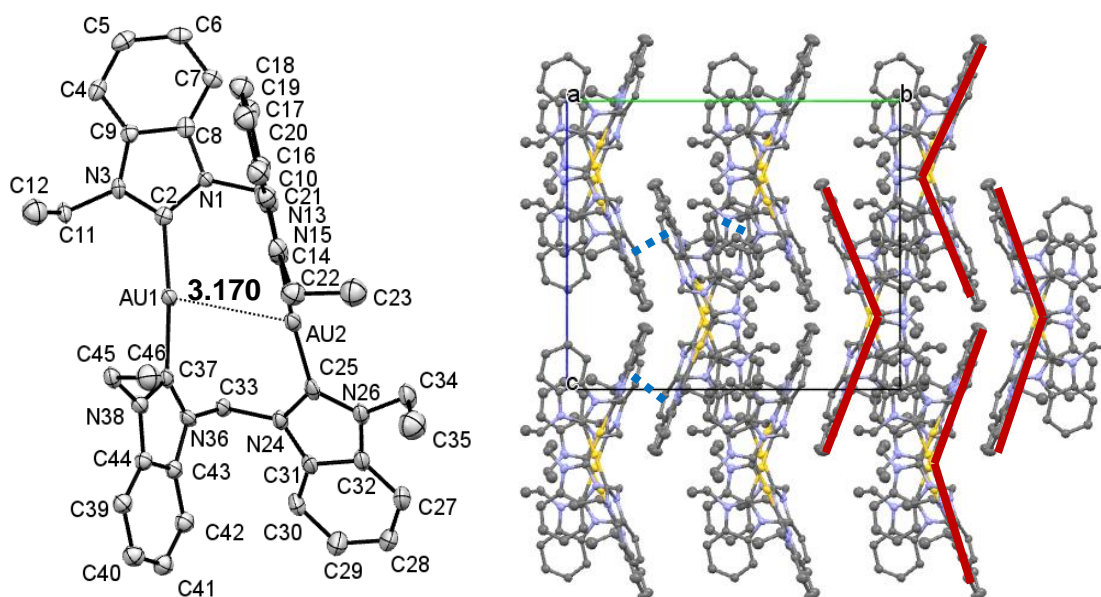

Figure 4.2. ORTEP drawing (left) and crystal packing (view along a axis, right) of complex **13a** (50% probability level for the thermal ellipsoids). Dimers of macrocycles are connected by intermolecular π−π interactions indicated by dotted blue lines. The formation of the dications is indicated by stylized red arrowheads. Hydrogen atoms, cocrystallized methanol and bromide anions have been omitted for clarity.

The macrocycle **14a** crystallizes in the monoclinic space group *C 2/c*. It shows a backfolded conformation with all-*gauche* ethylene linker (Figure 4.3, left). The resulting intramolecular gold-gold distance is short (3.5194(2) Å). Simultaneously, the NHC planes are not coplanar, neither on both sides of one gold atom in the macrocycle, nor in one ligand (twisted by approx. 50°, respectively). The ethyl side chains point to the same direction in one ligand and in the other direction for the other ligand. The conformational folding of the dication is so compact and twisted, that close arrangement with neighbouring macrocycles is restricted to a single π−π interaction per molecule (Figure 4.3, right).
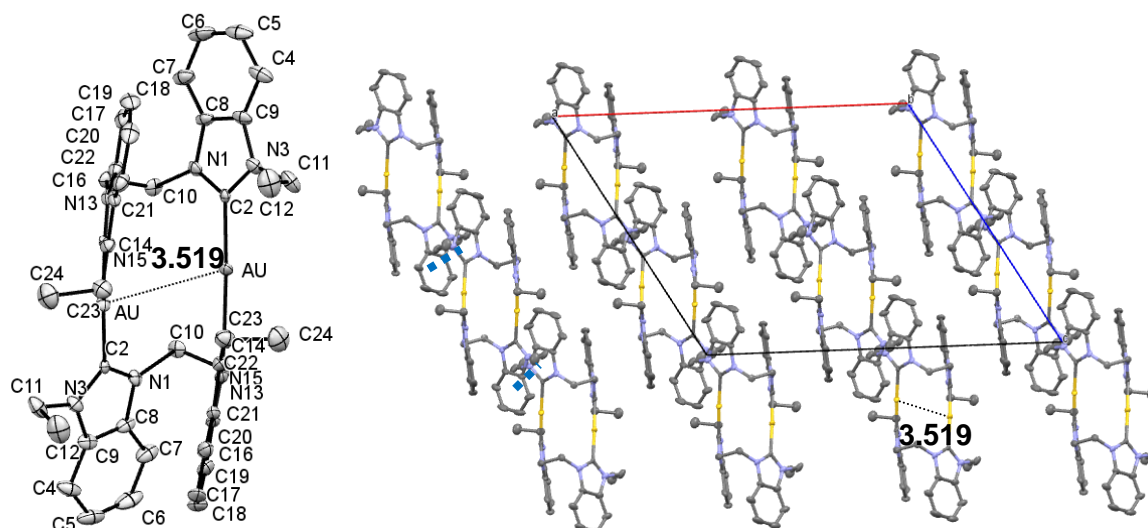
Figure 4.3. ORTEP drawing (left) and crystal packing (view along b axis, right) of complex **14a** (50% probability level for the thermal ellipsoids). Dimers of macrocycles are connected by intermolecular π−π interactions indicated by dotted blue lines. Hydrogen atoms, cocrystallized methanol and bromide anions have been omitted for clarity.

The only published ethylene-linked NHC-Au complex structurally characterized by X-ray bears a bulky alcohol-functionalized side group and PF_6^- anions[33]. Its conformation is backfolded with 50° twisted NHC planes and an intramolecular Au-Au bond in the range of 3.3 Å. The fact that all side chains point to the same side of the molecule thus is not enforced by hydrogen bonds between OH groups, because a similar conformation is retained by simple ethyl groups as well. In sight of the absence of strong intra- or intermolecular π−π interactions (imidazole-based ligands), the backfolded conformation should have an attractive aurophilic origin even though the two gold atoms are cationic.
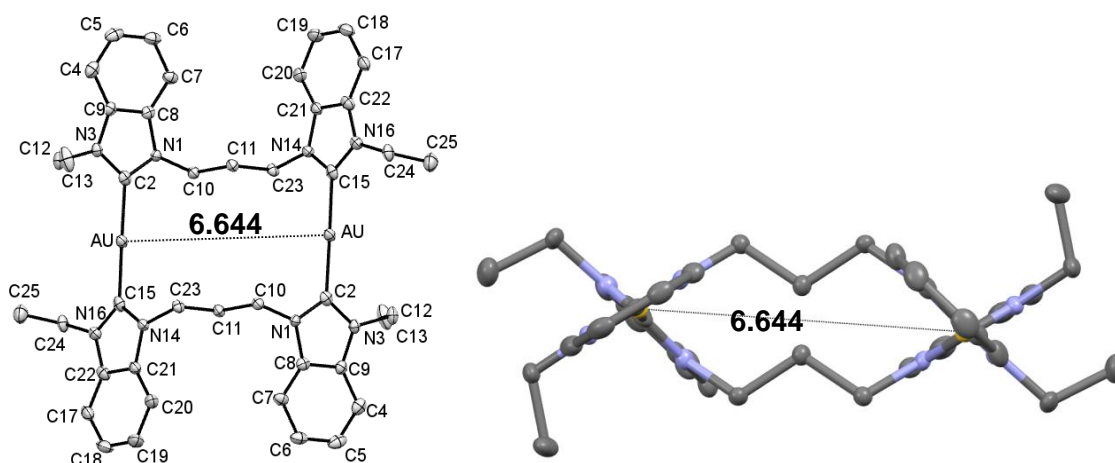

Figure 4.4. ORTEP drawing (left) and top view of one cation (right) of complex **15a** (50% probability level for the thermal ellipsoids). Hydrogen atoms and bromide anions have been omitted for clarity.
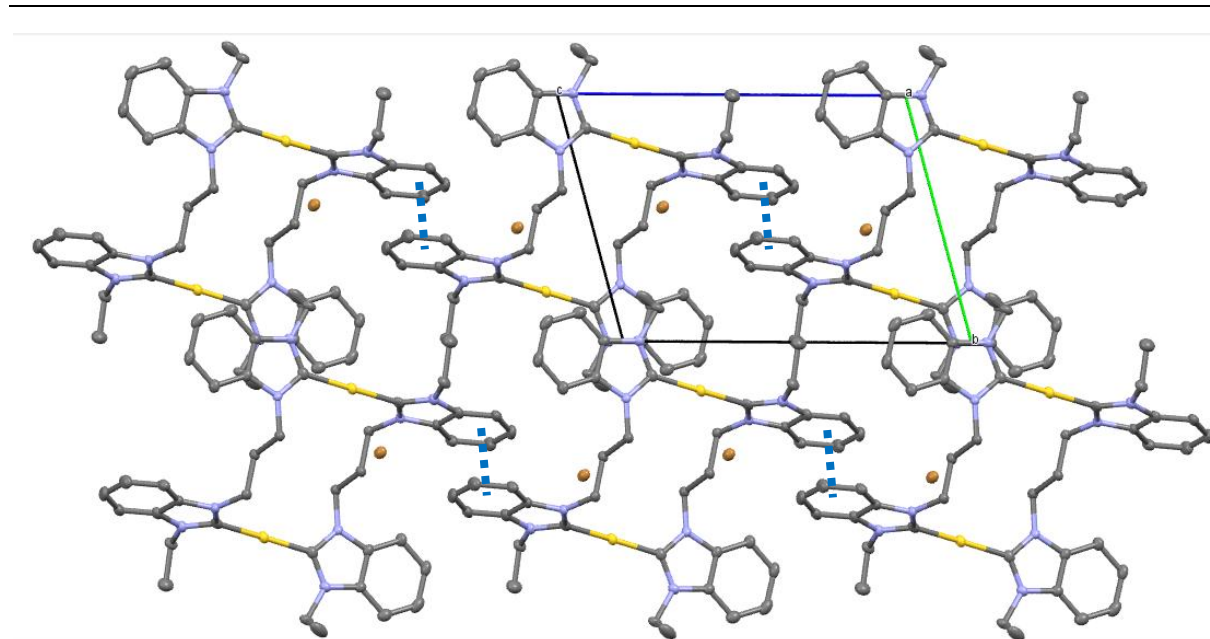
Figure 4.5. Crystal packing of complex **15a** (50% probability level for the thermal ellipsoids, view along a axis). Dimers of macrocycles are connected by intermolecular π−π interactions indicated by dotted blue lines. Hydrogen atoms have been omitted for clarity.

The complex **15a** crystallizes in the triclinic space group *P -1*. The dication with C$_3$-linked NHC ligands shows an open conformation with an all-*trans* propylene linker (Figure 4.4). The intramolecular Au-Au distance is long (6.6437(2) Å). The top view of the cation **15a** shows, that the NHCs on both sides of one gold atom are not coplanar and the ethyl side chains point to one direction: the cation is located around the inversion centre of the structure (Figure 4.4, right). Due to this twisted arrangement, a close intermolecular Au-Au contact is impossible, but polymers of macrocycles are formed by short intermolecular π−π interactions (Figure 4.5).

The complex **21a** crystallizes in the monoclinic space group *C 2/c*. Contrary to the ethyl side chain congener **15a**, this compound shows a backfolded and twisted conformation with a mixed *gauche/trans* propylene linker (Figure 4.6). The intramolecular Au-Au distance is by approx. 2 Å shorter than the analogous one in the complex with ethyl side chains **15a**, but still long (4.7375(6) Å). Here, the NHCs on both sides of one gold ion are coplanar, but the C-Au-C axes are twisted by 87.2°, which leads to a cross-like conformation (Figures 4.6 and 4.7). Due to this twisted and compact arrangement, the formation of polymers comparable to those of the other structures shown here, are possible through short intermolecular π−π interactions (Figure 4.6, right). The two complexes with propylene linkers **15a** and **21a** are

the only ones of the series shown here without any intra- or intermolecular close Au-Au contact.
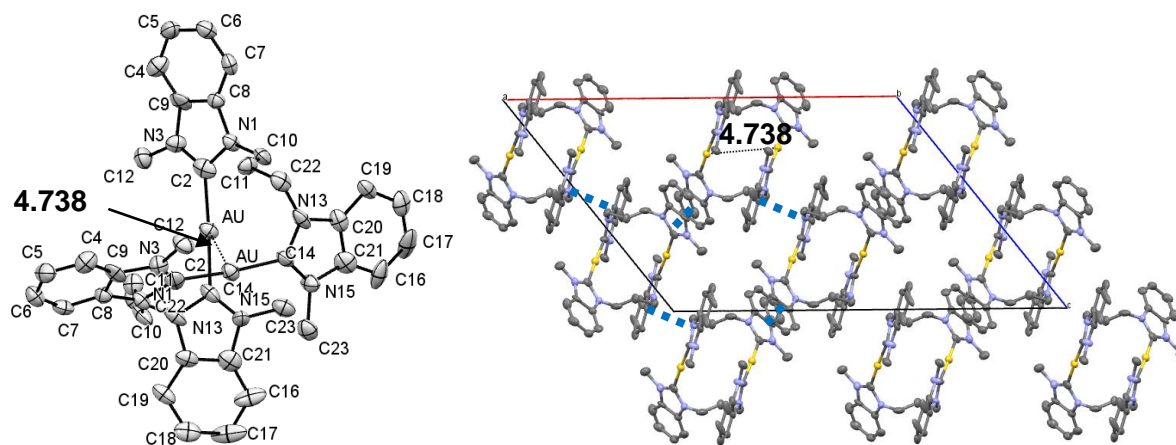

Figure 4.6. ORTEP drawing (left) and crystal packing (view along b axis, right) of complex **21a** (50% probability level for the thermal ellipsoids). Hydrogen atoms, cocrystallized diethylether and bromide anions have been omitted for clarity.
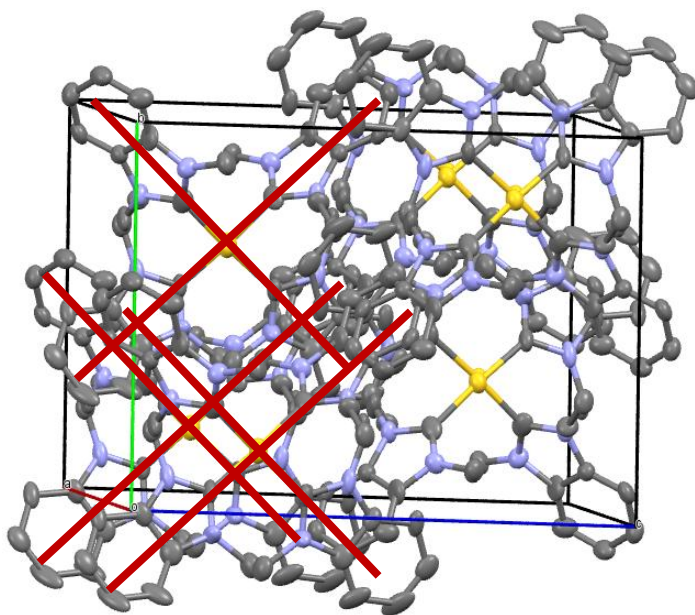
Figure 4.7. Crystal packing (view along no axis) of complex **21a** (50% probability level for the thermal ellipsoids). The formation of the dications is indicated by stylized red crosses. Hydrogen atoms, cocrystallized diethylether and bromide anions have been omitted for clarity.

Tubaro et al.[36] reported the crystal structure of cation **21a** with hexafluorophosphate as counter ion in 2013. It shows an open arrangement with coplanar NHCs and a resulting intramolecular Au-Au distance of 6.827(2) Å. It is the first and only dicarbene NHC gold complex with benzimidazole in literature so far. However, they showed a mixed

imidazole/benzimidazole dicarbene NHC gold complex with an all-*gauche* propylene linker and methyl side groups, which is backfolded with an intramolecular gold-gold distance of 3.0954(1) Å[36]. The same group[35] reported the crystal structure of a propylene bridged Au(I) NHC complex with methyl side chains and PF_6^- as counter ion (ligands based on imidazole) in 2012. Gil-Rubio et al.[24] crystallized the same cation with triflate anions in 2013. This time, a helical conformation with orthogonal NHC-Au-NHC bonds and a very small Au-Au-distance of 3.032 Å is realized. In both structures, the backfolded macrocycle form C3- and C2-symmetric columnar aggregates, respectively, with intermolecular Au-Au and π–π interactions of about d = 3.7 Å. In contrast, the last structurally characterized propylene-bridged complex of this type crystallizes in an open conformation and a double-layer packing without Au-Au interactions[32]. It comes from the Hemmert group and possesses PF_6^- anions and bulky side groups with hydroxyl functions. Thus, counter ion as well as the type of side group have an extreme effect on the molecular conformation of propylene-linked dinuclear NHC complexes of gold(I).

Figure 4.8. ORTEP drawing (left) and crystal packing (view along c axis, right) of complex **16a** (50% probability level for the thermal ellipsoids). Au-Au bound dimers of macrocycles are connected by intermolecular π–π interactions indicated by dotted blue lines. Hydrogen atoms have been omitted for clarity.

The complex **16a** crystallizes in the triclinic space group *P -1* with cocrystallized water bound in the structure. The cation shows an open conformation, with an all-*trans* butylenes linker. Due to this open arrangement, the intramolecular Au-Au distance is very long, but simultaneously the crystal packing allows the formation of columns of NHC-Au-NHC units with close intermolecular gold-gold distances of 3.2990(3) Å. Additionally, these columns are

stabilized by intermolecular $\pi-\pi$ interactions (Figure 4.8). The congener with methyl side chains **22a** shows a similar conformation with an intermolecular gold-gold distance of 3.6216(6) Å. It crystallizes in the monoclinic space group *C 2/c* with cocrystallized methanol bound in the structure (Figure 4.9). Both complexes with butylenes linkers **16a** and **22a** have intramolecular alkyl-alkyl interactions and intermolecular short gold-gold distances accompanied by $\pi-\pi$ interactions in common.
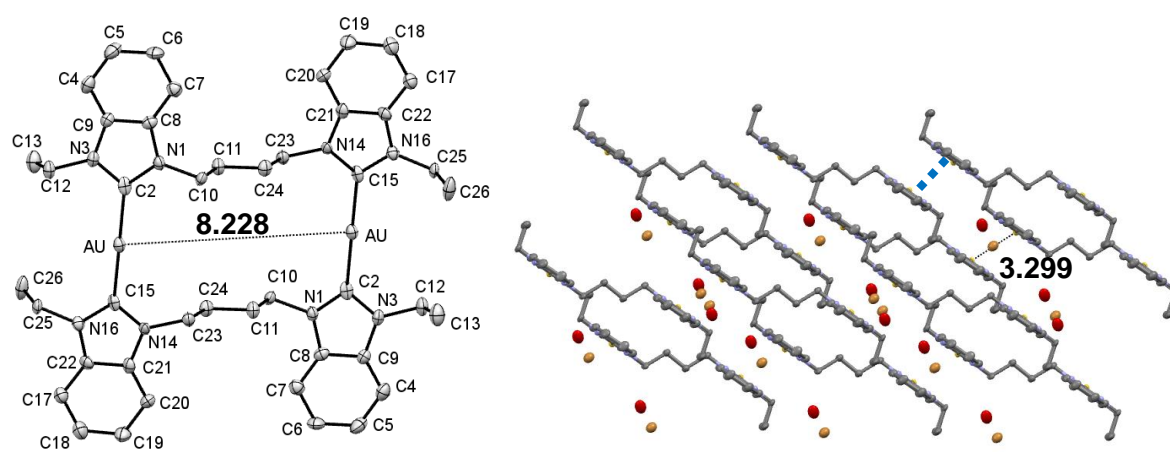

Figure 4.9. ORTEP drawing (left) and crystal packing (view along b axis, right) of complex **22a** (50% probability level for the thermal ellipsoids). Au-Au bound dimers of macrocycles are connected by intermolecular $\pi-\pi$ interactions indicated by dotted blue lines. Hydrogen atoms have been omitted for clarity.
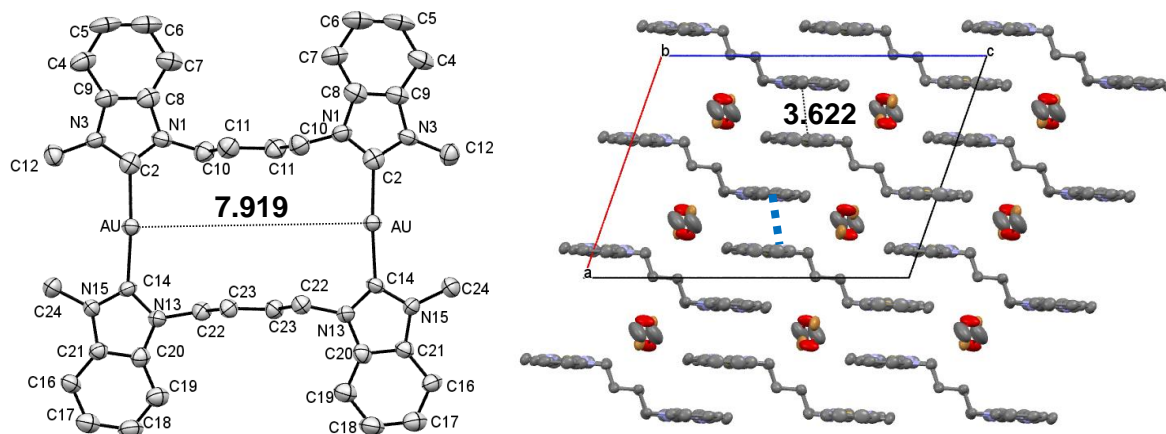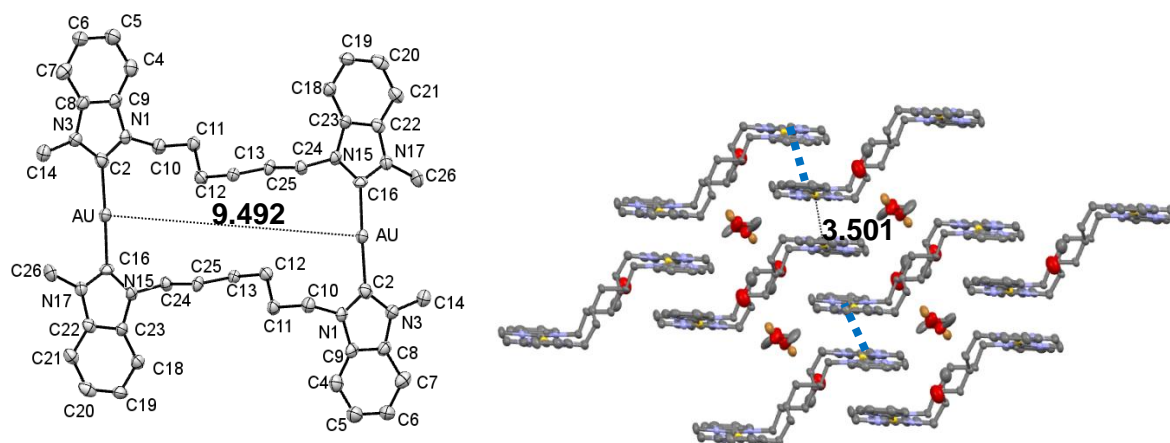

Figure 4.10. ORTEP drawing (left) and crystal packing (view along no axis, left) of complex **24a** (50% probability level for the thermal ellipsoids). Au-Au bound dimers of macrocycles are connected by intermolecular $\pi-\pi$ interactions indicated by dotted blue lines. Hydrogen atoms have been omitted for clarity.

The complex **24a** crystallizes in the monoclinic space group *P 2₁/n* with cocrystallized methanol bound in the structure (Figure 4.10). The cations show an open conformation, comparable to **15a** and **22a**, but with a mixture of *gauche* and *trans* conformation next to the NHC in the hexylene linkers. Due to this open arrangement, the intramolecular Au-Au distance is very long (9.4918(5) Å). Again, the crystal packing allows the formation of columns of NHC-Au-NHC units with close intermolecular gold-gold distances of 3.5005(2) Å. Contrary to the situations in the complexes **16a** and **22a**, the linker chains on both sides of the gold atoms in **24a** are not parallel. Unexpectedly, alkyl-alkyl interaction seems to have a minor role here.

Comparable complexes with NHCs on the basis of benzimidazole and butylene, pentylene or hexylene linkers are unkown so far.

The expected large influence of the enhanced π-system in the benzimidazole on the X-ray structures is visible in the conformation of the cations: every complex shown here is arranged in a way, that π-π interactions are intermolecularly accomplished. Additionally, intermolecular short Au-Au distances are possible through the parallel formation of the NHC-Au-NHC units with coplanar NHCs in the complexes with butylene (**16a**, **22a**) and hexylene (**24a**) linkers.

4.4 UV/Vis and fluorescence studies

Solution based structural studies for dinuclear Au(I) NHC complexes on the basis of benzimidazole, which display aurophilic interactions, are unkown to literature yet. To make a contribution to a better understanding of the triplet state exciplexes the ligand precursors **13**-**18** and the gold complexes **13a**-**18a** are studied here in acetonitrile at room temperature. In solid state, solely the complexes with methylene and ethylene linkers **13a** and **14a** performed a short intramolecular Au-Au distance.

All photophysical measurements were performed with 10^{-5} molar solutions of pure substances (results of the crystallization) in acetonitrile at room temperature. The first measurements in our group were perfomed in DMSO (measurement range <250 nm). To enlarge the measurement range to higher energies (<200 nm) the solvent was changed to ACN. The influence (possible solvation effects) of the solvent was insignificant. The results turned out to be hard to reproduce (variability of the absolute intensity), therefore measurements were

performed multiple times to eliminate weighing and diluting errors. The results shown here are well-established.
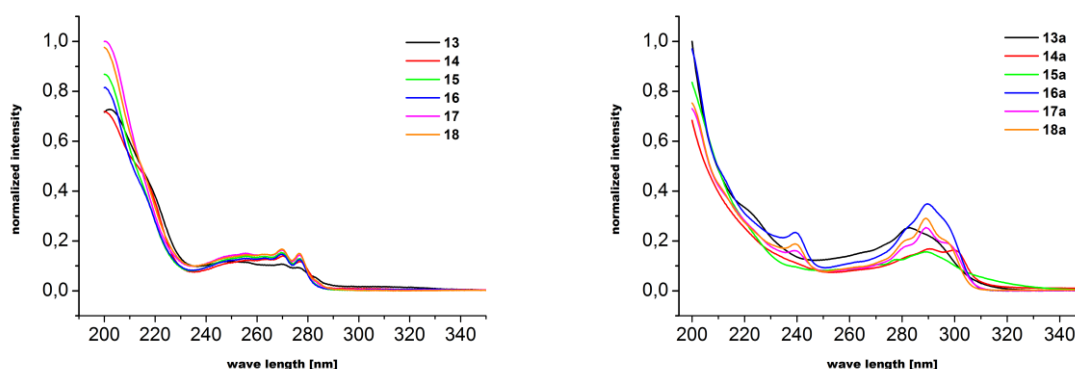

Figure 4.11. Graphics of the absorption measurements of ligand precursors **13**-**18** and complexes **13a**-**18a** in ACN at room temperature.

The ligand precursors **13**-**18** show the same line shape and absorption intensity with maxima at 280 nm and 270 nm (Figure 4.11, left). The same applies to the complexes with long linkers **16a**, **17a** and **18a** with maxima at 290 nm and 240 nm. The complex with the propylene linker **15a** is comparable in line shape, but less intensive. The complexes with the shorter linkers **13a** and **14a** have shifted maxima (**13a**: 280 nm; **14a**: 300 nm) (Figure 4.11, right).
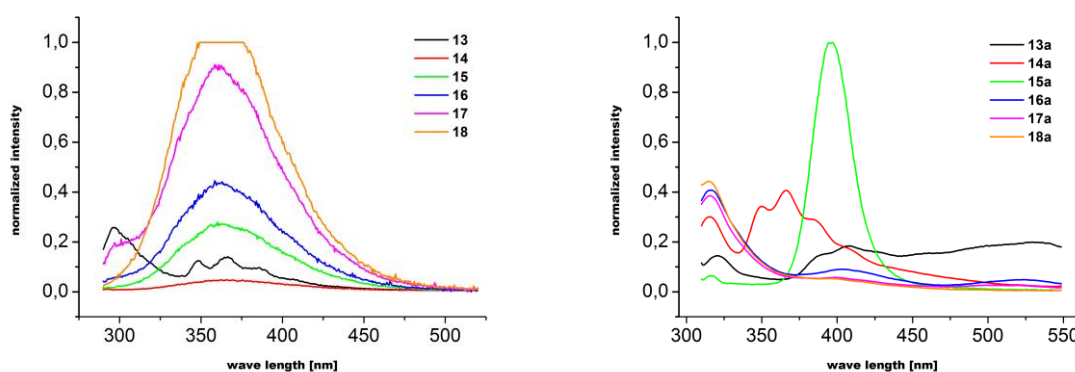

Figure 4.12. Graphics of the emission measurements of ligand precursors **13**-**18** and complexes **13a**-**18a** in ACN at room temperature. The exact excitation wave length used during measurements is 270 nm for **13**-**18** and 290 nm for **13a**-**18a**.

The emission of the ligand precursors **14**-**18** is rather unremarkable in acetonitrile and show the same band at 360 nm with variable intensity (Figure 4.12, left). Only the ligand precursor with the shortest linker **13** shows a different line shape with a promint maximum at 300 nm. The complexes **16a**-**18a** are able to form an association complex[24,35] between the macrocycle and bromide, which are hardly emissive here. The complexes with the long linkers **16a**-**18a** are weak emitters while the complex with the propylene linker **15a** is the strongest emitter, although the solid state structure suggests otherwise (open conformation with Au-Au 6.6437(2) Å intramolecularly). Despite this conformation, an explanation could be the formation of a stable exciplex (^{3}[dσ*pσ] excited state). Interestingly the complex with the ethylene linker **14a** seems to form a new kind of associated complex possibly including water with an emission band at 325 nm. The methylene-linked complex **13a** shows the same band at 375 nm, but the emission intensity stays nearly constant up to 550 nm (Figure 4.12, right).

4.5 Summary

Two systematic series of gold(I) NHC complexes on the basis of benzimidazole with ethyl or methyl side chains have been reported. The counter ion is bromide. The compounds vary in the length of the alkyl chain linking two NHC units, respectively.

The VT-NMR spectra reveal an interesting behaviour for the compound with the shortest linker **13a**. The free activation enthalpy for the conversion of the linker conformation could be extracted from an Eyring plot of exchange rates. The cation **15a** undergoes some interesting changes. At -40 °C, a complete new set of signal begins to appear, which can be explained by the aggregation of two cations, possibly stabilized by intermolecular Au-Au bonds and/or π-π interactions.

Seven out of twelve complexes were structurally characterized. The compounds consist of dicationic dinuclear complexes $Au_2L_2^{2+}$ with bridging dicarbene ligands L. The basic structural parameters fit the expectations: The gold atoms are doubly coordinated with C-Au-C angles close to linearity and mean C-Au bond lengths of 2.02 Å typical for gold(I) NHC compounds[1,2].

A short Au-Au distance is realized intramolecularly for the complexes with methylene (**13a**) and ethylene (**14a**) linkers. For the complexes with longer linkers stacking of the cations allows a short intermolecular Au-Au distance stabilized by π-π interactions. Exceptions are two complexes with propylene linkers **15a** and **21a**, which show a head-to-tail π-π

interactions and no short gold-gold distance is found intra- or intermolecularly. Unfortunately, a trend for the conformational differences between complexes with varying side chains can not be derived from the studies shown here.

UV/Vis and fluorescence spectra are measured in acetonitrile. Measurements should be repeated with degassed solvents and additionally solventfree with pure crystals. The complex with the propylene linker **15a** is by far the strongest emitter studied here. Despite the open conformation in solid state, an explanation could be the formation of a stable exciplex (^{3}[dσ*pσ] excited state)..

5. Conclusions

The spectroscopic characteristics and solid state molecular structures of seven systematic series of dicationic coin metal(I) NHC complexes with alkyl linker lengths ranging from one to six methylene units are reported. Both the counter ions bromide and hexafluorophosphate have been investigated, as well as gold(I) and silver(I) atoms, ethyl and methyl side chains and ligands based on imidazole and benzimidazole. Overall, 24 ligand precusors and 42 metal(I) NHC complexes have been analyzed.

The (benz)imidazolium bromide salts **1-24** were obtained by conversion of the corresponding N-substituted (benz)imidazole with the corresponding alkyldibromide in toluene[75,76,88-,90]. Additionally, the NHC precursors **13-16** and **18** can be obtained by the conversion of benzimidazole with the corresponding dialkylbromide and subsequent ethylation with ethylbromide. The corresponding NHC gold(I) bromide complexes **1a-24a** were synthesized by direct metallation of the respective imidazolium salt in the presence of sodium acetate in DMF according to a well-established procedure[27-29,32,33,35-37]. The complexes were purified by crystallization (slow diffusion of diethylether into a methanol solution). Subsequent anion exchange with KPF_6 in a methanol/water mixture gave the complexes **1b-12b** in excellent yields. The analogous silver(I) complexes **1c-6c** were obtained by direct metallation of the ethyl imidazolium bromide salts **1-6** with silver(I)oxide[77,78].

The room temperature ^{1}H and ^{13}C NMR spectra for the all complexes confirm the expected highly symmetrical structures. The formation of gold(I)-carbene complexes is accompanied by the disappearance of the acidic imidazolium proton signal at $\delta \sim 9.50$ ppm in the ^{1}H NMR spectrum and a typical shift of the $C_{carbene}$ signal from <140 ppm in the NHC precursor to >180 ppm in the gold(I) complex in the ^{13}C NMR spectrum[1,2]. In accordance to previously reported similar findings[24,27,32,33,35], neither the exocyclic NHC side chain nor the counter anion induce significant changes of the macrocycle resonances at room temperature, whereas an upfield shift in acetonitrile solution is more pronounced. The compounds **1c-6c** show the same changes to the NMR spectra, but the signals compared to those of the gold compounds are shifted downfield in the ^{1}H NMR spectra and upfiled for the ^{13}C NMR spectra[33].

The protons of the methylene linkers in compounds **1a/b**, **7a/b** and **13a** are not equivalent and appear as two separated doublets at room temperature, which was observed before for the iodide congener of **7a/b**[27]. They reversibly coalesce upon heating to 100 - 105 °C

(Figures 6.1.1, 6.2.1 and 6.3.1, Appendix), which has been attributed to an interconversion of exo- and endo-hydrogens by a kind of ring inversion[27]. Therefore the free activation enthalphy at 298 K is extracted from an Eyring plot of exchange rates (Figures 6.1.2, 6.2.2 and 6.3.2 and Tables 6.1.1, 6.2.1 and 6.3.1, Appendix) obtained by line shape analysis using the programme gNMR[80].

Additionally, the rotation of the N-CH$_2$ bond of the side chain in **1a/b** seems to be frozen at room temperature (two multiplets when measured with 500 MHz at room temperature in DMSO-d$_6$). Heating the sample leads to coalescence and appearance of a quartet signal expected for freely rotating ethyl groups. The signal for the pending methyl protons appears as triplet, which shifts very slightly downfield by 0.05 ppm at higher temperatures. The ethyl side chains of the two NHCs coordinating a gold atom come rather close (distance between the methylene carbon atoms $d = 4.350$ Å). Thus, the ethyl groups are jammed and their independent rotation is hindered. (vide infra, Figure 6.1.6, Appendix). For the corresponding benzimidazole complex **13a** the rotation around the N-CH$_2$ bond is not hindered at room temperature and the protons are equivalent (vide infra, Figure 6.3.7, Appendix).

The compounds **2a/b** and **8a/b** show a similar behaviour at lower temperatures, where the inversion of the ethylene-bridged macrocycle equilibrating exo and endo protons is frozen at -80 °C. However, the rotation of the ethyl side chains in **2a/b** is possible at every temperature studied here, but a concerted ethyl rotation of partly jammed ethyl side chains agains seems plausible. (vide infra, Figure 6.1.6, Appendix).

For substance **6a** with six methylene units in the linker, sample cooling reveals additional broad signals which could be interpreted as signs of a starting aggregation inspired by the solid state packing with dominant π-π interactions arranging the cations in long chains. The cation **15a** undergoes similar changes: At -40 °C, a complete new set of signals begins to appear, which has about the same intensity as the original signals at -50 °C. H,H-COSY NMR measurements at -50 °C show no bonding between the two sets of signals. Further cooling to -80 °C leads to the complete disappearance of the original signal set and only shows the new one with two separated broad singlets for the methylene protons next to the NHC (H10 and H12). The new set of signals can be explained by the aggregation of two cations, possibly stabilized by intermolecular Au-Au bonds and/or π-π interactions.

Single crystals suitable for X-ray diffraction could be obtained by slow diffusion of diethylether in a methanol solution (**1a-4a**, **6a**; **7a-10a**, **12a**; **13a-16a**, **21a**, **22a**, **24a**), an acetonitrile solution (**1b-6b**; **7b-12b**) or a DCM solution (**1c**, **3c**, **4c**). Thus, 32 out of 42 complexes were structurally characterized. The compounds containing gold as metal consist of dicationic dinuclear complexes $Au_2L_2^{2+}$ with bridging dicarbene ligands L. The basic structural parameters fit the expectations: The gold atoms are doubly coordinated with C-Au-C angles close to linearity and mean C-Au bond lengths of 2.02 Å typical for gold(I) NHC compounds[1,2].

The compounds **1c** and **3c** show the same macrocycles with dicationic dinuclear complexes $Ag_2L_2^{2+}$ containing bridging dicarbene ligands L. The compound **4c** shows a completely different organization with polymer chains instead of macrocycles. Two different ligands connect three instead of two silver ions. Nonetheless in all three silver compounds the silver atoms are doubly coordinated with C-Ag-C angles close to linearity and mean C-Ag bond lengths of 2.08 Å typical for silver(I) NHC compounds[79].

Owing to the almost linear C-M-C axis, the torsion angles can be measured between N-C-C-N of the two ligands in a cation to describe the position of these ligands. The torsion angle is close to zero when the NHC planes on opposite sides of the metal are coplanar. Each cation is accompanied by two bromide, $AgBr_2^-$ or hexafluorophosphate anions, respectively. In all cases, the complexes are arranged in a way that layers are formed consisting of organic ligands on the one hand and metal atoms with anions on the other. NHC ligands of neighboured complexes are interconnected by π-π interactions. Further, almost all solid state structures of the gold compounds (except for **3a**; **8a**, **10b**, **12a**; **15a**, **21a**) reveal a relatively short Au-Au distance, either intra- or intermolecularly; in four cases (**1a**; **7b**, **9a/b**) even both is realized. The silver compound **1c** is the only one shown here with a short Ag-Ag distance (3.47 Å). An overview of the solid state structures is given in Table 5.1. The structures are roughly categorized in rigid, backfolded, twisted and the most common open arrangement of the macrocycles.

Table 5.1. Summary of the studied complexes and their classification.

	n =	1	2	3	4	5	6	
imidazole	M = Au R = ethyl $X^- = Br^-$	1a*	2a*	3a*	4a*	5a*	6a*	Complexes Type 1
	M = Au R = ethyl $X^- = PF_6^-$	1b*	2b*	3b*	4b*	5b*	6b*	
	M = Ag R = ethyl $X^- = Br^-/$ $AgBr_2^-$	1c*	2c*	3c	4c*	5c*	6c*	
	M = Au R = methyl $X^- = Br^-$	7a	8a	9a	10a	11a*	12a*	Complexes Type 2
	M = Au R = methyl $X^- = PF_6^-$	7b	8b	9b	10b	11b*	12b*	
benzimidazole	M = Au R = ethyl $X^- = Br^-$	13a*	14a*	15a*	16a*	17a*	18a*	Complexes Type 3
	M = Au R = methyl $X^- = Br^-$	19a*	20a*	21a*	22a*	23a*	24a*	

* Syntheses not known to literature yet, ▥ rigid, ▨ backfolded, ▨ twisted, ▧ open

All six compounds with methylene linkers have a short M-M distance intramolecularly in common; the general constitution of the complexes dictates that: all N-C-N angles in the linker are ~111°. They represent the group of rigid complexes (Table 5.1). Two of the complexes (**1a**, **7b**) show an addional short Au-Au distance intermolecularly. Nonetheless, all complexes with a methylene linker form dimers stabilized by π-π interactions. Contrary to the silver congener (**1c**) and the gold(I) complex with ligands based on benzimidazole (**13a**), for the complexes with ligands an the basis of imidazole (**1a/b**, **7a/b**) the NHCs on both sides of the gold atom are coplanar. The position of the side chains seems to have no dominant role in the forming process of the solid state structure, given the variety found here. All ethyl side chains point inwards for the bromide salt **1a**, but show an in/out conformation for **1b** with PF_6^- (Figures 2.3 and 2.4). The ethyl side chains on both sides of the gold ions in the

benzimidazole congener are conformationally different; they are facing each other in one ligand and pointing in the same direction in the other one (Figure 4.2). The corresponding silver(I) structure **1c** shows an outward orientation of the ethyl side chains leading to a zig-zag pattern for the ligands (Figure 2.5). The gold(I) complexes **1a/b** and **7a/b** are very typical for this kind of compound, where the NHCs on both sides of the gold(I) atoms are coplanar and the C-Au-C axes are parallel[1,2].

The same applies to the complexes with an ethylene linker **8a/b** (Figure 3.4), whereas the other three complexes with an ethylene linker **2a/b** (Figure 2.7) and **14a** (Figure 4.3) have twisted C-Au-C axes. The overall conformation of the dicationic macrocycles **2a/b** and **14a** is unusual, but rather similar for the three complexes. A backfolded twisted geometry with gauche conformation in the ethylene linkers realizes a short intramolecular Au-Au distance (**2a**: 3.3988(1) Å, **2b**: 3.2328(2) Å, **14a**: 3.5194(2) Å). The two NHC planes bound to a gold atom are not coplanar, but twisted by approx. 50°, respectively, - probably to avoid steric repulsion of the ethylene linkers while retaining the short Au-Au distance. The conformational folding of the dications is so compact and twisted, that close arrangement with neighbouring macrocycles is restricted to a single π−π interaction per molecule. The complex **8b** shows an open conformation with all-*trans* ethylene linker. The resulting intramolecular gold-gold distance is quite long (5.5492(3) Å). The cation **8a** shows a mixture of the open conformation of macrocycle **8b** and the backfolded arrangement of the complexes **2a/b** and **14a** with one *trans* ethylene linker and one *gauche* ethylene linker, which leads to a shorter Au-Au distance (4.6320(3) Å) than the one found in the hexafluorophosphate congener **8b**. Again, the conformational folding of the dication is so compact and twisted that close arrangement with neighbouring macrocycles is restricted to a single π−π interaction per molecule for **2a/b**, **8b** and **14a**.

Like the compound **8b**, the dications **3a/b** and **15a** show an open, W-like conformation with an all-*trans* propylene linker (Figures 2.9 and 4.4). The intramolecular Au-Au distance is very long for the three structures. The dihedral angle of 103° - 105° between the two NHC planes of a ligand in **3b** and **15a** is widened to 126° when crystallized as the bromide salt **3a**. Dimers of macrocycles **3b** are formed by a short intermolecular Au-Au distance of 3.292 Å connected by π−π interactions (Figure 2.11). In contrast, the cations **3a** and **15a** form dimers stabilized by π-π interactions, but no short intermolecular gold-gold distance is found. The NHCs on both sides of one metal atom in **3c** and **15a** are not coplanar. While the cation **15a** (like **3a/b**)

shows an all-*trans* conformation in the propylene linker, the macrocycles **3c** and **21a** show a mixture of *gauche* and *trans*. In consequence, the complex **21a** shows a backfolded and twisted X-like conformation (Figures 4.6 and 4.7). The intramolecular Au-Au distance is by approx. 2 Å shorter than the analogous one in the complex with ethyl side chains **15a**, but still long (4.7375(6) Å). Here, the NHCs on both sides of one gold ion are coplanar, but the C-Au-C axes are twisted by 87.2°, which leads to the cross-like conformation. Due to this twisted and compact arrangement, the formation of dimers stabilized by π-π interactions is restricted to a single contact per dication (Figure 4.5). Both dications **9a/b** show a backfolded conformation with an all-*gauche* propylene linker (Figures 3.6 and 3.7). The intramolecular Au-Au distances are short (**9a**: 3.1153(2) Å, **9b**: 3.2283(4) Å). This is the result of a folded conformation: the torsion angle amounts to 66°-68° between the N-C-C linkers of a ligand. Polymers of macrocycles are formed by a short intermolecular Au-Au distance of 3.7 – 3.9 Å stabilized by π–π interactions (Figure 3.7).

The orientation of the cations **4a/b** (Figure 2.13) and **10b** (Figure 3.9) is similar. So all cations cannot, due to the open S-arrangement of the cation, realize a short intramolecular Au-Au distance. The conformation next to the NHC units is *gauche*, which results in a backfolded conformation comparable to **9b**, but due to the additional methylene unit in the linker with a *trans* conformation, the intramolecular gold-gold distance is still very long (**4a**: 6.7729(4) Å, **4b**: 6.972(6) Å, **10b**: 7.0525(5) Å). While the cation **10b** shows a head-to-tail connection for the NHC-Au-NHC units, thus inhibiting close Au-Au contacts while connecting polymers by intermolecular π–π interactions, the C-Au-C axes in **4a/b** are parallel. In contrast, **4c** shows a very unusual conformation: the $M_2L_2^{2+}$ macrocycles are replaced by a polymere structure with AgL^+ subunits forming long chains. Conformation next to the NHC is all-gauche for **4a/b/c**, but due to the polymerisation there is no possibility for short Ag-Ag distances or π–π interactions in **4c**.

The complexes **10a** (Figure 3.8), **16a** (Figure 4.8) and **22a** (Figure 4.9) show an open conformation, comparable to **8b**, with an all-*trans* butylenes linker. Due to this open arrangement, the intramolecular Au-Au distance is very long, but simultaneously the crystal packing allows the formation of columns of NHC-Au-NHC units with close intermolecular gold-gold distances (**10a**: 3.5842(2) Å, **16a**: 3.2990(3) Å, **22a**: 3.6216(6) Å). Additionally, these columns are stabilized by intermolecular π–π interactions.

Like the congeners with butylenes linkers, the complexes **6a/b** (Figures 6.1.8 and 6.1.9, Appendix) and **12a/b** (3.11) show an open conformation with a *gauche* conformation next to the NHC, but *trans* conformation in the hexylenes linker. As a consequence, the intramolecular Au-Au distance is very long for the dications (**6a**: 8.7084(7) Å, **6b**: 8.8268(7) Å, **12a**: 8.5616(6) Å; **12b**: 8.8762(8) Å). The crystal packing however differs. While the arrangement of the cations in **12a** (Figure 3.12, left) is comparable to **10b**, dimers are formed by stacking of NHC planes of different cations stabilized by intermolecular π−π interactions (head-to-tail), the cations of complexes **6a/b** (Figures 6.1.8 and 6.1.9, Appendix) and **12b** (Figure 3.12, right) show an arrangement comparable to complex **10a** with close intermolecular Au-Au distances (3.6224(2) Å) stabilized by intermolecular π−π interactions (head-to-head). The complex **24a** (Figure 4.10) shows an open conformation, comparable to **15a** (Figure 4.4) and **22a** (Figure 4.9), but with a mixture of *gauche* and *trans* conformation next to the NHC in the hexylenes linker. Due to this open arrangement, the intramolecular Au-Au distance is very long (9.4918(5) Å). Again, the crystal packing allows the formation of columns of NHC-Au-NHC units with close intermolecular gold-gold distances of 3.5005(2) Å. Nontheless, all eleven gold(I) compounds with butylenes (**4a/b**, **10a/b**, **16a**, **22a**) or hexylene (**6a/b**, **12a/b**, **24a**) linkers have the overall open conformation forming dimers stabilized by intermolecular π−π interactions in common.

The adjustment of the cations **5b** (Figure 2.15) and **11b** (Figure 3.10) is rather unusual compared to the other complexes of these series. The two C-Au-C axes are twisted and not parallel (**5b**: -64.2°, **11b**: -53.2°), resulting in a compact cation with a quite long intramolecular Au-Au distance (**5b**: 4.9425(2) Å, **11b**: 4.1307(2) Å). Due to the ethyl side chains facing inside in **5b**, close π-π interactions and a shorter intermolecular gold-gold distance of 3.548 Å are realized. The conformation next to the NHCs is a mixture of three *gauche* and one *trans* arrangement in **11b** (**5b**: all-*gauche*). The C-Au-C axes are forming columns with a shorter intermolecular gold-gold distance of 3.2582(2) Å, but the NHC planes are shifted, so intermolecular π−π interactions are impossible. The structure determining motif here seems to be the formation of close gold-gold bonds and stabilization through intermolecular π−π interactions is insignificant. The only other comparable cation arrangement is **21a** (Figures 4.6 and 4.7), with NHC based on benzimidazole and a propylene linker, which indicates even-odd alternation. The similarity of the compounds with butylenes and hexylene linkers confirms that obvervation.

UV/Vis and fluorescence spectra are measured in acetonitrile (additionally a mixture of acetonitrile and 20% water for **1a**/**b-6a**/**b**). Irrespective of the counter ion, the solvent, the side chain and even the type of NHC in the complex, the strongest emitter is the propylene linked compound. Independent of the arrangement in the solid state, all these dications are probably forming a stable exciplex (^{3}[dσ*pσ] excited state) with a suggested formal Au-Au single bond, even though the X-ray structures suggest otherwise. The situation for the ethylene linked compounds is similar although with less intensity, apart from the benzimidazole-based complex **14a**. The same behavior would be expected for the methylene linked compounds (short Au-Au distances in the X-ray structures), but they are hardly emissive at all and influenced by the choice of the solvent. The compounds with longer linkers show the expected dependence on the counter ion and the solvent. In general, the bromide congeners are capable of forming association complexes of the dication and the anion, which can be dissolved through hydration. The compounds with the bulky hexafluorophosphate are not able to associate with the dications.

All studies shown in this work make a contribution to a better understanding of the balance of weak interactions (aurophilicity vs. π-π interaction) in several systematic series varying different features of dinuclear gold(I) NHC complexes. Additionally, the results could be useful as an experimental reference for quantum-chemical studies targeting aurophilic interactions.

6. Appendix
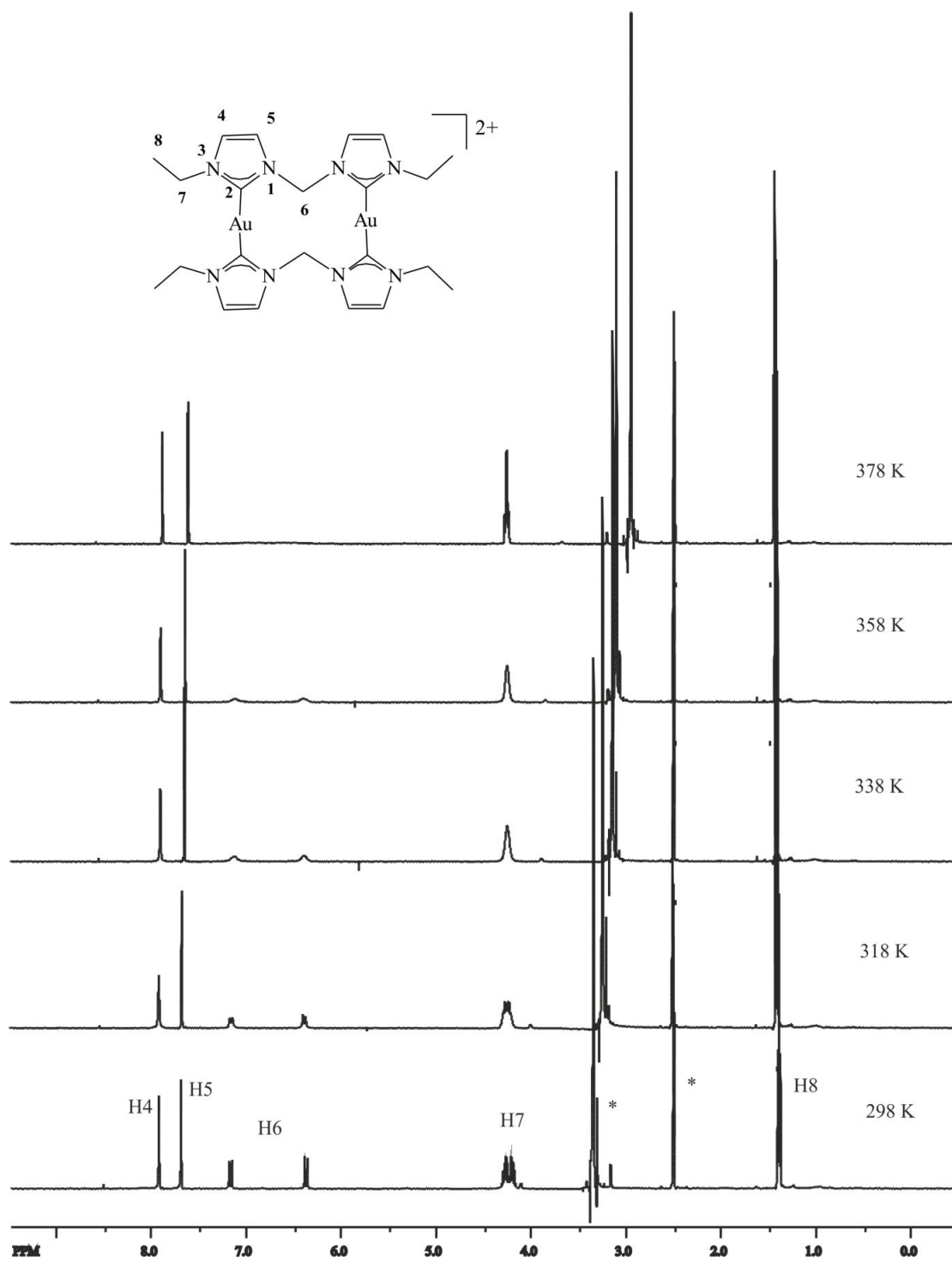
6.1 Complexes Type 1

6.1.1. VT-NMR

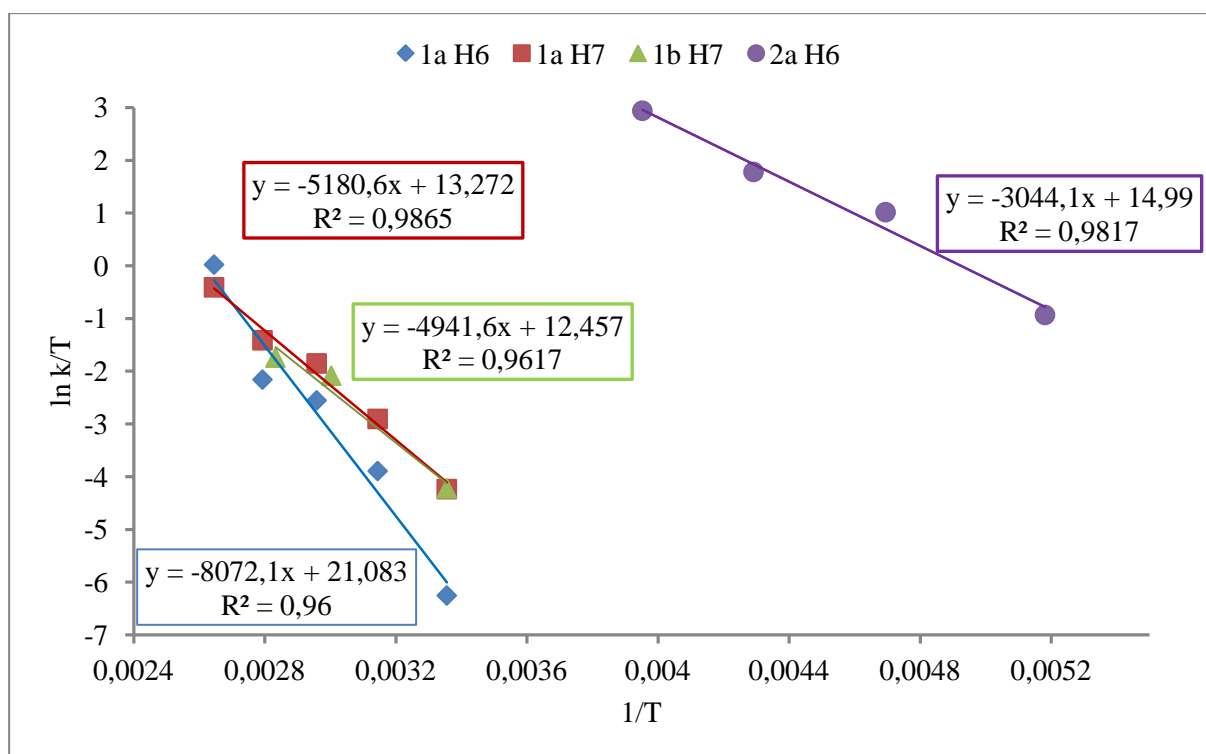**Figure 6.1.1.** High temperature ^{1}H NMR spectra (500.13 MHz, DMSO[D6]) of **1a**/**b**.

Figure 6.1.2: Eyring plots for the kinetic rate constants given in Table x obtained from line shape analysis of the VT-NMR spectra shown in Figure x and Figure x

Table 6.1.1. Thermal activation parameters determined from the Eyring plots in Figure S2 for the dynamic behaviour observed for the metallamacrocyclic systems **1a/b** and **2a**.

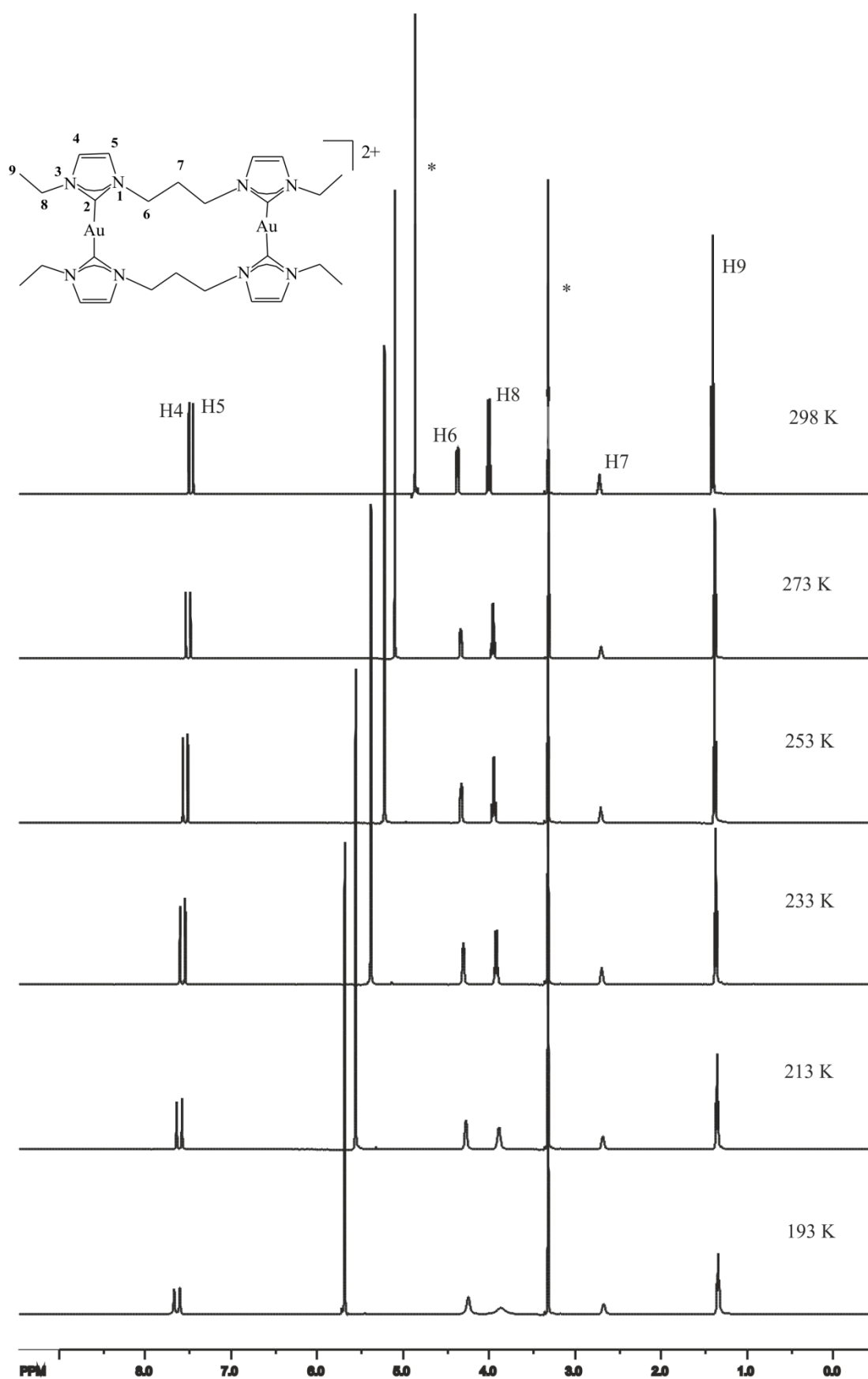| compound	anion	linker	signal	$\Delta H^{\ddagger}$ / kJ mol^{-1}	$\Delta S^{\ddagger}$ / J mol^{-1}K^{-1}	$\Delta G^{\ddagger}_{(298K)}$ / kJ mol^{-1}
1a	Br$^-$	CH$_2$	H6	67 ± 7	-22 ± 24	74 ± 11
2a	Br$^-$	C$_2$H$_4$	H6	25 ± 2	-73 ± 11	47 ± 4
1a	Br$^-$	CH$_2$	H7	43 ± 3	-87 ± 9	69 ± 4
1b	PF$_6^-$	CH$_2$	H7	41 ± 8	-94 ± 25	69 ± 11

Figure 6.1.3. Low temperature ^{1}H NMR spectra (500.13 MHz, CD$_3$OD) of **3a**.
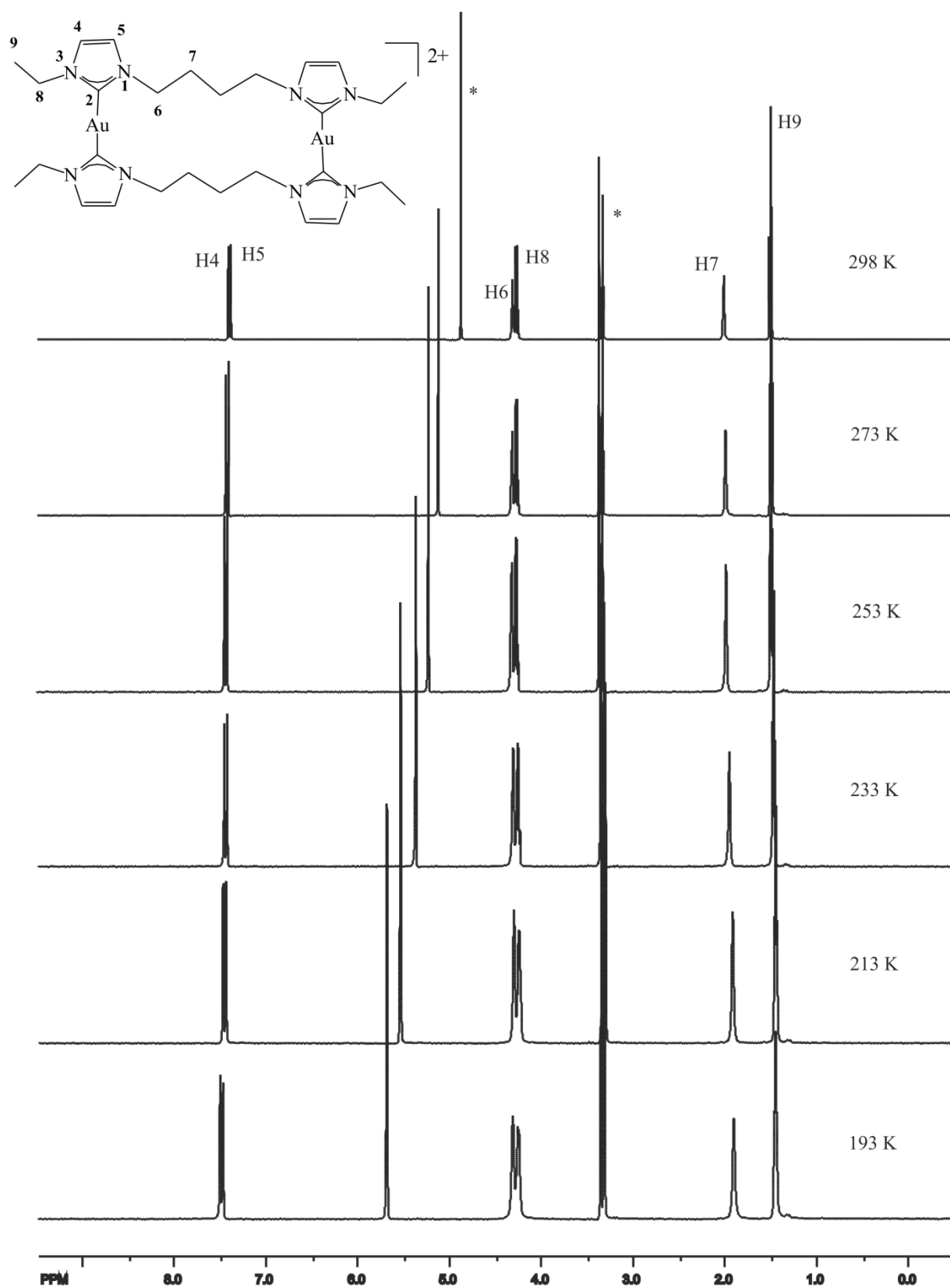
Figure 6.1.4. Low temperature ^{1}H NMR spectra (500.13 MHz, CD$_3$OD) of **4a**.
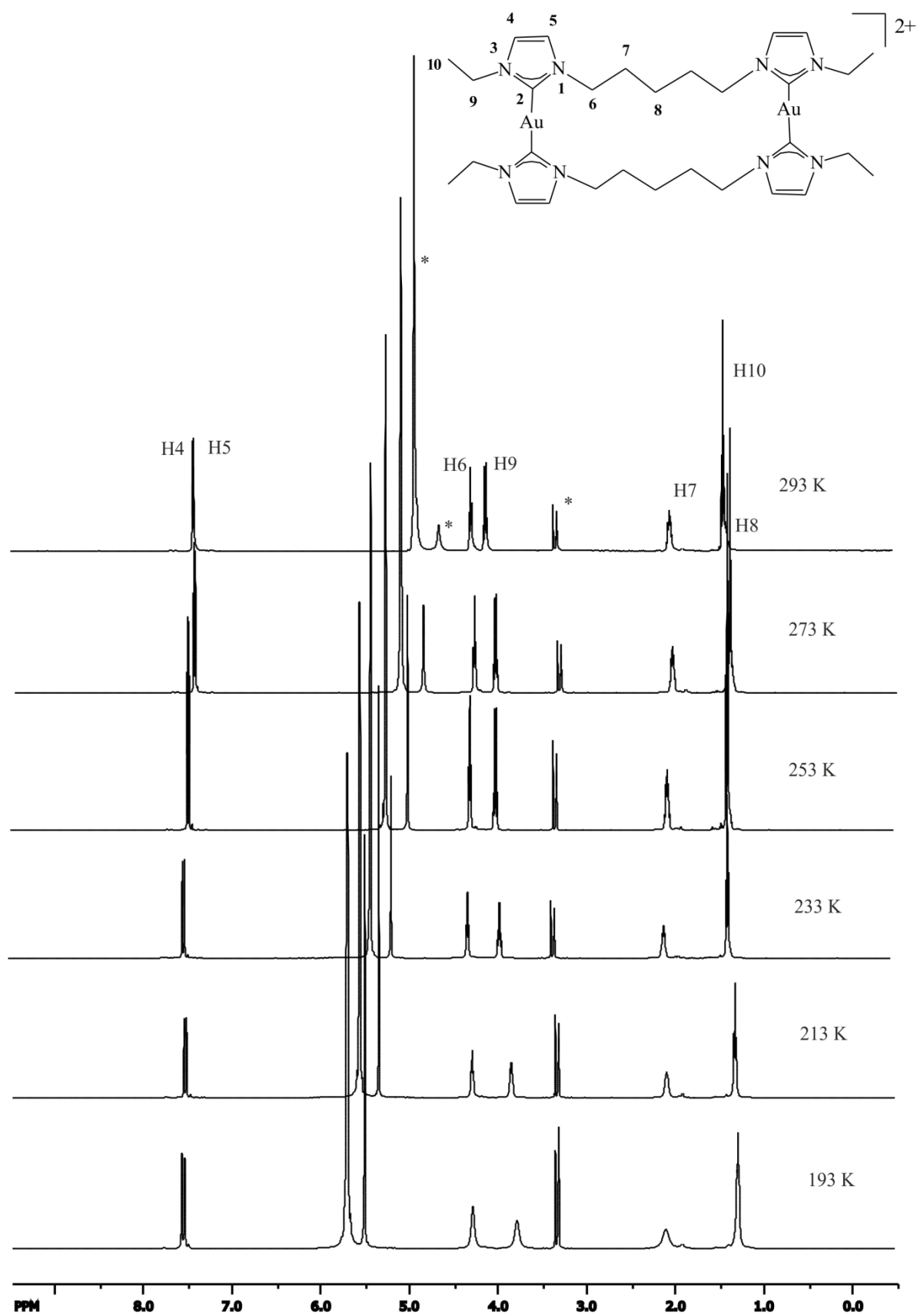
Figure 6.1.5. Low temperature ^{1}H NMR spectra (500.13 MHz, CD$_3$OD) of **6a**.
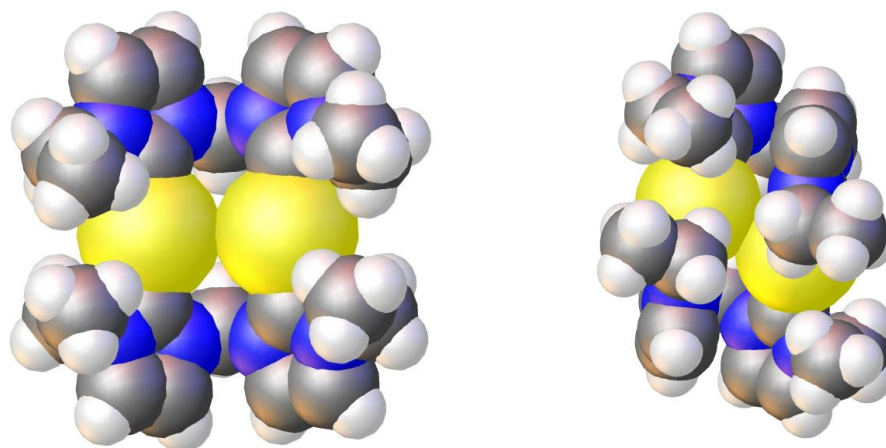
6.1.2. X-ray

Figure 6.1.6. Spacefill drawing of complex **1a** (left) and **2a** (right) of **4b**.

Figure 6.1.7. ORTEP drawing of complex (left) and crystal packing (right, view along no axis) of **4b** (50% probability level for the thermal ellipsoids). Au-Au bound dimers of macrocycles are connected by intermolecular π−π interactions indicated by dotted blue lines. Hydrogen atoms have been omitted for clarity.
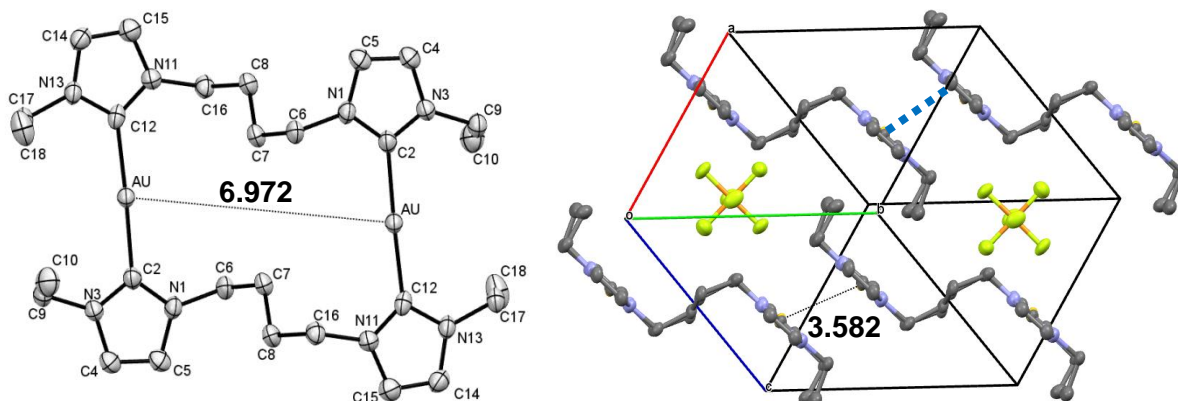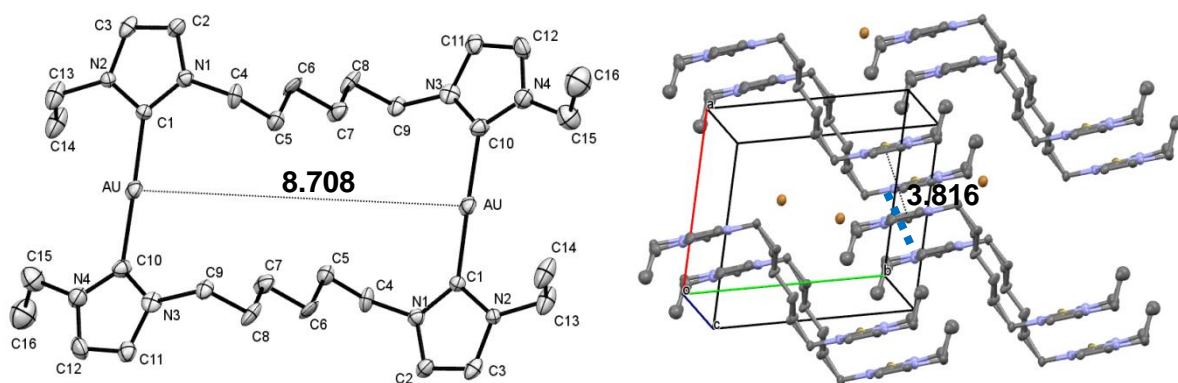

Figure 6.1.8. ORTEP drawing of complex (left) and crystal packing (right, view along no axis) of **6a** (50% probability level for the thermal ellipsoids). Au-Au bound dimers of macrocycles are connected by intermolecular π−π interactions indicated by dotted blue lines. Hydrogen atoms have been omitted for clarity.

Figure 6.1.9. ORTEP drawing of complex (left) and crystal packing (right, view along no axis) of **6b** (50% probability level for the thermal ellipsoids). Dimers of macrocycles are connected by intermolecular π–π interactions indicated by dotted blue lines. Hydrogen atoms have been omitted for clarity.
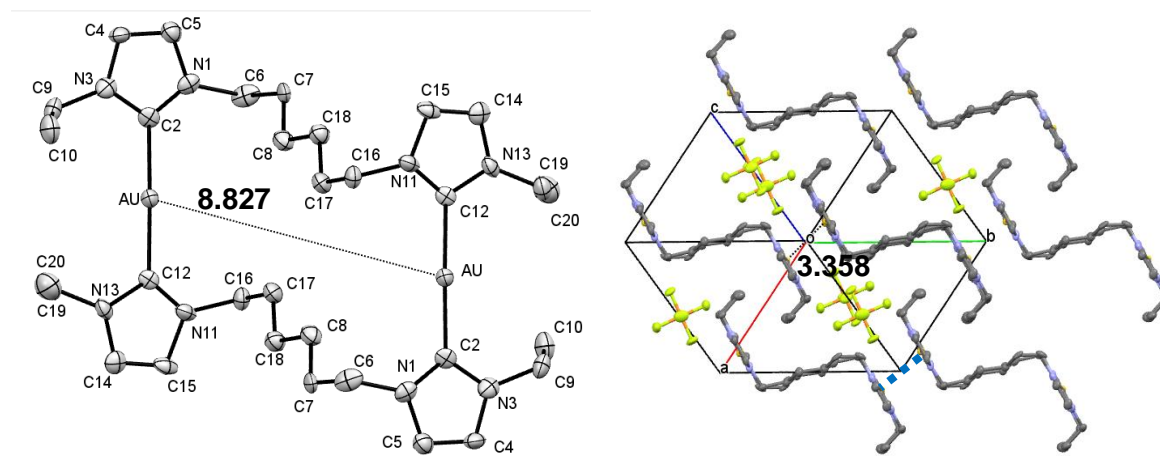
6.1.3. General Experimental Details & Substance Characterization

HPLC-grade solvents were used as received unless otherwise stated. The ligand precursor **1** was synthesized according to the literature procedure[75]. All reactions involving silver compounds were performed with the exclusion of light. NMR spectra were measured on Bruker Avance 300, 400 or 500 instruments. The references for NMR spectra were as follows: ^{1}H (methanol-d3 (3.31 ppm), DMSO-d5 (2.50 ppm), ACN-d2 (1.94 ppm)), ^{13}C{^{1}H} (methanol-d4 (49.0 ppm), DMSO-d6 (39.5 ppm), ACN-d3 (1.3 ppm)). Abbreviations used: br (broad), s (singlet), d (doublet), t (triplet), q (quartet), quint (quintet), sept (septet), m (multiplet). Assignments of ^{1}H and ^{13}C{^{1}H} NMR spectra are based on COSY, HMQC and HMBC experiments, when necessary. Numeration of the cations can be found in the VT-NMR spectra. ESI-MS spectra were measured on Bruker Daltonik microToF-Q. UV/Vis and fluorescence spectra were measured with 10^{-5}mol solutions in ACN in precision cuvettes (SUPRASIL$^®$) with 10 mm thickness. For UV/Vis measurements a Perkin Elmer Lambda 18 was used, for fluorescence a Perkin LS50B. Scan rate was 120 nm/s between 200 nm and 700 nm.

1a. 1 (109.8 mg, 0.3 mmol) and Au(SMe$_2$)Cl (88.37 mg, 0.3 mmol) were dissolved in dry DMF (7 mL). To maintain a clear solution the mixture was heated to 100 °C, if applicable. NaOAc (62.27 mg, 0.75 mmol) was added and the solution was stirred for 2 h at 120 °C. After cooling to room temperature, diethylether (15 mL) was added to precipitate the

complex. The white powder was filtered, washed with diethylether and dried in vacuo. The complex was purified by crystallization (slow diffusion of diethylether into a solution in methanol). Yield 99%. ^{1}H NMR (300 MHz, CD$_3$OD, 25°C): δ=7.74 (s, 4H; H-4), 7.53 (d, ^3J(H,H)=2 Hz, 4H; H-5), 7.21 (d, ^2J(H,H)=14 Hz, 2H; H-6a), 6.31 ppm (d, ^2J(H,H)=14 Hz, 2H; H-6b), 4.31 (q, ^3J(H,H)=7 Hz, 8H; H-7), 1.48 (t, ^3J(H,H)=7 Hz, 8H; H-8); ^{1}H NMR (500 MHz, DMSO-d6, 25°C): δ=7.94 (d, ^3J(H,H)=2 Hz 4H; H-4), 7.71 (d, ^3J(H,H)=2 Hz, 4H; H-5), 7.19 (d, ^2J(H,H)=14 Hz, 2H; H-6a), 6.39 ppm (d, ^2J(H,H)=14 Hz, 2H; H-6b), 4.28 (dq, ^3J(H,H)=7 Hz, ^2J(H,H)=14 Hz, 4H; H-7a), 4.21 (dq, ^3J(H,H)=7 Hz, ^2J(H,H)=14 Hz, 4H; H-7b), 1.39 (t, ^3J(H,H)=7 Hz, 8H; H-8); ^{13}C NMR (75 MHz, CD$_3$OD, 25°C): δ=184.7 (C-2), 123.9 (C-5), 122.8 (C-4), 64.1 (C-6), 48.1 (C-7), 17.2 (C-8). UV/Vis (ACN): λ_{max} (ε)=252, 240, 216 nm; fluorescence (ACN): λ_{ex}=255 nm; λ_{em}=306 nm; ESI (+): m/z (%): 401.2 (100) [M-2Br]$^{2+}$, 881.2 (5) [M−Br]$^+$, HRMS (ESI): m/z calcd for C$_{22}$H$_{32}$Au$_2$N$_8$$^{2+}$: 401.1035 [$M$-2Br]$^{2+}$; found: 401.1037.

1b. 1a (96.2 mg, 0.1 mmol) was dissolved in methanol (3 mL). A solution of KPF$_6$ (36.8 mg, 0.15 mmol) in water (4 mL) was added to precipitate the corresponding complex. The white powder was filtered, washed with water and methanol and dried in vacuo. The complex was purified by crystallization (slow diffusion of diethylether into a solution in acetonitrile). Yield 99%. ^{1}H NMR (300 MHz, CD$_3$CN, 25°C): δ=7.48 (d, ^3J(H,H)=2 Hz, 4H; H-4), 7.32 (d, ^3J(H,H)=2 Hz, 4H; H-5), 6.89 (d, ^2J(H,H)=14 Hz, 2H; H-6a), 6.08 ppm (d, ^2J(H,H)=14 Hz, 2H; H-6b), 4.22 (q, ^3J(H,H)=7 Hz, 8H; H-7), 1.41 (t, ^3J(H,H)=7 Hz, 8H; H-8); ^{1}H NMR (500 MHz, [D6]DMSO, 25°C): δ=7.89 (d, ^3J(H,H)=2 Hz 4H; H-4), 7.69 (d, ^3J(H,H)=2 Hz, 4H; H-5), 7.14 (d, ^2J(H,H)=14 Hz, 2H; H-6a), 6.35 ppm (d, ^2J(H,H)=14 Hz, 2H; H-6b), 4.28 (dq, ^3J(H,H)=7 Hz, ^2J(H,H)=14 Hz, 4H; H-7a), 4.21 (dq, ^3J(H,H)=7 Hz, ^2J(H,H)=14 Hz, 4H; H-7b), 1.38 (t, ^3J(H,H)=7 Hz, 8H; H-8); ^{13}C NMR (75 MHz, CD$_3$CN, 25°C): δ=184.4 (C-2), 123.7 (C-5), 122.4 (C-4), 63.9 (C-6), 47.9 (C-7), 17.1 (C-8); ^{19}F NMR (282 MHz, CD$_3$CN, 25°C): δ=-72.3 (d); ^{31}P NMR (121 MHz, CD$_3$CN, 25°C): δ=-143.1 (sept). UV/Vis (ACN): λ_{max} (ε)=252, 241 nm; fluorescence (ACN): λ_{ex}=255 nm; λ_{em}=305 nm; ESI (+): m/z (%): 401.1 (100) [M-2PF$_6$]$^{2+}$ 947.2 (3) [M−PF$_6$]$^+$; ESI (-): m/z (%): 145.0 (100) [PF_6]$^-$.

1c. 1 (219.7 mg, 0.6 mmol) and Ag$_2$O (139.04 mg, 0.6 mmol) were dissolved in dry DCM (50 mL) and stirred for 24 h. The solid was filtered and the filtrate was concentrated to 10 mL. Diethylether (15 mL) was added to precipitate the complex. The white powder was filtered, washed with diethylether and dried in vacuo. The complex was purified by

crystallization (slow diffusion of diethylether into a solution in ACN). Yield 89%. ^{1}H NMR (400 MHz, [D6]DMSO, 25°C): δ=7.85 (d, ^3J(H,H)=2 Hz, 4H; H-4), 7.53 (d, ^3J(H,H)=2 Hz, 4H; H-5), 6.68 (s, 4H; H-6), 4.18 (q, ^3J(H,H)=7 Hz, 8H; H-7), 1.36 (t, ^3J(H,H)=7 Hz, 8H; H-8); ^{13}C NMR (100 MHz, [D6]DMSO, 25°C): δ=180.5 (C-2), 122.4 (C-5), 121.8 (C-4), 63.2 (C-6), 46.6 (C-7), 16.9 (C-8). ESI (+): m/z (%): 311.1 (100) [M-$2Br$]$^{2+}$, 703.1 (9) [M−Br]$^+$, HRMS (ESI): m/z calcd for $C_{22}H_{32}Ag_2N_8Br^+$: 701.0030 [M-Br]$^+$; found: 701.0026.

2. Ethyldibromide (0.43 mL, 5 mmol) and N-ethylimidazole (1 mL, 10.4 mmol) were dissolved in dry toluene (15 mL) and stirred for 1 d at 110 °C. After cooling to room temperature, the white precipitate was filtered, washed with dry toluene/diethylether and dried in vacuo. Yield 67%. The NMR data agree with those previously reported[76].

2a. **2** (114.0 mg, 0.3 mmol) and Au(SMe$_2$)Cl (88.37 mg, 0.3 mmol) were dissolved in dry DMF (7 mL). To maintain a clear solution the mixture was heated to 100 °C, if applicable. NaOAc (62.27 mg, 0.75 mmol) was added and the solution was stirred for 2 h at 120 °C. After cooling to room temperature, diethylether (15 mL) was added to precipitate the complex. The white powder was filtered, washed with diethylether and dried in vacuo. The complex was purified by crystallization (slow diffusion of diethylether into a solution in methanol). Yield 94%. ^{1}H NMR (300 MHz, CD$_3$OD, 25°C): δ=7.38 (d, ^3J(H,H)=2 Hz, 4H; H-4), 7.33 (d, ^3J(H,H)=2 Hz, 4H; H-5), 4.90 (s, 8H; H-6), 4.23 (q, ^3J(H,H)=7 Hz, 8H; H-7), 1.44 (t, ^3J(H,H)=7 Hz, 8H; H-8); ^{13}C NMR (75 MHz, CD$_3$OD, 25°C): δ=184.4 (C-2), 123.6 (C-5), 122.8 (C-4), 51.5 (C-6), 47.7 (C-7), 17.6 (C-8). UV/Vis (ACN): λ_{max} (ε)=252, 217 nm; fluorescence (ACN): λ_{ex}=255 nm; λ_{em}=364 nm; ESI (+): m/z (%): 415.2 (100) [M-$2Br$]$^{2+}$, 909.2 (2) [M−Br]$^+$, HRMS (ESI): m/z calcd for $C_{24}H_{36}Au_2N_8^{2+}$: 415.1192 [M-2Br]$^{2+}$; found: 415.1197.

2b. **2a** (99.0 mg, 0.1 mmol) was dissolved in methanol (3 mL). A solution of KPF$_6$ (36.8 mg, 0.15 mmol) in water (4 mL) was added to precipitate the corresponding complex. The white powder was filtered, washed with water and methanol and dried in vacuo. The complex was purified by crystallization (slow diffusion of diethylether into a solution in acetonitrile). Yield 99%. ^{1}H NMR (300 MHz, CD$_3$CN, 25°C): δ=7.16 (d, ^3J(H,H)=2 Hz, 4H; H-4), 7.07 (d, ^3J(H,H)=2 Hz, 4H; H-5), 4.75 (s, 8H; H-6), 4.14 (q, ^3J(H,H)=7 Hz, 8H; H-7), 1.37 (t, ^3J(H,H)=7 Hz, 8H; H-8); ^{13}C NMR (75 MHz, CD$_3$CN, 25°C): δ=184.1 (C-2), 123.2 (C-5), 122.6 (C-4), 51.2 (C-6), 47.4 (C-7), 17.4 (C-8); ^{19}F NMR (282 MHz, CD$_3$CN, 25°C): δ=-72.3 (d); ^{31}P NMR (121 MHz, CD$_3$CN, 25°C): δ=-143.1 (sept). UV/Vis (ACN): λ_{max} (ε)=251,

221 nm; fluorescence (ACN): λ_{ex}=255 nm; λ_{em}=365 nm; ESI (+): m/z (%): 415.1 (100) [M-$2PF_6$]$^{2+}$ 975.2 (4) [$M-PF_6$]$^+$; ESI (-): m/z (%): 145.0 (100) [PF_6]$^-$.

2c. **2** (228.1 mg, 0.6 mmol) and Ag_2O (139.04 mg, 0.6 mmol) were dissolved in dry DCM (50 mL) and stirred for 24 h. The solid was filtered and the filtrate was concentrated to 10 mL. Diethylether (15 mL) was added to precipitate the complex. The white powder was filtered, washed with diethylether and dried in vacuo. The complex was purified by crystallization (slow diffusion of diethylether into a solution in ACN). Yield 84%. ^{1}H NMR (400 MHz, [D6]DMSO, 25°C): δ=7.45 (d, ^3J(H,H)=2 Hz, 4H; H-4), 7.30 (d, ^3J(H,H)=2 Hz, 4H; H-5), 4.58 (s, 8H; H-6), 4.06 (q, ^3J(H,H)=7 Hz, 8H; H-7), 1.31 (t, ^3J(H,H)=7 Hz, 8H; H-8); ^{13}C NMR (100 MHz, [D6]DMSO, 25°C): δ=178.8 (C-2), 122.0 (C-5), 121.7 (C-4), 51.4 (C-6), 46.2 (C-7), 17.1 (C-8). ESI (+): m/z (%): 325.1 (100) [M-$2Br$]$^{2+}$, 729.0 (12) [$M-Br$]$^+$, HRMS (ESI): m/z calcd for $C_{24}H_{36}Ag_2N_8{}^{2+}$: 729.0343 [$M$-2Br]$^{2+}$; found: 729.0351.

3. Propyldibromide (0.51 mL, 5 mmol) and N-ethylimidazole (1 mL, 10.4 mmol) were dissolved in dry toluene (15 mL) and stirred for 1 d at 110 °C. After cooling to room temperature, the white precipitate was filtered, washed with dry toluene/diethylether and dried in vacuo. Yield 80%. The NMR data agree with those previously reported[76].

3a. **3** (118.2 mg, 0.3 mmol) and Au(SMe$_2$)Cl (88.37 mg, 0.3 mmol) were dissolved in dry DMF (7 mL). To maintain a clear solution the mixture was heated to 100 °C, if applicable. NaOAc (62.27 mg, 0.75 mmol) was added and the solution was stirred for 2 h at 120 °C. After cooling to room temperature, diethylether (15 mL) was added to precipitate the complex. The white powder was filtered, washed with diethylether and dried in vacuo. The complex was purified by crystallization (slow diffusion of diethylether into a solution in methanol). Yield 97%. ^{1}H NMR (300 MHz, CD$_3$OD, 25°C): δ=7.51 (d, ^3J(H,H)=2 Hz, 4H; H-4), 7.45 (d, ^3J(H,H)=2 Hz, 4H; H-5), 4.37 (t, ^3J(H,H)=6 Hz, 8H; H-6), 4.01 (q, ^3J(H,H)=7 Hz, 8H; H-8), 2.68-2.76 (bm, 4H; H-7), 1.39 (m, 12H; H-9); ^{13}C NMR (75 MHz, CD$_3$OD, 25°C): δ=184.1 (C-2), 123.6 (C-5), 122.4 (C-4), 48.1 (C-6), 47.3 (C-8), 30.8 (C-7), 17.2 (C-9). UV/Vis (ACN): λ_{max} (ε)=260 nm; fluorescence (ACN): λ_{ex}=255 nm; λ_{em}=372 nm; ESI (+): m/z (%): 429.2 (100) [M-$2Br$]$^{2+}$, HRMS (ESI): m/z calcd for $C_{26}H_{40}Au_2N_8{}^{2+}$: 429.1348 [$M$-2Br]$^{2+}$; found: 429.1363.

3b. **3a** (101.8 mg, 0.1 mmol) was dissolved in methanol (3 mL). A solution of KPF$_6$ (36.8 mg, 0.15 mmol) in water (4 mL) was added to precipitate the corresponding complex. The white

powder was filtered, washed with water and methanol and dried in vacuo. The complex was purified by crystallization (slow diffusion of diethylether into a solution in acetonitrile). Yield 99%. ^{1}H NMR (300 MHz, CD_3CN, 25°C): δ=7.25 (d, [3]J(H,H)=2 Hz, 4H; H-4), 7.22 (d, [3]J(H,H)=2 Hz, 4H; H-5), 4.28 (t, [3]J(H,H)=6 Hz, 8H; H-6), 3.92 (q, [3]J(H,H)=7 Hz, 8H; H-8), 2.54-2.61 (bm, 4H; H-7), 1.32 (t, [3]J(H,H)=7 Hz, 12H; H-9); ^{13}C NMR (75 MHz, CD_3CN, 25°C): δ=183.7 (C-2), 123.1 (C-5), 122.0 (C-4), 49.0 (C-6), 46.9 (C-8), 30.2 (C-7), 17.0 (C-9); ^{19}F NMR (282 MHz, CD_3CN, 25°C): δ=-72.3 (d); ^{31}P NMR (121 MHz, CD_3CN, 25°C): δ=-143.1 (sept). UV/Vis (ACN): λ_{max} (ε)=259 nm; fluorescence (ACN): λ_{ex}=255 nm; λ_{em}=372 nm; ESI (+): m/z (%): 429.1 (100) $[M-2PF_6]^{2+}$ 1003.2 (10) $[M-PF_6]^+$; ESI (-): m/z (%): 145.0 (100) $[PF_6]^-$. The NMR data agree with those previously reported[74]. The classification is now non-ambiguous.

3c. **3** (236.5 mg, 0.6 mmol) and Ag_2O (139.04 mg, 0.6 mmol) were dissolved in dry DCM (50 mL) and stirred for 24 h. The solid was filtered and the filtrate was concentrated to 10 mL. Diethylether (15 mL) was added to precipitate the complex. The white powder was filtered, washed with diethylether and dried in vacuo. The complex was purified by crystallization (slow diffusion of diethylether into a solution in ACN).Yield 87%. ^{1}H NMR (400 MHz, [D6]DMSO, 25°C): δ=7.57 (s, 8H; H-4/5), 4.03 (m, 16H; H-6/8), 2.45 (m, 4H; H-7), 1.32 (t, [3]J(H,H)=7 Hz, 12H; H-9); ^{13}C NMR (75 MHz, [D6]DMSO, 25°C): δ=180.7 (C-2), 124.1 (C-5), 120.1 (C-4), 46.6 (C-6), 37.9 (C-8), 29.4 (C-7), 15.4 (C-9). ESI (+): m/z (%): 339.1 (100) $[M-2Br]^{2+}$ 757.1 (12) $[M-Br]^+$, HRMS (ESI): m/z calcd for $C_{26}H_{40}Ag_2N_8Br^+$: 757.0656 $[M-Br]^+$; found: 757.0613.

4. Butyldibromide (0.60 mL, 5 mmol) and N-ethylimidazole (1 mL, 10.4 mmol) were dissolved in dry toluene (15 mL) and stirred for 1 d at 110 °C. After cooling to room temperature, the white precipitate was filtered, washed with dry toluene/diethylether and dried in vacuo. Yield 99%. The NMR data agree with those previously reported[76].

4a. **4** (122.5 mg, 0.3 mmol) and Au(SMe$_2$)Cl (88.37 mg, 0.3 mmol) were dissolved in dry DMF (7 mL). To maintain a clear solution the mixture was heated to 100 °C, if applicable. NaOAc (62.27 mg, 0.75 mmol) was added and the solution was stirred for 2 h at 120 °C. After cooling to room temperature diethylether (15 mL) was added to precipitate the complex. The white powder was filtered, washed with diethylether and dried in vacuo. The complex was purified by crystallization (slow diffusion of diethylether into a solution in methanol). Yield 99%. ^{1}H NMR (400 MHz, CD_3OD, 25°C,): δ=7.40 (m, 8H; H-4/5), 4.31 (bs, 8H; H-6),

4.26 (q, ^3J(H,H)=7 Hz, 8H; H-8), 2.00 (bs, 8H; H-7), 1.48 (t, ^3J(H,H)=7 Hz, 12H; H-9); ^{13}C NMR (75 MHz, CD$_3$OD, 25°C): δ=184.3 (C-2), 123.2 (C-5), 122.7 (C-4), 51.9 (C-6), 47.4 (C-8), 30.1 (C-7), 17.4 (C-9). UV/Vis (ACN): λ_{max} (ε)=259, 232, 219 nm; fluorescence (ACN): λ_{ex}=255 nm; λ_{em}=328 nm; ESI (+): m/z (%): 443.1 (100) $[M$-2Br$]^{2+}$ 965.2 (5) $[M-$Br$]^+$, HRMS (ESI): m/z calcd for C$_{28}$H$_{44}$Au$_2$N$_8$Br$^+$: 965.2198 $[M$-Br$]^+$; found: 965.2202.

4b. 4a (104.4 mg, 0.1 mmol) was dissolved in methanol (3 mL). A solution of KPF$_6$ (36.8 mg, 0.15 mmol) in water (4 mL) was added to precipitate the corresponding complex. The white powder was filtered, washed with water and methanol and dried in vacuo. The complex was purified by crystallization (slow diffusion of diethylether into a solution in acetonitrile). Yield 99%. ^{1}H NMR (300 MHz, CD$_3$CN, 25°C): δ=7.21 (d, ^3J(H,H)=2 Hz, 4H; H-4), 7.16 (d, ^3J(H,H)=2 Hz, 4H; H-5), 4.18 (m, 16H; H-6/8), 1.90 (bs, 8H; H-7), 1.41 (t, ^3J(H,H)=7 Hz, 12H; H-9); ^{13}C NMR (75 MHz, CD$_3$CN, 25°C): δ=184.0 (C-2), 122.8 (C-5), 122.4 (C-4), 51.6 (C-6), 47.1 (C-8), 29.5 (C-7), 17.3 (C-9); ^{19}F NMR (282 MHz, CD$_3$CN, 25°C): δ=-72.3 (d); ^{31}P NMR (121 MHz, CD$_3$CN, 25°C): δ=-143.1 (sept)). UV/Vis (ACN): λ_{max} (ε)=258, 243 nm; fluorescence (ACN): λ_{ex}=255 nm; λ_{em}=377 nm; ESI (+): m/z (%): 443.2 (100) $[M$-2PF$_6]^{2+}$ 1031.3 (4) $[M-$PF$_6]^+$; ESI (-): m/z (%): 145.0 (100) $[PF_6]^-$.

4c. 4 (244.9 mg, 0.6 mmol) and Ag$_2$O (139.04 mg, 0.6 mmol) were dissolved in dry DCM (50 mL) and stirred for 24 h. The solid was filtered and the filtrate was concentrated to 10 mL. Diethylether (15 mL) was added to precipitate the complex. The white powder was filtered, washed with diethylether and dried in vacuo. The complex was purified by crystallization (slow diffusion of diethylether into a solution in ACN).Yield 89%. ^{1}H NMR (400 MHz, [D6]DMSO, 25°C,): δ=7.50 (d, ^3J(H,H)=2 Hz, 4H; H-4), 7.46 (d, ^3J(H,H)=2 Hz, 4H; H-5), 4.13 (m, 16H; H-6/8), 1.78 (bs, 8H; H-7), 1.35 (t, ^3J(H,H)=7 Hz, 12H; H-9); ^{13}C NMR (75 MHz, [D6]DMSO, 25°C): δ=178.5 (C-2), 121.8 (C-5), 121.4 (C-4), 50.3 (C-6), 46.1 (C-8), 28.1 (C-7), 16.9 (C-9). ESI (+): m/z (%): 353.1 (100) $[M$-Br$]^+$ 785.1 (2) $[2M-$Br$]^+$, HRMS (ESI): m/z calcd for C$_{28}$H$_{44}$Ag$_2$N$_8$Br$^+$: 785.0969 $[M$-Br$]^+$; found: 785.0926.

5. Pentyldibromide (0.68 mL, 5 mmol) and N-ethylimidazole (1 mL, 10.4 mmol) were dissolved in dry toluene (15 mL) and stirred for 1 d at 110 °C. After cooling to room temperature, the white precipitate was filtered, washed with dry toluene/diethylether and dried in vacuo. Yield 88%. The NMR data agree with those previously reported[76].

5a. 5 (126.7 mg, 0.3 mmol) and Au(SMe$_2$)Cl (88.37 mg, 0.3 mmol) were dissolved in dry DMF (7 mL). To maintain a clear solution the mixture was heated to 100 °C, if applicable. NaOAc (62.27 mg, 0.75 mmol) was added and the solution was stirred for 2 h at 120 °C. After cooling to room temperature, diethylether (15 mL) was added to precipitate the complex. The white powder was filtered, washed with diethylether and dried in vacuo. The complex was purified by crystallization (slow diffusion of diethylether into a solution in methanol). Yield 99%. ^{1}H NMR (400 MHz, CD$_3$OD, 25°C): δ=7.41 (m, 8H; H-4/5), 4.28 (t, ^3J(H,H)=7 Hz, 8H; H-6), 4.14 (q, ^3J(H,H)=7 Hz, 8H; H-9), 2.02 ppm (quint, ^3J(H,H)=7 Hz, 8H; H-7), 1.43 (t, ^3J(H,H)=7 Hz, 12H; H-10), 1.36-1.40 (bm, 4H, H-8); ^{13}C NMR (100 MHz, CD$_3$OD, 25°C): δ=184.4 (C-2), 122.9 (C-5), 122.8 (C-4), 52.0 (C-6), 47.2 (C-9), 31.9 (C-7), 24.6 (C-8), 17.5 (C-10). UV/Vis (ACN): λ_{max} (ε)=260, 244, 232, 219 nm; fluorescence (ACN): λ_{ex}=255 nm; λ_{em}=333 nm; ESI (+): m/z (%): 457.2 (100) [M-2Br]$^{2+}$, HRMS (ESI): m/z calcd for C$_{30}$H$_{48}$Au$_2$N$_8$$^{2+}$: 457.1661 [$M$-2Br]$^{2+}$; found: 457.1660.

5b. 5a (107.5 mg, 0.1 mmol) was dissolved in methanol (3 mL). A solution of KPF$_6$ (36.8 mg, 0.15 mmol) in water (4 mL) was added to precipitate the corresponding complex. The white powder was filtered, washed with water and methanol and dried in vacuo. The complex was purified by crystallization (slow diffusion of diethylether into a solution in acetonitrile). Yield 99%. ^{1}H NMR (300 MHz, CD$_3$CN, 25°C): δ=7.23 (d, ^3J(H,H)=2 Hz, 4H; H-4), 7.20 (d, ^3J(H,H)=2 Hz, 4H; H-5), 4.18 (t, ^3J(H,H)=7 Hz, 8H; H-6), 4.06 (q, ^3J(H,H)=7 Hz, 8H; H-9), 1.90 (m, 8H; H-7), 1.37 (t, ^3J(H,H)=7 Hz, 12H; H-10), 1.31 (m, 4H, H-8); ^{13}C NMR (75 MHz, CD$_3$CN, 25°C): δ=184.0 (C-2), 122.6 (C-5), 122.4 (C-4), 51.7 (C-6), 46.9 (C-9), 31.3 (C-7), 24.1 (C-8), 17.3 (C-10); ^{19}F NMR (282 MHz, CD$_3$CN, 25°C): δ=-72.3 (d); ^{31}P NMR (121 MHz, CD$_3$CN, 25°C): δ=-143.1 (sept). UV/Vis (ACN): λ_{max} (ε)=261, 245 nm; fluorescence (ACN): λ_{ex}=255 nm; λ_{em}=378 nm; ESI (+): m/z (%): 457.2 (100) [M-2PF$_6$]$^{2+}$ 1059.3 (3) [M−PF$_6$]$^+$; ESI (-): m/z (%): 145.0 (100) [PF_6]$^-$.

5c. 5 (253.3 mg, 0.6 mmol) and Ag$_2$O (139.04 mg, 0.6 mmol) were dissolved in dry DCM (50 mL) and stirred for 24 h. The solid was filtered and the filtrate was concentrated to 10 mL. Diethylether (15 mL) was added to precipitate the complex. The white powder was filtered, washed with diethylether and dried in vacuo. The complex was purified by crystallization (slow diffusion of diethylether into a solution in ACN).Yield 89%. ^{1}H NMR (400 MHz, [D6]DMSO, 25°C): δ=7.49 (d, ^3J(H,H)=2 Hz, 4H; H-4), 7.46 (d, ^3J(H,H)=2 Hz, 4H; H-5), 4.14 (m, 16H; H-6/9), 1.81 ppm (m, 8H; H-7), 1.35 (t, ^3J(H,H)=7 Hz, 12H; H-10),

1.22 (m, 4H, H-8); ^{13}C NMR (100 MHz, [D6]DMSO, 25°C): δ=178.9 (C-2), 121.6 (C-5), 121.4 (C-4), 50.6 (C-6), 46.0 (C-9), 30.3 (C-7), 22.7 (C-8), 16.9 (C-10 ESI (+): m/z (%): 367.1 (100) $[M\text{-}2Br]^{2+}$ 813.1 (2) $[M-Br]^+$, HRMS (ESI): m/z calcd for $C_{30}H_{48}Ag_2N_8Br^+$: 813.1282 $[M\text{-}Br]^+$; found: 813.1227.

6. Hexyldibromide (0.76 mL, 5 mmol) and N-ethylimidazole (1 mL, 10.4 mmol) were dissolved in dry toluene (15 mL) and stirred for 1 d at 110 °C. After cooling to room temperature, the white precipitate was filtered, washed with dry toluene/diethylether and dried in vacuo. Yield 86%. The NMR data agree with those previously reported[76].

6a. 6 (130.9 mg, 0.3 mmol) and Au(SMe$_2$)Cl (88.37 mg, 0.3 mmol) were dissolved in dry DMF (7 mL). To maintain a clear solution the mixture was heated to 100 °C, if applicable. NaOAc (62.27 mg, 0.75 mmol) was added and the solution was stirred for 3 h at 120 °C. After cooling to room temperature, diethylether (15 mL) was added to precipitate the complex. The white powder was filtered, washed with diethylether and dried in vacuo. The complex was purified by crystallization (slow diffusion of diethylether into a solution in methanol). Yield 98%. ^{1}H NMR (400 MHz, CD$_3$OD, 25°C): δ=7.39 (m, 8H; H-4/5), 4.24-4.31 (bm, 16H; H-6/9), 1.92 (bs, 8H; H-7), 1.51 (t, ^3J(H,H)=7 Hz, 12H; H-10), 1.41 (bs, 8H, H-8); ^{13}C NMR (100 MHz, CD$_3$OD, 25°C): δ=184.4 (C-2), 123.0 (C-5), 122.6 (C-4), 52.3 (C-6), 47.3 (C-9), 32.9 (C-7), 27.8 (C-8), 17.4 (C-10). UV/Vis (ACN): λ_{max} (ε)=260, 245, 232, 218 nm; fluorescence (ACN): λ_{ex}=255 nm; λ_{em}=328 nm; ESI (+): m/z (%): 471.2 (100) $[M\text{-}2Br]^{2+}$, HRMS (ESI): m/z calcd for $C_{32}H_{52}Au_2N_8^{2+}$: 471.1818 $[M\text{-}2Br]^{2+}$; found: 471.1816.

6b. 6a (110.3 mg, 0.1 mmol) was dissolved in methanol (3 mL). A solution of KPF$_6$ (36.8 mg, 0.15 mmol) in water (4 mL) was added to precipitate the corresponding complex. The white powder was filtered, washed with water and methanol and dried in vacuo. The complex was purified by crystallization (slow diffusion of diethylether into a solution in acetonitrile). Yield 99%. ^{1}H NMR (400 MHz, CD$_3$CN, 25°C): δ=7.21 (d, ^3J(H,H)=2 Hz, 4H; H-4), 7.18 (d, ^3J(H,H)=2 Hz, 4H; H-5), 4.19 (m, 16H; H-6/9), 1.84 (bs, 8H; H-7), 1.45 (t, ^3J(H,H)=7 Hz, 12H; H-10), 1.33 (bs, 8H, H-8); ^{13}C NMR (75 MHz, CD$_3$CN, 25°C): δ=184.1 (C-2), 122.9 (C-5), 122.6 (C-4), 52.1 (C-6), 47.1 (C-9), 32.3 (C-7), 27.2 (C-8), 17.3 (C-10); ^{19}F NMR (282 MHz, CD$_3$CN, 25°C): δ=-72.3 (d); ^{31}P NMR (121 MHz, CD$_3$CN, 25°C): δ=-143.1 (sept). UV/Vis (ACN): λ_{max} (ε)=260, 244 nm; fluorescence (ACN): λ_{ex}=255 nm; λ_{em}=382 nm; ESI (+): m/z (%): 471.2 (100) $[M\text{-}2PF_6]^{2+}$; ESI (-): m/z (%): 145.0 (100) $[PF_6]^-$.

6c. 6 (261.7 mg, 0.6 mmol) and Ag_2O (139.04 mg, 0.6 mmol) were dissolved in dry DCM (50 mL) and stirred for 24 h. The solid was filtered and the filtrate was concentrated to 10 mL. Diethylether (15 mL) was added to precipitate the complex. The white powder was filtered, washed with diethylether and dried in vacuo. The complex was purified by crystallization (slow diffusion of diethylether into a solution in ACN).Yield 88%. ^{1}H NMR (400 MHz, [D6]DMSO, 25°C): δ=7.53 (d, ^3J(H,H)=2 Hz, 4H; H-4), 7.49 (d, ^3J(H,H)=2 Hz, 4H; H-5), 4.15 (m, 16H; H-6/9), 1.77 (bs, 8H; H-7), 1.40 (t, ^3J(H,H)=7 Hz, 12H; H-10), 1.23 (bs, 8H, H-8); ^{13}C NMR (100 MHz, [D6]DMSO, 25°C): δ=178.6 (C-2), 122.6 (C-5), 122.4 (C-4), 50.3 (C-6), 46.5 (C-9), 28.8 (C-7), 26.2 (C-8), 15.2 (C-10). ESI (+): m/z (%): 381.1 (100) $[M\text{-}2Br]^{2+}$ 841.2 (3) $[M\text{-}Br]^+$, HRMS (ESI): m/z calcd for $C_{32}H_{52}Ag_2N_8Br^+$: 841.1595 $[M\text{-}Br]^+$; found: 841.1625.

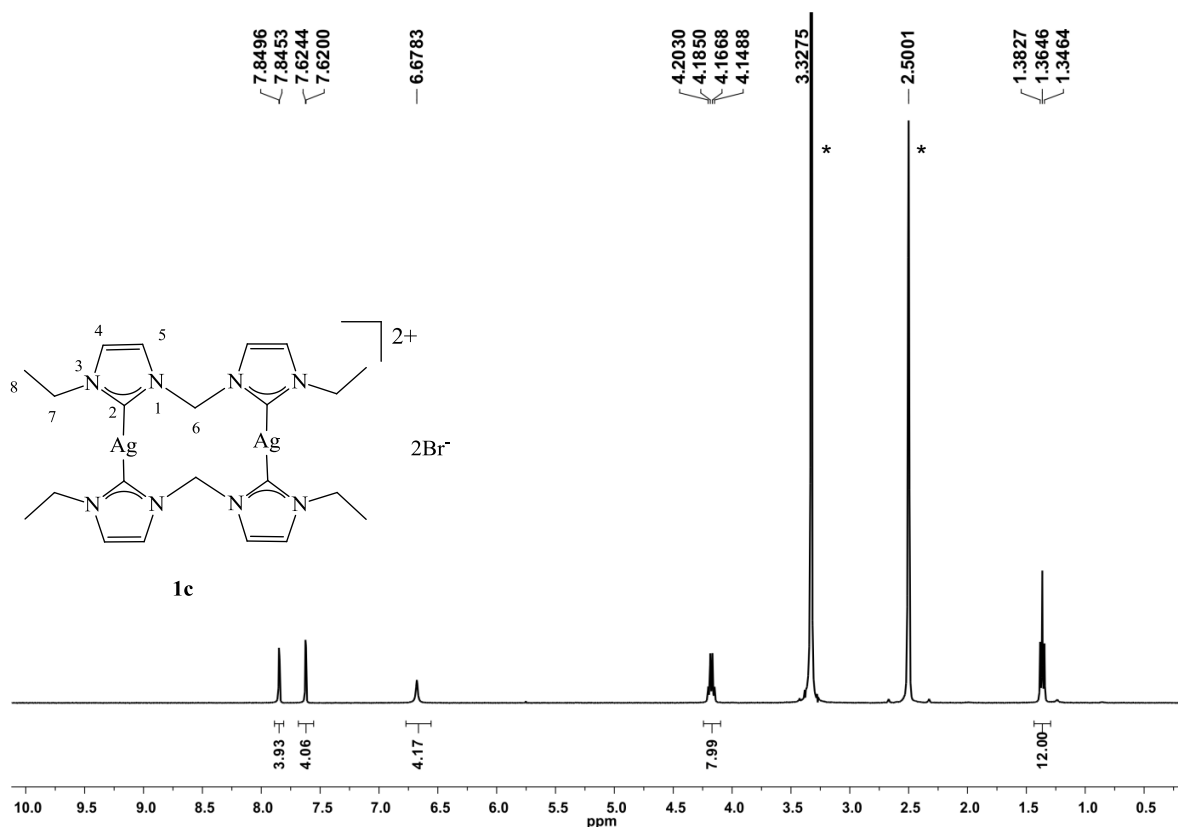Characterization of unpublished substances without VT-NMR spectra

Figure 6.1.10. ^{1}H NMR (400 MHz, [D6]DMSO, r. t.) spectrum of **1c**. *partially deuterated and undeuterated DMSO and water, respectively.
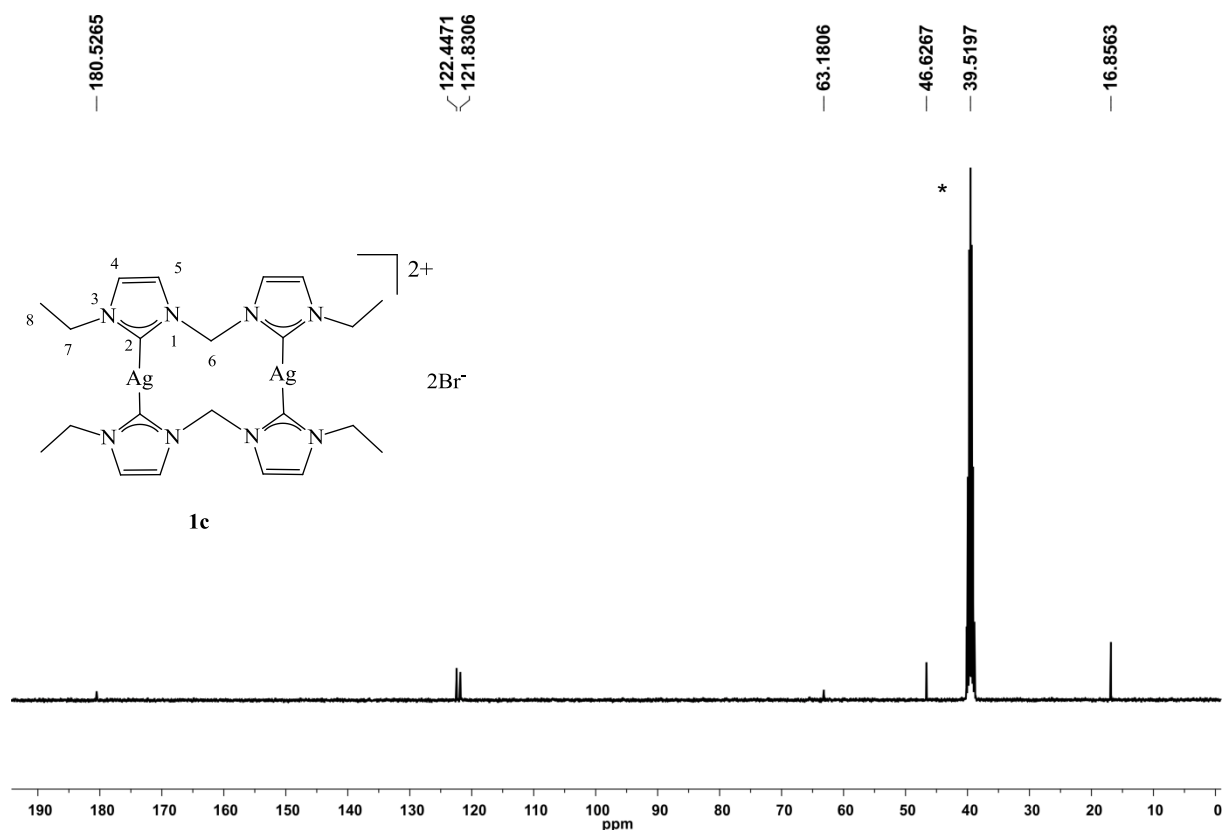
Figure 6.1.11. ^{13}C NMR (100 MHz, [D6]DMSO, r. t.) spectrum of **1c**. *partially deuterated and undeuterated DMSO, respectively.
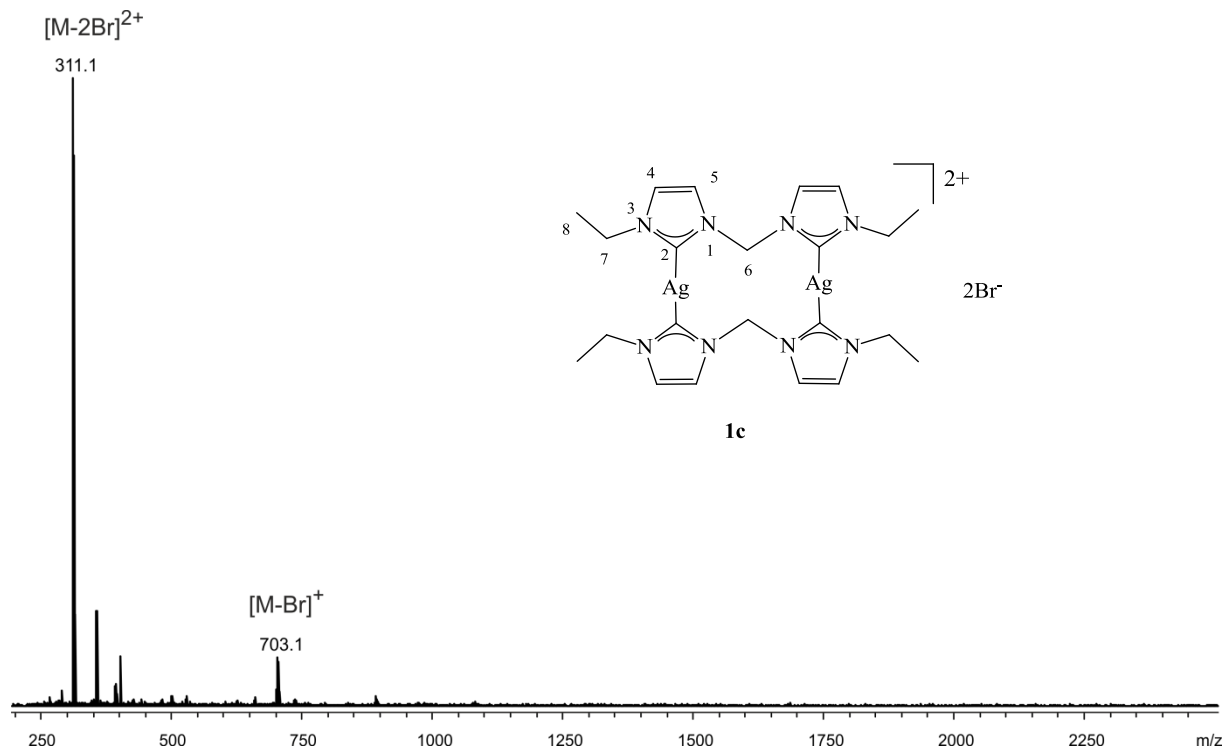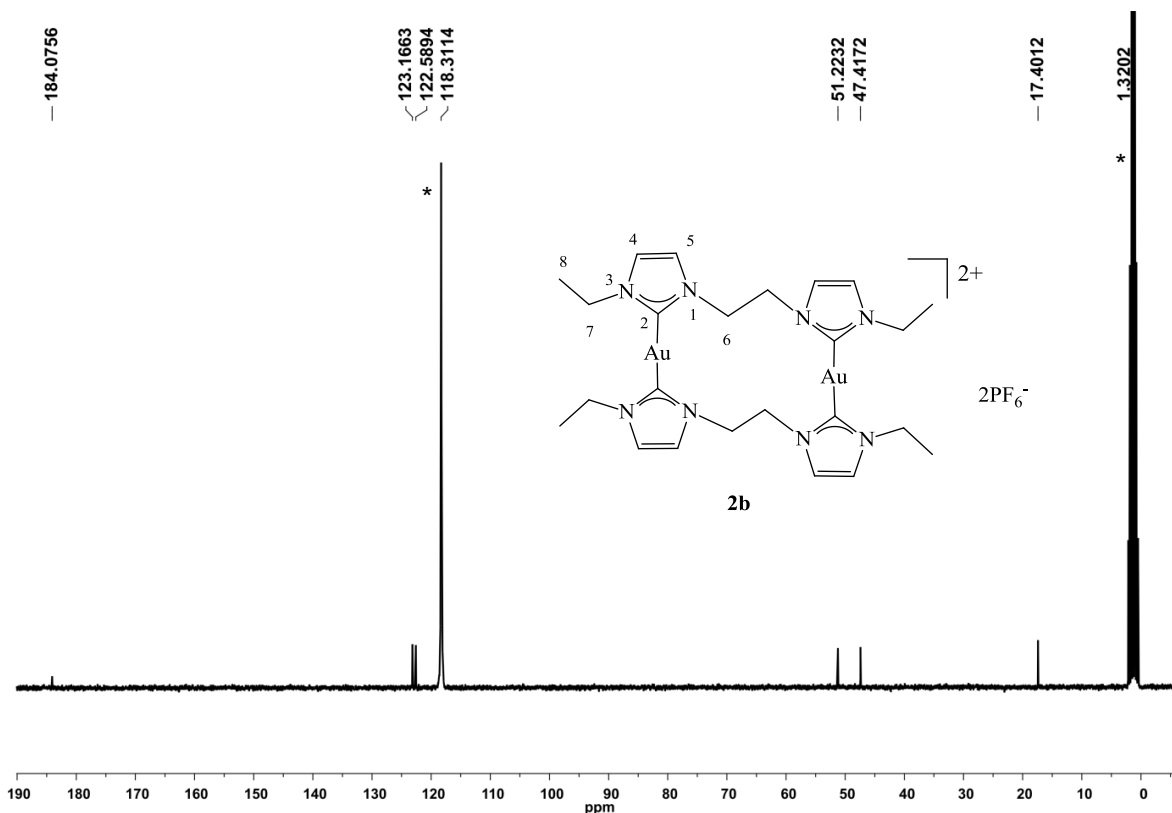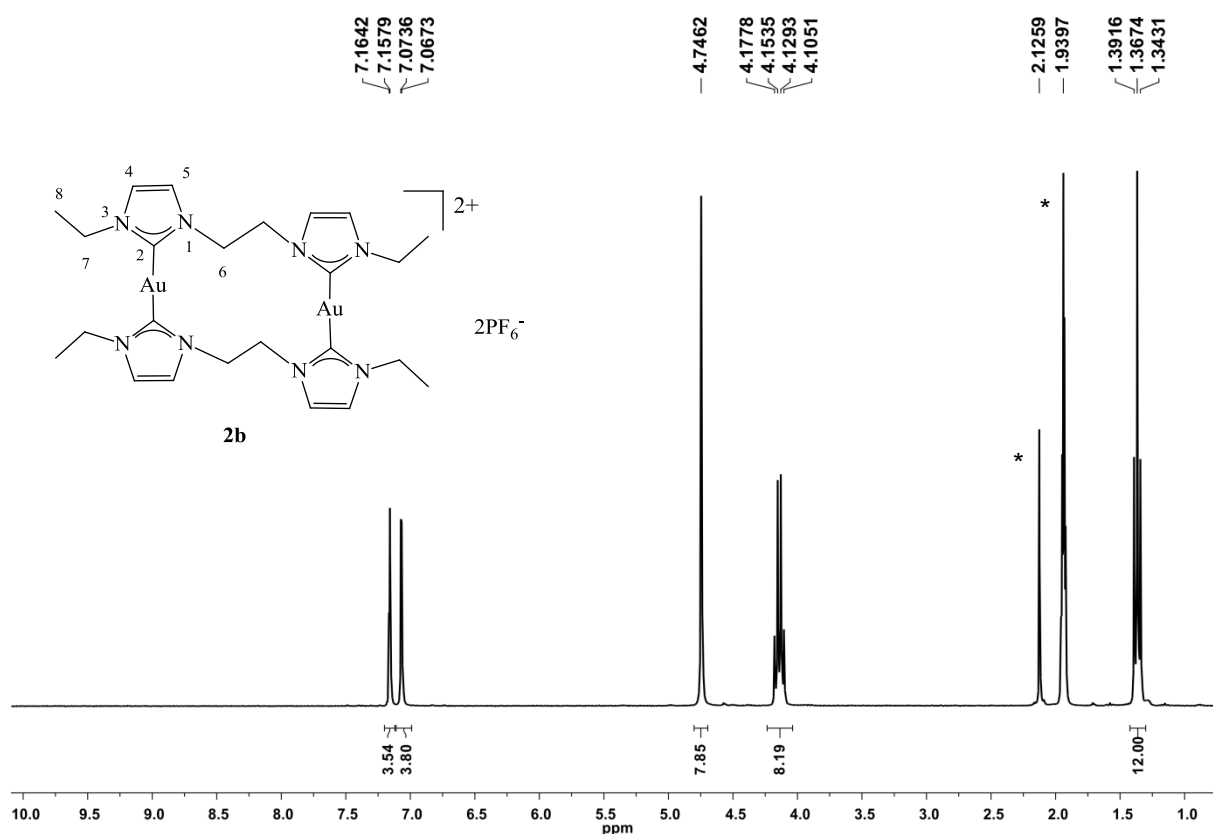

Figure 6.1.12. microTof-Q ESI(+) mass spectrum of **1c** in ACN. *memory signal, respectively.

Figure 6.1.13. ^{1}H NMR (300 MHz, CD$_3$CN, r. t.) spectrum of **2b**. *partially deuterated and undeuterated ACN and water, respectively.

Figure 6.1.14. ^{13}C NMR (75 MHz, CD$_3$CN, r. t.) spectrum of **2b**. *partially deuterated and undeuterated ACN, respectively.
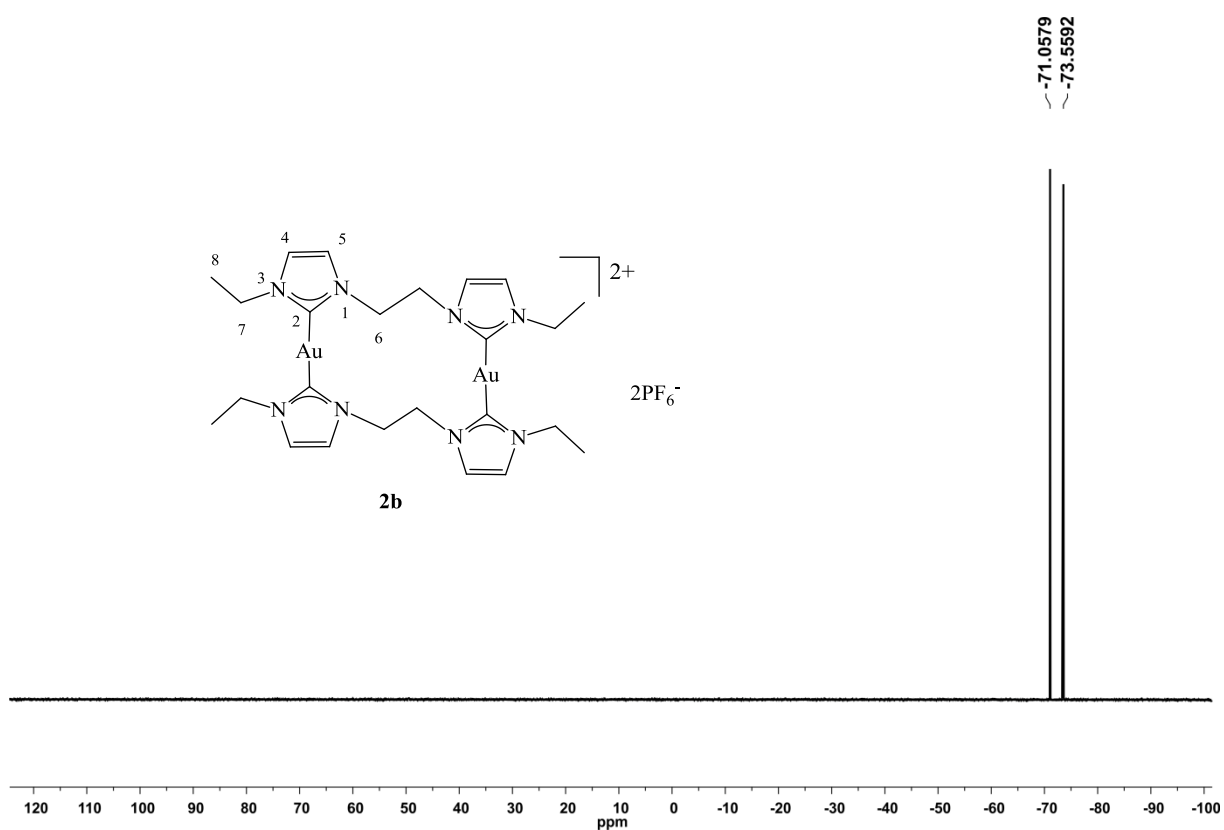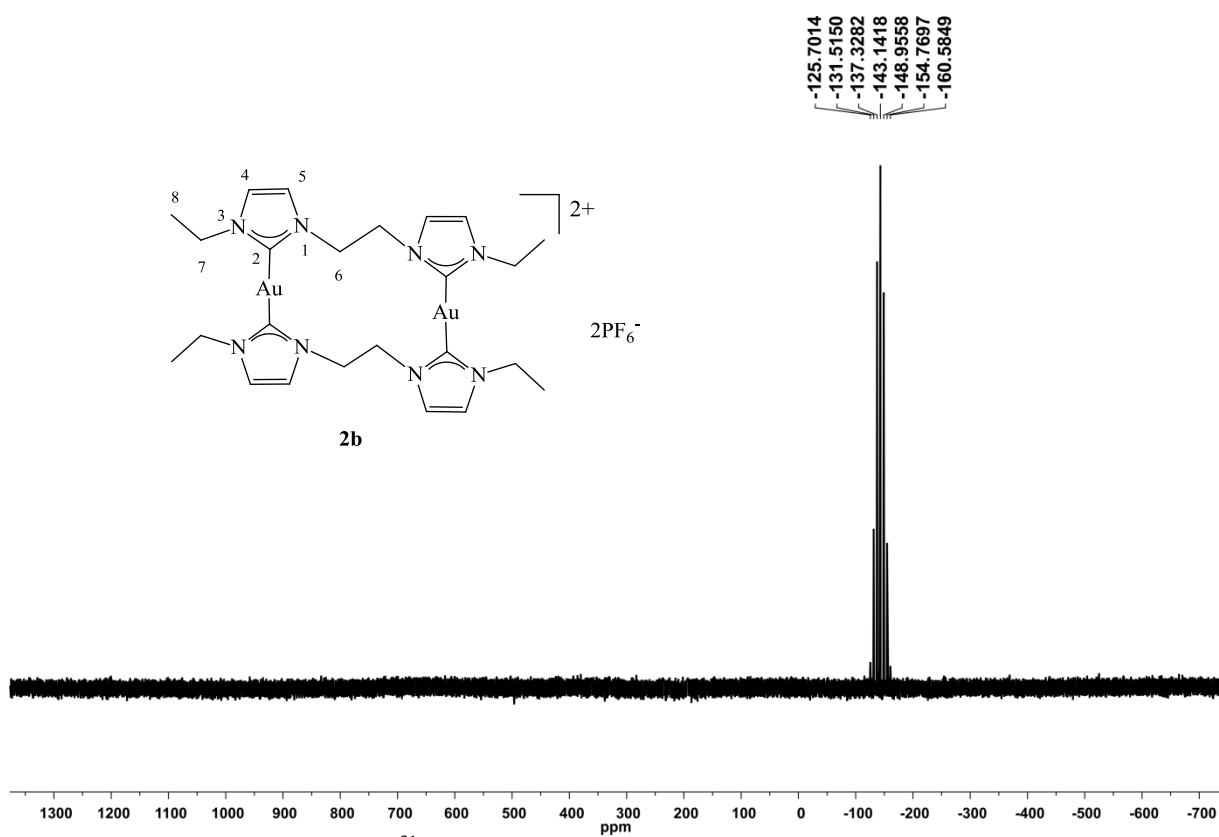
Figure 6.1.15. ^{19}F NMR (282 MHz, CD3CN, r. t.) spectrum of **2b**.

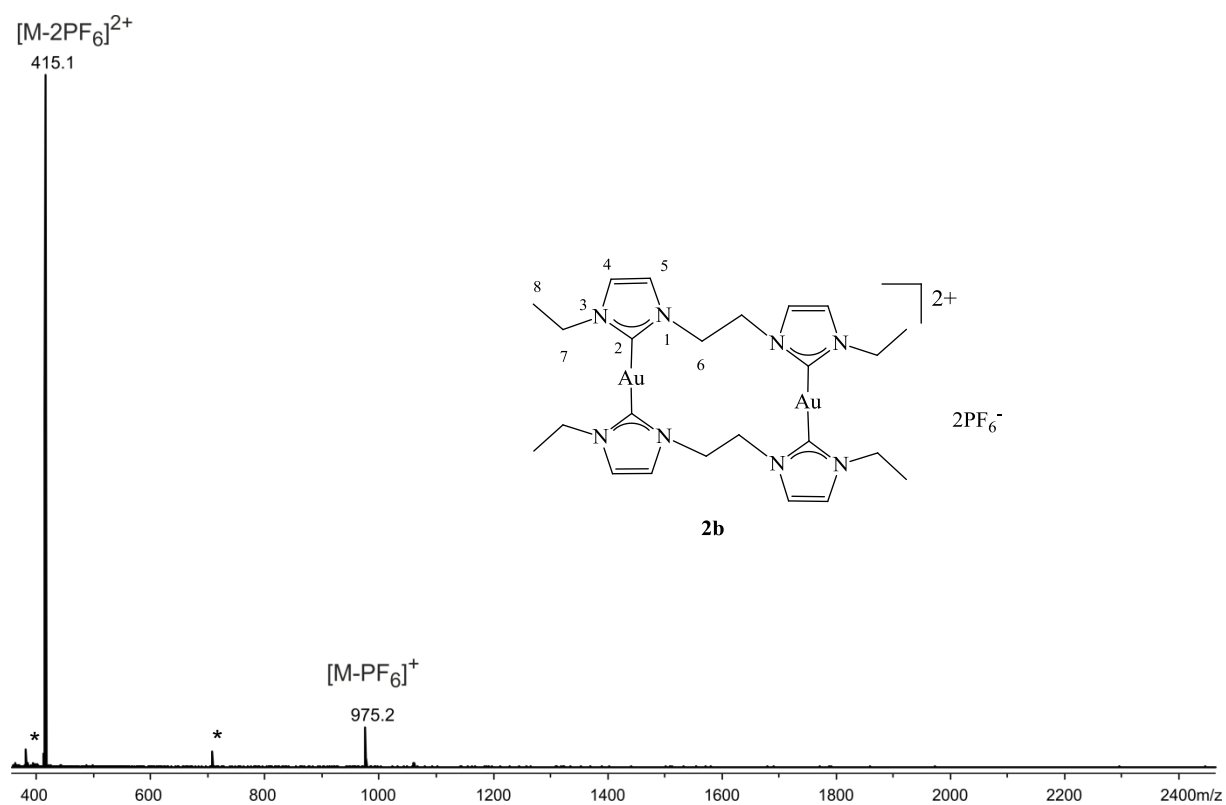**Figure 6.1.16.** ^{31}P NMR (121 MHz, CD$_3$CN, r. t.) spectrum of **2b**.

$[M-2PF_6]^{2+}$
415.1

$[M-PF_6]^+$
975.2

2b

$2PF_6^-$

Figure 6.1.17. microTof-Q ESI(+) mass spectrum of **2b** in ACN. *memory signal, respectively.

$[PF_6]^-$
145.0

2b

$2PF_6^-$

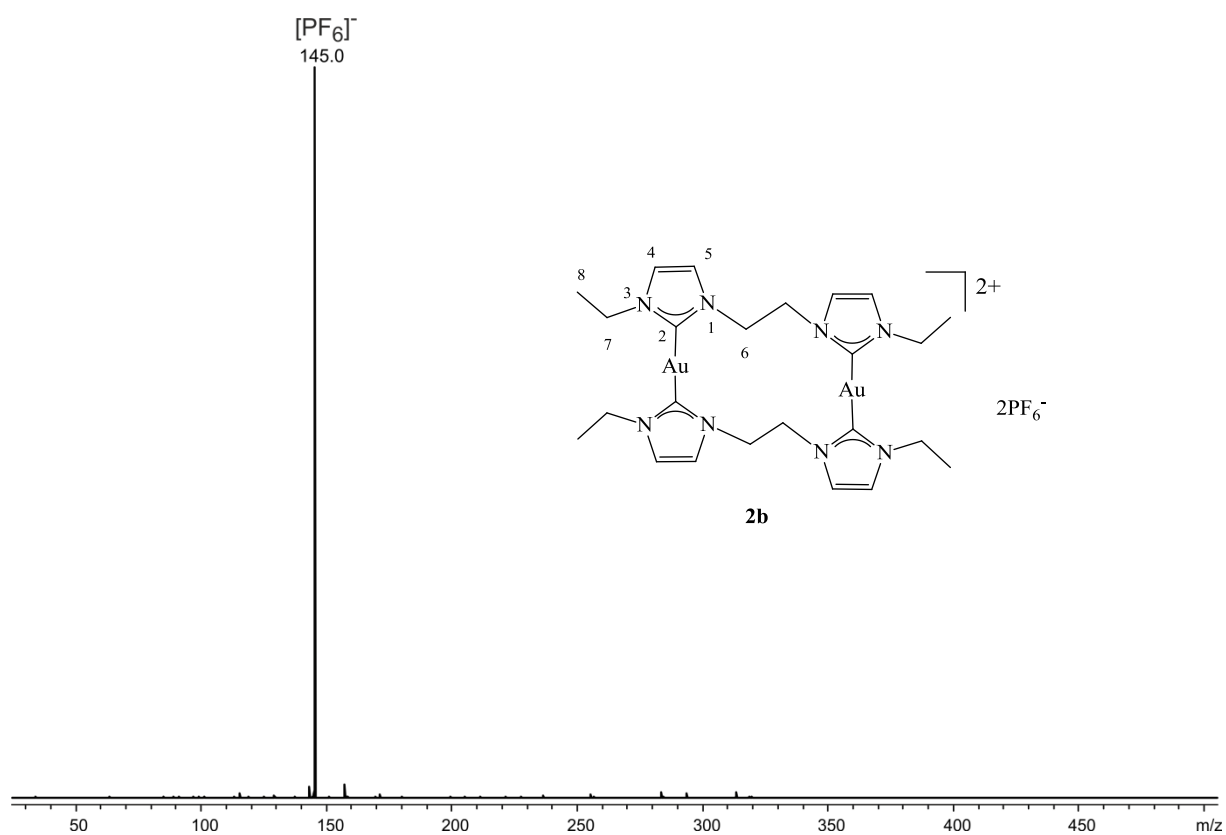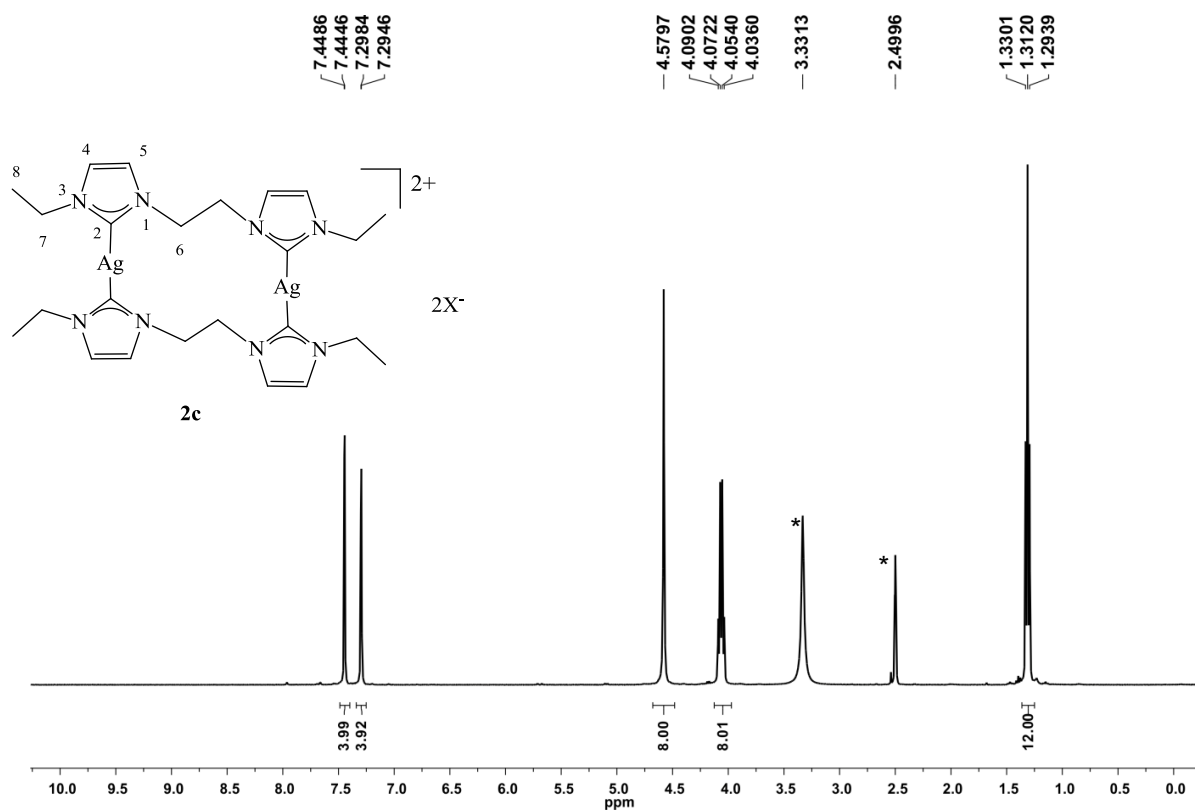**Figure 6.1.18.** microTof-Q ESI(-) mass spectrum of **2b** in ACN.

Figure 6.1.19. ^{1}H NMR (400 MHz, [D6]DMSO, r. t.) spectrum of **2c**. *partially deuterated and undeuterated DMSO and water, respectively.

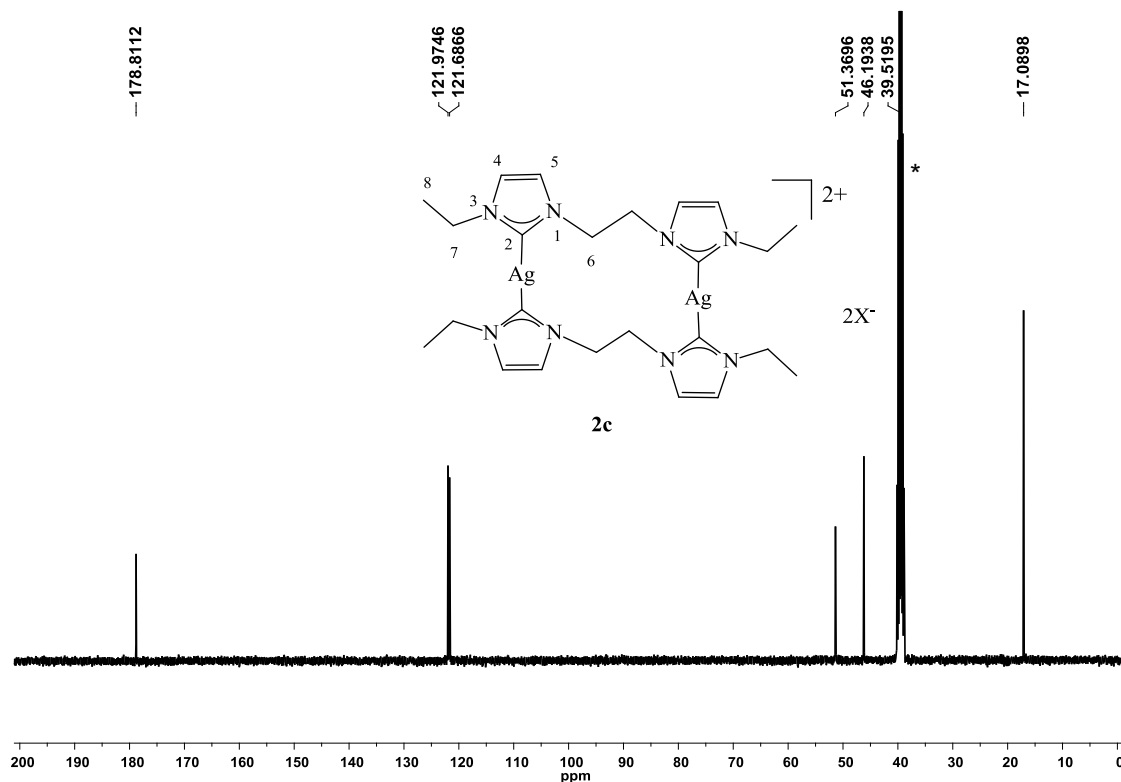**Figure 6.1.20.** ^{13}C NMR (100 MHz, [D6]DMSO, r. t.) spectrum of **2c**. *partially deuterated and undeuterated DMSO, respectively.
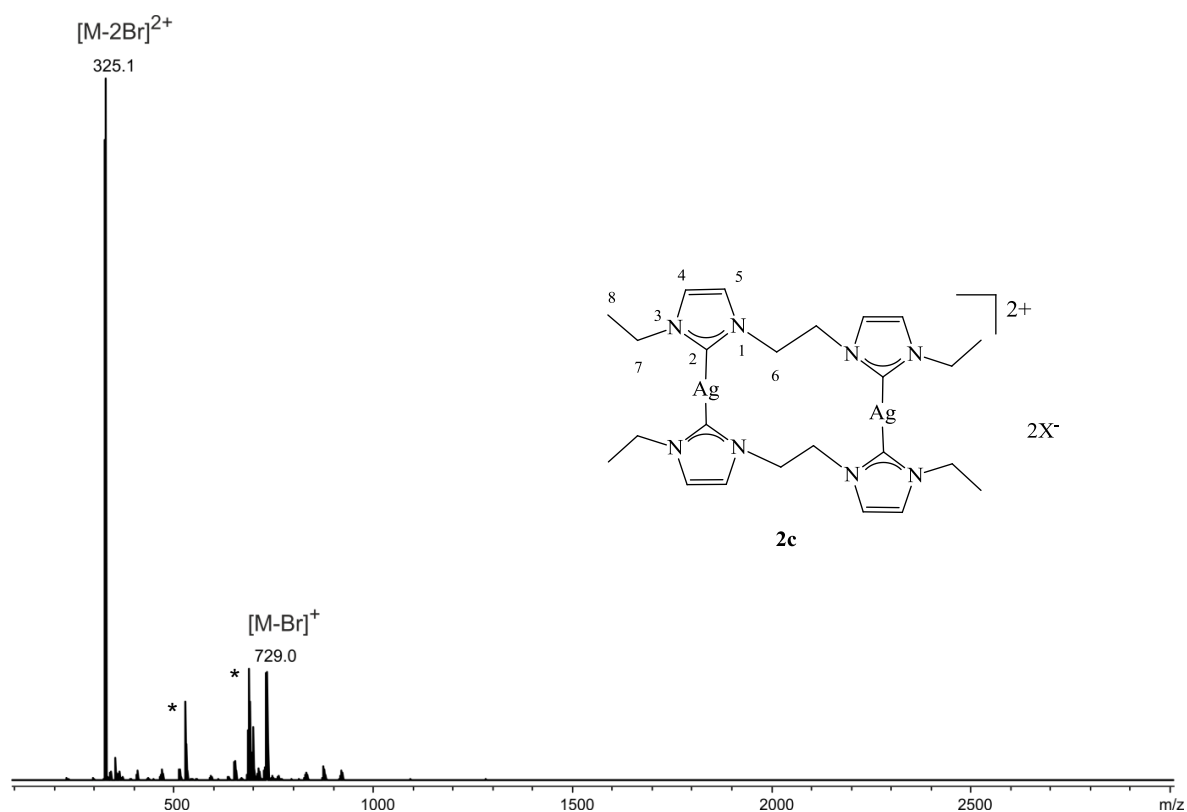
Figure 6.1.21. microTof-Q ESI(+) mass spectrum of **2c** in ACN. *memory signal, respectively.

Figure 6.1.22. ¹H NMR (300 MHz, CD₃CN, r. t.) spectrum of **3b**. *partially deuterated and undeuterated ACN and water, respectively.

Figure 6.1.23. ^{13}C NMR (75 MHz, CD$_3$CN, r. t.) spectrum of **3b**. *partially deuterated and undeuterated ACN, respectively.

Figure 6.1.24. ^{19}F NMR (282 MHz, CD$_3$CN, r. t.) spectrum of **3b**.

Figure 6.1.25. ^{31}P NMR (121 MHz, CD$_3$CN, r. t.) spectrum of **3b**.

Figure 6.1.26. microTof-Q ESI(+) mass spectrum of **3b** in ACN.
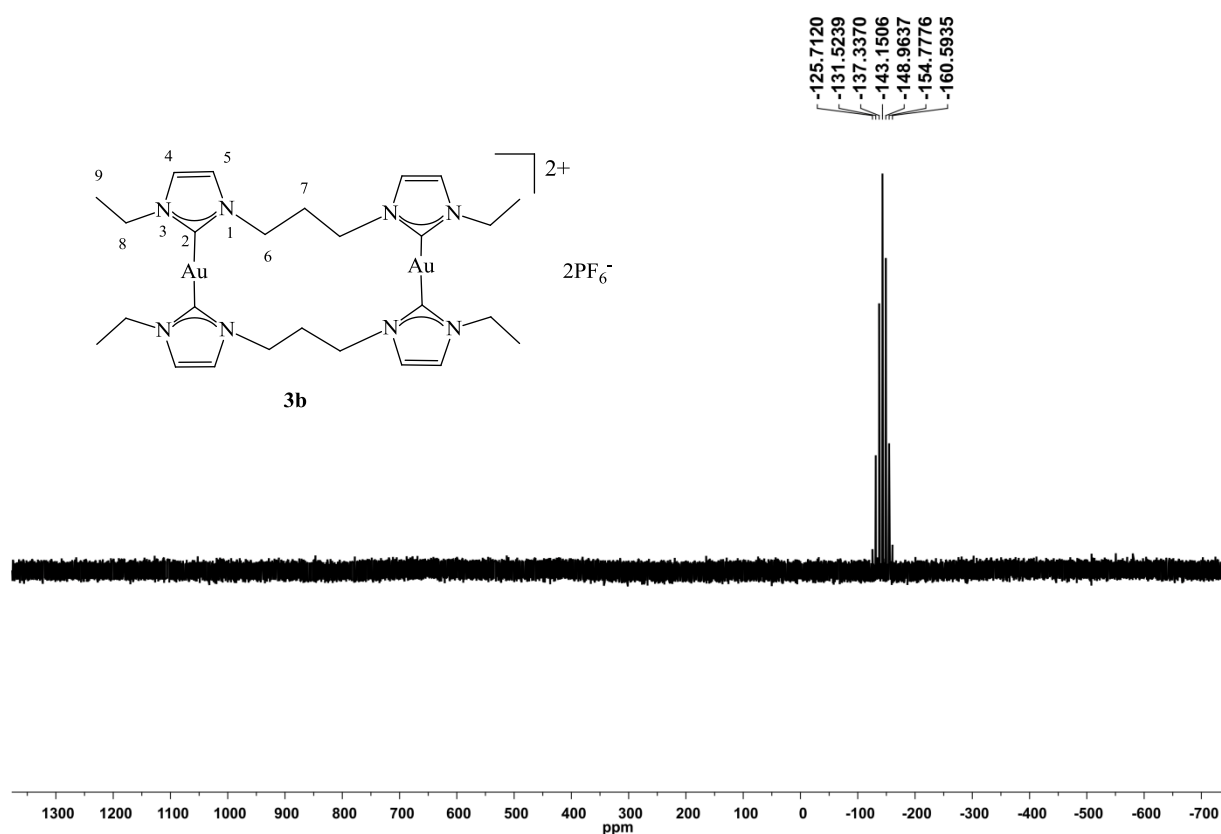
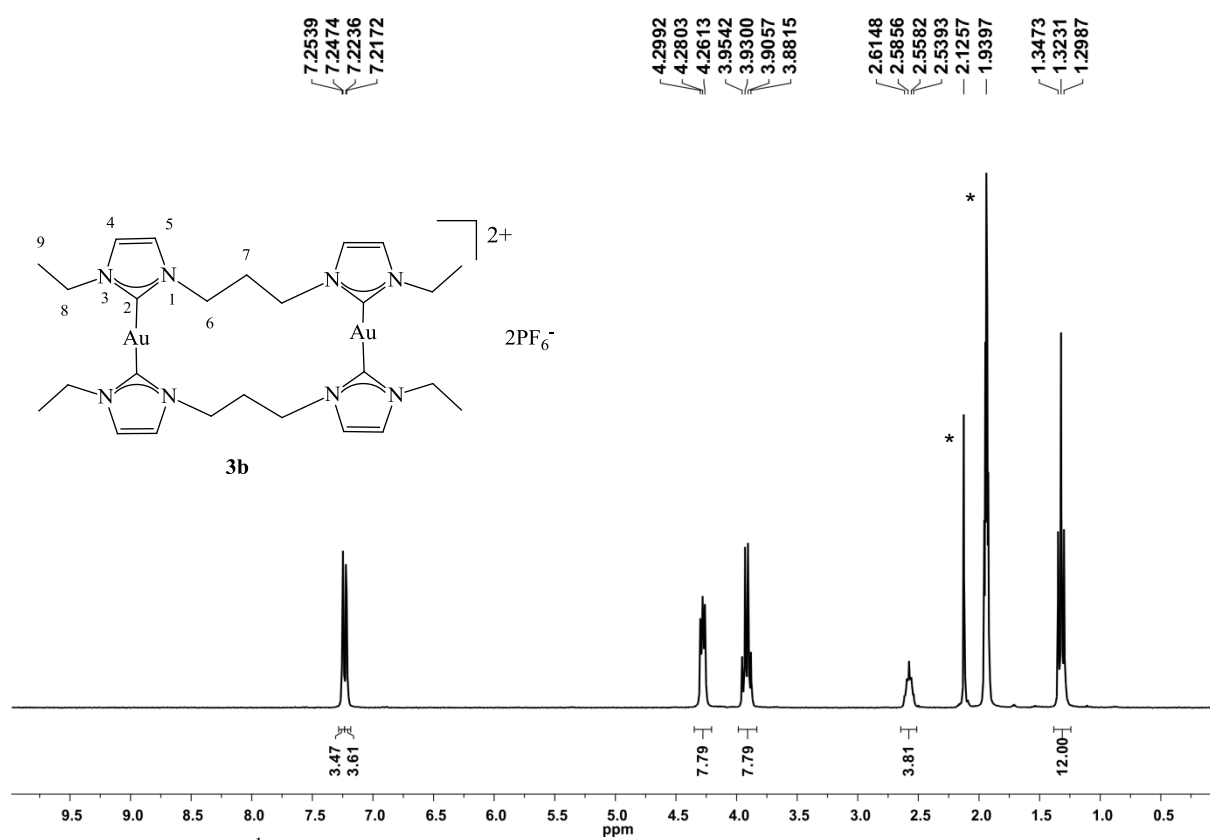**Figure 6.1.27.** microTof-Q ESI(-) mass spectrum of **3b** in ACN.

Figure 6.1.28. ^{1}H NMR (300 MHz, CD$_3$CN, r. t.) spectrum of **4b**. *partially deuterated and undeuterated ACN and water, respectively.
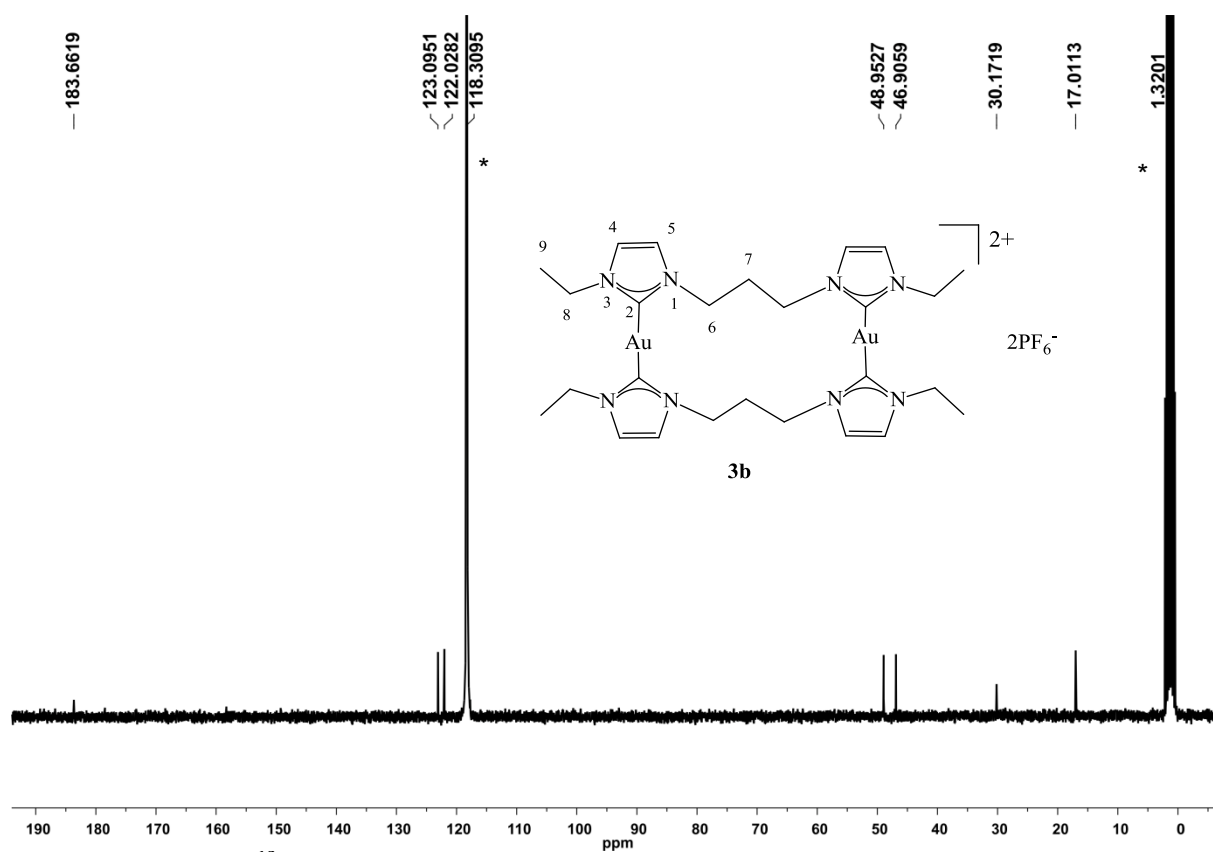
Figure 6.1.29. ^{13}C NMR (75 MHz, CD$_3$CN, r. t.) spectrum of **4b**. *partially deuterated and undeuterated ACN, respectively.

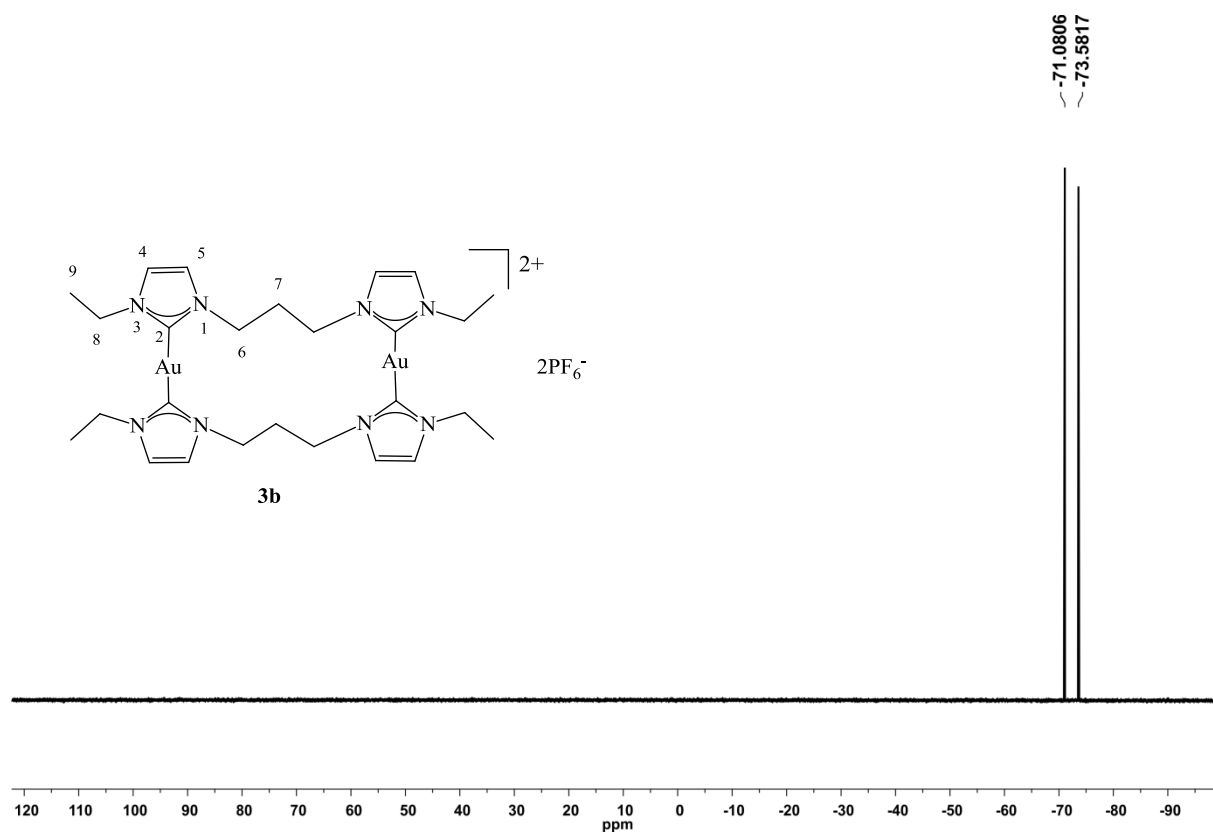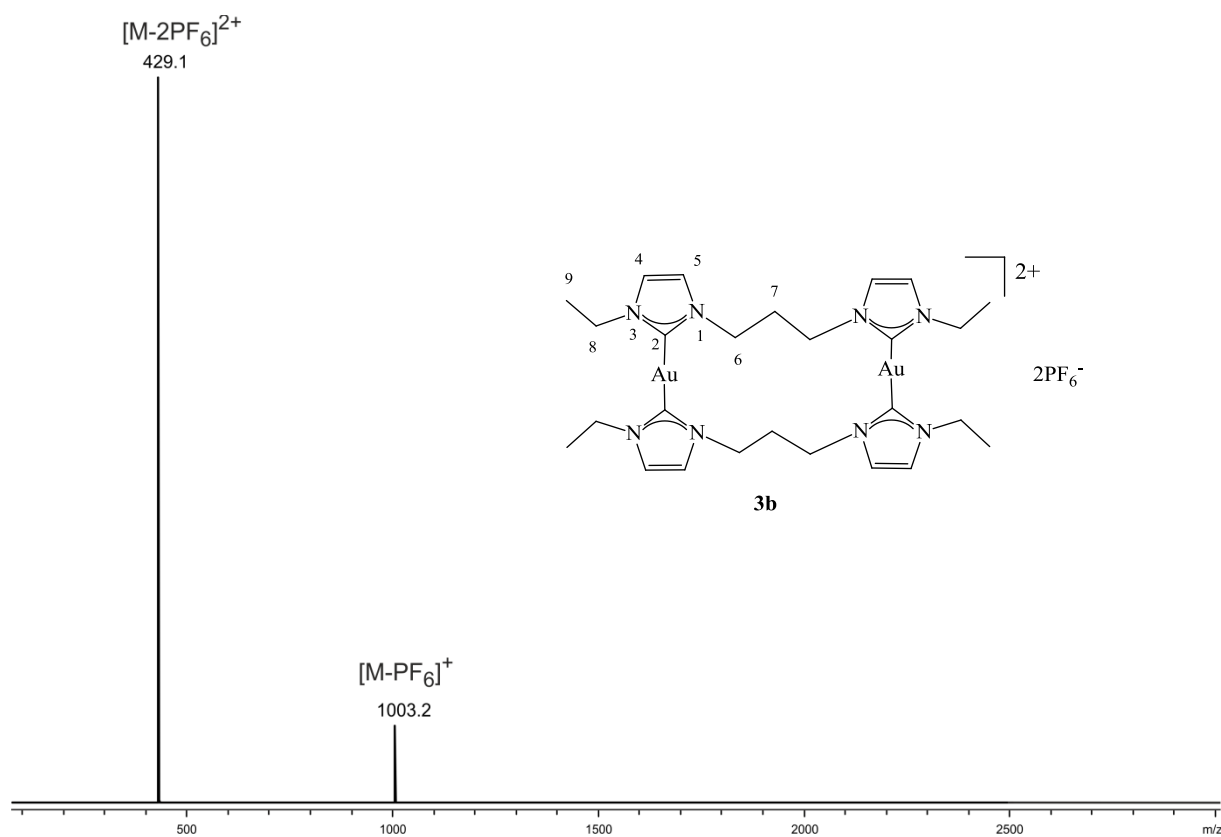
Figure 6.1.30. ^{19}F NMR (282 MHz, CD$_3$CN, r. t.) spectrum of **4b**.

Figure 6.1.31. ^{31}P NMR (121 MHz, CD$_3$CN, r. t.) spectrum of **4b**.

Figure 6.1.32. microTof-Q ESI(+) mass spectrum of **4b** in ACN. *memory signal.

Figure 6.1.33. microTof-Q ESI(-) mass spectrum of **4b** in ACN.

Figure 6.1.34. ¹H NMR (400 MHz, [D6]DMSO, r. t.) spectrum of **4c**. *partially deuterated and undeuterated DMSO and water, respectively.

Figure 6.1.35. ^{13}C NMR (100 MHz, [D6]DMSO, r. t.) spectrum of **4c**. *partially deuterated and undeuterated DMSO-d6, respectively.
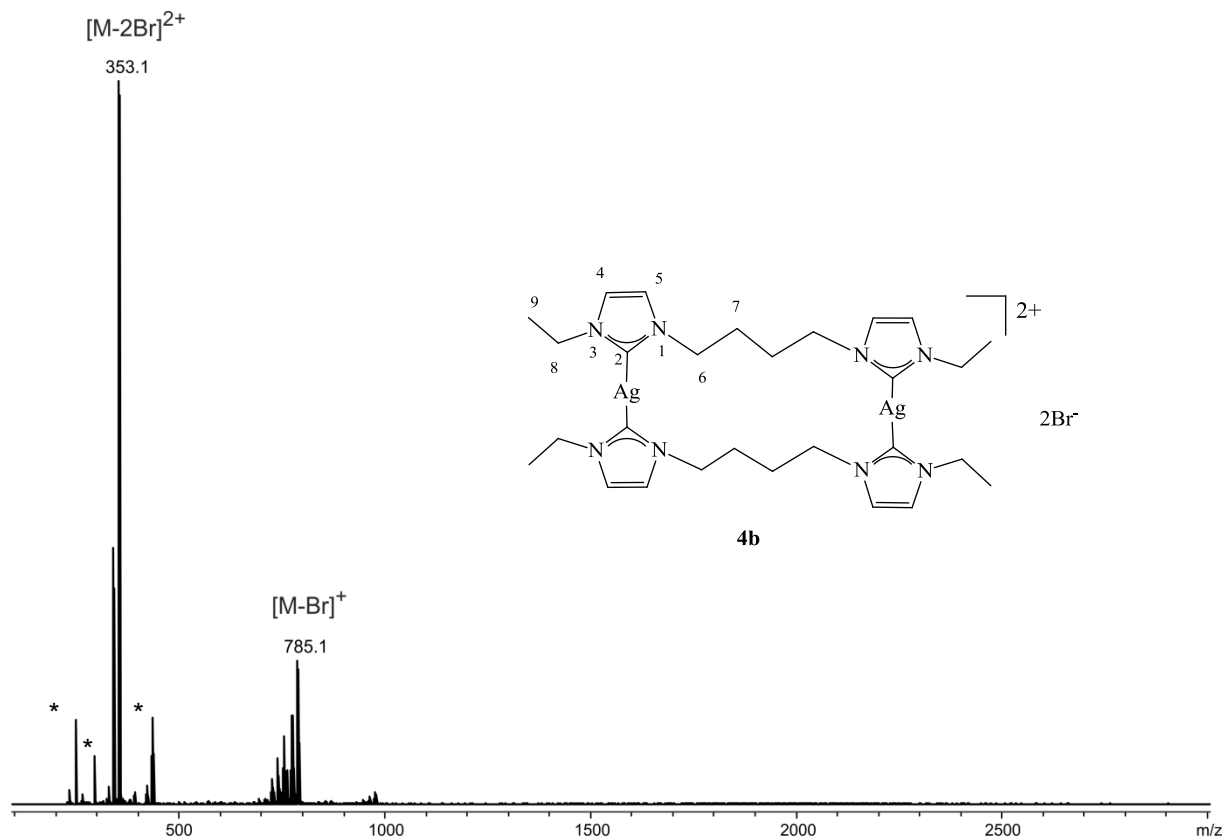
Figure 6.1.36. microTof-Q ESI(+) mass spectrum of **4c** in ACN. *memory signal, respectively.
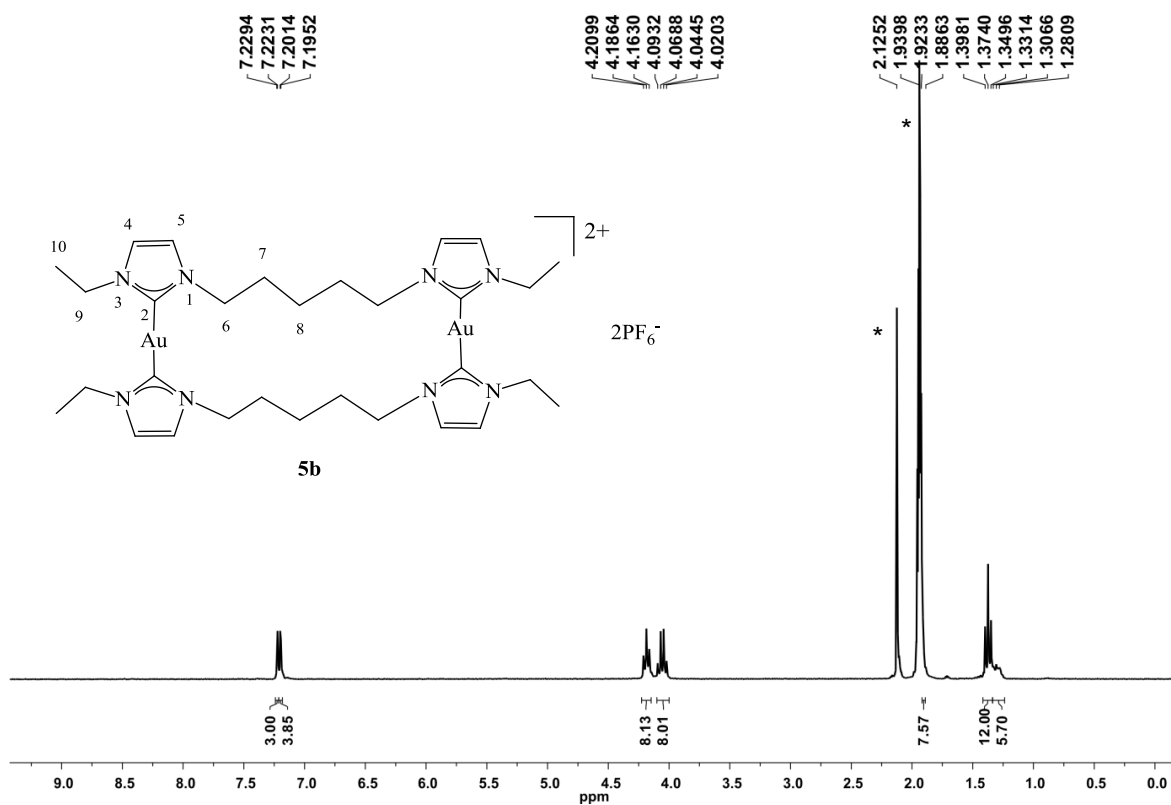
Figure 6.1.37. ^{1}H NMR (300 MHz, CD$_3$CN, r. t.) spectrum of **5b**. *partially deuterated and undeuterated ACN and water, respectively.

Figure 6.1.38. ^{13}C NMR (75 MHz, CD$_3$CN, r. t.) spectrum of **5b**. *partially deuterated and undeuterated ACN, respectively.

-71.1046
-73.6055

Figure 6.1.39. ^{19}F NMR (282 MHz, CD$_3$CN, r. t.) spectrum of **5b**.

-125.9085
-131.5288
-137.3432
-143.1559
-148.9697
-154.7823
-160.5934
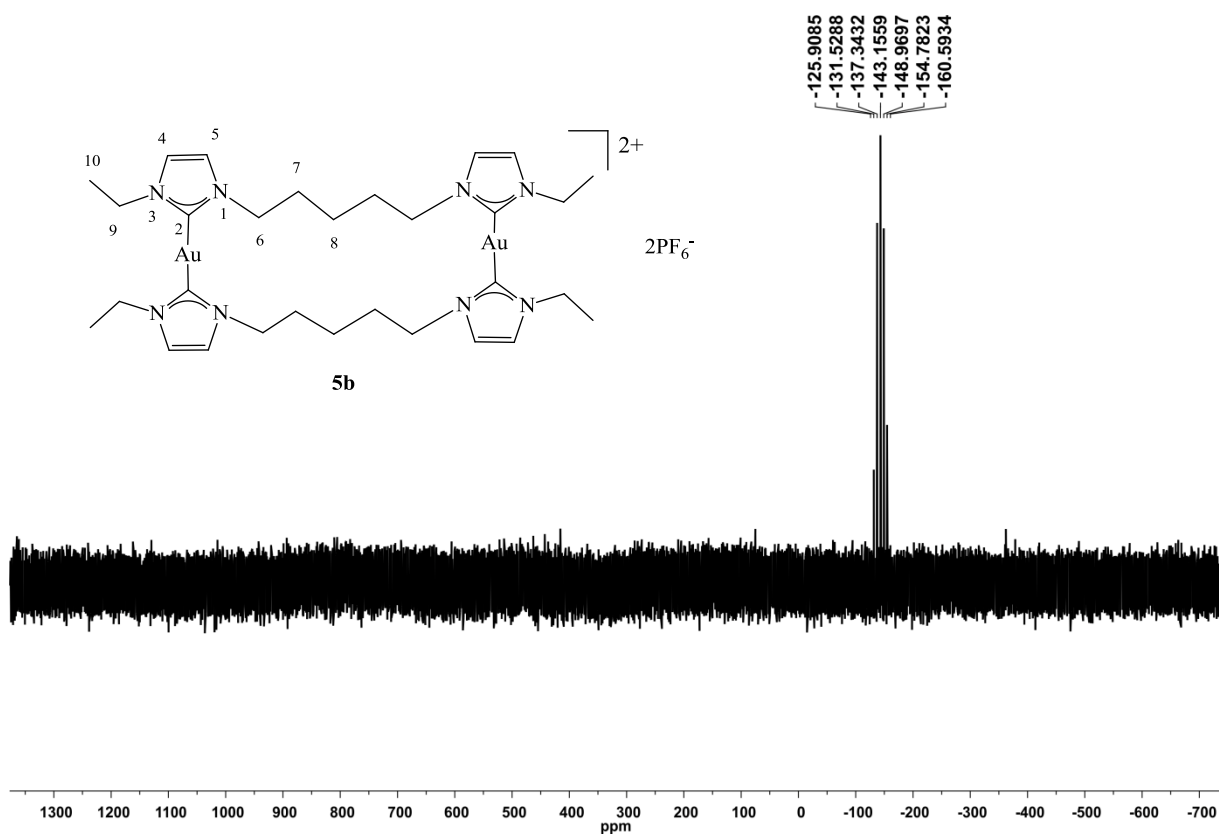
Figure 6.1.40. ^{31}P NMR (121 MHz, CD$_3$CN, r. t.) spectrum of **5b**.
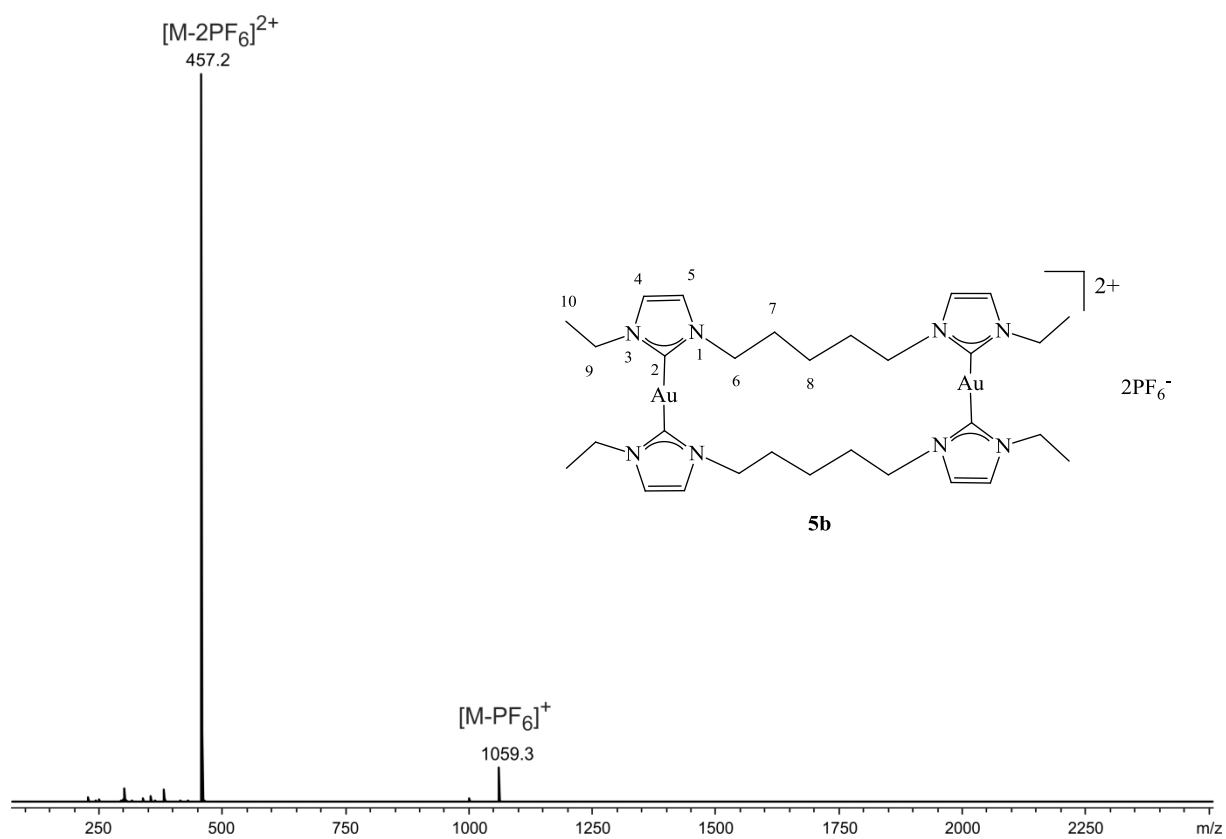
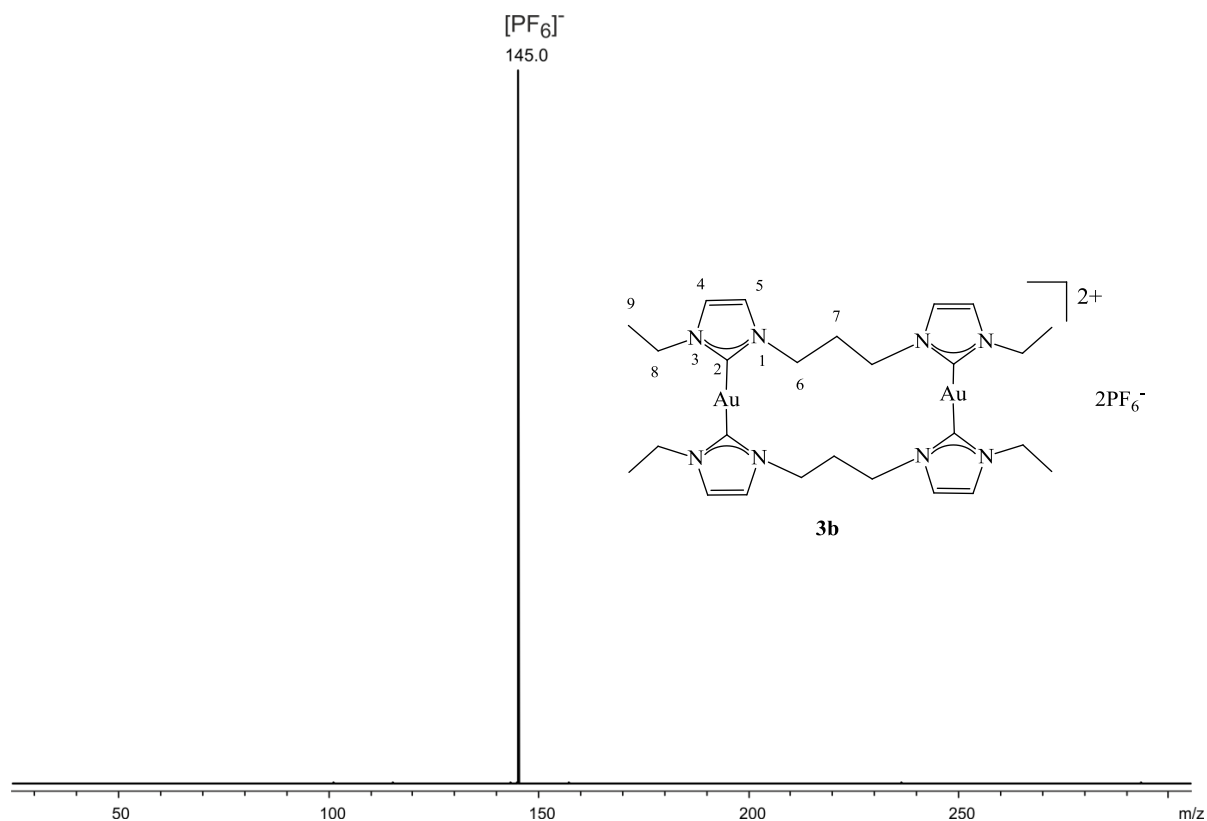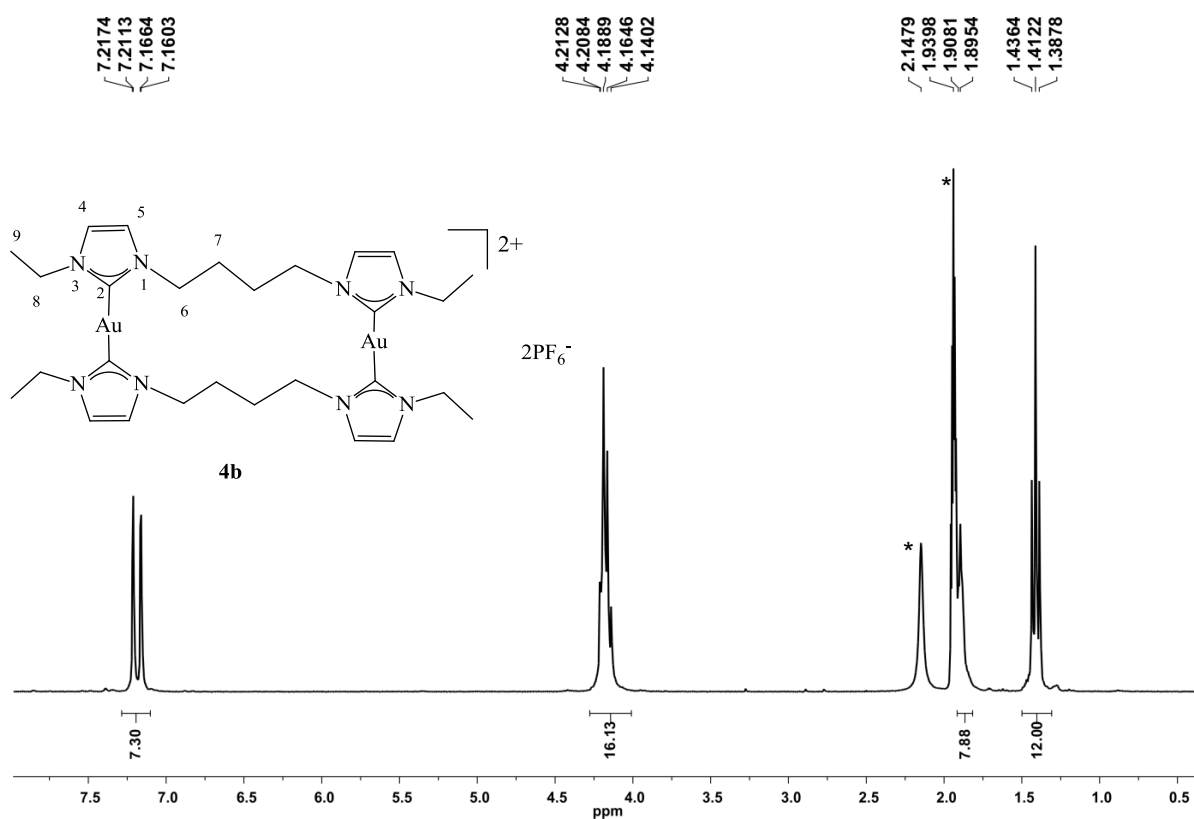**Figure 6.1.41.** microTof-Q ESI(+) mass spectrum of **5b** in ACN.
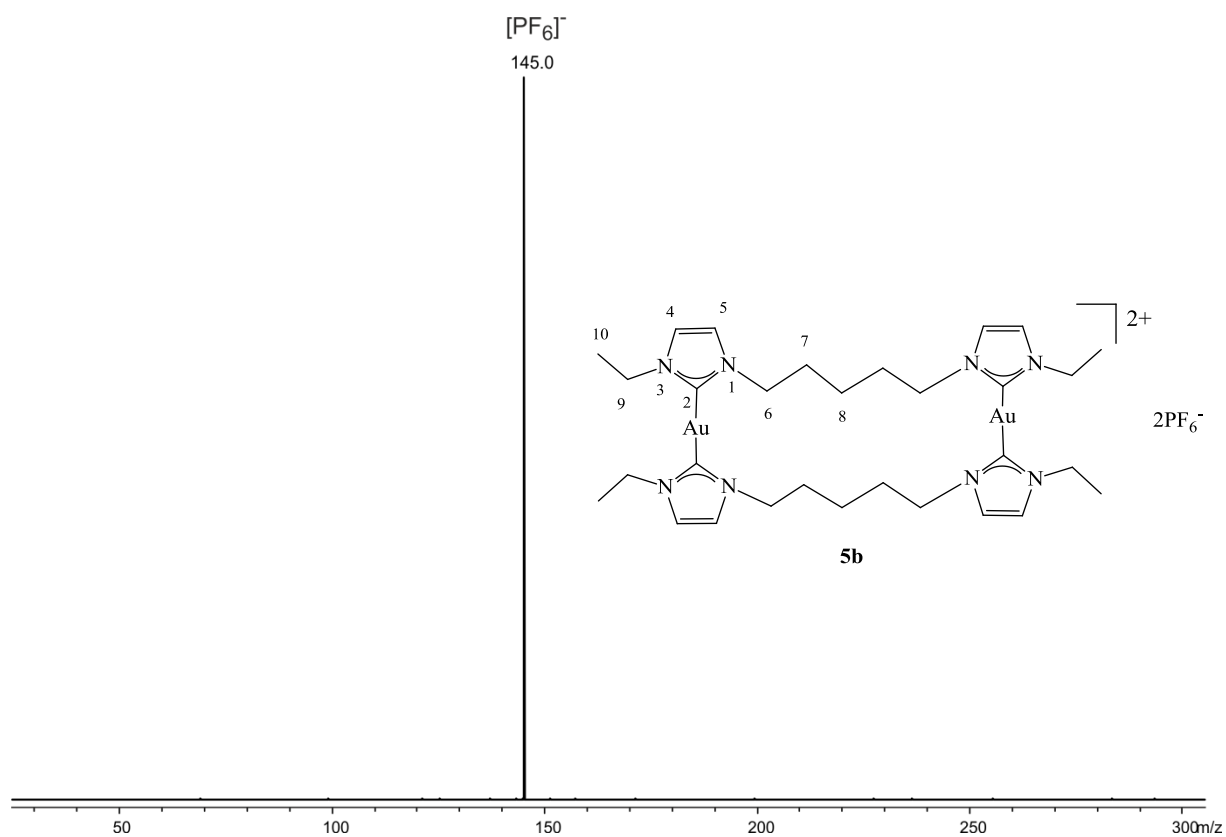
Figure 6.1.42. microTof-Q ESI(-) mass spectrum of **5b** in ACN.
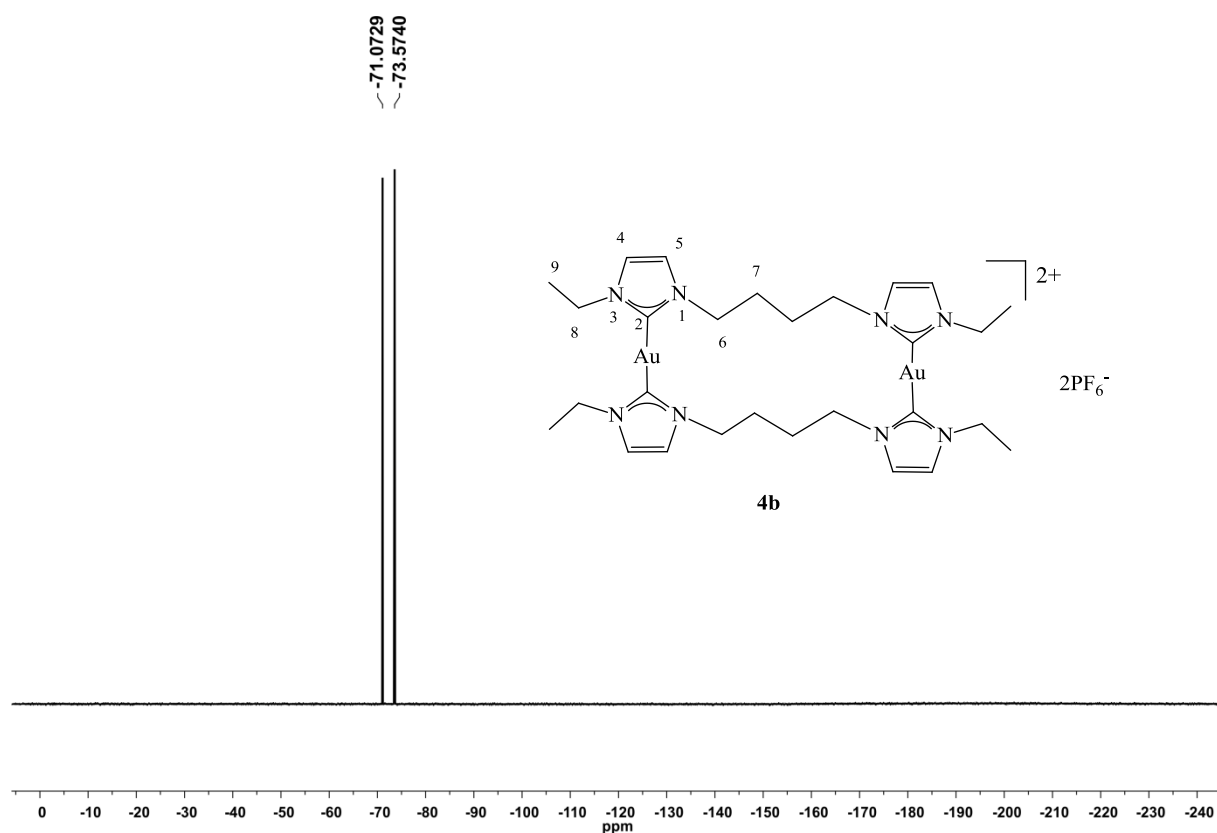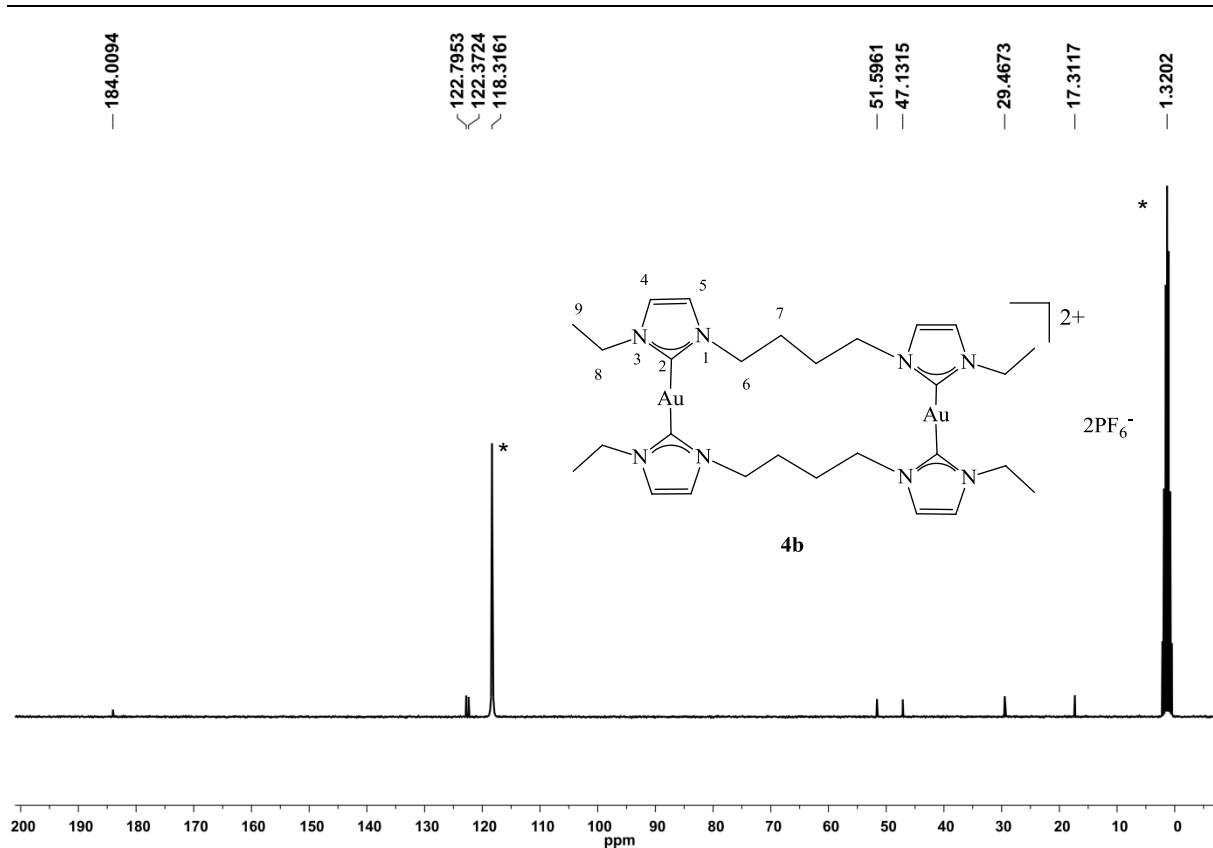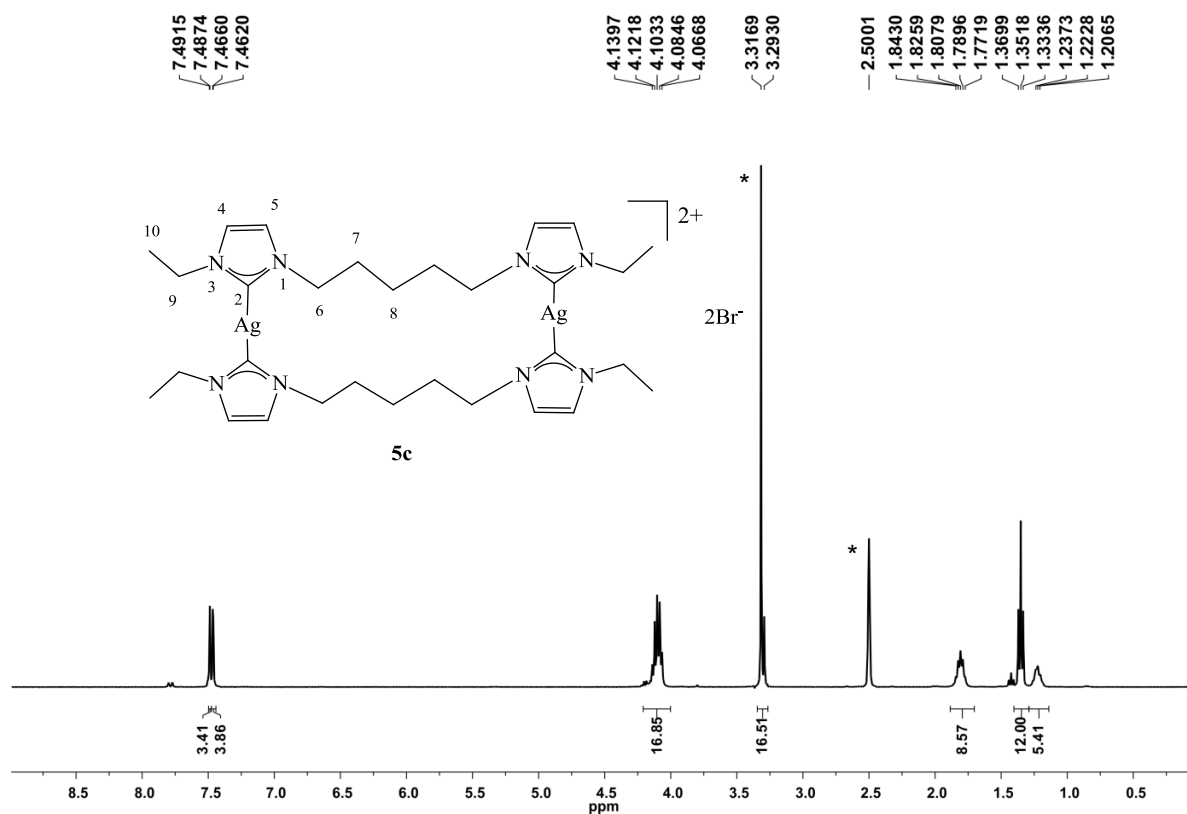
Figure 6.1.43. ^{1}H NMR (400 MHz, DMSO[D6], r. t.) spectrum of **5c**. *partially deuterated and undeuterated ACN and water, respectively.
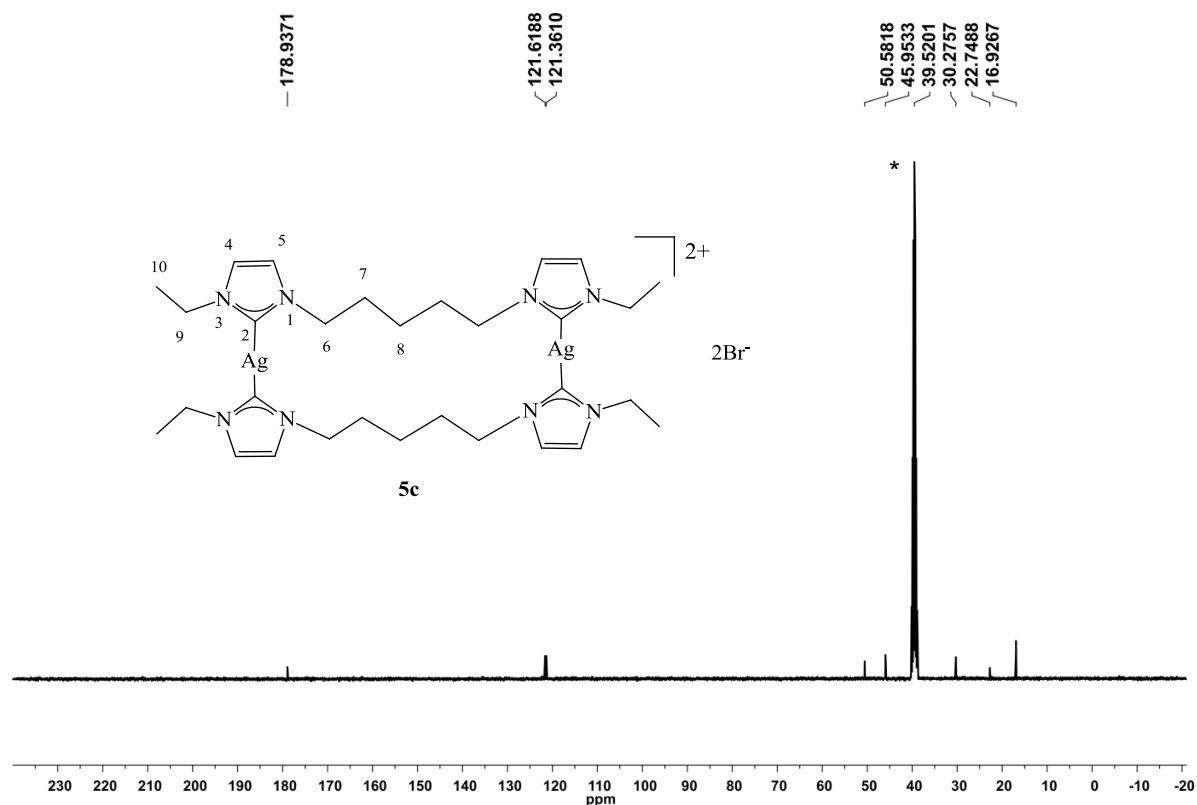
Figure 6.1.44. ^{13}C NMR (100 MHz, [D6]DMSO, r. t.) spectrum of **5c**. *partially deuterated and undeuterated DMSO, respectively.
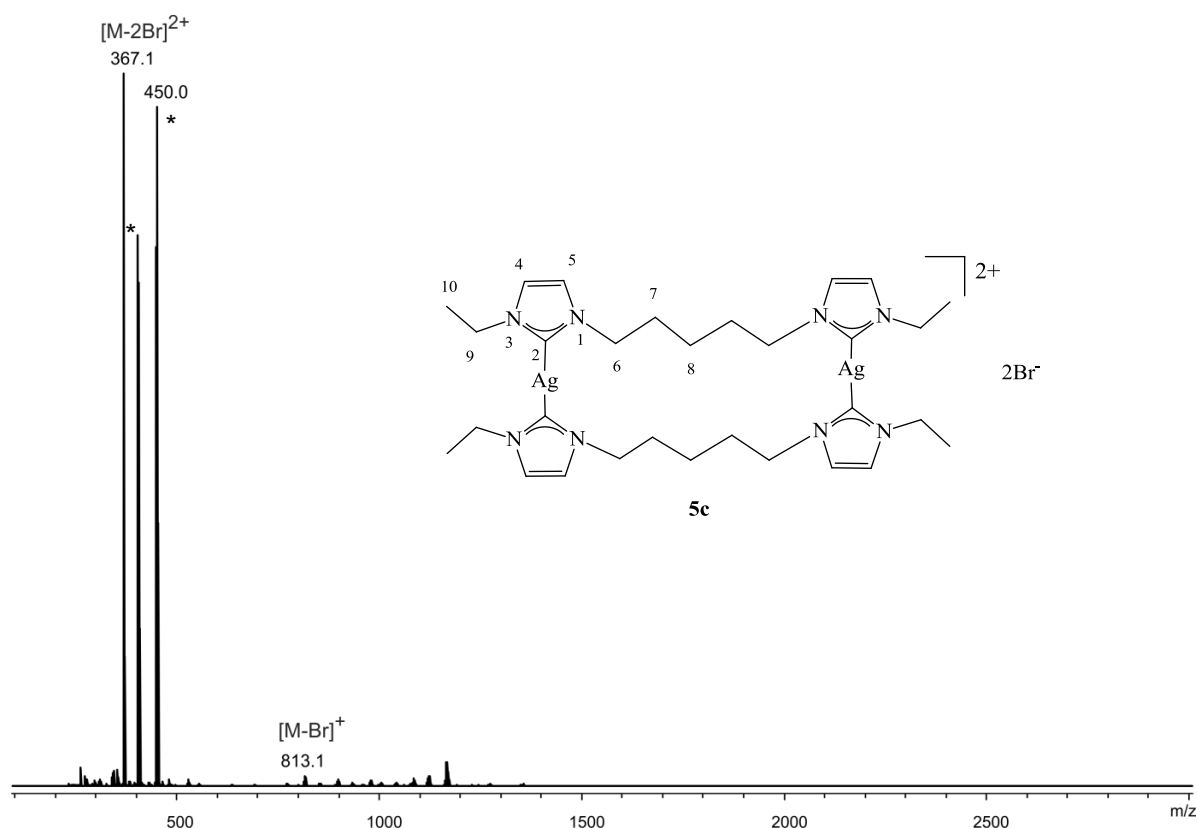
Figure 6.1.45. microTof-Q ESI(+) mass spectrum of **5c** in ACN.
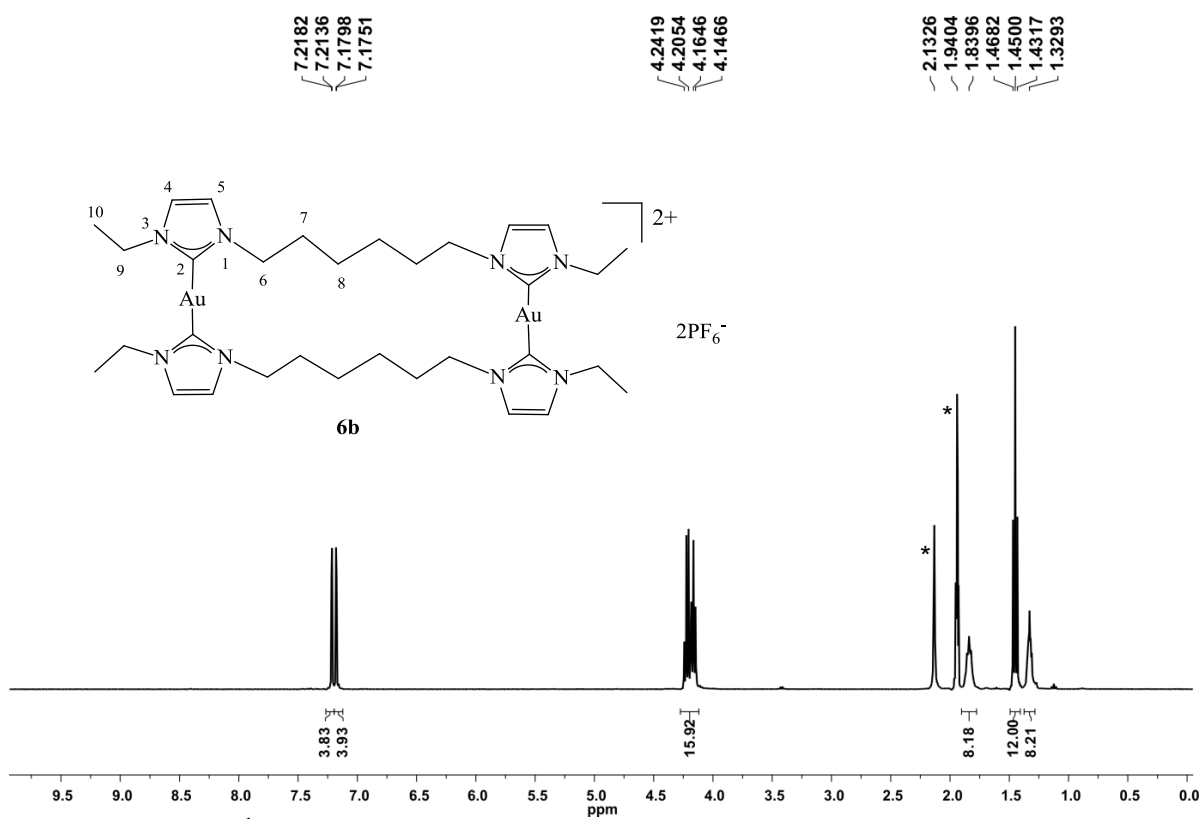
Figure 6.1.46. ¹H NMR (400 MHz, CD₃CN, r. t.) spectrum of **6b**. *partially deuterated and undeuterated ACN and water, respectively.
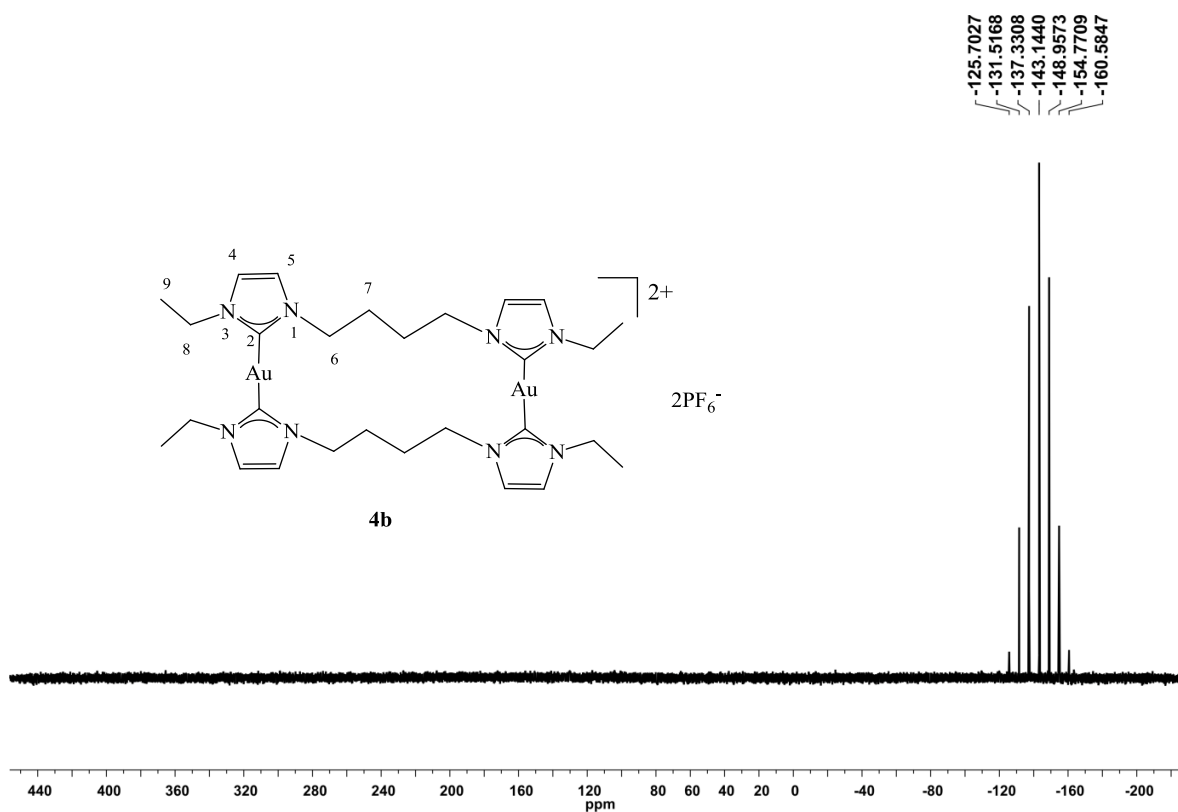
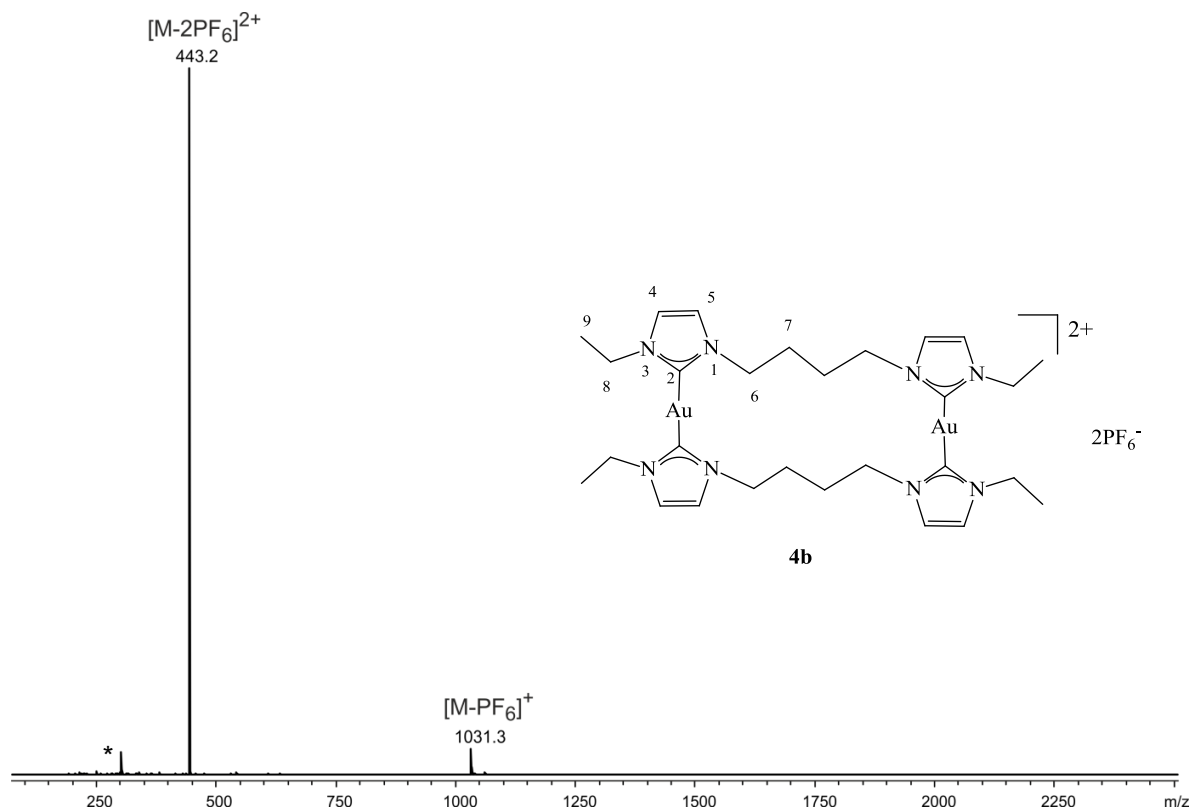**Figure 6.1.47.** ^{13}C NMR (75 MHz, CD$_3$CN, r. t.) spectrum of **6b**. *partially deuterated and undeuterated ACN, respectively.

Figure 6.1.48. ^{19}F NMR (282 MHz, CD$_3$CN, r. t.) spectrum of **6b**.
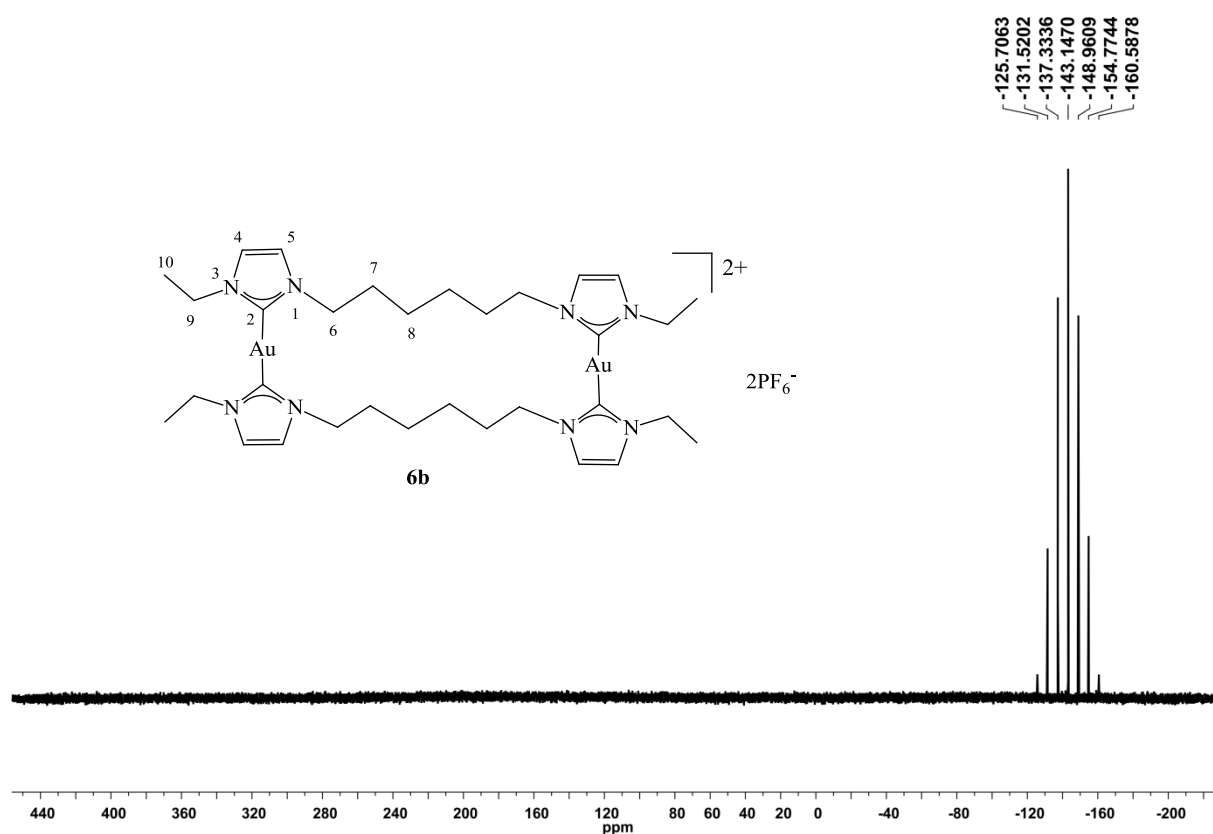
Figure 6.1.49. ^{31}P NMR (121 MHz, CD$_3$CN, r. t.) spectrum of **6b**.
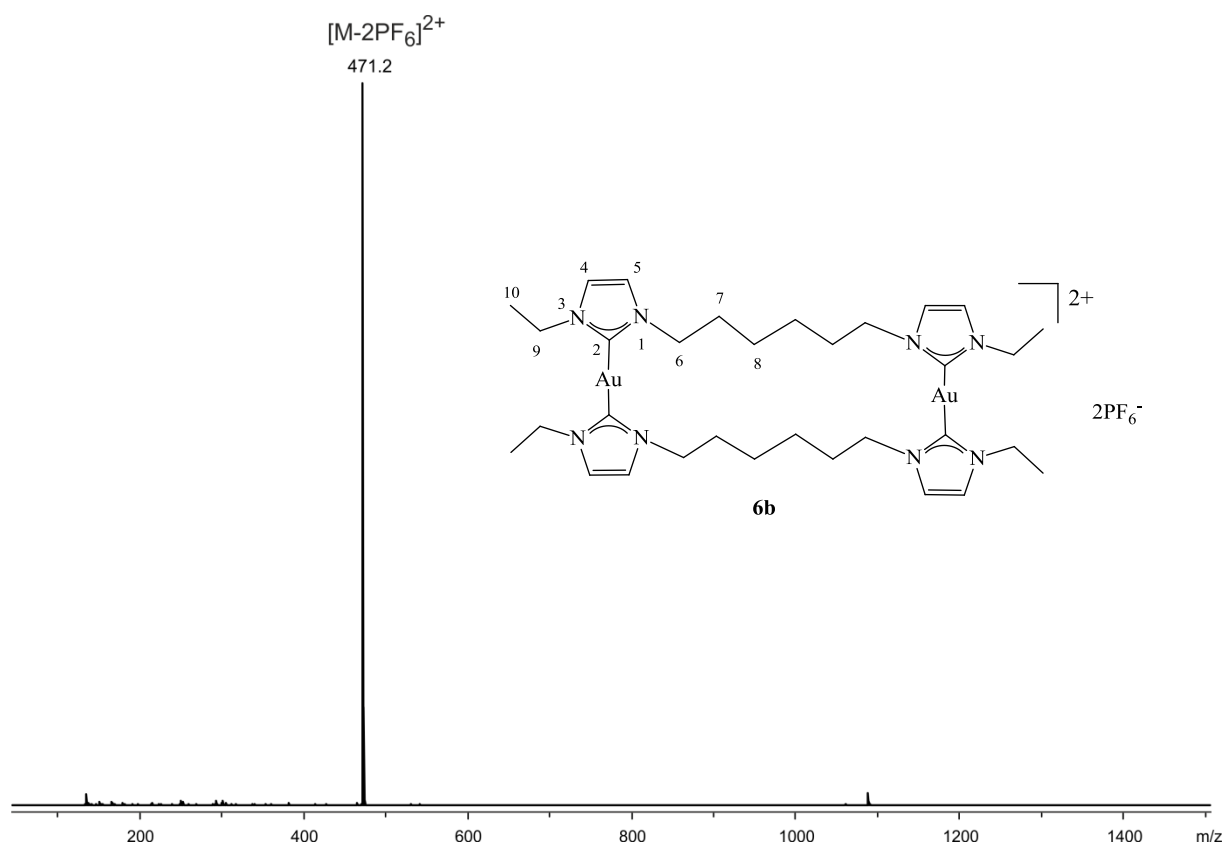
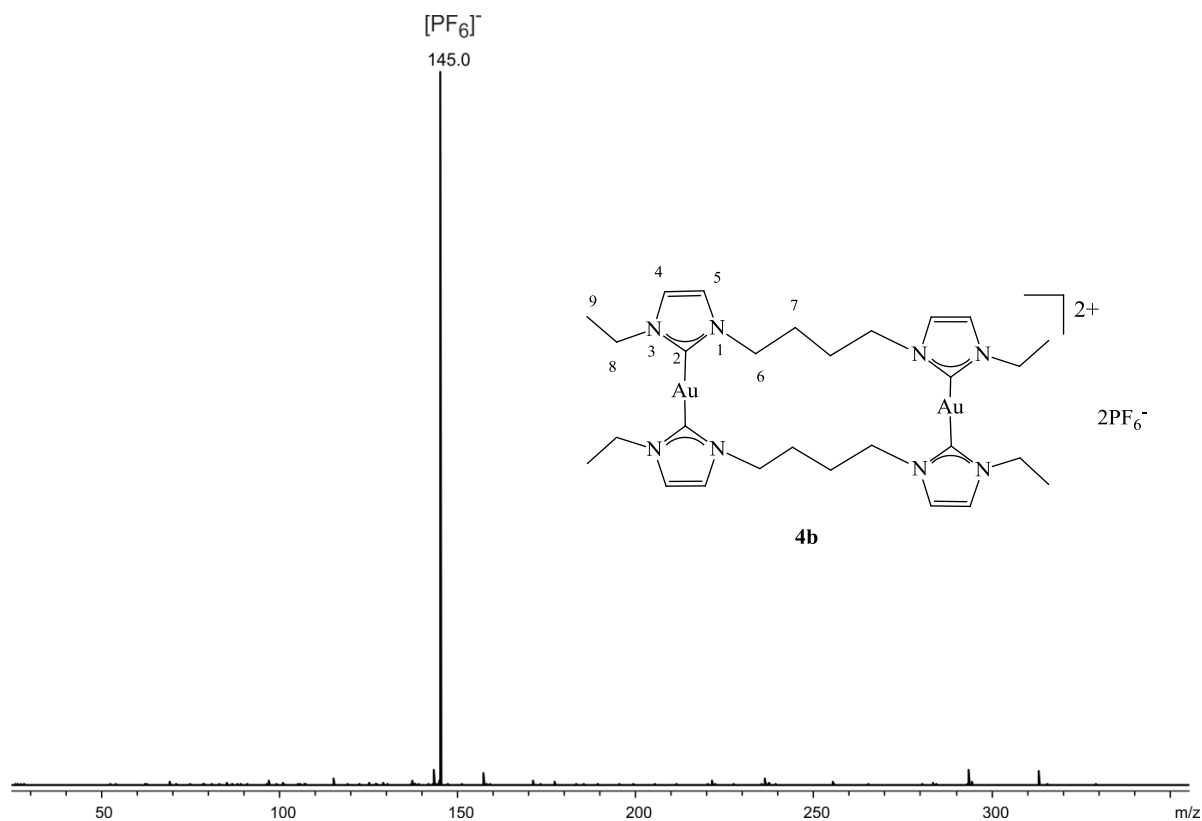**Figure 6.1.50.** microTof-Q ESI(+) mass spectrum of **6b** in ACN.
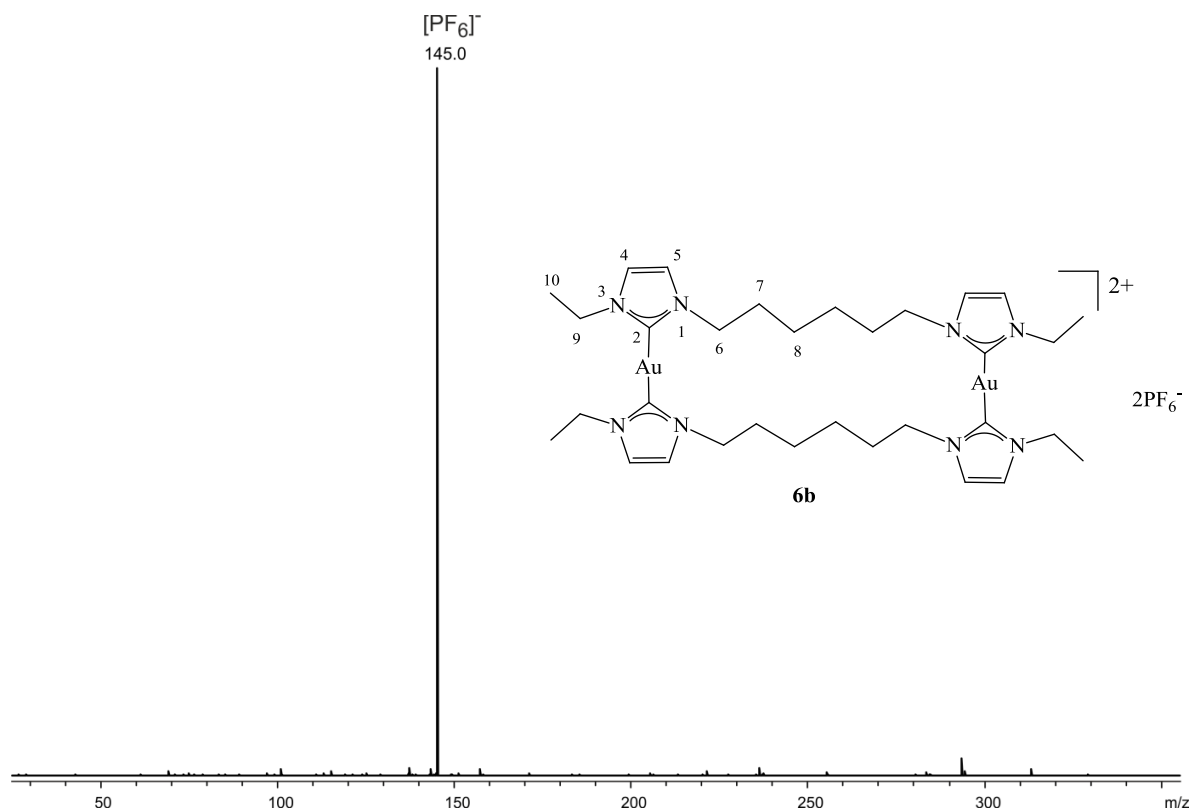
Figure 6.1.51. microTof-Q ESI(-) mass spectrum of **6b** in ACN.
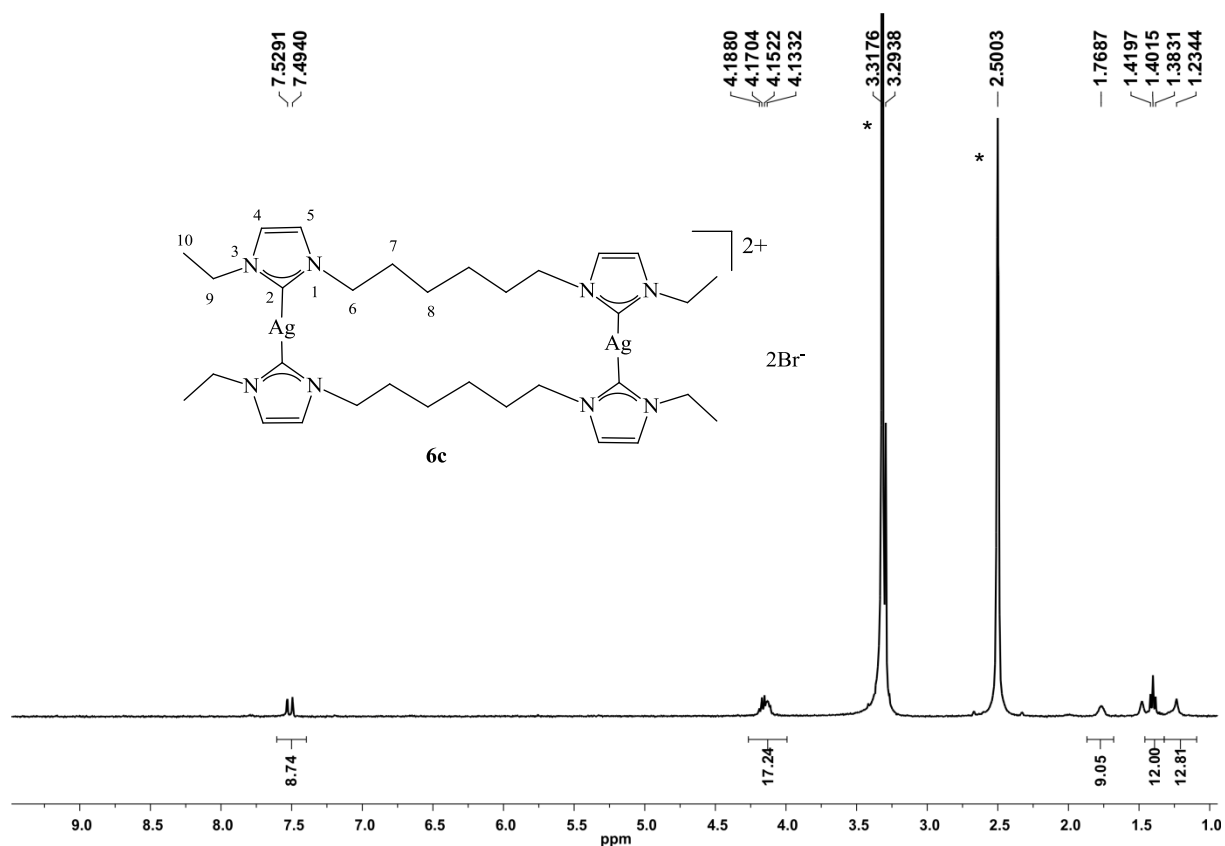
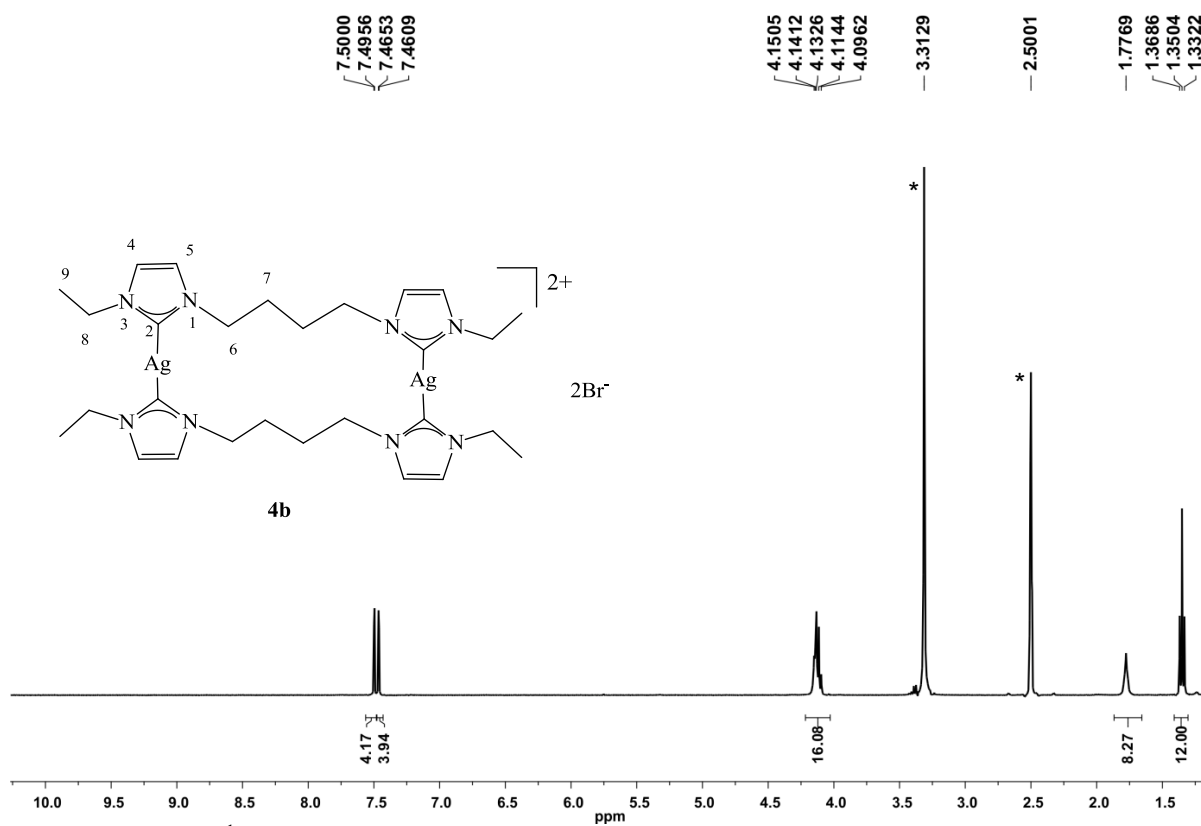**Figure 6.1.52.** ^{1}H NMR (400 MHz, DMSO[D6], r. t.) spectrum of **6c**. *partially deuterated and undeuterated DMSO and water, respectively.
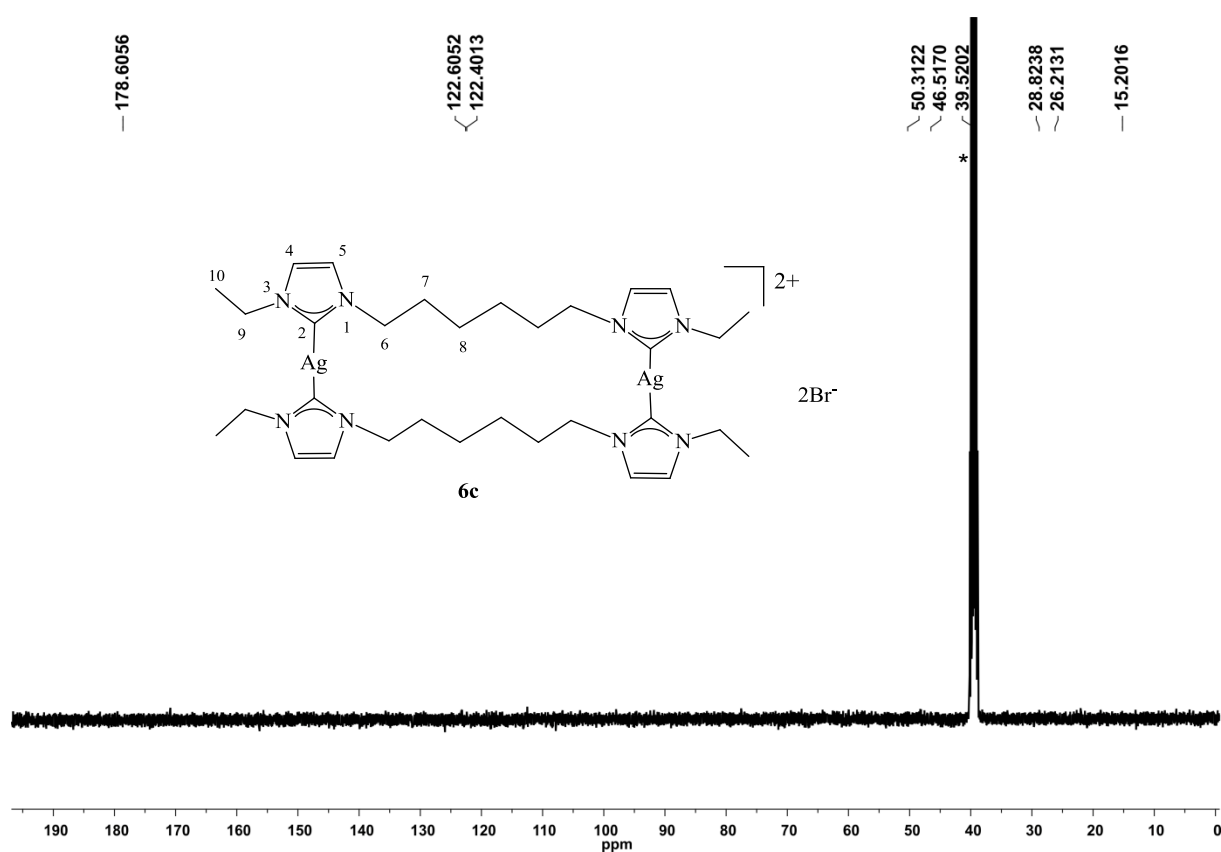
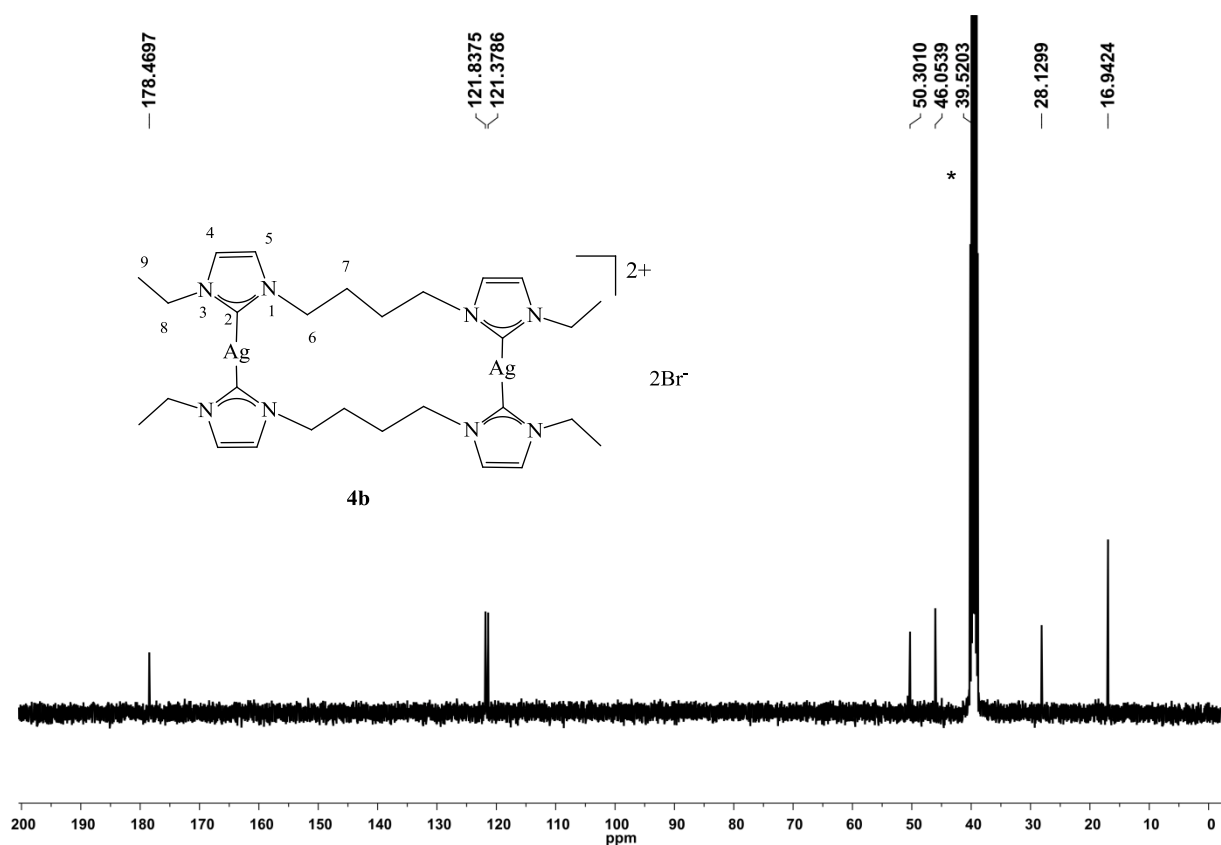**Figure 6.1.53.** ^{13}C NMR (100 MHz, DMSO[D6], r. t.) spectrum of **6c**. *partially deuterated and undeuterated ACN, respectively.
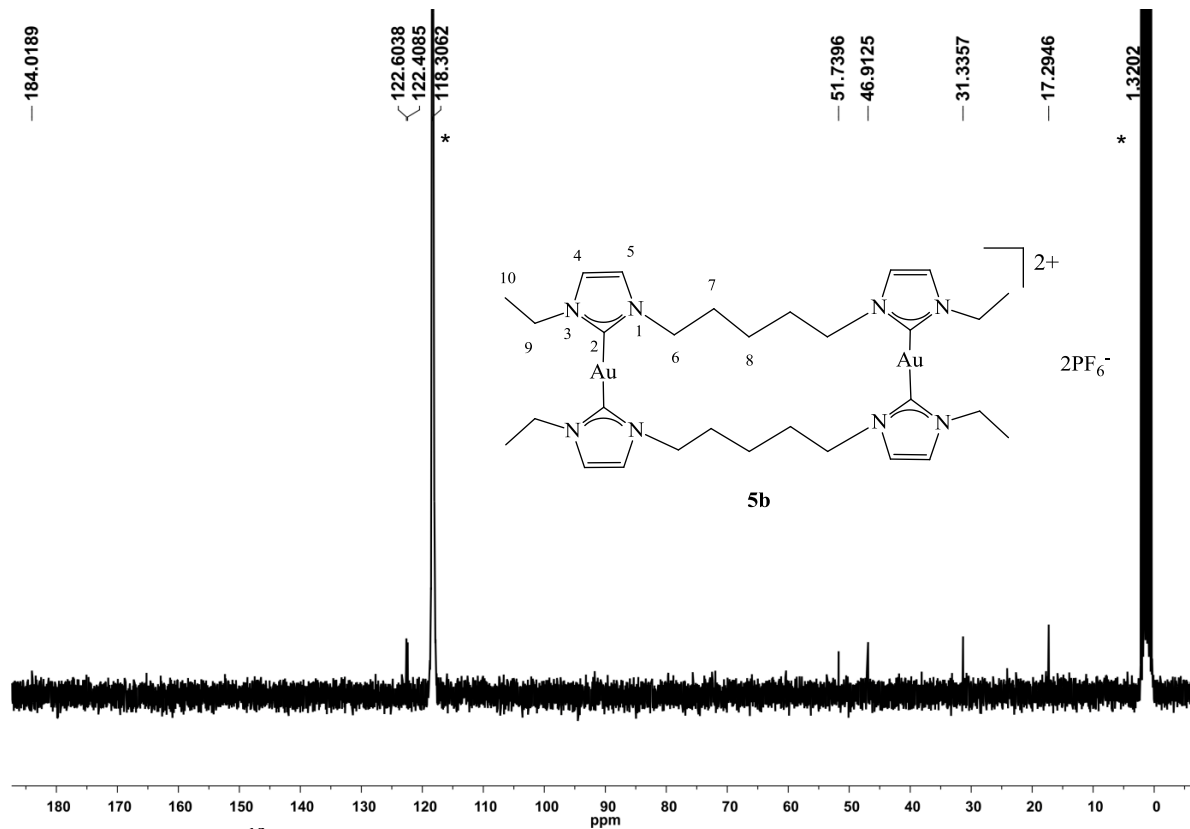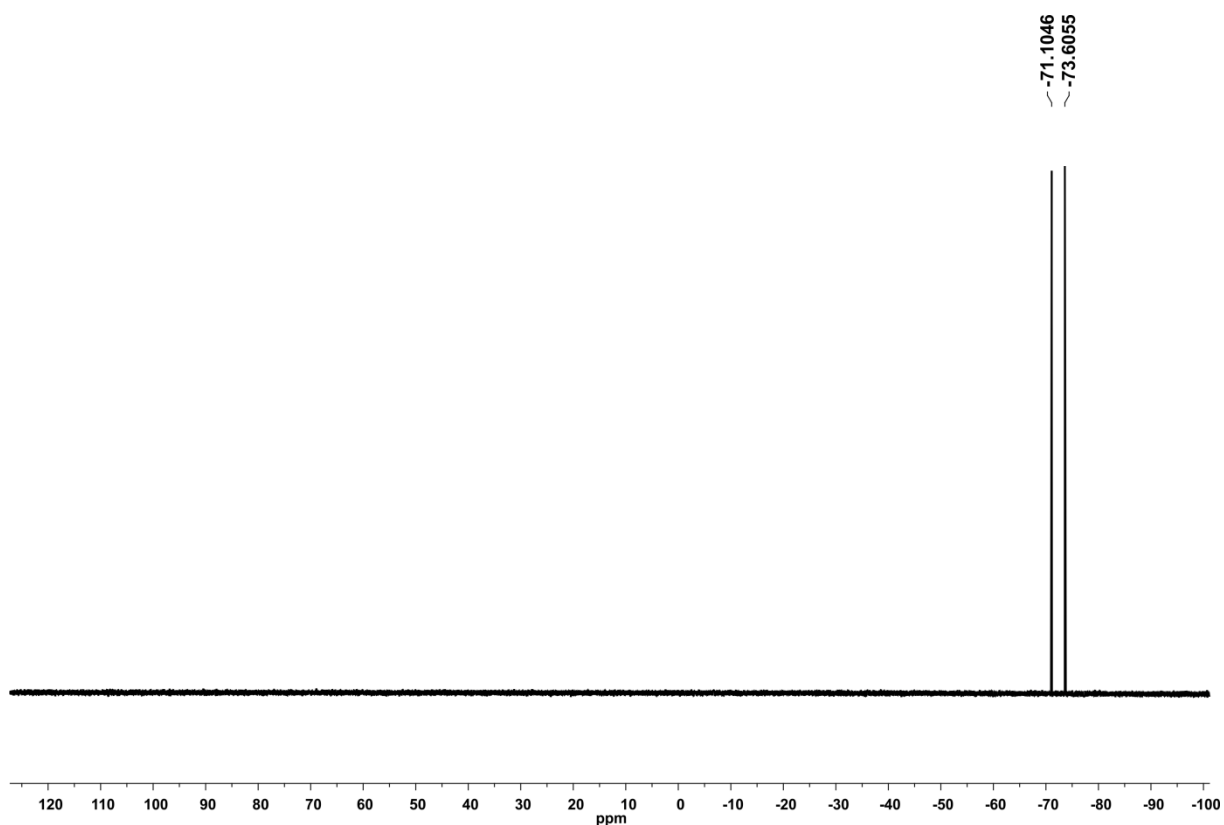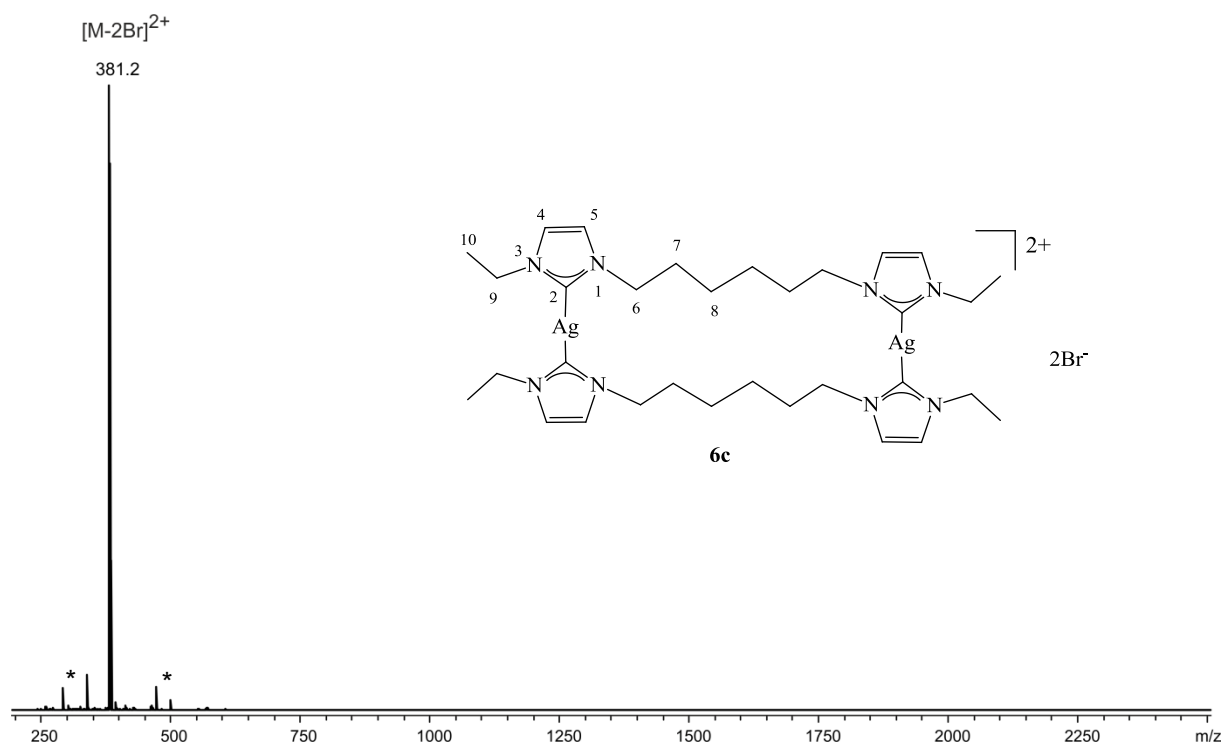

Figure 6.1.54. microTof-Q ESI(+) mass spectrum of **6c** in ACN.

6.1.4. Crystallographic Data

Crystal structure determination: Data for the X-ray crystallographic analyses were performed on a Nonius KappaCCD diffractometer (**1a, 1c**, **3a**, **3b**, **4a**, **6a**, **6b**), a Bruker X8 KappaApexII diffractometer (**1b**, **2a**, **2b**, **5b**) or a STOE IPDS2T diffractometer (**4b**) using graphite monochromated Mo-Kα radiation (λ = 0.71073 Å). Intensities were measured by fine-slicing φ- and ω-scans and corrected for background, polarization and Lorentz effects. A semi-empirical absorption correction was applied for the data sets following Blessing's method[94]. The structures were solved by direct methods and refined anisotropically by the least squares procedure implemented in the ShelX programme system[95]. The hydrogen atoms were included isotropically using the riding model on the carbon atoms.

Table 6.1.2. Crystallographic Data of **1a/b/c**.

|	1a	1b	1c
formula	$C_{22}H_{32}Au_2N_8Br_2*CH_3OH$	$C_{22}H_{32}Au_2N_8P_2F_{12}$	$C_{22}H_{32}Ag_2N_8Br_2$
cryst size (mm^3)	0.32 x 0.25 x 0.08	0.22 x 0.14 x 0.04	0.18 x 0.08 x 0.04
cryst syst	monoclinic	monoclinic	monoclinic
space group	$P2_1/n$	C 2/m	$P2_1/c$
a (Å)	13.3644(6)	18.360(3)	8.0414(3)
b (Å)	12.1912(5)	13.0075(19)	16.2599(7)
c (Å)	18.6685(8)	14.499(2)	12.1967(5)
$α$ (deg)	90	90	90
$β$ (deg)	107.723(3)	105.846(5)	121.189(2)
$γ$ (deg)	90	90	90
V ($Å^3$)	2897.3(2)	3330.9(9)	1364.25(10)
Z	4	4	2
$ρ_{calcd}$ (mg m^3)	2.280	2.178	1.909
F_{000}	1864	2064	768
$μ$ (mm^{-1})	12.905	8.991	4.391
transmissions	0.4250-0.1042	0.7150-0.2424	0.8439-0.5054
$Θ$ range (deg)	2.36-28.00	2.23-28.00	2.51-27.99
reflns collected	18686	38334	24780
R_{int}	0.1246	0.0598	0.0841
GOF	1.045	1.029	1.052
R1	0.0701-0.0994	0.0327-0.0437	0.0402-0.0567
wR2	0.1976-0.2117	0.0743-0.0797	0.1031-0.1097
largest diff peak (e $Å^{-3}$)	5.716	3.007	1.831

Table 6.1.3. Crystallographic Data of **2a/b**.

	2a	2b
formula	$C_{24}H_{36}Au_2N_8Br_2 * CH_3OH * H_2O$	$C_{24}H_{36}Au_2N_8P_2F_{12}$
cryst size (mm^3)	0.32 x 0.25 x 0.08	0.20 x 0.10 x 0.05
cryst syst	monoclinic	monoclinic
space group	$P2_1/n$	$P2_1/c$
a (Å)	12.4982(6)	16.1337(7)
b (Å)	19.0817(9)	16.6581(8)
c (Å)	13.4521(7)	14.4451(7)
α (deg)	90	90
β (deg)	91.013(2)	116.201(2)
γ (deg)	90	90
V (Å^3)	3207.6(3)	3483.3(3)
Z	4	4
ρ_{calcd} (mg m^3)	2.154	2.137
F_{000}	1968	2128
μ (mm^{-1})	11.664	8.600
transmissions	0.6526-0.1180	0.6730-0.2781
Θ range (deg)	2.62-28.00	2.82-28.00
reflns collected	46922	42238
R_{int}	0.0464	0.0697
GOF	1.0078	1.030
R1	0.0311-0.0402	0.0195-0.0263
wR2	0.0622-0.0651	0.0398-0.0418
largest diff peak (e Å^{-3})	2.531	0.685

Table 6.1.4. Crystallographic Data of **3a/b**.

	3a	3b	3c
formula	$C_{26}H_{40}Au_2N_8Br_2$	$2C_{26}H_{40}Au_2N_8P_2F_{12}$ $_*Et_2O$	$C_{26}H_{40}Ag_4N_8Br_4$
cryst size (mm^3)	0.56 x 0.28 x 0.06	0.18 x 0.12 x 0.08	0.18 x 0.08 x 0.06
cryst syst	orthorhombic	triclinic	triclinic
space group	Pmmn	P-1	P-1
a (Å)	14.8235(6)	12.0982(18)	9.4471(11)
b (Å)	12.0677(8)	12.5843(18)	9.7787(11)
c (Å)	9.3272(7)	14.952(2)	10.2050(11)
α (deg)	90	77.062(5)	71.165(3)
β (deg)	90	78.543(5)	84.131(4)
γ (deg)	90	63.762(5)	83.233(4)
V (Å^3)	1668.50(18)	1977.1(5)	883.97(17)
Z	2	1	1
ρ_{calcd} (mg m^3)	2.027	1.992	2.284
F_{000}	960	1138	580
μ (mm^{-1})	11.205	7.583	6.733
transmissions	0.5529-0.0619	0.5822-0.3422	0.6881-0.3770
Θ range (deg)	2.76-28.00	2.47-28.00	2.18-26.99
reflns collected	9715	102783	3875
R_{int}	0.0487	0.0918	0.0593
GOF	1.052	1.029	1.124
R1	0.0311-0.0405	0.0456-0.00693	0.0419-0.00796
wR2	0.0753-0.0780	0.1357-0.1551	0.0772-0.0923
largest diff peak (e Å^{-3})	3.404	2.190	2.646

Table 6.1.5. Crystallographic Data of **4a/b/c**.

	4a	4b	4c
formula	$C_{28}H_{44}Au_2N_8Br_2 *$ $2CH_3OH$	$C_{28}H_{44}Au_2N_8P_2F_{12}$	$C_{14}H_{22}AgN_4Br_3$
cryst size (mm^3)	0.60 x 0.30 x 0.28	0.15 x 0.12 x 0.09	0.18 x 0.16 x 0.14
cryst syst	triclinic	triclinic	triclinic
space group	P-1	P-1	P-1
a (Å)	9.5196(5)	9.946(5)	7.472(3)
b (Å)	10.6053(4)	10.113(8)	7.540(3)
c (Å)	11.2021(6)	11.269(9)	9.448(3)
α (deg)	95.973(3)	65.56(5)	67.584(11)
β (deg)	114.100(2)	85.99(5)	79.880(11)
γ (deg)	111.925(3)	68.14(5)	74.743 (12)
V (Å^3)	912.70(8)	953.0(12)	473.0(3)
Z	1	1	1
ρ_{calcd} (mg m^3)	2.021	2.050	2.085
F_{000}	532	564	286
μ (mm^{-1})	10.255	7.864	7.402
transmissions	0.12831-0.04964	0.5379-0.3850	0.4239-0.3492
Θ range (deg)	2.52-28.00	3.13-28.00	2.34-28.00
reflns collected	9908	9602	9675
R_{int}	0.0595	0.0697	0.0563
GOF	1.003	1.029	1.047
R1	0.0292-0.0655	0.0492-0.0536	0.0732-0.0968
wR2	0.0342-0.0670	0.1282-0.1307	0.2193-0.2426
largest diff peak (e Å^{-3})	2.214	2.080	5.039

Table 6.1.6. Crystallographic Data of **5b**.

	5b
formula	$C_{30}H_{48}Au_2N_8P_2F_{12}$
cryst size (mm^3)	0.24 x 0.13 x 0.08
cryst syst	monoclinic
space group	C2/c
a (Å)	20.1425(7)
b (Å)	20.9547(8)
c (Å)	11.5734(4)
α (deg)	90
β (deg)	123.6960(10)
γ (deg)	90
V (Å^3)	4064.2(3)
Z	4
ρ_{calcd} (mg m^3)	1.969
F_{000}	2320
μ (mm^{-1})	7.379
transmissions	0.5898-0.2704
$\varTheta$ range (deg)	3.11-28.00
reflns collected	65226
R_{int}	0.0425
GOF	1.065
R1	0.0218-0.0556
wR2	0.0262-0.0573
largest diff peak (e Å^{-3})	1.272

Table 6.1.7. Crystallographic Data of **6a/b**.

	6a	**6b**
formula	$C_{32}H_{52}Au_2N_8Br_2$	$C_{32}H_{52}Au_2N_8P_2F_{12}$
cryst size (mm^3)	0.44 x 0.24 x 0.11	0.18 x 0.09 x 0.04
cryst syst	triclinic	triclinic
space group	P-1	P-1
a (Å)	9.4795(8)	10.3753(7)
b (Å)	10.1252(9)	10.8525(8)
c (Å)	11.5109(9)	11.5698(8)
α (deg)	64.343(3)	113.079(4)
β (deg)	75.524(3)	90.440(4)
γ (deg)	71.486(3)	115.080(3)
V (Å^3)	936.15(14)	1061.59(14)
Z	1	1
ρ_{calcd} (mg m^3)	1.956	1.928
F_{000}	528	596
μ (mm^{-1})	9.994	7.064
transmissions	0.0461-0.0964	0.7653-0.3628
Θ range (deg)	2.82-25.25	2.28-26.00
reflns collected	6681	10919
R_{int}	0.0372	0.0750
GOF	1.156	1.162
R1	0.0536-0.0637	0.0653-0.0770
wR2	0.1212-0.1317	0.1715-0.1768
largest diff peak (e Å^{-3})	3.071	5.040

6.1.5. UV/Vis and Fluorescence Graphics
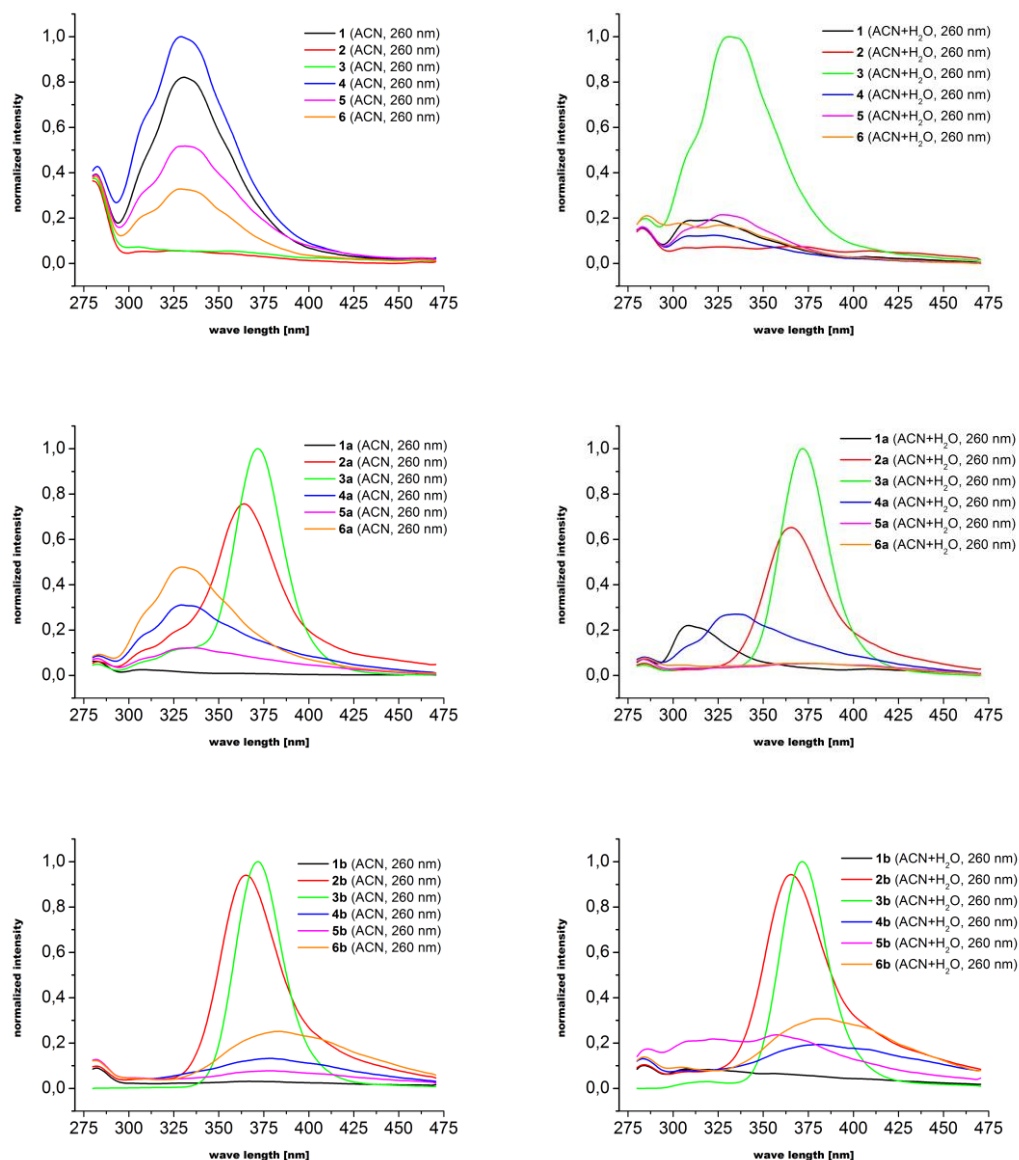
Figure 6.1.55. Graphics of the emission measurements of ligand precursors **1-6** and complexes **1a/b-6a/b** in pure ACN and ACN with 10% H_2O at room temperature. Excitation wave length used during measurements is given in the legend.
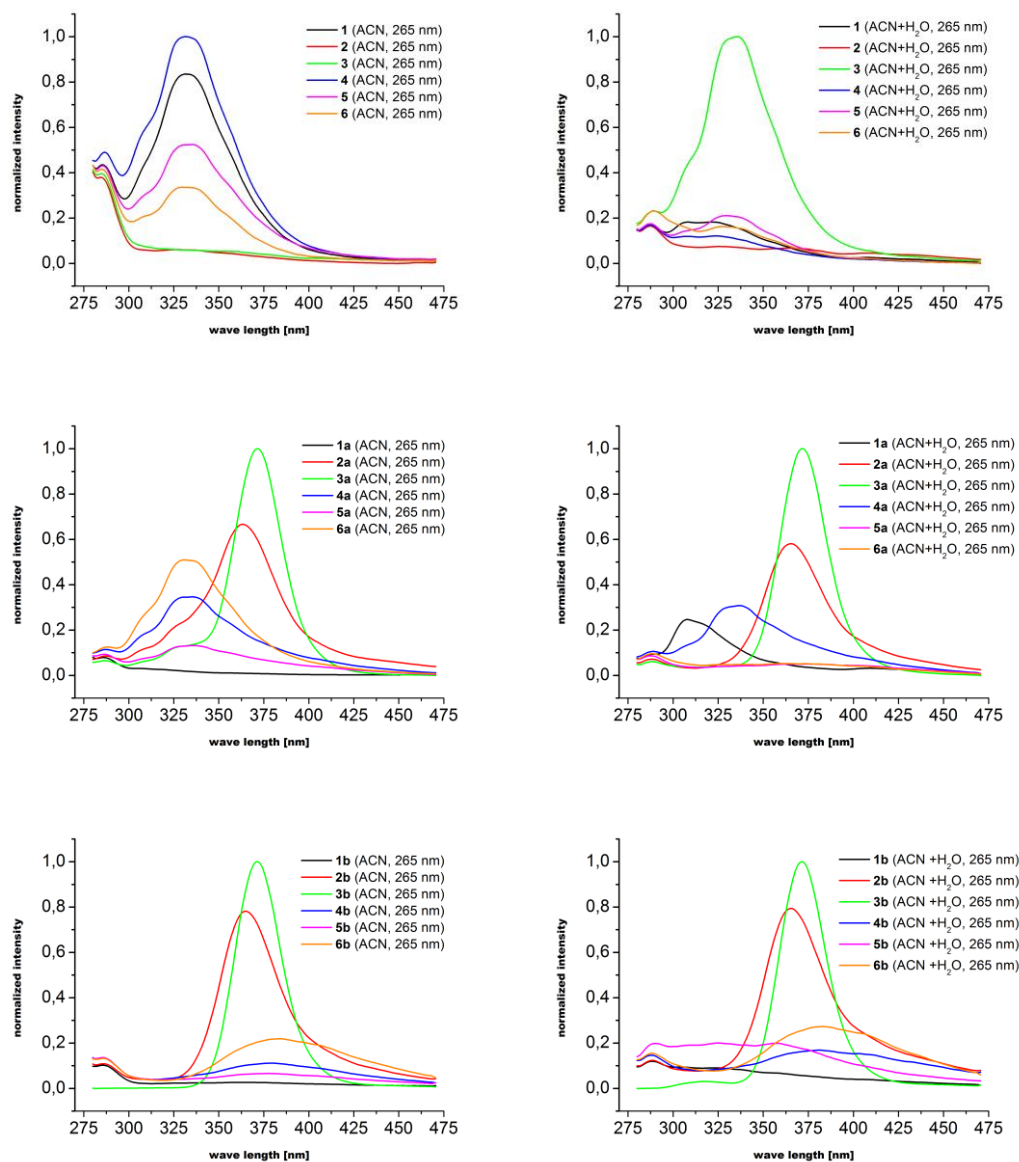
Figure 6.1.56. Graphics of the emission measurements of ligand precursors **1**-**6** and complexes **1a**/**b**-**6a**/**b** in pure ACN and ACN with 10% H_2O at room temperature. Excitation wave length used during measurements is given in the legend.

6.2 Complexes Type 2

6.2.1 VT NMR
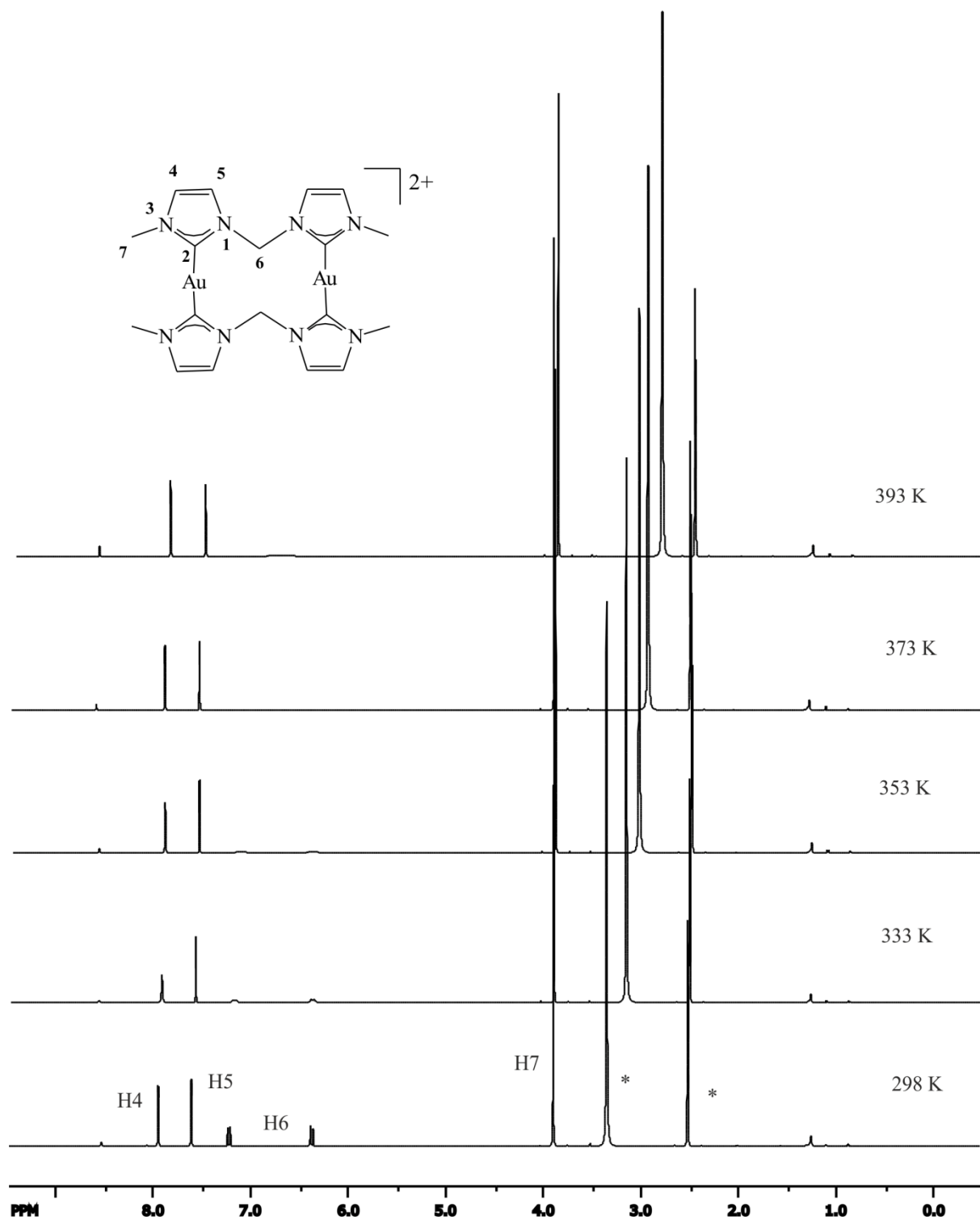
Figure 6.2.1. High temperature ^{1}H NMR spectra (500.13 MHz, DMSO[D6]) of **7a/b**.
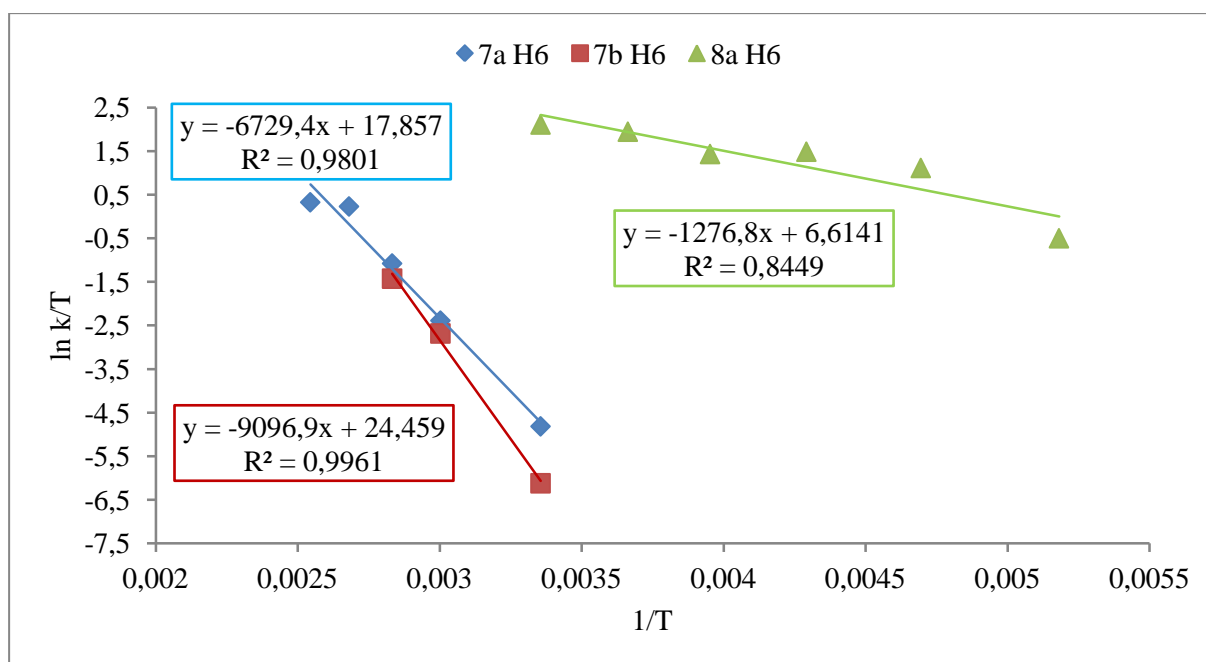
Figure 6.2.2: Eyring plots for the kinetic rate constants given in Table x obtained from line shape analysis of the VT-NMR spectra shown in Figure x and Figure x

Table 6.2.1. Thermal activation parameters determined from the Eyring plots in Figure x for the dynamic behaviour observed for the metallamacrocyclic systems **7a/b** and **8a**.

compound	anion	linker	signal	$\Delta H^{\ddagger}$ / kJ mol^{-1}	$\Delta S^{\ddagger}$ / J mol^{-1}K^{-1}	$\Delta G^{\ddagger}_{(298K)}$ / kJ mol^{-1}
7a	Br$^-$	CH$_2$	H6	56 ± 5	-5 ± 13	71 ± 6
7b	PF$_6^-$	CH$_2$	H6	76 ± 5	6 ± 15	74 ± 6
8a	Br$^-$	C$_2$H$_4$	H6	11 ± 2	-1 ± 9	53 ± 4
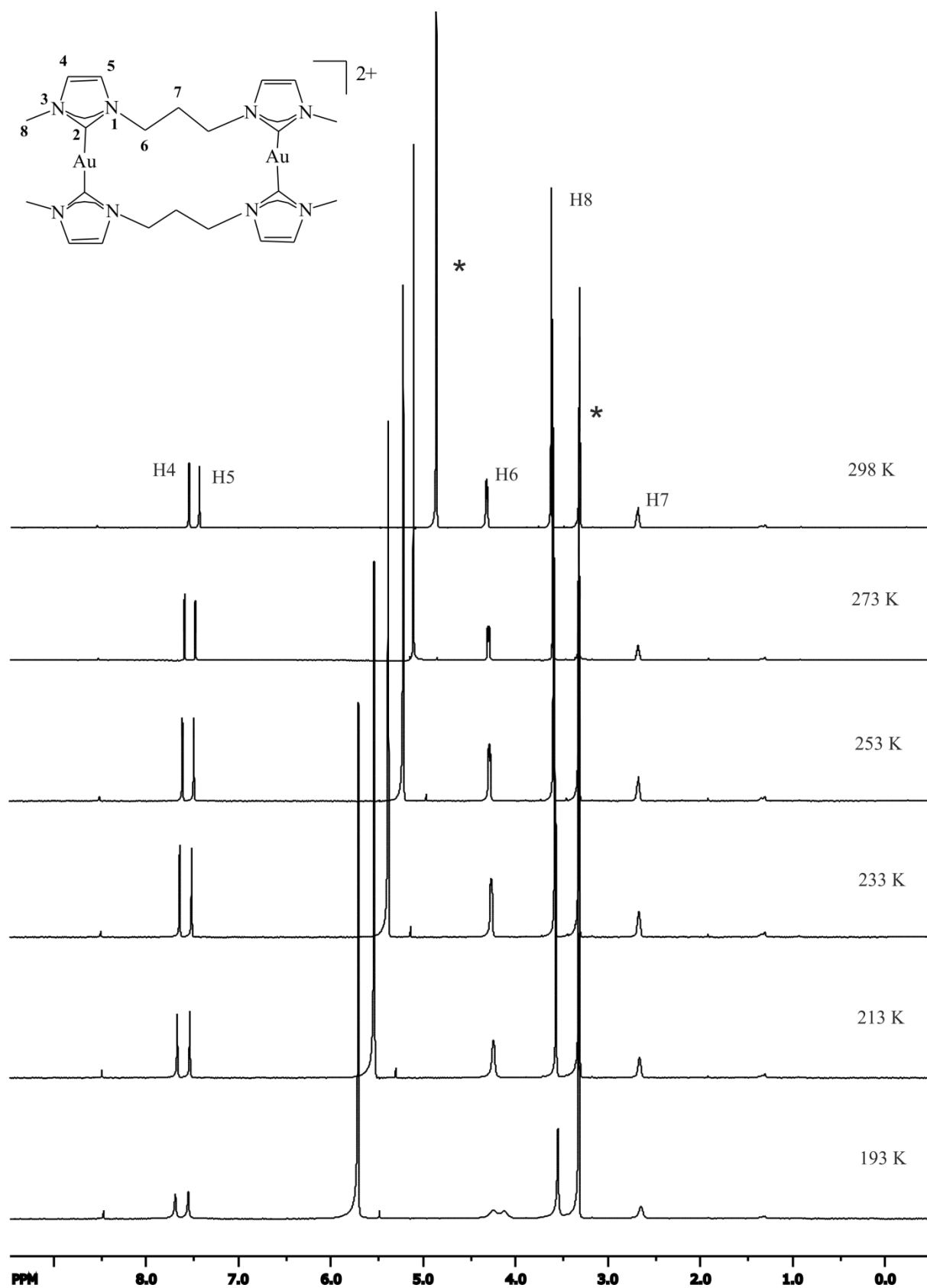
Figure 6.2.3. Low temperature ^{1}H NMR spectra (500.13 MHz, CD$_3$OD) of **9a**.
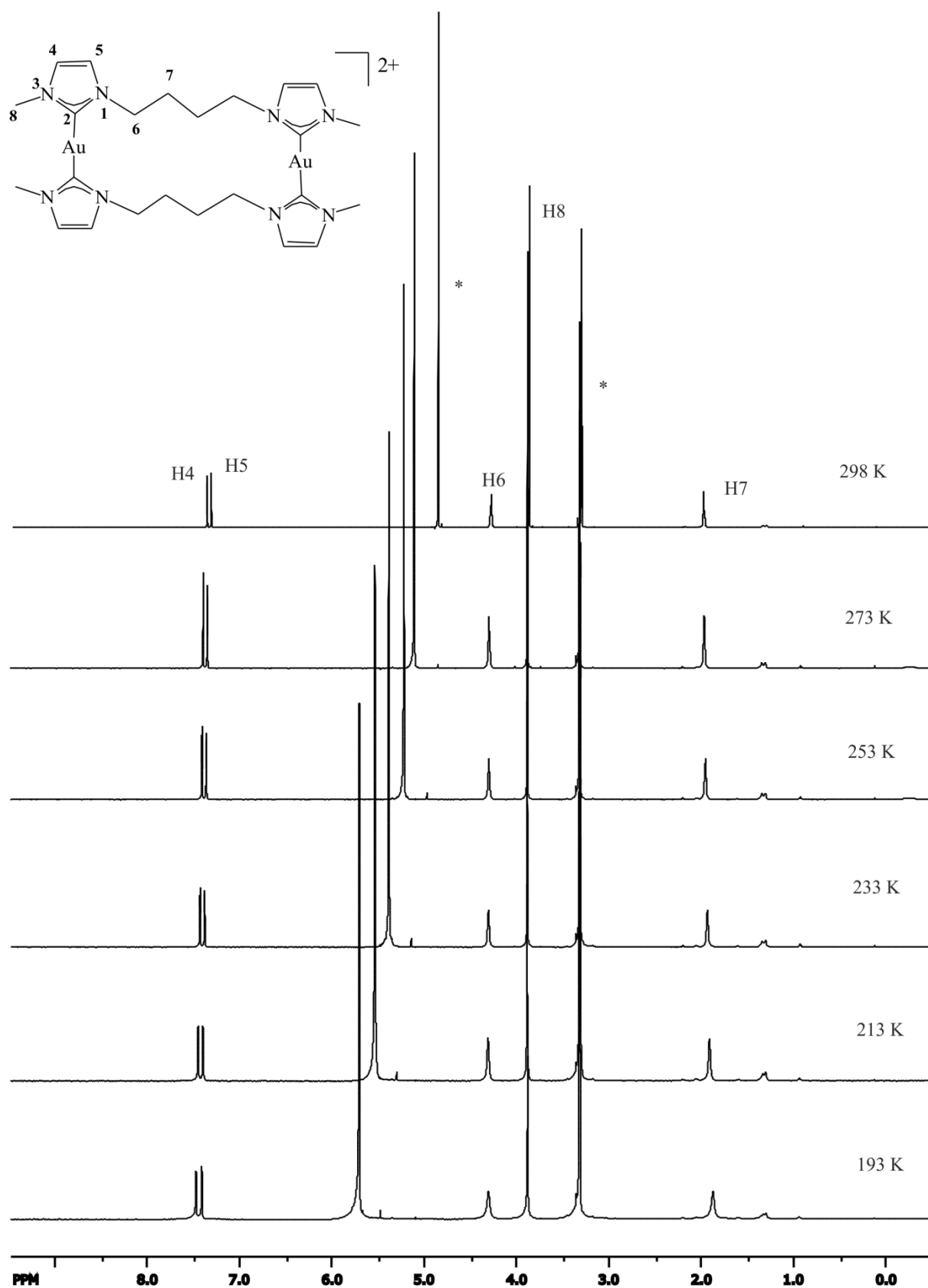
Figure 6.2.4. Low temperature ^{1}H NMR spectra (500.13 MHz, CD$_{3}$OD) of **10a**.
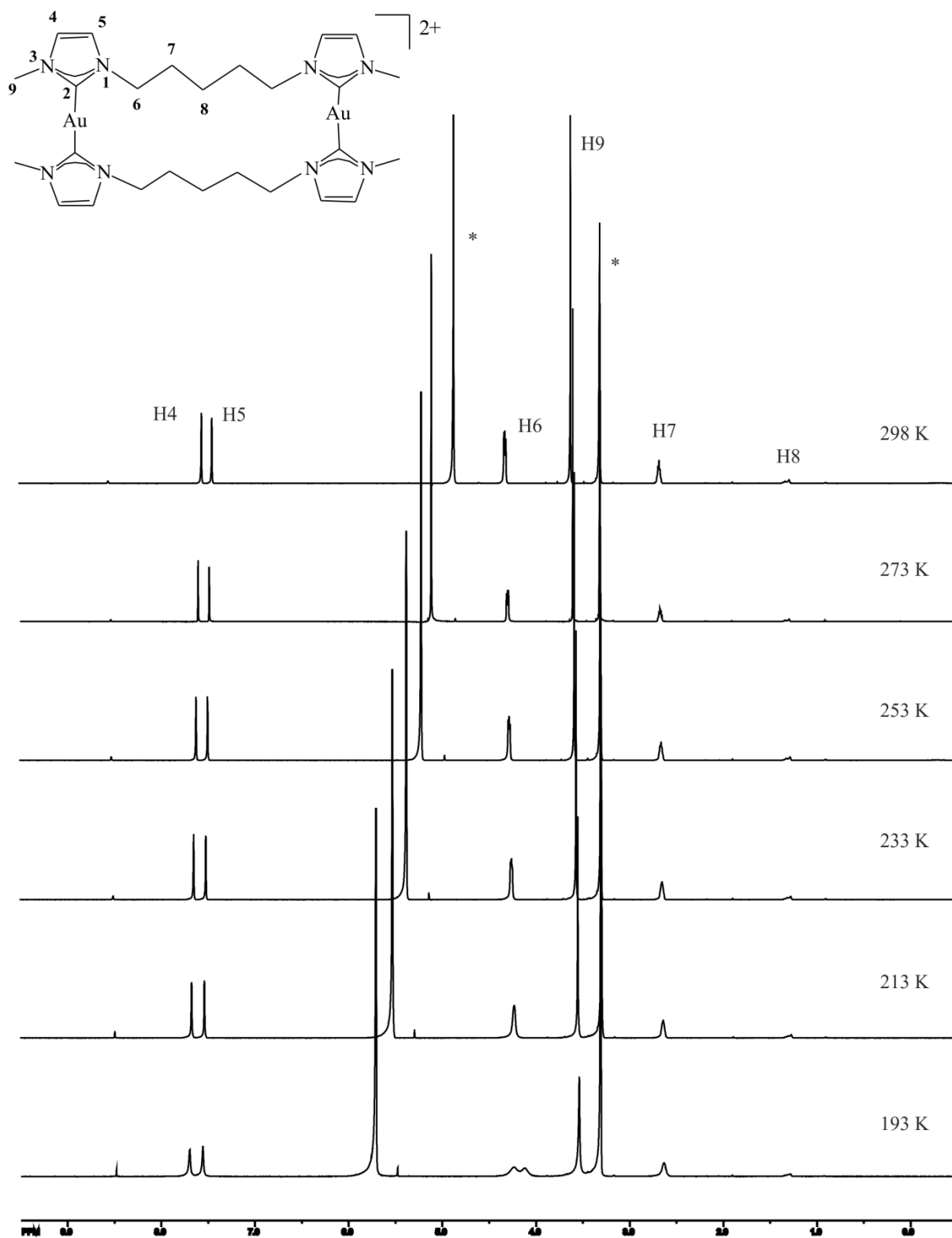
Figure 6.2.5. Low temperature ^{1}H NMR spectra (500.13 MHz, CD$_3$OD) of **11a**.
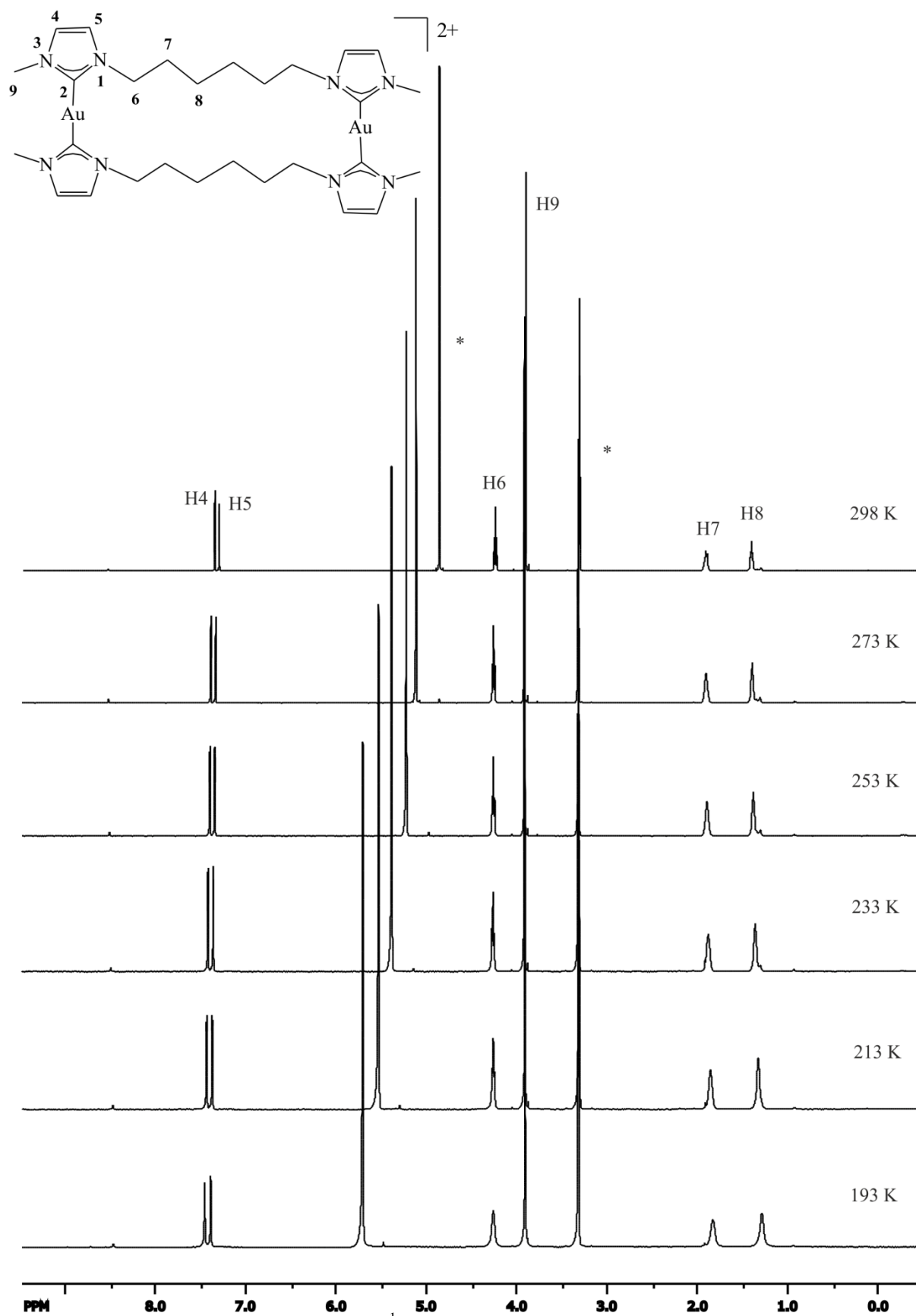
Figure 6.2.6. Low temperature ^{1}H NMR spectra (500.13 MHz, CD$_3$OD) of **11a**.

6.2.2. General Experimental Details & Substance Characterization

HPLC-grade solvents were used as received unless otherwise stated. NMR spectra were measured on Bruker Avance 300, 400 or 500 instruments. The references for NMR spectra were as follows: ^{1}H (methanol-d3 (3.31 ppm), DMSO-d5 (2.50 ppm), ACN-d2 (1.94 ppm)), ^{13}C{^{1}H} (methanol-d4 (49.0 ppm), [D6]DMSO (39.5 ppm), ACN-d3 (1.3 ppm)). Abbreviations used: br (broad), s (singlet), d (doublet), t (triplet), q (quartet), quint (quintet), sept (septet), m (multiplet). Assignments of ^{1}H and ^{13}C{^{1}H} NMR spectra are based on COSY, HMQC and HMBC experiments, when necessary. Numeration of the cations can be found in the VT-NMR spectra. ESI-MS spectra were measured on Bruker Daltonik microToF-Q. UV/Vis and fluorescence spectra were measured with 10^{-5} mol solutions in ACN in precision cuvettes (SUPRASIL®) with 10 mm thickness. For UV/Vis measurements a Perkin Elmer Lambda 18 was used, for fluorescence a Perkin LS50B. Scan rate was 120 nm/s between 200 nm and 700 nm.

7-12. Preparations of imidazolium derivatives are modified from literature procedure[87]. Alkyldibromide (5 mmol) and N-methylimidazole (1 mL, 10.4 mmol) were dissolved in dry toluene (15 mL) and stirred for 1 d at 110 °C. After cooling to room temperature, the white precipitate was filtered, washed with dry toluene/diethylether and dried in vacuo. The NMR data agree with those previously reported[87].

7a. 7 (101.4 mg, 0.3 mmol) and Au(SMe$_2$)Cl (88.37 mg, 0.3 mmol) were dissolved in dry DMF (7 mL). To maintain a clear solution the mixture was heated to 100 °C, if applicable. NaOAc (62.27 mg, 0.75 mmol) was added and the solution was stirred for 2 h at 120 °C. After cooling to room temperature, diethylether (15 mL) was added to precipitate the complex. The white powder was filtered, washed with diethylether and dried in vacuo. The complexes were purified by crystallization (slow diffusion of diethylether into a solution in methanol). Yield 99%. ^{1}H NMR (300 MHz, [D$_6$]DMSO, 25°C): δ=7.95 (s, 4H; H-4), 7.61 (d, ^3J(H,H)=2 Hz, 4H; H-5), 7.22 (d, ^2J(H,H)=14 Hz, 2H; H-6a), 6.37 (d, ^2J(H,H)=14 Hz, 2H; H-6b), 3.89 (s, 12H; H-7); ^{1}H NMR (300 MHz, CD$_3$OD, 25°C): δ=7.72 (s, 4H; H-4), 7.45 (d, ^3J(H,H)=2 Hz, 4H; H-5), 7.19 (d, ^2J(H,H)=14 Hz, 2H; H-6a), 6.27 (d, ^2J(H,H)=14 Hz, 2H; H-6b), 3.94 (s, 12H; H-7); ^{13}C NMR (75 MHz, CD$_3$OD, 25°C): δ=185.8 (C-2), 125.6 (C-5), 122.6 (C-4), 63.8 (C-6), 38.8 (C-7). UV/Vis (ACN): λ_{max} (ε)=253, 240 nm; fluorescence (ACN): λ_{ex}=255 nm; λ_{em}=327 nm; ESI (+): m/z (%): 373.1 (100) [M-2Br]$^{2+}$, 825.1 (5) [M−Br]$^+$, HRMS (ESI): m/z calcd for C$_{18}$H$_{24}$Au$_2$N$_8$$^{2+}$: 373.0722 [$M$-2Br]$^{2+}$; found: 373.0744. The NMR data agree with those previously reported[35]. The classification is now non-ambiguous.

7b. 7a (90.6 mg, 0.1 mmol) was dissolved in methanol (3 mL). A solution of KPF$_6$ (36.8 mg, 0.15 mmol) in water (4 mL) was added to precipitate the corresponding complex. The white powder was filtered, washed with water and methanol and dried in vacuo. The complex was purified by

crystallization (slow diffusion of diethylether into a solution in acetonitrile). Yield 99%. ^{1}H NMR (300 MHz, [D$_6$]DMSO, 25°C): δ=7.91 (s, 4H; H-4), 7.60 (d, ^3J(H,H)=2 Hz, 4H; H-5), 7.19 (d, ^2J(H,H)=14 Hz, 2H; H-6a), 6.34 (d, ^2J(H,H)=14 Hz, 2H; H-6b), 3.88 (s, 12H; H-7); ^{1}H NMR (300 MHz, CD$_3$CN, 25°C): δ=7.49 (d, ^3J(H,H)=2 Hz, 4H; H-4), 7.26 (d, ^3J(H,H)=2 Hz, 4H; NH-5), 6.92 (d, ^2J(H,H)=14 Hz, 2H; H-6a), 6.07 (d, ^2J(H,H)=14 Hz, 2H; H-6b), 3.85 (s, 12H; H-7) ; ^{13}C NMR (75 MHz, CD$_3$CN, 25°C): δ=185.3 (C-2), 125.5 (C-5), 122.3 (C-4), 63.6 (C-6), 39.2 (C-7); ^{19}F NMR (282 MHz, CD$_3$CN, 25°C): δ=-72.3 (d); ^{31}P NMR (121 MHz, CD$_3$CN, 25°C): δ=-143.2 (sept). UV/Vis (ACN): λ_{max} (ε)=254, 241 nm; fluorescence (ACN): λ_{ex}=255 nm; λ_{em}=356 nm; ESI (+): m/z (%): 373.1 (100) [M-2PF$_6$]$^{2+}$ 891.1 (10) [M−PF$_6$]$^+$. The NMR data agree with those previously reported[35]. The classification is now non-ambiguous.

8a. 8 (105.6 mg, 0.3 mmol) and Au(SMe$_2$)Cl (88.37 mg, 0.3 mmol) were dissolved in dry DMF (7 mL). To maintain a clear solution the mixture was heated to 100 °C, if applicable. NaOAc (62.27 mg, 0.75 mmol) was added and the solution was stirred for 2 h at 120 °C. After cooling to room temperature, diethylether (15 mL) was added to precipitate the complex. The white powder was filtered, washed with diethylether and dried in vacuo. The complexes were purified by crystallization (slow diffusion of diethylether into a solution in methanol). Yield 99%. ^{1}H NMR (400 MHz, CD$_3$OD, 25°C): δ=7.30 (s, 8H; H-4/5), 4.87 (s, 8H; H-6), 3.86 (s, 12H; H-7); ^{13}C NMR (75 MHz, CD$_3$OD, 25°C): δ=185.3 (C-2), 124.5 (C-5), 123.5 (C-4), 51.6 (C-6), 38.6 (C-7). UV/Vis (ACN): λ_{max} (ε)=249 nm; fluorescence (ACN): λ_{ex}=255 nm; λ_{em}=368 nm; ESI (+): m/z (%): 387.1 (100) [M-2Br]$^{2+}$, 855.1 (10) [M−Br]$^+$, HRMS (ESI): m/z calcd for C$_{20}$H$_{28}$Au$_2$N$_8$$^{2+}$: 387.0878 [$M$-2Br]$^{2+}$; found: 387.0878. The NMR data agree with those previously reported[35]. The classification is now non-ambiguous.

8b. 8a (93.4 mg, 0.1 mmol) was dissolved in methanol (3 mL). A solution of KPF$_6$ (36.8 mg, 0.15 mmol) in water (4 mL) was added to precipitate the corresponding complex. The white powder was filtered, washed with water and methanol and dried in vacuo. The complex was purified by crystallization (slow diffusion of diethylether into a solution in acetonitrile). Yield 99%. ^{1}H NMR (300 MHz, CD$_3$CN, 25°C): δ=7.11 (d, ^3J(H,H)=2 Hz, 4H; H-4), 7.06 (d, ^3J(H,H)=2 Hz, 4H; H-5), 4.73 (s, 8H; H-6), 3.77 (s, 12H; H-7); ^{13}C NMR (75 MHz, CD$_3$CN, 25°C): δ=184.9 (C-2), 124.3 (C-5), 123.0 (C-4), 51.2 (C-6), 38.8 (C-7); ^{19}F NMR (282 MHz, CD$_3$CN, 25°C): δ=-72.3 (d); ^{31}P NMR (121 MHz, CD$_3$CN, 25°C): δ=-143.2 (sept). UV/Vis (ACN): λ_{max} (ε)=251, 221 nm; fluorescence (ACN): λ_{ex}=255 nm; λ_{em}=369 nm; ESI (+): m/z (%): 387.6 (100) [M-2PF$_6$]$^{2+}$ 919.1 (17) [M−PF$_6$]$^+$. The NMR data agree with those previously reported[35]. The classification is now non-ambiguous.

9a. 9 (109.8 mg, 0.3 mmol) and Au(SMe$_2$)Cl (88.37 mg, 0.3 mmol) were dissolved in dry DMF (7 mL). To maintain a clear solution the mixture was heated to 100 °C, if applicable. NaOAc (62.27 mg, 0.75 mmol) was added and the solution was stirred for 2 h at 120 °C. After cooling to room

temperature, diethylether (15 mL) was added to precipitate the complex. The white powder was filtered, washed with diethylether and dried in vacuo. The complexes were purified by crystallization (slow diffusion of diethylether into a solution in methanol). Yield 99%. ^{1}H NMR (400 MHz, CD$_3$OD, 25°C): δ=7.56 (d, ^3J(H,H)=2 Hz, 4H; H-4), 7.45 (d, ^3J(H,H)=2 Hz, 4H; H-5), 4.32 (m, 8H; H-6), 3.63 (s, 12H; H-8), 2.68 (m, 4H; H-7); ^{13}C NMR (75 MHz, CD$_3$OD, 25°C): δ=184.7 (C-2), 125.4 (C-5), 122.2 (C-4), 48.1 (C-6), 37.8 (C-8), 30.5 (C-7). UV/Vis (ACN): λ_{max} (ε)=264 nm; fluorescence (ACN): λ_{ex}=255 nm; λ_{em}=373 nm; ESI (+): m/z (%): 401.1 (100) $[M\text{-}2Br]^{2+}$,883.2 (10) $[M-Br]^+$, HRMS (ESI): m/z calcd for C$_{22}$H$_{32}$Au$_2$N$_8$$^{2+}$: 401.1035 $[M\text{-}2Br]^{2+}$; found: 401.1042. The NMR data agree with those previously reported[35]. The classification is now non-ambiguous.

9b. **9a** (96.0 mg, 0.1 mmol) was dissolved in methanol (3 mL). A solution of KPF$_6$ (36.8 mg, 0.15 mmol) in water (4 mL) was added to precipitate the corresponding complex. The white powder was filtered, washed with water and methanol and dried in vacuo. The complex was purified by crystallization (slow diffusion of diethylether into a solution in acetonitrile). Yield 99%. ^{1}H NMR (400 MHz, CD$_3$CN, 25°C): δ=7.30 (d, ^3J(H,H)=2 Hz, 4H; H-4), 7.23 (d, ^3J(H,H)=2 Hz, 4H; H-5), 4.23 (m, 8H; H-6), 3.53 (s, 12H; H-8), 2.54 (m, 4H; H-7); ^{13}C NMR (75 MHz, CD$_3$CN, 25°C): δ=184.2 (C-2), 125.0 (C-5), 121.9 (C-4), 48.0 (C-6), 38.0 (C-8), 30.0 (C-7); ^{19}F NMR (282 MHz, CD$_3$CN, 25°C): δ=-72.4 (d); ^{31}P NMR (121 MHz, CD$_3$CN, 25°C): δ=-143.2 (sept). UV/Vis (ACN): λ_{max} (ε)=263 nm; fluorescence (ACN): λ_{ex}=255 nm; λ_{em}=374 nm; ESI (+): m/z (%): 401.1 (100) $[M\text{-}2PF_6]^{2+}$ 947.2 (10) $[M-PF_6]^+$. The NMR data agree with those previously reported[35]. The classification is now non-ambiguous.

10a. **10** (114.0 mg, 0.3 mmol) and Au(SMe$_2$)Cl (88.37 mg, 0.3 mmol) were dissolved in dry DMF (7 mL). To maintain a clear solution the mixture was heated to 100 °C, if applicable. NaOAc (62.27 mg, 0.75 mmol) was added and the solution was stirred for 2 h at 120 °C. After cooling to room temperature, diethylether (15 mL) was added to precipitate the complex. The white powder was filtered, washed with diethylether and dried in vacuo. The complexes were purified by crystallization (slow diffusion of diethylether into a solution in methanol). Yield 99%. ^{1}H NMR (400 MHz, CD$_3$OD, 25°C,): δ=7.38 (d, ^3J(H,H)=2 Hz, 4H; H-4), 7.33 (d, ^3J(H,H)=2 Hz, 4H; H-5), 4.29 (bs, 8H; H-6), 3.88 (s, 12H; H-8), 1.98 (m, 8H; H-7); ^{13}C NMR (75 MHz, CD$_3$OD, 25°C): δ=185.3 (C-2), 124.3 (C-5), 123.0 (C-4), 51.7 (C-6), 38.3 (C-8), 29.9 (C-8). UV/Vis (ACN): λ_{max} (ε)=260, 233, 218 nm; fluorescence (ACN): λ_{ex}=255 nm; λ_{em}=370, 326 nm; ESI (+): m/z (%): 415.1 (100) $[M\text{-}2Br]^{2+}$, HRMS (ESI): m/z calcd for C$_{24}$H$_{36}$Au$_2$N$_8$: 415.1192 $[M\text{-}2Br]^{2+}$; found: 415.1195. The NMR data agree with those previously reported[35]. The classification is now non-ambiguous.

10b. **10a** (98.8 mg, 0.1 mmol) was dissolved in methanol (3 mL). A solution of KPF$_6$ (36.8 mg, 0.15 mmol) in water (4 mL) was added to precipitate the corresponding complex. The white powder was filtered, washed with water and methanol and dried in vacuo. The complex was purified by

crystallization (slow diffusion of diethylether into a solution in acetonitrile). Yield 99%. ^{1}H NMR (400 MHz, CD$_3$CN, 25°C): δ=7.17 (s, 8H; H-4/5), 4.19 (s, 8H; H-6), 3.80 (s, 12H; H-8), 1.89 (s, 8H; H-7); ^{13}C NMR (75 MHz, CD$_3$CN, 25°C): δ=184.9 (C-2), 124.1 (C-5), 122.7 (C-4), 51.4 (C-6), 38.5 (C-8), 29.4 (C-7); ^{19}F NMR (282 MHz, CD$_3$CN, 25°C): δ=-72.4 (d); ^{31}P NMR (121 MHz, CD$_3$CN, 25°C): δ=-143.2 (sept)). UV/Vis (ACN): λ_{max} (ε)=259, 244, 233, 219 nm; fluorescence (ACN): λ_{ex}=255 nm; λ_{em}=374 nm; ESI (+): m/z (%): 415.1 (100) [M-2PF$_6$]$^{2+}$ 975.2 (26) [M−PF$_6$]$^+$. The NMR data agree with those previously reported[35]. The classification is now non-ambiguous.

11a. 11 (118.2 mg, 0.3 mmol) and Au(SMe$_2$)Cl (88.37 mg, 0.3 mmol) were dissolved in dry DMF (7 mL). To maintain a clear solution the mixture was heated to 100 °C, if applicable. NaOAc (62.27 mg, 0.75 mmol) was added and the solution was stirred for 2 h at 120 °C. After cooling to room temperature, diethylether (15 mL) was added to precipitate the complex. The white powder was filtered, washed with diethylether and dried in vacuo. The complexes were purified by crystallization (slow diffusion of diethylether into a solution in methanol). Yield 99%. ^{1}H NMR (400 MHz, CD$_3$OD, 25°C): δ=7.42 (d, ^3J(H,H)=2 Hz, 4H; H-4), 7.38 (d, ^3J(H,H)=2 Hz, 4H; H-5), 4.30 (t, ^3J(H,H)=7 Hz, 8H; H-6), 3.67 (s, 12H; H-9), 2.04 (quint, ^3J(H,H)=7 Hz, 8H; H-7), 1.42 (m, 4H, H-8); ^{13}C NMR (75 MHz, CD$_3$OD, 25°C): δ=185.4 (C-2), 124.6 (C-5), 122.8 (C-4), 51.8 (C-6), 38.0 (C-9), 31.7 (C-7), 24.9 (C-8). UV/Vis (ACN): λ_{max} (ε)=256, 245, 233 nm; fluorescence (ACN): λ_{ex}=255 nm; λ_{em}=373 nm; ESI (+): m/z (%): 429.1(100) [M-2Br]$^{2+}$, 883.2 (10) [M−Br]$^+$,, HRMS (ESI): m/z calcd for C$_{26}$H$_{40}$Au$_2$N$_8$$^{2+}$: 429.1348 [$M$-2Br]$^{2+}$; found: 429.1413.

11b. 11a (101.6 mg, 0.1 mmol) was dissolved in methanol (3 mL). A solution of KPF$_6$ (36.8 mg, 0.15 mmol) in water (4 mL) was added to precipitate the corresponding complex. The white powder was filtered, washed with water and methanol and dried in vacuo. The complex was purified by crystallization (slow diffusion of diethylether into a solution in acetonitrile). Yield 99%. ^{1}H NMR (400 MHz, CD$_3$CN, 25°C): δ=7.23 (d, ^3J(H,H)=2 Hz, 4H; H-4), 7.21 (d, ^3J(H,H)=2 Hz, 4H; H-5), 4.22 (t, ^3J(H,H)=7 Hz, 8H; H-6), 3.54 (s, 12H; H-9), 1.94 (m, 8H; H-7), 1.33 (m, 4H, H-8); ^{13}C NMR (75 MHz, CD$_3$CN, 25°C): δ=184.9 (C-2), 124.4 (C-5), 122.4 (C-4), 51.6 (C-6), 38.1 (C-9), 31.0 (C-7), 24.4 (C-8); ^{19}F NMR (282 MHz, CD$_3$CN, 25°C): δ=-72.4 (d); ^{31}P NMR (121 MHz, CD$_3$CN, 25°C): δ=-143.2 (sept). UV/Vis (ACN): λ_{max} (ε)=256, 245 nm; fluorescence (ACN): λ_{ex}=255 nm; λ_{em}=322 nm; ESI (+): m/z (%): 429.1 (100) [M-2PF$_6$]$^{2+}$ 1003.2 (9) [M−PF$_6$]$^+$.

12a. 12 (122.5 mg, 0.3 mmol) and Au(SMe$_2$)Cl (88.37 mg, 0.3 mmol) were dissolved in dry DMF (7 mL). To maintain a clear solution the mixture was heated to 100 °C, if applicable. NaOAc (62.27 mg, 0.75 mmol) was added and the solution was stirred for 3 h at 120 °C. After cooling to room temperature, diethylether (15 mL) was added to precipitate the complex. The white powder was filtered, washed with diethylether and dried in vacuo. The complexes were purified by crystallization (slow diffusion of diethylether into a solution in methanol). Yield 93%. ^{1}H NMR (400 MHz, CD$_3$OD,

25°C): δ=7.37 (d, ^3J(H,H)=2 Hz, 4H; H-4), 7.32 (d, ^3J(H,H)=2 Hz, 4H; H-5), 4.25 (t, ^3J(H,H)=7 Hz, 8H; H-6), 3.91 (s, 12H; H-9),1.91 (m, 8H; H-7), 1.40 (m, 8H, H-8); ^{13}C NMR (75 MHz, CD$_3$OD, 25°C): δ=185.3 (C-2), 124.2 (C-5), 122.9 (C-4), 52.2 (C-6), 38.2 (C-9), 32.9 (C-7), 27.8 (C-8). UV/Vis (ACN): λ_{max} (ε)=260, 244, 233, 218 nm; fluorescence (ACN): λ_{ex}=255 nm; λ_{em}=381 nm; ESI (+): m/z (%): 443.2 (100) [M-2Br]$^{2+}$, HRMS (ESI): m/z calcd for C$_{28}$H$_{44}$Au$_2$N$_8$$^{2+}$: 443.1505 [$M$-2Br]$^{2+}$; found: 443.1508.

12b. 12a (104.4 mg, 0.1 mmol) was dissolved in methanol (3 mL). A solution of KPF$_6$ (36.8 mg, 0.15 mmol) in water (4 mL) was added to precipitate the corresponding complex. The white powder was filtered, washed with water and methanol and dried in vacuo. The complex was purified by crystallization (slow diffusion of diethylether into a solution in acetonitrile). Yield 92%. ^1H NMR (400 MHz, CD$_3$CN, 25°C): δ=7.18 (d, ^3J(H,H)=2 Hz, 4H; H-4), 7.16 (d, ^3J(H,H)=2 Hz, 4H; H-5), 4.16 (t, ^3J(H,H)=7 Hz, 8H; H-6), 3.84(s, 12H, H-9), 1.83 (m, 8H; H-7), 1.33 (m, 8H, H-8); ^{13}C NMR (75 MHz, CD$_3$CN, 25°C): δ=184.9 (C-2), 124.0 (C-5), 122.6 (C-4), 51.9 (C-6), 38.5 (C-9), 32.3 (C-7), 27.2 (C-8); ^{19}F NMR (282 MHz, CD$_3$CN, 25°C): δ=-72.4 (d); ^{31}P NMR (121 MHz, CD$_3$CN, 25°C): δ=-143.2 (sept). UV/Vis (ACN): λ_{max} (ε)=260, 244 nm; fluorescence (ACN): λ_{ex}=255 nm; λ_{em}=326 nm; ESI (+): m/z (%): 443.2 (100) [M-2PF$_6$]$^{2+}$ 1031.3 (4) [M−PF$_6$]$^+$.

Characterization of unpublished substances without VT-NMR spectra

Figure 6.2.7. ^1H NMR (400 MHz, CD$_3$CN, r. t.) spectrum of **11b**. *partially deuterated and undeuterated ACN and water, respectively.

Figure 6.2.8. ^{13}C NMR (75 MHz, CD$_3$CN, r. t.) spectrum of 11**b**. *partially deuterated and undeuterated ACN, respectively.

Figure 6.2.9. microTof-Q ESI(+) mass spectrum of **11b** in ACN.

Figure 6.2.10. ^{1}H NMR (400 MHz, CD$_3$CN, r. t.) spectrum of **12b**. *partially deuterated and undeuterated ACN and water, respectively.

Figure 6.2.11. ^{13}C NMR (75 MHz, CD$_3$CN, r. t.) spectrum of **12b**. *partially deuterated and undeuterated ACN, respectively.

Figure 6.2.12. microTof-Q ESI(+) mass spectrum of **12b** in ACN.

6.2.4. Crystallographic Data

Crystal structure determination: Data for the X-ray crystallographic analyses were performed on a Nonius KappaCCD diffractometer (**7a**, **8a**, **8b**, **9a**, **9b**, **10a**, **11b**, **12b**), a Bruker X8 KappaApexII diffractometer (**7b**, **10b**) or a STOE IPDS2T diffractometer (**12a**) using graphite monochromated Mo-Kα radiation (λ = 0.71073 Å). Intensities were measured by fine-slicing φ- and ω-scans and corrected for background, polarization and Lorentz effects. A semi-empirical absorption correction was applied for the data sets following Blessing's method[94]. The structures were solved by direct methods and refined anisotropically by the least squares procedure implemented in the ShelX programme system[95]. The hydrogen atoms were included isotropically using the riding model on the carbon atoms.

Table 6.2.2. Crystallographic Data of **7a/b**.

	7a	7b
formula	$C_{22}H_{32}Au_2N_8Br_2$	$C_{22}H_{32}Au_2N_8P_2F_{12}$
cryst size (mm^3)	0.25 x 0.08 x 0.06	0.12 x 0.06 x 0.05
cryst syst	triclinic	monoclinic
space group	P-1	C 2/m
a (Å)	7.5549(9)	17.0766(5)
b (Å)	12.2807(14)	13.3831(4)
c (Å)	13.3725(17)	12.7710(4)
α (deg)	70.942(4)	90
β (deg)	82.744(4)	105.0990(10)
γ (deg)	88.960(4)	90
V (Å^3)	1162.9(2)	2817.90(15)
Z	2	4
ρ_{calcd} (mg m^3)	2.588	2.443
F_{000}	832	1936
μ (mm^{-1})	16.059	10.620
transmissions	0.4458-0.1079	0.6188-0.3622
Θ range (deg)	2.75-27.48	3.04-27.99
reflns collected	48844	3534
R_{int}	0.0608	0.0449
GOF	1.052	1.218
R1	0.0368-0.0555	0.0187-0.0203
wR2	0.0830-0.0943	0.0534-0.0540
largest diff peak (e Å^{-3})	2.866	1.243

Table 6.2.3. Crystallographic Data of **8a/b**.

	8a	8b
formula	$C_{24}H_{36}Au_2N_8Br_2$	$C_{24}H_{36}Au_2N_8P_2F_{12}$
cryst size (mm^3)	0.34 x 0.20 x 0.04	0.20 x 0.10 x 0.05
cryst syst	triclinic	monoclinic
space group	P-1	C 2/m
a (Å)	9.7703(7)	14.2284(8)
b (Å)	11.2794(8)	13.1742(5)
c (Å)	12.7721(9)	8.6638(5)
α (deg)	71.643(2)	90
β (deg)	69.989(2)	116.197(2)
γ (deg)	82.087(3)	90
V (Å^3)	1254.54(15)	1457.19(13)
Z	2	2
ρ_{calcd} (mg m^3)	2.473	2.426
F_{000}	864	1000
μ (mm^{-1})	14.891	10.272
transmissions	0.5873-0.0808	0.3079-0.1048
Θ range (deg)	2.20-28.00	2.62-27.00
reflns collected	39576	4940
R_{int}	0.0764	0.0512
GOF	1.054	1.061
R1	0.0556-0.0704	0.0256-0.0634
wR2	0.1515-0.1658	0.0287-0.0645
largest diff peak (e Å^{-3})	4.633	1.959

Table 6.2.4. Crystallographic Data of **9a/b**.

	9a	**9b**
formula	$C_{26}H_{40}Au_2N_8Br_2 * CH_3OH$	$C_{26}H_{40}Au_2N_8P_2F_{12}$
cryst size (mm^3)	0.21 x 0.10 x 0.06	0.20 x 0.16 x 0.08
cryst syst	monoclinic	hexagonic
space group	C2/c	P 3_1 1 2
a (Å)	13.1421(11)	11.9420(2)
b (Å)	17.5172(16)	11.9420(2)
c (Å)	13.8320(11)	18.9955(4)
α (deg)	90	90
β (deg)	117.786(2)	90
γ (deg)	90	120
V ($Å^3$)	2817.1(4)	2346.04(7)
Z	4	3
ρ_{calcd} (mg m^3)	2.344	2.320
F_{000}	1864	1548
μ (mm^{-1})	13.273	9.574
transmissions	0.5031-0.1670	0.5147-0.2504
Θ range (deg)	2.11-28.00	1.07-28.00
reflns collected	31616	30574
R_{int}	0.0780	0.0676
GOF	1.024	1.029
R1	0.0684-0.1013	0.0246-0.0268
wR2	0.1525-0.1770	0.0516-0.0522
largest diff peak (e $Å^{-3}$)	6.610	0.756

Table 6.2.5. Crystallographic Data of **10a/b**.

	10a	10b
formula	$C_{28}H_{44}Au_2N_8Br_2 * H_2O$	$C_{28}H_{44}Au_2N_8P_2F_{12}$
cryst size (mm^3)	0.22 x 0.08 x 0.06	0.22 x 0.08 x 0.06
cryst syst	monoclinic	triclinic
space group	P 2_1/c	P-1
a (Å)	16.3882(8)	9.2748(7)
b (Å)	12.0180(4)	9.6942(7)
c (Å)	15.5492(8)	10.2449(7)
α (deg)	90	78.494(3)
β (deg)	96.270(2)	71.803(3)
γ (deg)	90	70.517(3)
V (Å^3)	3044.2(2)	820.28(10)
Z	4	1
ρ_{calcd} (mg m^3)	2.200	2.268
F_{000}	1896	532
μ (mm^{-1})	12.284	9.130
transmissions	0.5260-0.1730	0.0089-0.0076
Θ range (deg)	2.11-26.00	2.42-25.24
reflns collected	19663	2973
R_{int}	0.1413	0.0950
GOF	1.055	1.076
R1	0.0614-0.0804	0.0542-0.0568
wR2	0.1564-0.1644	0.1436-0.1458
largest diff peak (e Å^{-3})	3.800	8.021

Table 6.2.6. Crystallographic Data of **11b**.

	11b
formula	$C_{30}H_{48}Au_2N_8P_2F_{12}$
cryst size (mm^3)	0.80 x 0.04 x 0.03
cryst syst	monoclinic
space group	$P\,2_1$
a (Å)	7.3836(4)
b (Å)	19.6572(11)
c (Å)	12.3320(7)
α (deg)	90
β (deg)	97.411(2)
γ (deg)	90
V (Å^3)	1774.93(17)
Z	2
ρ_{calcd} (mg m^3)	2.149
F_{000}	1096
μ (mm^{-1})	8.442
transmissions	0.7858-0.0565
Θ range (deg)	2.97-28.00
reflns collected	40048
R_{int}	0.0435
GOF	1.023
R1	0.0244-0.0394
wR2	0.0452-0.0498
largest diff peak (e Å^{-3})	1.250

Table 6.2.7. Crystallographic Data of **12a/b**.

	12a	12b
formula	$C_{32}H_{52}Au_2N_8Br_2 * 2CH_3OH$	$C_{32}H_{52}Au_2N_8P_2F_{12}$
cryst size (mm^3)	0.08 x 0.06 x 0.03	0.40 x 0.12 x 0.08
cryst syst	triclinic	triclinic
space group	P-1	P-1
a (Å)	9.2768(6)	9.2356(6)
b (Å)	9.4559(7)	10.5057(7)
c (Å)	10.9034(7)	11.3946(7)
α (deg)	103.894(5)	114.630(2)
β (deg)	90.784(5)	91.570(2)
γ (deg)	100.918(6)	109.390(2)
V (Å^3)	909.90(11)	930.11(11)
Z	1	1
ρ_{calcd} (mg m^3)	2.027	2.101
F_{000}	532	564
μ (mm^{-1})	10.287	8.058
transmissions	0.7478-0.4933	0.5650-0.1409
Θ range (deg)	2.85-25.25	3.40-27.99
reflns collected	6194	23495
R_{int}	0.0928	0.0753
GOF	1.016	1.025
R1	0.0674-0.0786	0.0421-0.0704
wR2	0.1724-0.1774	0.0897-0.1005
largest diff peak (e Å^{-3})	2.861	2.080

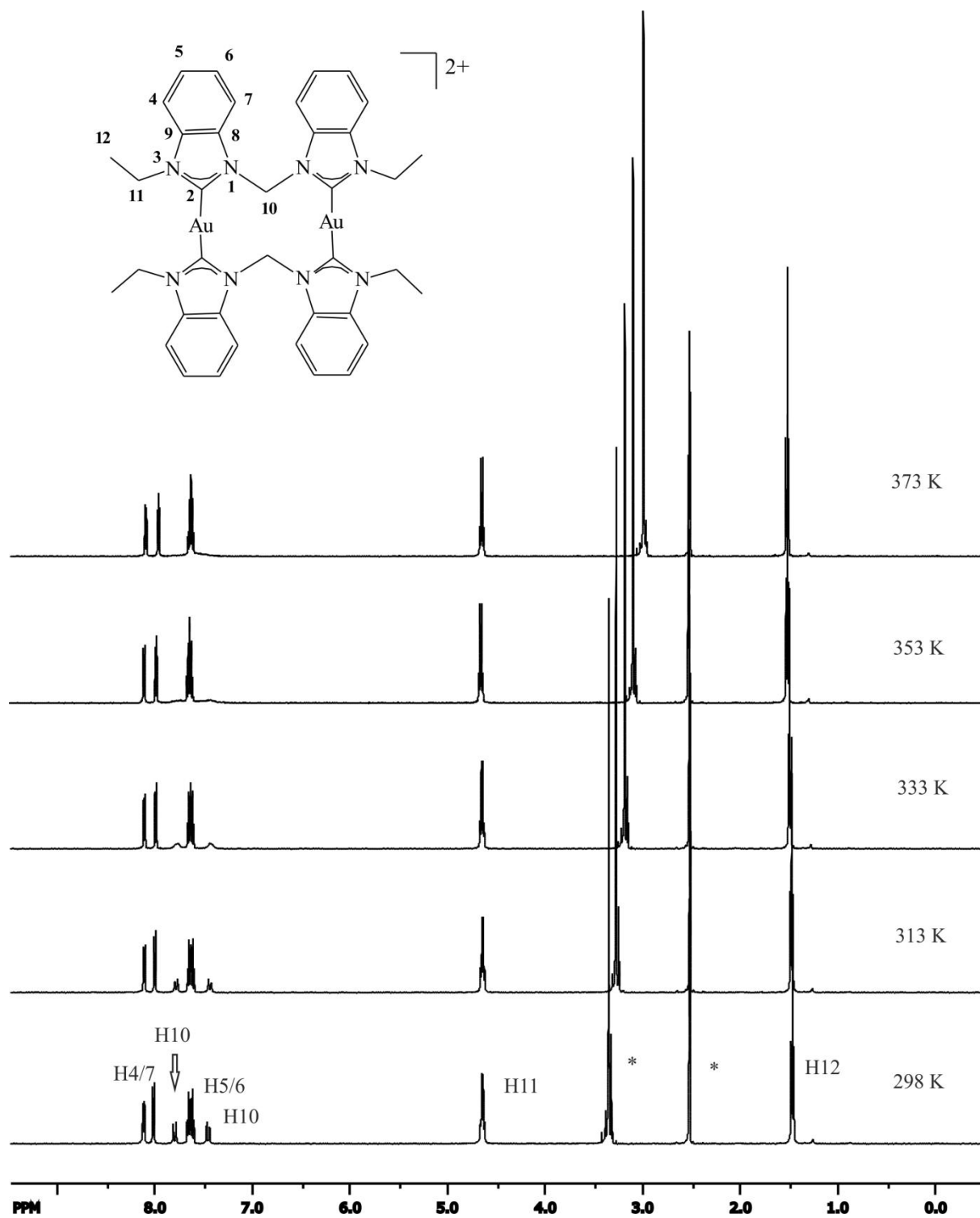## 6.3 Anhang zu BIm Komplexe

6.3.1. VT-NMR

Figure 6.3.1. High temperature ^{1}H NMR spectra (500.13 MHz, CD$_3$OD) of **13a**.

Figure 6.3.2: Eyring plots for the kinetic rate constants given in Table x obtained from line shape analysis of the VT-NMR spectra shown in Figure x

Table 6.3.1. Thermal activation parameters determined from the Eyring plots in Figure x for the dynamic behaviour observed for the metallamacrocyclic system **13a**.

compound	anion	linker	signal	$\Delta H^{\ddagger}$ / kJ mol^{-1}	$\Delta S^{\ddagger}$ / J mol^{-1}K^{-1}	$\Delta G^{\ddagger}_{(298K)}$ / kJ mol^{-1}
13a	Br$^-$	CH$_2$	H6	56 ± 6	-5 ± 18	70 ± 8

Figure 6.3.3. Low temperature ^{1}H NMR spectra (500.13 MHz, CD$_3$OD) of **14a**.

Figure 6.3.4. Low temperature ^{1}H NMR spectra (500.13 MHz, CD$_3$OD) of **16a**.
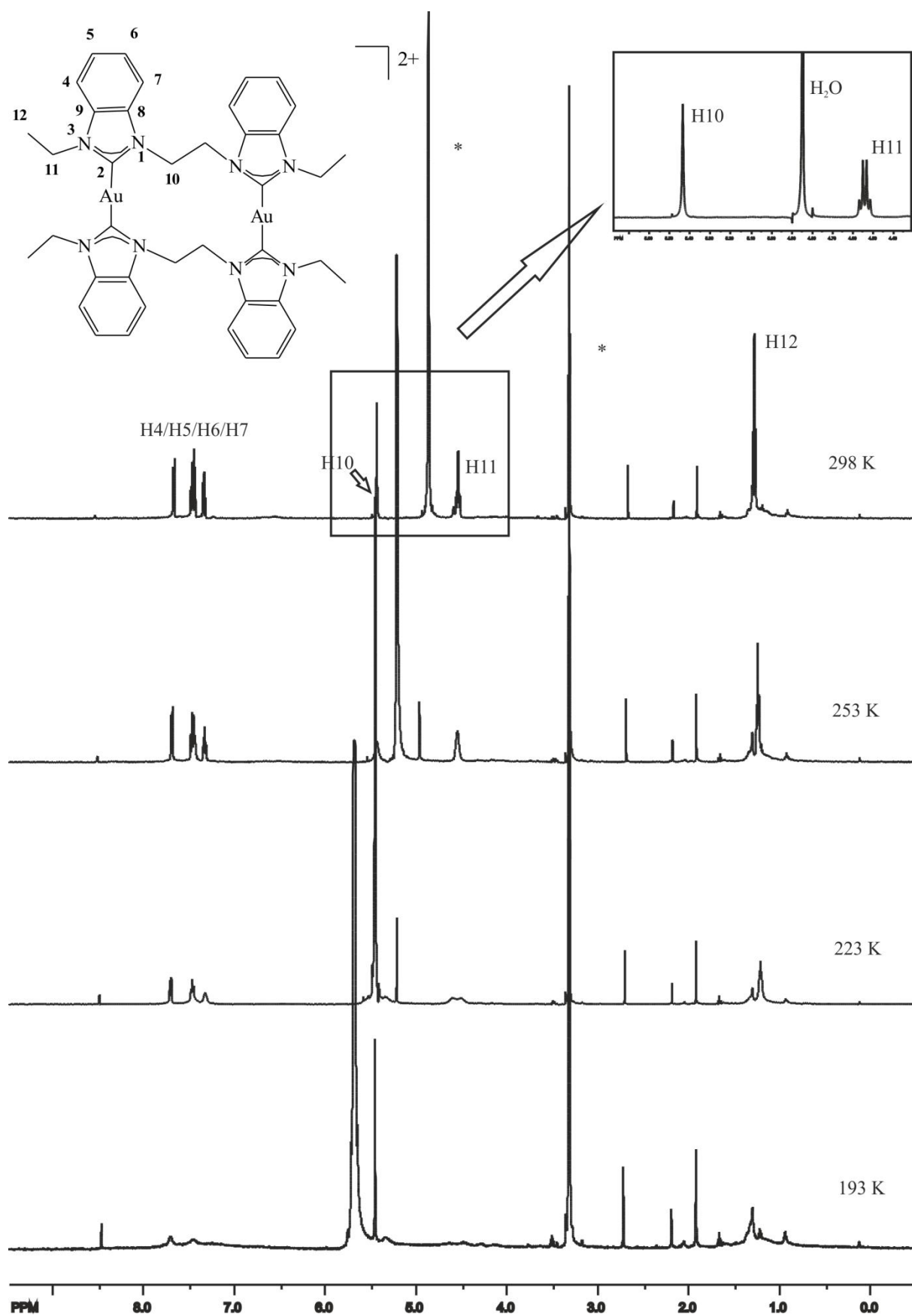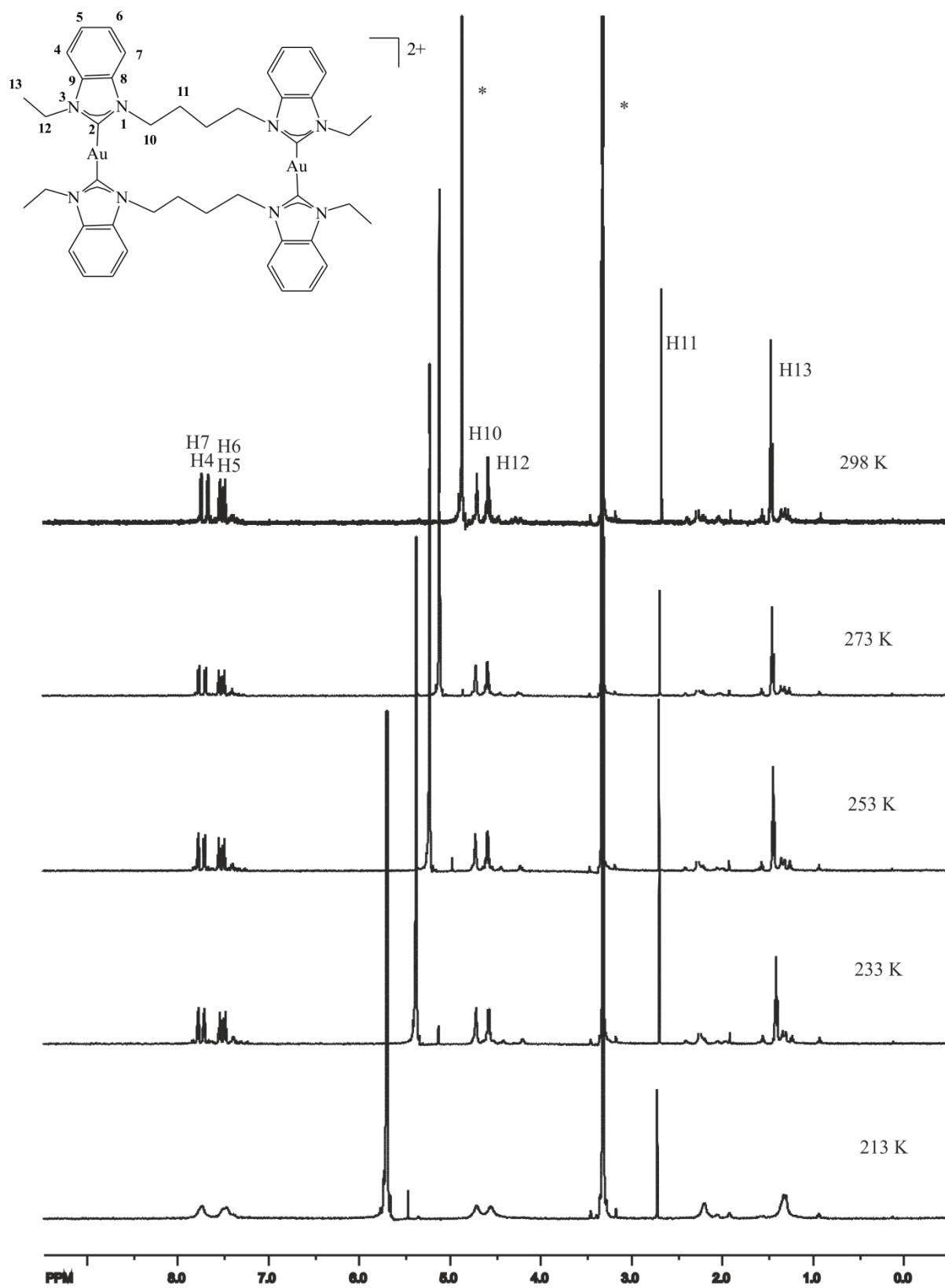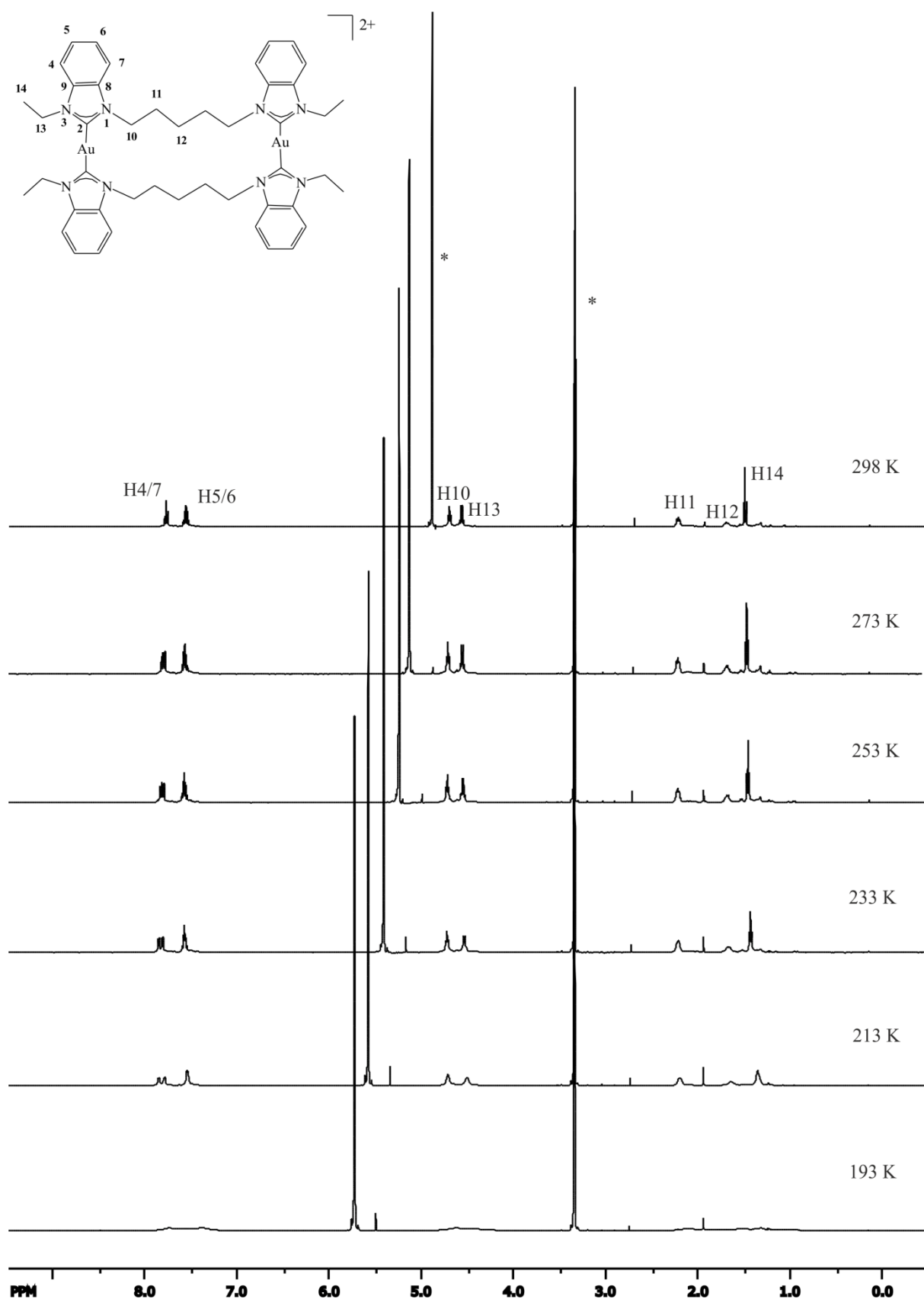
Figure 6.3.5. Low temperature ^{1}H NMR spectra (500.13 MHz, CD$_3$OD) of **17a**.
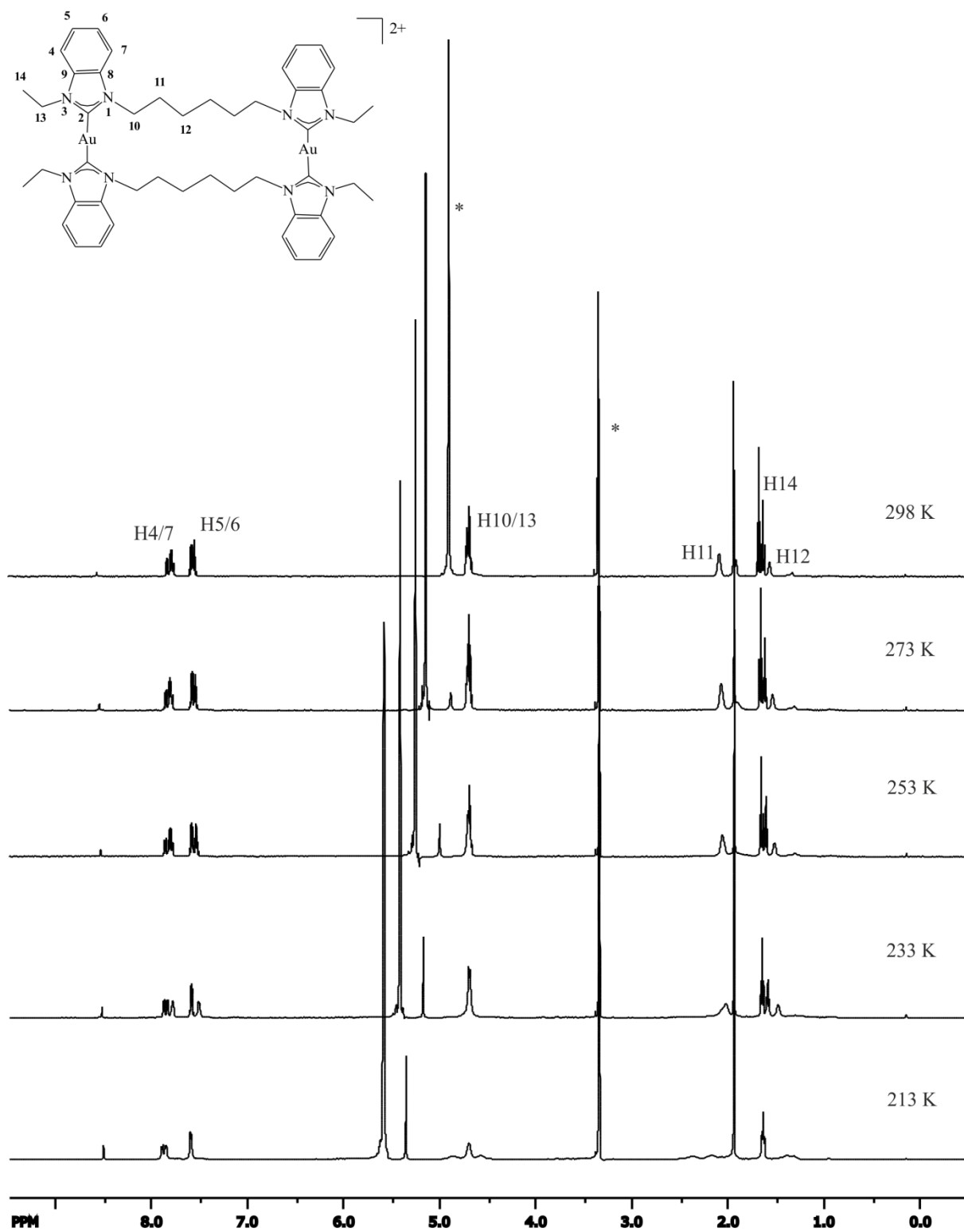
Figure 6.3.6. Low temperature ^{1}H NMR spectra (500.13 MHz, CD$_3$OD) of **17a**.
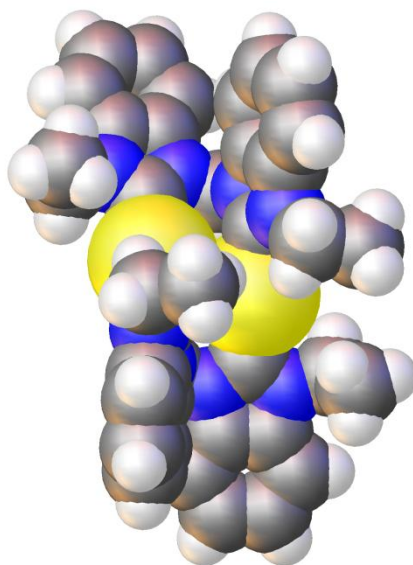
6.3.2. X-ray

Figure 6.3.7. Spacefill drawing of complex **13a**.

6.3.3. General Experimental Details & Substance Characterization

HPLC-grade solvents and N-methylbenzimidazole were used as received unless otherwise stated. N-Ethylbenzimidazole was synthesized according to the literature procedure[88]. NMR spectra were measured on Bruker Avance 300, 400 or 500 instruments. The references for NMR spectra were as follows: ^{1}H (methanol-d3 (3.31 ppm), DMSO-d5 (2.50 ppm),), ^{13}C{^{1}H} (methanol-d4 (49.0 ppm), DMSO-d6 (39.5 ppm),). Abbreviations used: br (broad), s (singlet), d (doublet), t (triplet), q (quartet), quint (quintet), sept (septet), m (multiplet). Assignments of ^{1}H and ^{13}C{^{1}H} NMR spectra are based on COSY, HMQC and HMBC experiments, when necessary. Numeration of the cations can be found in the VT-NMR spectra. ESI-MS spectra were measured on Bruker Daltonik microToF-Q. UV/Vis and fluorescence spectra were measured with 10^{-5}mol solutions in ACN in precision cuvettes (SUPRASIL®) with 10 mm thickness. For UV/Vis measurements a Perkin Elmer Lambda 18 was used, for fluorescence a Perkin LS50B. Scan rate was 120 nm/s between 200 nm and 700 nm.

13. Methyldibromide (0.26 mL, 3.75 mmol) and N-ethylbenzimidazole (0.731 g, 5 mmol) were dissolved in dry toluene (10 mL) and stirred for 21 d at 110 °C. After cooling to room temperature, the white precipitate was filtered, washed with dry toluene/diethylether and dried in vacuo. Yield 82%. ^{1}H NMR (400 MHz, CD$_3$OD, 25°C): δ=10.30 (s, 2H, H-2), 8.32 (m, 2H; H-4), 8.09 (m, 2H; H-7), 7.81 (m, 4H; H-5/6), 7.49 (s, 2H; H-10), 4.66 (q, ^3J(H,H)=7 Hz, 4H; H-11), 1.72 (t, ^3J(H,H)=7 Hz, 4H; H-12); ^{13}C NMR (75 MHz, CD$_3$OD, 25°C): δ=144.1 (C-2), 132.8 (C-8), 132.3 (C-9), 129.4 (C-5), 128.9 (C-6), 115.2 (C-7), 114.4 (C-4), 56.7 (C-10), 44.6 (C-11), 14.4 (C-12). ESI (+): m/z (%): 153.1 (80) [M-2Br]$^{2+}$, 305.2 (100) [M−H-2Br]$^+$, HRMS (ESI): m/z calcd for C$_{19}$H$_{21}$N$_4^+$: 305.1761 [M-H-2Br]$^+$; found: 305.1774.

13a. 13 (139.9 mg, 0.3 mmol) and Au(SMe$_2$)Cl (88.37 mg, 0.3 mmol) were dissolved in dry DMF (7 mL). To maintain a clear solution the mixture was heated to 100 °C, if applicable. NaOAc (62.27 mg, 0.75 mmol) was added and the solution was stirred for 2 h at 120 °C. After cooling to room temperature, diethylether (15 mL) was added to precipitate the complex. The white powder was filtered, washed with diethylether and dried in vacuo. The complexes were purified by crystallization (slow diffusion of diethylether into a solution in methanol). Yield 99%. ^{1}H NMR (400 MHz, CD$_3$OD, 25°C): δ=8.02 (m, 4H; H-4), 7.89 (m, 4H; H-7), 7.78 (d, ^3J(H,H)=14 Hz, 4H; H-10a), 7.63 (m, 8H; H-5, H-6), 7.26 (d, ^2J(H,H)=14 Hz, 2H; H-10b), 4.66 (m, 8H; H-11), 1.54 (t, ^3J(H,H)=7 Hz, 12H; H-12); ^{13}C NMR (100 MHz, CD$_3$OD, 25°C): δ=191.5 (C-2), 134.3 (C-8 or C-9), 134.2 (C-8 or C-9), 127.2 (C-5 or C-6), 127.1 (C-5 or C-6), 113.9 (C-4 or C-7), 113.0 (C-4 or C-7), 59.9 (C-10), 45.9 (C-11), 16.2 (C-12). UV/Vis (ACN): λ_{max} (ε)=283 nm; fluorescence (ACN): λ_{ex}=273 nm; λ_{em}=398 nm; ESI (+): m/z (%): 501.2 (100) $[M$-2Br$]^{2+}$, 1081.3 (1) $[M-$Br$]^+$, HRMS (ESI): m/z calcd for C$_{38}$H$_{40}$Au$_2$N$_8$Br^{2+}: 1081.1885 $[M$-2Br$]^{2+}$; found: 1081.1881.

14. Ethyldibromide (0.33 mL, 3.75 mmol) and N-ethylbenzimidazole (0.731 g, 5 mmol) were dissolved in dry toluene (10 mL) and stirred for 9 d at 110 °C. After cooling to room temperature, the white precipitate was filtered, washed with dry toluene/diethylether and dried in vacuo. Yield 90%. The NMR data agree with those previously reported[88].

14a. 14 (144.1 mg, 0.3 mmol) and Au(SMe$_2$)Cl (88.37 mg, 0.3 mmol) were dissolved in dry DMF (7 mL). To maintain a clear solution the mixture was heated to 100 °C, if applicable. NaOAc (62.27 mg, 0.75 mmol) was added and the solution was stirred for 2 h at 120 °C. After cooling to room temperature, diethylether (15 mL) was added to precipitate the complex. The white powder was filtered, washed with diethylether and dried in vacuo. The complexes were purified by crystallization (slow diffusion of diethylether into a solution in methanol). Yield 91%. ^{1}H NMR (400 MHz, CD$_3$OD, 25°C): δ=7.68 (d, ^3J(H,H)=8 Hz, 4H; H-4 or H-7), 7.48 (m, 8H; H-4 or H-7, H-5 or H-6), 7.34 (m, 4H; H-5 or H-6), 5.44 (bs, 8H; H-10), 4.54 (q, ^3J(H,H)=7 Hz, 8H; H-11), 1.27 (t, ^3J(H,H)=7 Hz, 12H; H-12); ^{13}C NMR (100 MHz, CD$_3$OD, 25°C): δ=191.0 (C-2), 134.9 (C-8 or C-9), 134.0 (C-8 or C-9), 126.4 (C-5 or C-6), 126.2 (C-5 or C-6), 113.1 (C-4 or C-7), 112.7 (C-4 or C-7), 48.1 (C-10), 45.2 (C-11), 16.3 (C-12). UV/Vis (ACN): λ_{max} (ε)=290 nm; fluorescence (ACN): λ_{ex}=328, 274, 234 nm; λ_{em}=366 nm; ESI (+): m/z (%): 515.2 (100) $[M$-2Br$]^{2+}$, HRMS (ESI): m/z calcd for C$_{40}$H$_{44}$Au$_2$N$_8$$^{2+}$: 515.1505 $[M$-2Br$]^{2+}$; found: 515.1506.

15. Propyldibromide (0.38 mL, 3.75 mmol) and N-ethylbenzimidazole (0.731 g, 5 mmol) were dissolved in dry toluene (10 mL) and stirred for 3 d at 110 °C. After cooling to room temperature, the white precipitate was filtered, washed with dry toluene/diethylether and dried in vacuo. Yield 75%. The NMR data agree with those previously reported[89,90].

15a. 15 (148.3 mg, 0.3 mmol) and Au(SMe$_2$)Cl (88.37 mg, 0.3 mmol) were dissolved in dry DMF (7 mL). To maintain a clear solution the mixture was heated to 100 °C, if applicable. NaOAc (62.27 mg, 0.75 mmol) was added and the solution was stirred for 2 h at 120 °C. After cooling to room temperature, diethylether (15 mL) was added to precipitate the complex. The white powder was filtered, washed with diethylether and dried in vacuo. The complexes were purified by crystallization (slow diffusion of diethylether into a solution in methanol). Yield 92%. ^{1}H NMR (400 MHz, CD$_3$OD, 25°C): δ=7.65 (d, ^3J(H,H)=8 Hz, 4H; H-7), 7.51 (d, ^3J(H,H)=8 Hz, 4H; H-4), 7.26 (m, 8H; H-5, H-6), 5.11 (bs, 8H; H-10), 4.58 (m, 8H; H-12), 3.25 (bs, 4H; H-11), 1.49 (m, 12H; H-13); ^{13}C NMR (100 MHz, CD$_3$OD, 25°C): δ=191.0 (C-2), 133.9 (C-8), 133.8 (C-9), 126.2 (C-5), 126.0 (C-6), 113.7 (C-7), 112.5 (C-4), 50.2 (C-10), 45.0 (C-12), 27.5 (C-11), 16.3 (C-13). UV/Vis (ACN): λ_{max} (ε)=288 nm; fluorescence (ACN): λ_{ex}=298, 270 nm; λ_{em}=395 nm; ESI (+): m/z (%): 529.2 (100) [M-$2Br$]$^{2+}$, HRMS (ESI): m/z calcd for C$_{42}$H$_{48}$Au$_2$N$_8$$^{2+}$: 529.1661 [$M$-2Br]$^{2+}$; found: 529.1659.

16. Butyldibromide (0.45 mL, 3.75 mmol) and N-ethylbenzimidazole (0.731 g, 5 mmol) were dissolved in dry toluene (10 mL) and stirred for 2 d at 110 °C. After cooling to room temperature, the white precipitate was filtered, washed with dry toluene/diethylether and dried in vacuo. Yield 92%. The NMR data agree with those previously reported[90].

16a. 16 (152.5 mg, 0.3 mmol) and Au(SMe$_2$)Cl (88.37 mg, 0.3 mmol) were dissolved in dry DMF (7 mL). To maintain a clear solution the mixture was heated to 100 °C, if applicable. NaOAc (62.27 mg, 0.75 mmol) was added and the solution was stirred for 2 h at 120 °C. After cooling to room temperature, diethylether (15 mL) was added to precipitate the complex. The white powder was filtered, washed with diethylether and dried in vacuo. The complexes were purified by crystallization (slow diffusion of diethylether into a solution in methanol). Yield 80%. ^{1}H NMR (400 MHz, [D$_6$]DMSO, 25°C,): δ=7.86 (m, 8H; H-4, H-7), 7.50 (bm, 8H; H-5, H-6), 4.65 (bs, 8H; H-10), 4.54 (m, 8H; H-12), 2.13 (bs, 8H; H-11), 1.29 (m, 12H; H-13); ^{13}C NMR (100 MHz, CD$_3$OD, 25°C): δ=189.3 (C-2), 132.9 (C-8 or C-9), 132.3 (C-8 or C-9), 124.8 (C-5 or C-6), 124.7 (C-5 or C-6), 112.3 (C-4 or C-7), 112.2 (C-4 or C-7), 47.7 (C-10), 43.2 (C-12), 27.9 (C-11), 15.8 (C-13). UV/Vis (ACN): λ_{max} (ε)=290, 240 nm; fluorescence (ACN): λ_{ex}=263 nm; λ_{em}=403 nm; ESI (+): m/z (%): 543.2 (100) [M-$2Br$]$^{2+}$, HRMS (ESI): m/z calcd for C$_{44}$H$_{52}$Au$_2$N$_8$$^+$: 543.1808 [$M$-2Br]$^+$; found: 543.1818.

17. Pentyldibromide (0.51 mL, 3.75 mmol) and N-ethylbenzimidazole (0.731 g, 5 mmol) were dissolved in dry toluene (10 mL) and stirred for 1 d at 110 °C. After cooling to room temperature, the white precipitate was filtered, washed with dry toluene/diethylether and dried in vacuo. Yield 88%. ^{1}H NMR (400 MHz, [D$_6$]DMSO, 25°C): δ=10.08 (s, 2H; H-2), 8.12 (m, 4H; H-4/7), 7.68 (m, 4H; H-5/6), 4.55 (m, 8H; H-10/13), 2.01 (m, 4H; H-11), 1.55 (t, ^3J(H,H)=7 Hz, 6H; H-14), 1.46 (m, 2H, H-12); ^{13}C NMR (75 MHz, [D$_6$]DMSO, 25°C): δ=141.9 (C-2), 131.1 (C-8), 130.8 (C-9), 126.5 (C-5/6), 113.7 (C-4/7), 46.4 (C-10), 42.0 (C-13), 28.0 (C-11), 22.7 (C-12), 14.2 (C-14). ESI (+): m/z (%): 181.2

(100) [M-2Br]$^{2+}$, 441.2 (7) [$M-$Br]$^+$, HRMS (ESI): m/z calcd for C$_{23}$H$_{30}$N$_4$Br$^+$: 441.1648 [M-Br]$^+$; found: 441.1642.

17a. 17 (156.7 mg, 0.3 mmol) and Au(SMe$_2$)Cl (88.37 mg, 0.3 mmol) were dissolved in dry DMF (7 mL). To maintain a clear solution the mixture was heated to 100 °C, if applicable. NaOAc (62.27 mg, 0.75 mmol) was added and the solution was stirred for 3 h at 120 °C. After cooling to room temperature, diethylether (15 mL) was added to precipitate the complex. The white powder was filtered, washed with diethylether and dried in vacuo. The complexes were purified by crystallization (slow diffusion of diethylether into a solution in methanol). Yield 88%. ^{1}H NMR (400 MHz, [D$_6$]DMSO, 25°C): δ=7.90 (m, 8H; H-4, H-7), 7.54 (m, 8H; H-5, H-6), 4.59 (m, 16H; H-10, H-13), 2.06 (m, 8H; H-11), 1.39 (t, ^{3}J(H,H)=7 Hz, 12H; H-14), 1.23 (m, 4H, H-12); ^{13}C NMR (75 MHz, [D$_6$]DMSO, 25°C): δ=189.2 (C-2), 132.7 (C-8 or C-9), 132.5 (C-8 or C-9), 124.9 (C-5 or C-6), 124.8 (C-5 or C-6), 112.5 (C-4 or C-7), 112.2 (C-4 or C-7), 48.3 (C-10), 43.2 (C-13), 29.8 (C-11), 24.0 (C-12), 15.9 (C-14). UV/Vis (ACN): λ_{max} (ε)=289, 239 nm; fluorescence (ACN): λ_{ex}=358 nm; λ_{em}=398 nm; ESI (+): m/z (%): 557.2 (100) [M-2Br]$^{2+}$, 1193.3 (8) [$M-$Br]$^+$, HRMS (ESI): m/z calcd for C$_{46}$H$_{56}$Au$_2$N$_8$Br^{2+}: 1193.3137 [M-2Br]$^{2+}$; found: 1193.3143.

18. Hexyldibromide (0.57 mL, 3.75 mmol) and N-ethylbenzimidazole (0.731 g, 5 mmol) were dissolved in dry toluene (10 mL) and stirred for 3 d at 110 °C. After cooling to room temperature, the white precipitate was filtered, washed with dry toluene/diethylether and dried in vacuo. Yield 90%. ^{1}H NMR (400 MHz, CD$_3$OD, 25°C): δ=9.74 (s, 2H; H-2), 8.02 (m, 4H; H-4/7), 7.72 (m, 4H; H-5/6), 4.60 (m, 8H; H-10/13), 2.09 (m, 4H; H-11), 1.68 (t, ^{3}J(H,H)=7 Hz, 6H; H-14), 1.57 (m, 4H, H-12); ^{13}C NMR (100 MHz, CD$_3$OD, 25°C): δ=142.4 (C-2), 133.0 (C-8), 132.8 (C-9), 128.2 (C5 or C-6), 128.1 (C5 or C-6), 114.7 (C4 or C-7), 114.5 (C4 or C-7), 48.3 (C-10), 43.8 (C-13), 30.0 (C-11), 26.9 (C-12), 14.7 (C-14). ESI (+): m/z (%): 188.1 (100) [M-2Br]$^{2+}$, 457.2 (6) [$M-$Br]$^+$, HRMS (ESI): m/z calcd for C$_{24}$H$_{32}$N$_4$$^{2+}$: 188.1308 [$M$]$^{2+}$; found: 188.1305.

18a. 18 (160.9 mg, 0.3 mmol) and Au(SMe$_2$)Cl (88.37 mg, 0.3 mmol) were dissolved in dry DMF (7 mL). To maintain a clear solution the mixture was heated to 100 °C, if applicable. NaOAc (62.27 mg, 0.75 mmol) was added and the solution was stirred for 3 h at 120 °C. After cooling to room temperature, diethylether (15 mL) was added to precipitate the complex. The white powder was filtered, washed with diethylether and dried in vacuo. The complexes were purified by crystallization (slow diffusion of diethylether into a solution in methanol). Yield 92%. ^{1}H NMR (400 MHz, CD$_3$OD, 25°C): δ=7.76 (m, 8H; H-4, H-7), 7.53 (m, 8H; H-5, H-6), 4.67 (m, 16H; H-10, H-13), 2.04 (bs, 8H; H-11), 1.59 (t, ^{3}J(H,H)=7 Hz, 12H; H-14), 1.52 (bs, 8H; H-12); ^{1}H NMR (300 MHz, [D$_6$]DMSO, 25°C): δ=7.90 (m, 8H; H-4, H-7), 7.49 (m, 8H; H-5, H-6), 4.63 (m, 16H; H-10, H-13), 1.89 (bs, 8H; H-11), 1.48 (t, ^{3}J(H,H)=7 Hz, 12H; H-14), 1.38 (bs, 8H, H-12); ^{13}C NMR (75 MHz, [D$_6$]DMSO, 25°C): δ=189.3 (C-2), 132.8 (C-8, C-9), 124.7 (C-5, C-6), 112.4 (C-4 or C-7), 112.2 (C-4 or C-7), 48.5

(C-10), 43.3 (C-13), 30.2 (C-11), 26.7 (C-12), 16.0 (C-14). UV/Vis (ACN): λ_{max} (ε)=289, 239 nm; fluorescence (ACN): λ_{ex}=359 nm; λ_{em}=396 nm; ESI (+): m/z (%): 571.2 (100) [M-2Br]$^{2+}$, HRMS (ESI): m/z calcd for $C_{48}H_{60}Au_2N_8^{2+}$: 571.2131 [M-2Br]$^{2+}$; found: 571.2137.

19. Methyldibromide (0.26 mL, 3.75 mmol) and N-methylbenzimidazole (0.661 g, 5 mmol) were dissolved in dry toluene (10 mL) and stirred for 14 d at 110 °C. After cooling to room temperature, the white precipitate was filtered, washed with dry toluene/diethylether and dried in vacuo. Yield 74%. The NMR data agree with those previously reported[91].

19a. 19 (131.4 mg, 0.3 mmol) and Au(SMe$_2$)Cl (88.37 mg, 0.3 mmol) were dissolved in dry DMF (7 mL). To maintain a clear solution the mixture was heated to 100 °C, if applicable. NaOAc (62.27 mg, 0.75 mmol) was added and the solution was stirred for 3 h at 120 °C. After cooling to room temperature, diethylether (15 mL) was added to precipitate the complex. The white powder was filtered, washed with diethylether and dried in vacuo. The complexes were purified by crystallization (slow diffusion of diethylether into a solution in methanol). Yield 91%. ^{1}H NMR (400 MHz, CD$_3$OD/CD$_2$Cl$_2$, 25°C): δ=7.97 (m, 4H; H-4), 7.77 (m, 2H; H7, H10a), 7.61 (m, 8H; H-5/6), 7.19 (d, ^2J(H,H)=15 Hz, 2H; H10b), 4.14 (s, 12H; H-11); ^{13}C NMR (75 MHz, CD$_3$OD/CD$_2$Cl$_2$, 25°C): δ=191.5 (C-2), 135.0 (C-8 or C-9), 133.6 (C-8 or C-9), 126.9 (C-5 or C-6), 126.7 (C-5 or C-6), 113.4 (C-4 or C-7), 112.5 (C-4 or C-7), 68.6 (C-10), 39.9 (C-11). ESI (+): m/z (%): 473.2 (100) [M-2Br]$^{2+}$, 1027.2 (3) [M−Br]$^+$, HRMS (ESI): m/z calcd for $C_{34}H_{32}Au_2N_8Br^+$: 1025.1259 [M-Br]$^+$; found: 1025.1264.

20. Ethyldibromide (0.33 mL, 3.75 mmol) and N-methylbenzimidazole (0.661 g, 5 mmol) were dissolved in dry toluene (10 mL) and stirred for 4 d at 110 °C. After cooling to room temperature, the white precipitate was filtered, washed with dry toluene/diethylether and dried in vacuo. Yield 78%. The NMR data agree with those previously reported[91].

20a. 20 (135.7 mg, 0.3 mmol) and Au(SMe$_2$)Cl (88.37 mg, 0.3 mmol) were dissolved in dry DMF (7 mL). To maintain a clear solution the mixture was heated to 100 °C, if applicable. NaOAc (62.27 mg, 0.75 mmol) was added and the solution was stirred over night at 120 °C. After cooling to room temperature, diethylether (15 mL) was added to precipitate the complex. The white powder was filtered, washed with diethylether and dried in vacuo. The complexes were purified by crystallization (slow diffusion of diethylether into a solution in methanol). Yield 88%. ^{1}H NMR (400 MHz, [D$_6$]DMSO, 25°C): δ=7.71 (d, ^3J(H,H)=8 Hz, 4H; H-4 or H-7), 7.64 (d, ^3J(H,H)=8 Hz, 4H; H-4 or H-7), 7.44 (m, 8H; H-5 or H-6), 7.33 (m, 8H; H-5 or H-6), 5.39 (s, 8H; H-10), 4.00 (s, 12H; H-11); ^{13}C NMR (100 MHz, [D$_6$]DMSO, 25°C): δ=189.7 (C-2), 133.2 (C-8 or C-9), 132.7 (C-8 or C-9), 124.8 (C-5 or C-6), 124.6 (C-5 or C-6), 112.3 (C-4 or C-7), 111.6 (C-4 or C-7), 35.3 (C-10), 25.3 (C-11). ESI (+): m/z (%): 487.1 (100) [M-2Br]$^{2+}$, 1055.2 (6) [M−Br]$^+$, HRMS (ESI): m/z calcd for $C_{36}H_{36}Au_2N_8Br^+$: 1053.1572 [M-Br]$^+$; found: 1053.1574.

21. Propyldibromide (0.38 mL, 3.75 mmol) and N-methylbenzimidazole (0.661 g, 5 mmol) were dissolved in dry toluene (10 mL) and stirred for 2 d at 110 °C. After cooling to room temperature, the white precipitate was filtered, washed with dry toluene/diethylether and dried in vacuo. Yield 90%. The NMR data agree with those previously reported[91,92].

21a. 21 (139.9 mg, 0.3 mmol) and Au(SMe$_2$)Cl (88.37 mg, 0.3 mmol) were dissolved in dry DMF (7 mL). To maintain a clear solution the mixture was heated to 100 °C, if applicable. NaOAc (62.27 mg, 0.75 mmol) was added and the solution was stirred over night at 120 °C. After cooling to room temperature, diethylether (15 mL) was added to precipitate the complex. The white powder was filtered, washed with diethylether and dried in vacuo. The complexes were purified by crystallization (slow diffusion of diethylether into a solution in methanol). Yield 95%. ^{1}H NMR (400 MHz, CD$_3$OD/CD$_2$Cl$_2$, 25°C): δ=7.56 (d, ^3J(H,H)=8 Hz, 4H; H-4 or H-7), 7.47 (d, ^3J(H,H)=8 Hz, 4H; H-4 or H-7), 7 36 (m, 8H; H-5 or H-6), 7 26 (m, 8H; H-5 or H-6), 5.01 (t, ^3J(H,H)=6 Hz, 8H; H-10), 4.06 (s, 12H; H-12), 3.17 (m, 4H; H-11); ^{13}C NMR (75 MHz, CD$_3$OD/CD$_2$Cl$_2$, 25°C): δ=190.7 (C-2), 134.6 (C-9), 133.1 (C-8), 126.0 (C-5, C-6), 113.0 (C-4 or C-7), 112.2 (C-4 or C-7), 49.3 (C-10), 35.6 (C-12), 24.2 (C-11). ESI (+): m/z (%): 501.2 (100) [M-$2Br$]$^{2+}$, 1081.3 (3) [M−Br]$^+$, HRMS (ESI): m/z calcd for C$_{38}$H$_{40}$Au$_2$N$_8$Br$^+$: 1081.1885 [M-Br]$^+$; found: 1081.1886.

22. Butyldibromide (0.45 mL, 3.75 mmol) and N-methylbenzimidazole (0.661 g, 5 mmol) were dissolved in dry toluene (10 mL) and stirred for 2 d at 110 °C. After cooling to room temperature, the white precipitate was filtered, washed with dry toluene/diethylether and dried in vacuo. Yield 88%. The NMR data agree with those previously reported[92].

22a. 22 (144.1 mg, 0.3 mmol) and Au(SMe$_2$)Cl (88.37 mg, 0.3 mmol) were dissolved in dry DMF (7 mL). To maintain a clear solution the mixture was heated to 100 °C, if applicable. NaOAc (62.27 mg, 0.75 mmol) was added and the solution was stirred over night at 120 °C. After cooling to room temperature, diethylether (15 mL) was added to precipitate the complex. The white powder was filtered, washed with diethylether and dried in vacuo. The complexes were purified by crystallization (slow diffusion of diethylether into a solution in methanol). Yield 91%. ^{1}H NMR (400 MHz, CD$_3$OD/CD$_2$Cl$_2$, 25°C,): δ=7.64 (m, 8H; H-4, H-7), 7.54 (m, 4H; H-5, H-6), 4.67 (bs, 8H; H-10), 4.11 (s, 12H; H-12), 2.23 (m, 8H; H-11); ^{13}C NMR (75 MHz, CD$_3$OD/CD$_2$Cl$_2$, 25°C): δ=190.9 (C-2), 134.8 (C-9), 133.8 (C-8), 125.9 (C-5, C-6), 112.5 (C-4, C-7), 53.7 (C-10), 35.6 (C-12), 28.8 (C-11). ESI (+): m/z (%): 515.2 (100) [M-$2Br$]$^{2+}$, 1109.2 (2) [M−Br]$^+$, HRMS (ESI): m/z calcd for C$_{40}$H$_{44}$Au$_2$N$_8$Br$^+$: 1109.2198 [M-Br]$^+$; found: 1109.2188.

23. Pentyldibromide (0.51 mL, 3.75 mmol) and N-methylbenzimidazole (0.661 g, 5 mmol) were dissolved in dry toluene (10 mL) and stirred for 3 d at 110 °C. After cooling to room temperature, the white precipitate was filtered, washed with dry toluene/diethylether and dried in vacuo. Yield 81%.

^{1}H NMR (400 MHz, [D$_6$]DMSO, 25°C): δ=9.83 (s, 2H; H-2), 8.06 (m, 4H; H-4/7), 7.70 (m, 4H; H-5/6), 4.51 (t, ^{3}J(H,H)=7 Hz, 4H; H-10), 4.09 (s, 6H; H-13), 1.97 (m, 4H; H-11), 1.43 (m, 2H; H-12), ^{13}C NMR (75 MHz, [D$_6$]DMSO, 25°C): δ=142.7 (C-2), 131.8 (C-9), 130.9 (C-8), 126.5 (C-5/6), 113.6 (C-4 or C-7), 113.5 (C-4 or C-7), 46.3 (C-10), 33.3 (C-13), 28.0 (C-11), 22.6 (C-12). ESI (+): m/z (%): 167.1 (100) [M-$2Br$]$^{2+}$, 413.2 (3) [M−Br]$^+$, HRMS (ESI): m/z calcd for C$_{21}$H$_{26}$N$_4$Br$^+$: 413.1335 [M-Br]$^+$; found: 413.1321.

23a. 23 (148.3 mg, 0.3 mmol) and Au(SMe$_2$)Cl (88.37 mg, 0.3 mmol) were dissolved in dry DMF (7 mL). To maintain a clear solution the mixture was heated to 100 °C, if applicable. NaOAc (62.27 mg, 0.75 mmol) was added and the solution was stirred over night at 120 °C. After cooling to room temperature, diethylether (15 mL) was added to precipitate the complex. The white powder was filtered, washed with diethylether and dried in vacuo. The complexes were purified by crystallization (slow diffusion of diethylether into a solution in methanol). Yield 86%. ^{1}H NMR (400 MHz, CD$_3$OD/CD$_2$Cl$_2$, 25°C): δ=7.71 (m, 4H; H-4 or H-7), 7.66 (m, 4H; H-4 or H-7), 7.56 (m, 8H; H-5, H-6), 4.63 (d, ^{3}J(H,H)=7 Hz. 8H; H-10), 4.03 (s, 12H; H-13), 2.17 (m, 8H; H-11), 1.67 (m, 4H, H-12); ^{13}C NMR (75 MHz, CD$_3$OD/CD$_2$Cl$_2$, 25°C): δ=191.2 (C-2), 135.0 (C-9), 134.0 (C-8), 126.1 (C-5, C-6), 112.7 (C-4, C-7), 49.4 (C-10), 35.5 (C-13), 31.2 (C-11), 25.6 (C-12). ESI (+): m/z (%): 529.2(100) [M-$2Br$]$^{2+}$, 1137.3 (3) [M−Br]$^+$,, HRMS (ESI): m/z calcd for C$_{42}$H$_{48}$Au$_2$N$_8$Br$^+$: 1137.2511 [M-Br]$^+$; found: 1137.2517.

24. Hexyldibromide (0.57 mL, 3.75 mmol) and N-methylbenzimidazole (0.661 g, 5 mmol) were dissolved in dry toluene (10 mL) and stirred for 3 d at 110 °C. After cooling to room temperature, the white precipitate was filtered, washed with dry toluene/diethylether and dried in vacuo. Yield 88%. The NMR data agree with those previously reported[93].

24a. 24 (152.5 mg, 0.3 mmol) and Au(SMe$_2$)Cl (88.37 mg, 0.3 mmol) were dissolved in dry DMF (7 mL). To maintain a clear solution the mixture was heated to 100 °C, if applicable. NaOAc (62.27 mg, 0.75 mmol) was added and the solution was stirred over night at 120 °C. After cooling to room temperature, diethylether (15 mL) was added to precipitate the complex. The white powder was filtered, washed with diethylether and dried in vacuo. The complexes were purified by crystallization (slow diffusion of diethylether into a solution in methanol). Yield 93%. ^{1}H NMR (400 MHz, CD$_3$OD/CD$_2$Cl$_2$, 25°C): δ=7.65 (m, 8H; H-4, H-7), 7.54 (m, 8H; H-5, H-6), 4.60 (t, ^{3}J(H,H)=7 Hz, 8H; H-10), 4.15 (s, 12H; H-13), 2.03 (m, 8H; H-11), 1.49 (m, 8H, H-12); ^{13}C NMR (75 MHz, CD$_3$OD/CD$_2$Cl$_2$, 25°C): δ=191.0 (C-2), 134.9 (C-9), 133.8 (C-8), 125.8 (C-5, C-6), 112.5 (C-4, C-7), 54.4 (C-10), 35.5 (C-13), 31.2 (C-11), 28.0 (C-12). ESI (+): m/z (%): 543.3 (100) [M-$2Br$]$^{2+}$, HRMS (ESI): m/z calcd for C$_{44}$H$_{52}$Au$_2$N$_8$Br$^+$: 543.1818 [M-2Br]$^{2+}$; found: 543.1831.

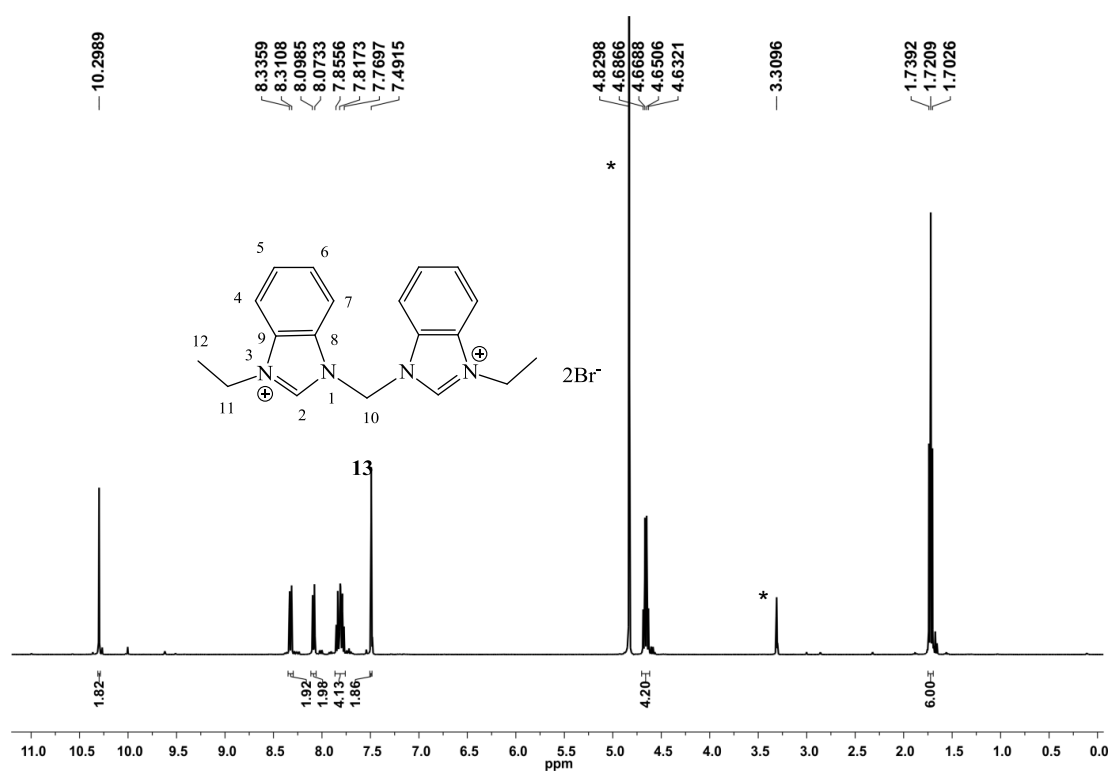Characterization of unpublished substances without VT-NMR spectra

Figure 6.3.8. ^{1}H NMR (400 MHz, CD$_3$OD, r. t.) spectrum of **13**. *partially deuterated and undeuterated MeOH and water, respectively.
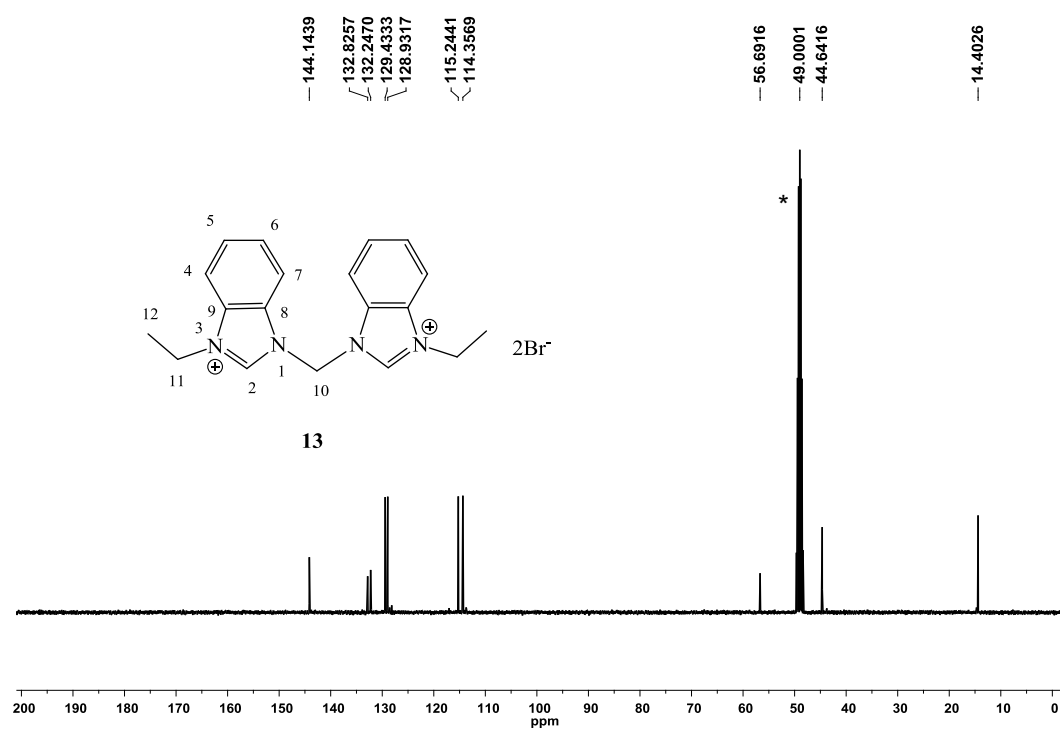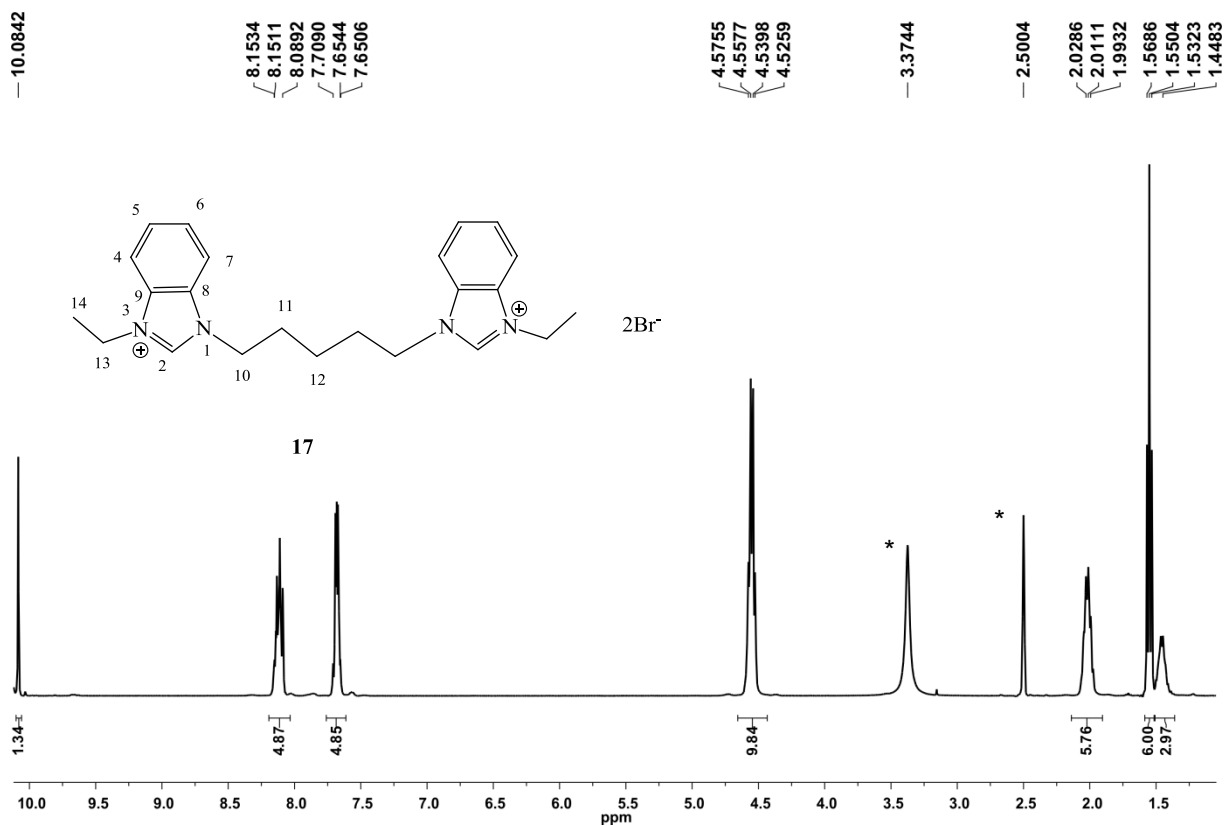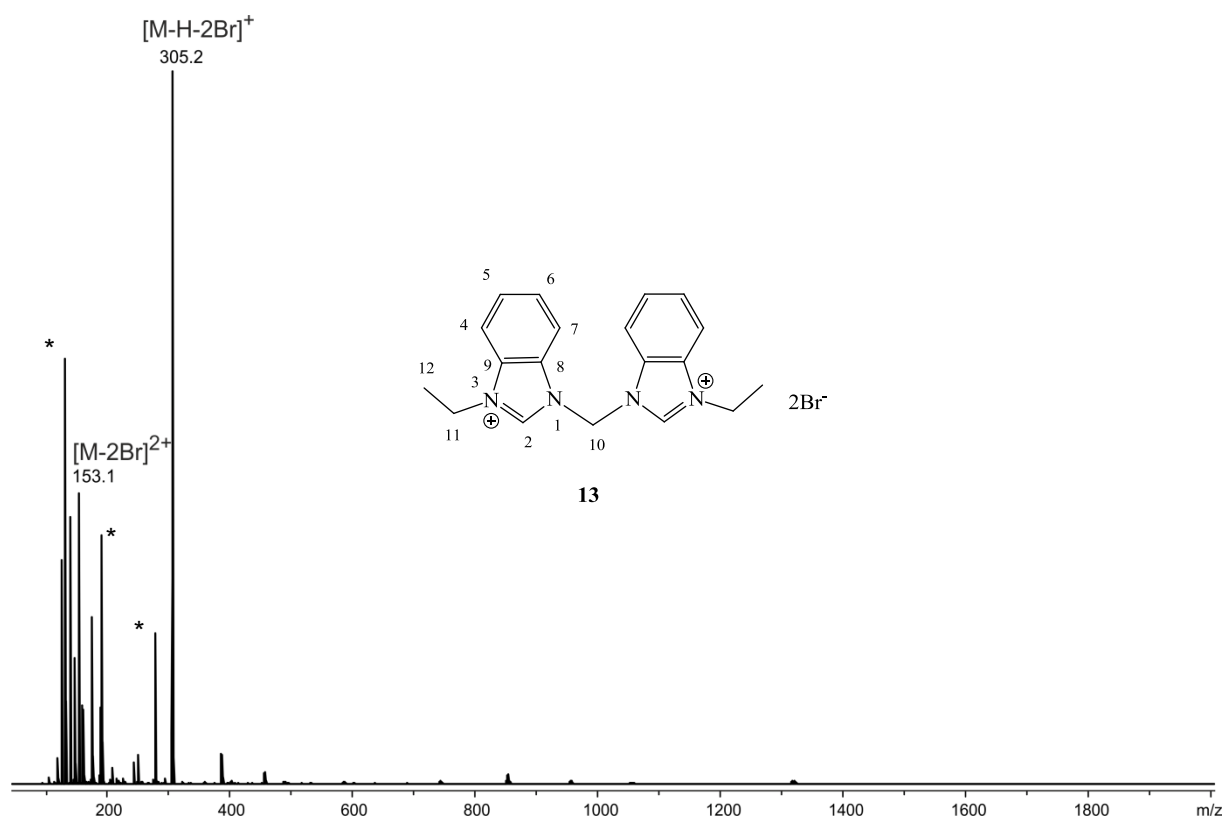

Figure 6.3.9. ^{13}C NMR (100 MHz, CD$_3$OD, r. t.) spectrum of **13**. *partially deuterated and undeuterated MeOH, respectively.
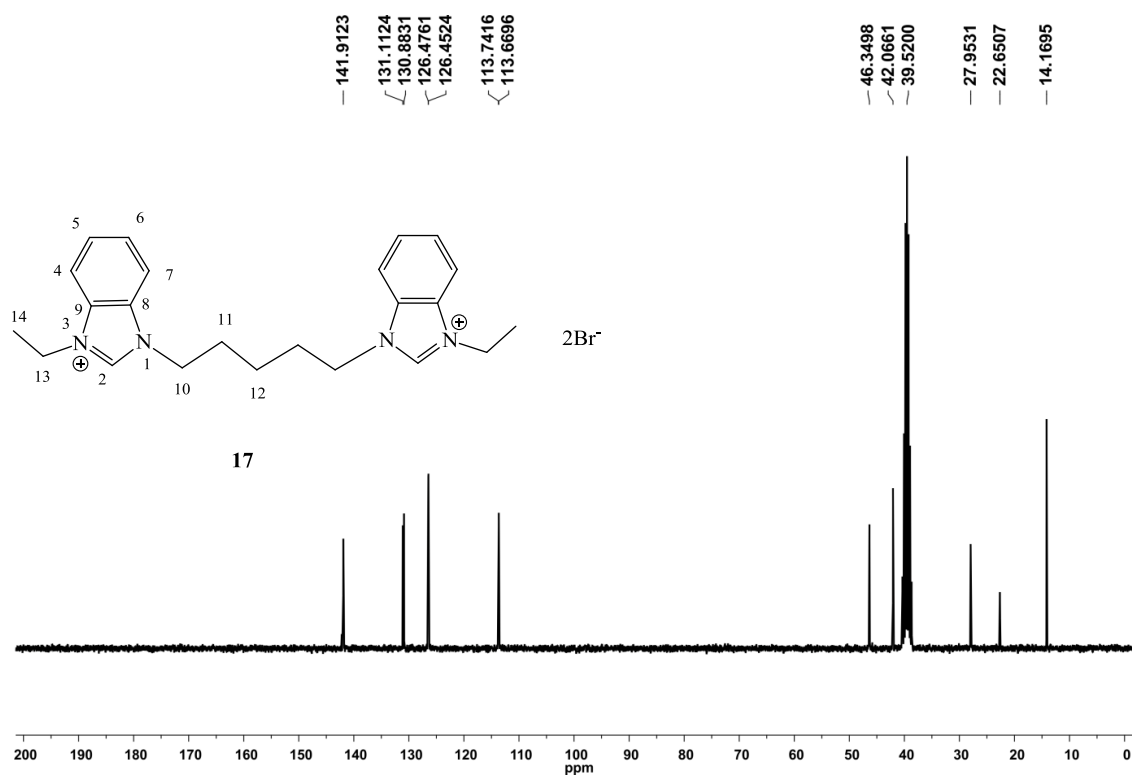
Figure 6.3.10. microTof-Q ESI(+) mass spectrum of **13** in MeOH. * memory signal, respectively.

Figure 6.3.11. ^{1}H NMR (400 MHz, [D$_6$]DMSO, r. t.) spectrum of **17**. *partially deuterated and undeuterated DMSO and water, respectively.

Figure 6.3.12. ^{13}C NMR (75 MHz, [D6]DMSO, r. t.) spectrum of **17**. *partially deuterated and undeuterated DMSO, respectively.
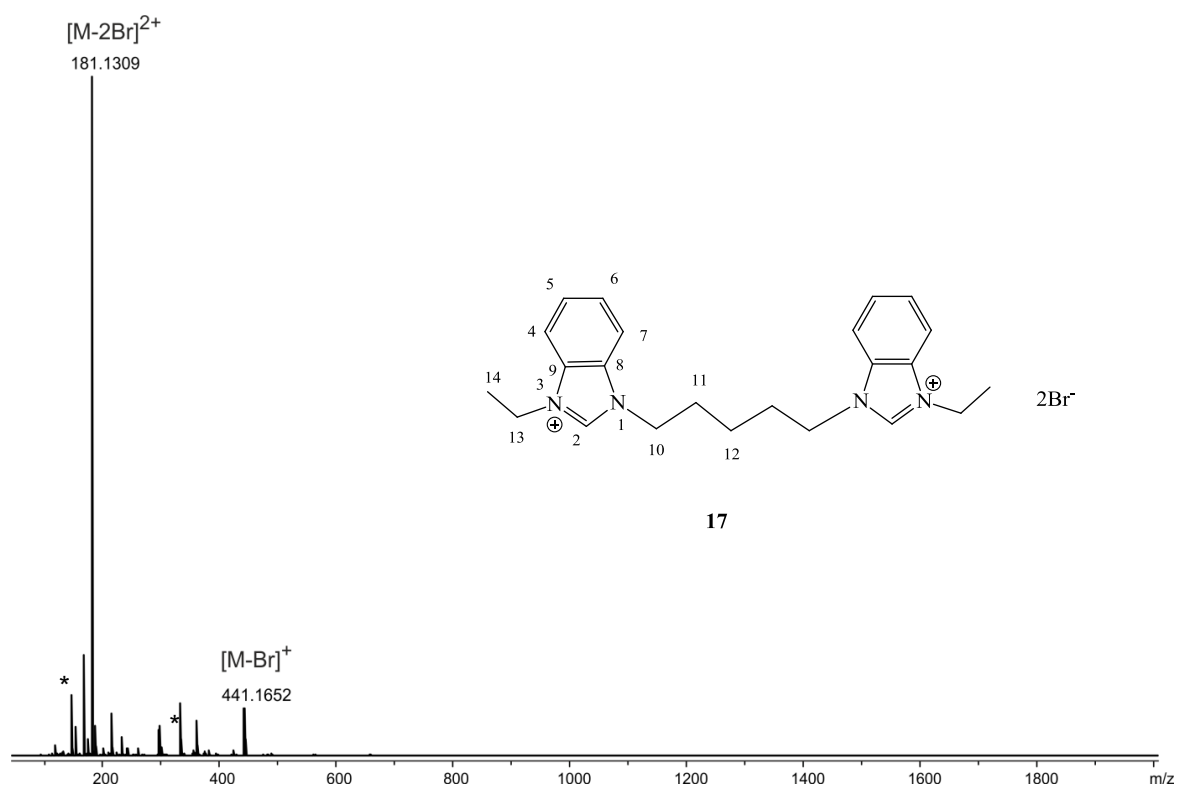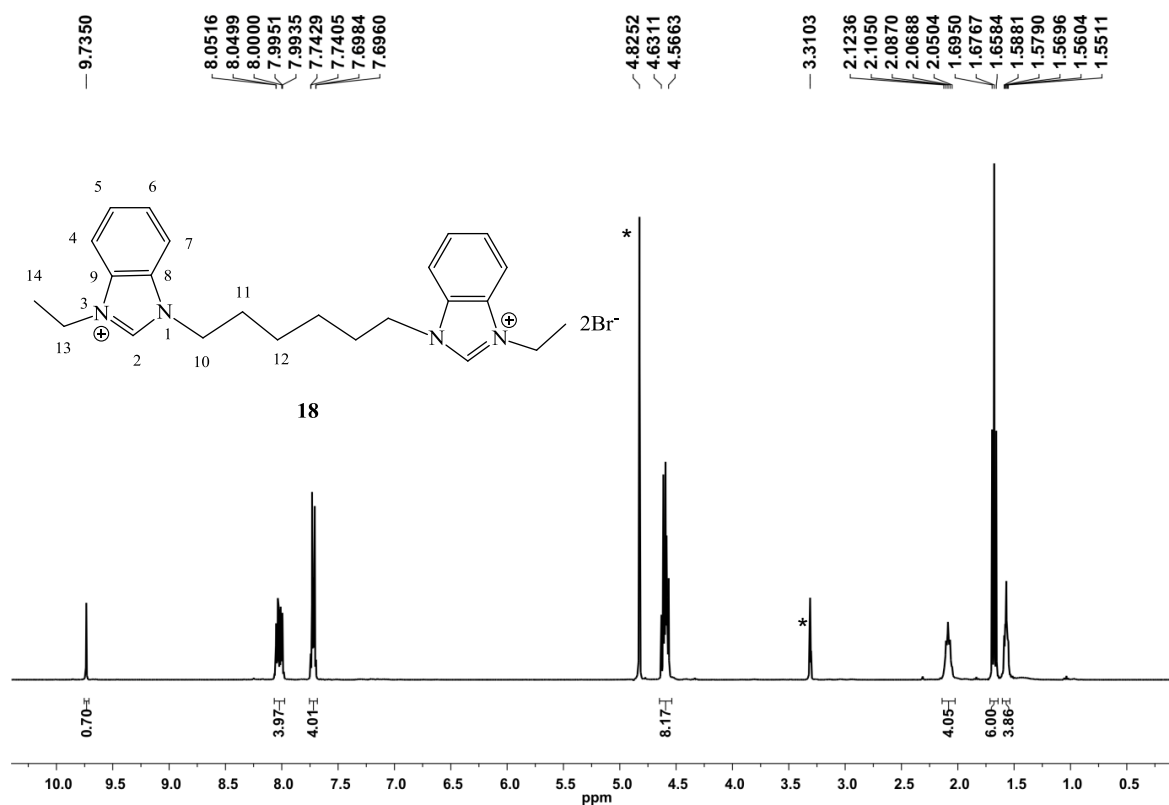

Figure 6.3.13. microTof-Q ESI(+) mass spectrum of **17** in MeOH. * memory signal, respectively.

Figure 6.3.14. ^{1}H NMR (400 MHz, CD$_3$OD, r. t.) spectrum of **18**. *partially deuterated and undeuterated MeOH and water, respectively.
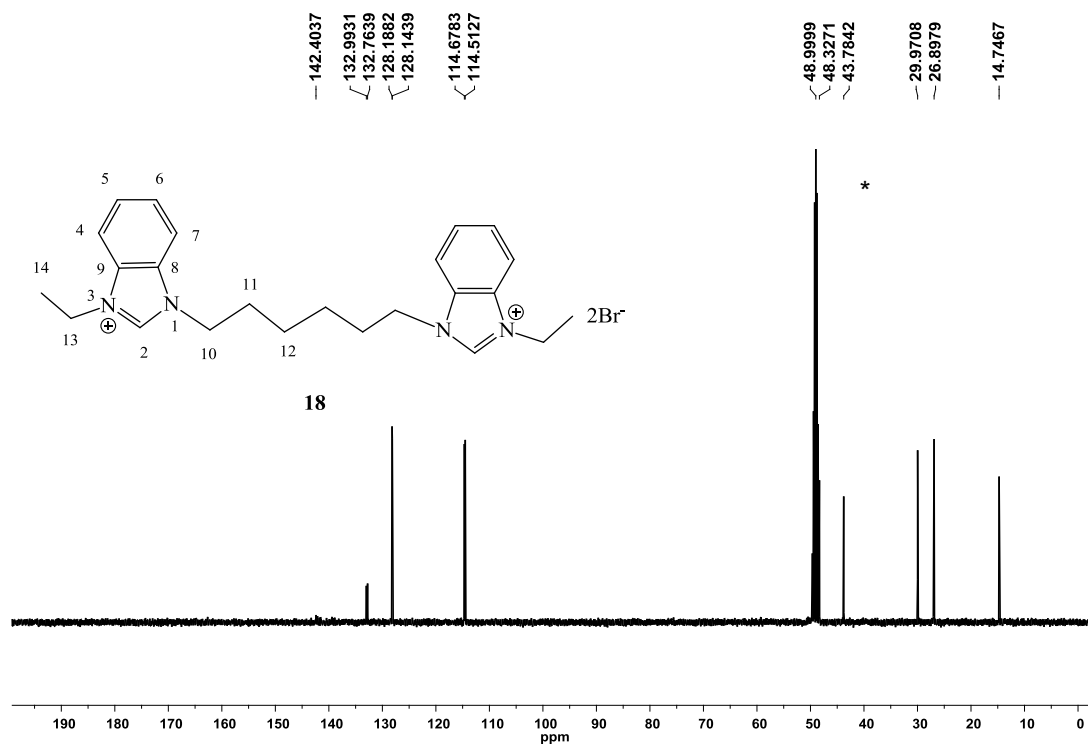

Figure 6.3.15. ^{13}C NMR (100 MHz, CD$_3$OD, r. t.) spectrum of **18**. *partially deuterated and undeuterated MeOH, respectively.
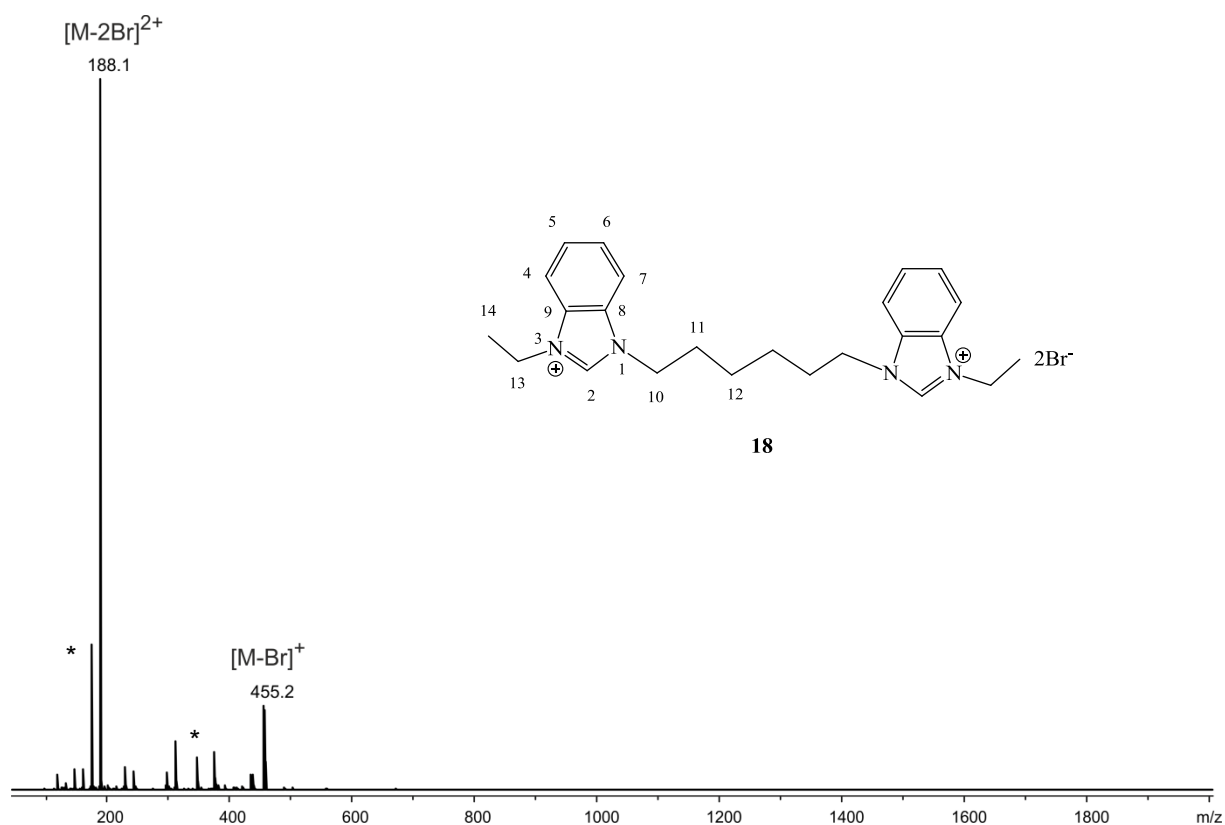
Figure 6.3.16. microTof-Q ESI(+) mass spectrum of **18** in MeOH. * memory signal, respectively.
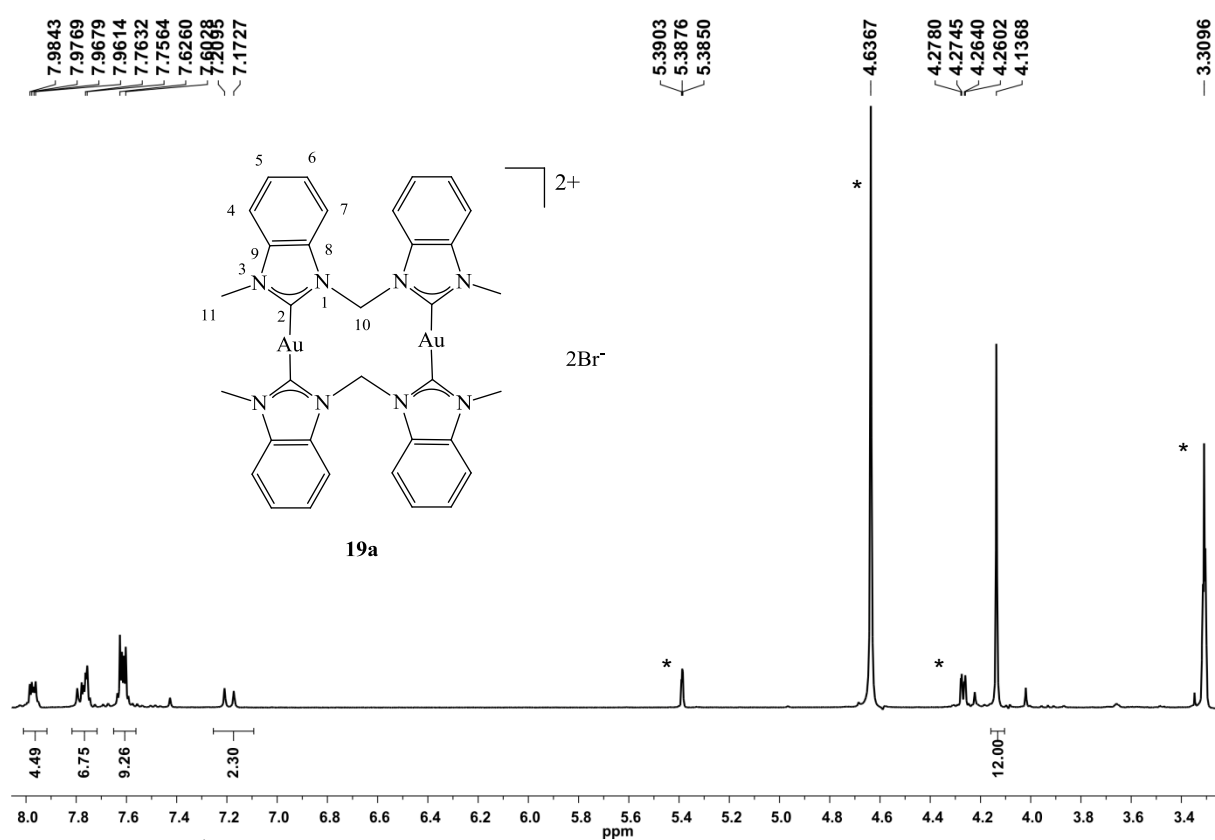

Figure 6.3.17. ^{1}H NMR (400 MHz, CD$_3$OD/CD$_2$Cl$_2$, r. t.) spectrum of **19a**. *partially deuterated and undeuterated MeOH and DCM and water, respectively.

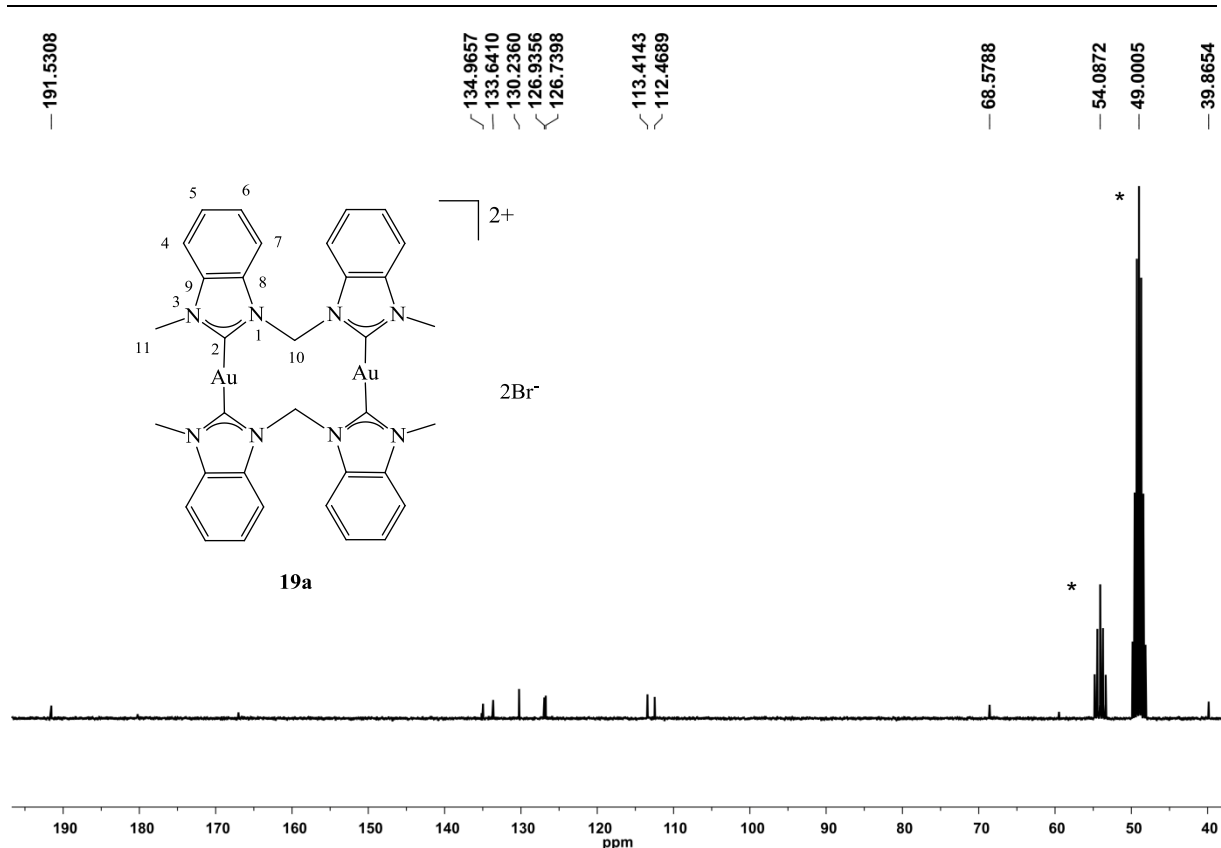**Figure 6.3.18.** ^{13}C NMR (75 MHz, CD$_3$OD/CD$_2$Cl$_2$, r. t.) spectrum of **19a**. *partially deuterated and undeuterated MeOH and DCM, respectively.
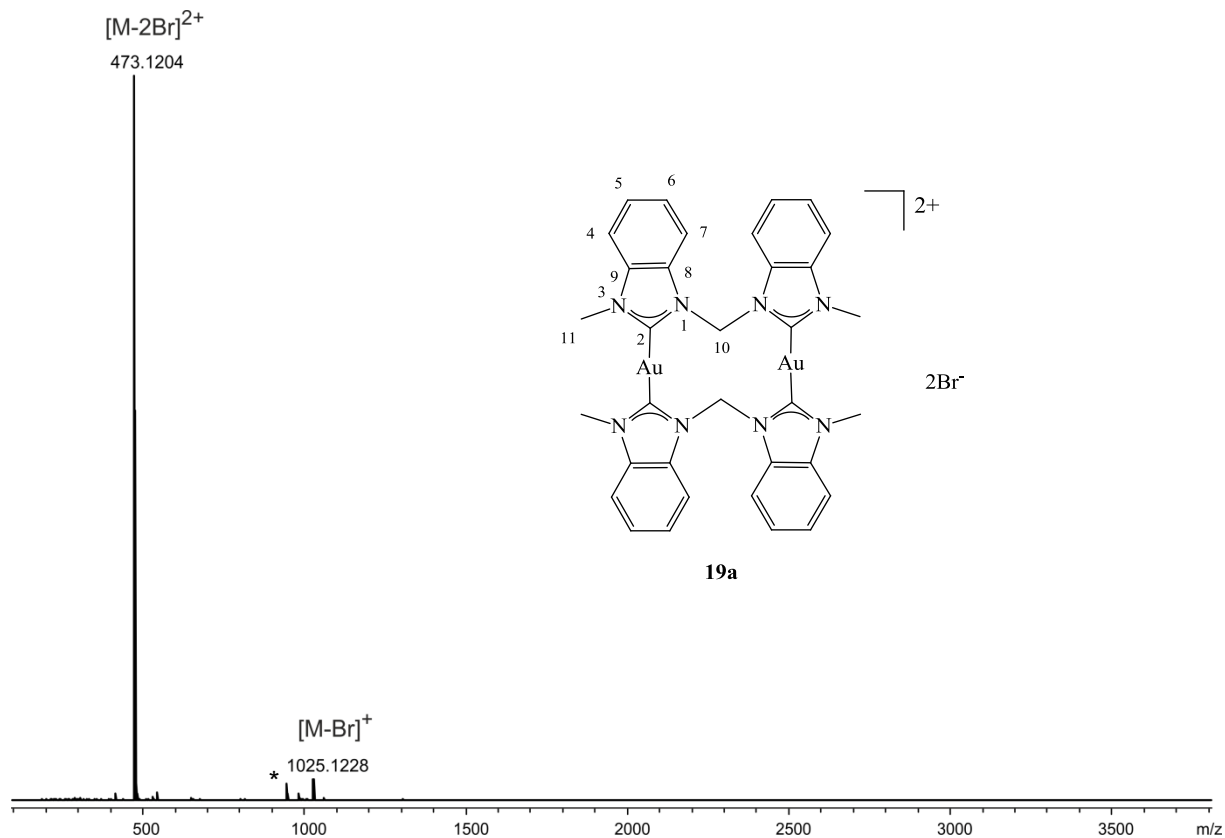

Figure 6.3.19. microTof-Q ESI(+) mass spectrum of **19a** in MeOH. * memory signal.

Figure 6.3.20. ^{1}H NMR (400 MHz, [D6]DMSO, r. t.) spectrum of **20a**. *partially deuterated and undeuterated DMSO and water, respectively.

Figure 6.3.21. ^{13}C NMR (100 MHz, [D6]DMSO, r. t.) spectrum of **20a**. *partially deuterated and undeuterated DMSO, respectively.

Figure 6.3.22. microTof-Q ESI(+) mass spectrum of **20a** in MeOH. * memory signal, respectively.

Figure 6.3.23. ^{1}H NMR (400 MHz, CD$_3$OD/CD$_2$Cl$_2$, r. t.) spectrum of **21a**. *partially deuterated and undeuterated MeOH and DCM and water, respectively.

Figure 6.3.24. ^{13}C NMR (100 MHz, CD$_3$OD/CD$_2$Cl$_2$, r. t.) spectrum of **21a**. *partially deuterated and undeuterated MeOH and DCM, respectively.
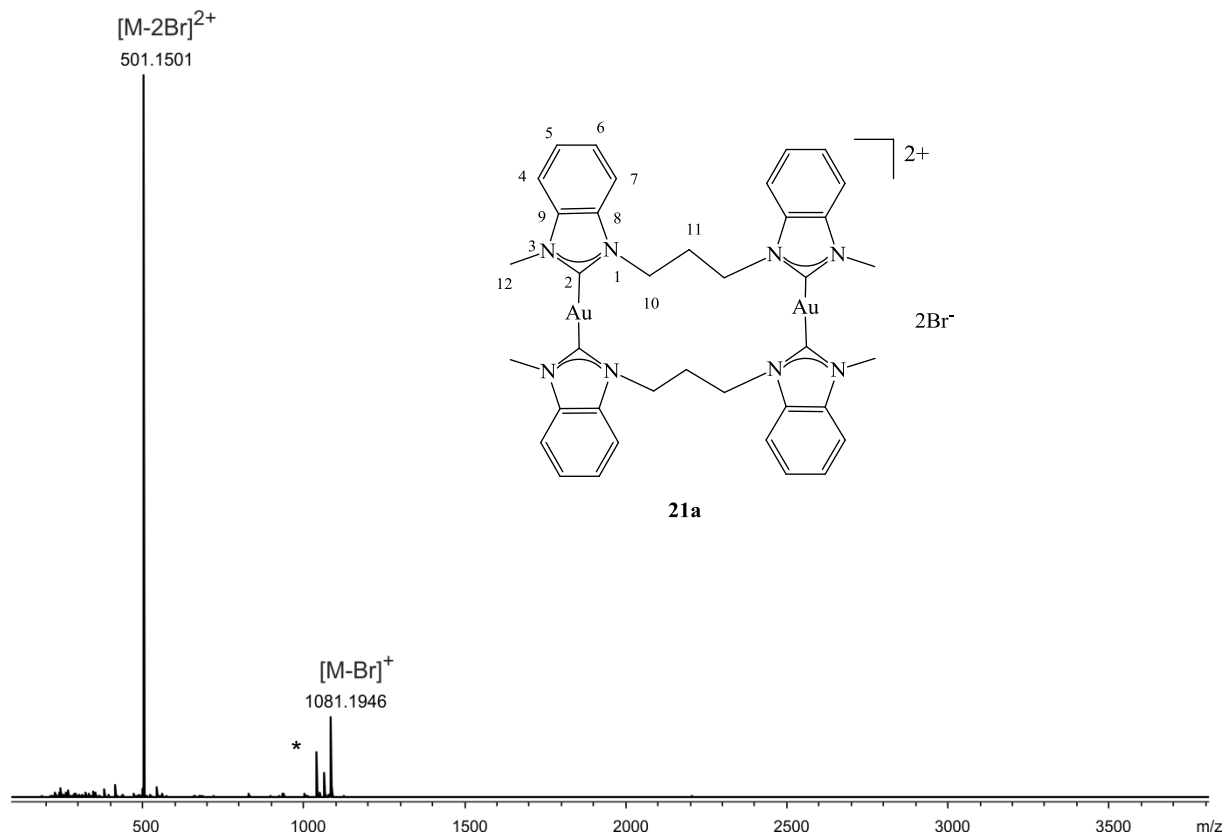
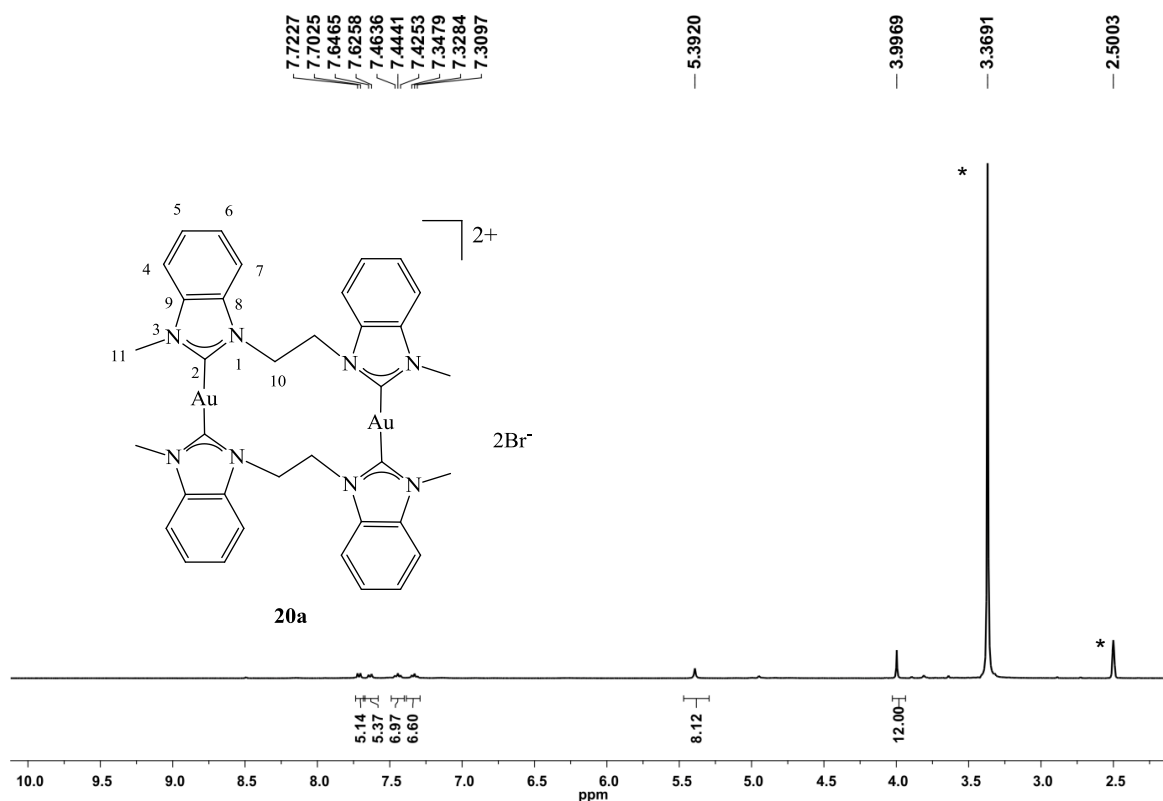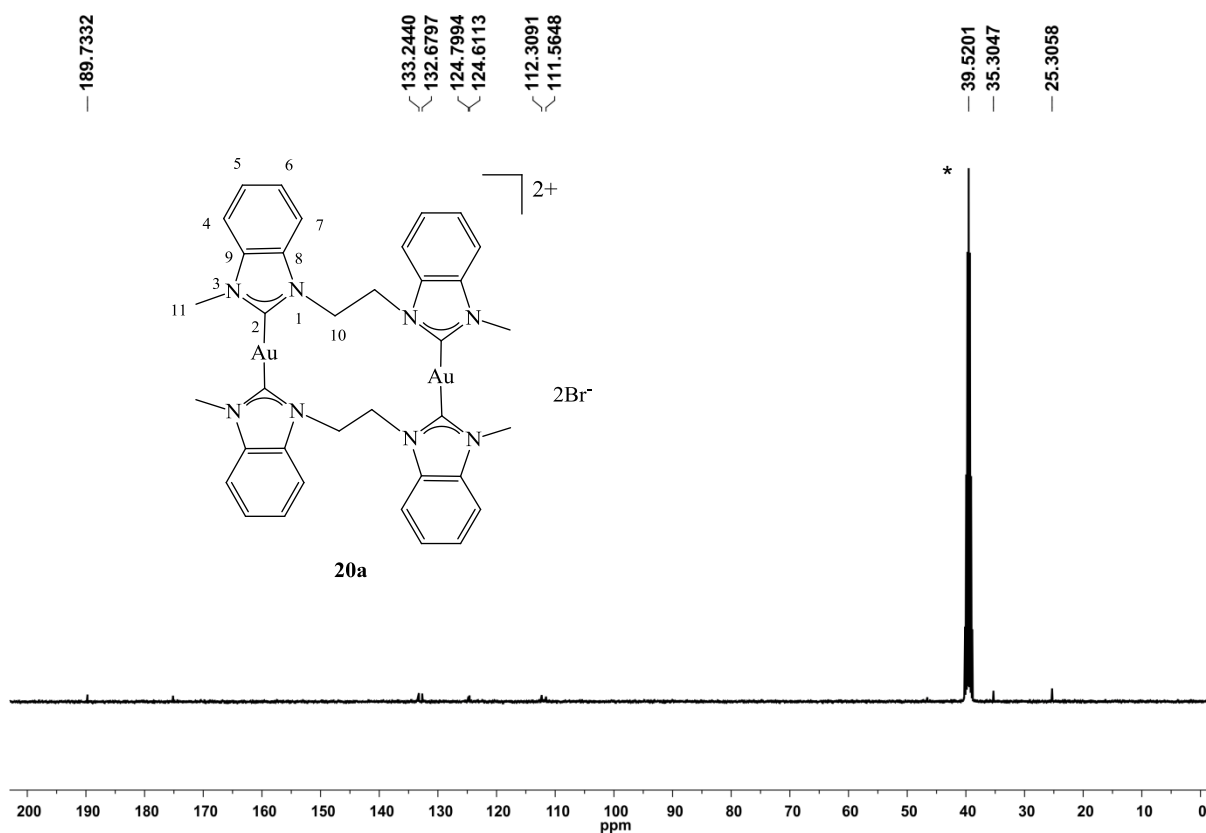**Figure 6.3.25.** microTof-Q ESI(+) mass spectrum of **21a** in MeOH. * memory signal.

Figure 6.3.26. ^{1}H NMR (400 MHz, CD$_3$OD/CD$_2$Cl$_2$, r. t.) spectrum of **22a**. *partially deuterated and undeuterated MeOH and DCM and water, respectively.

Figure 6.3.27. ^{13}C NMR (100 MHz, CD$_3$OD/CD$_2$Cl$_2$, r. t.) spectrum of **22a**. *partially deuterated and undeuterated MeOH and DCM, respectively.

Figure 6.3.28. microTof-Q ESI(+) mass spectrum of **22a** in MeOH.

Figure 6.3.29. ¹H NMR (400 MHz, [D6]DMSO, r. t.) spectrum of **23**. *partially deuterated and undeuterated DMSO and water, respectively.
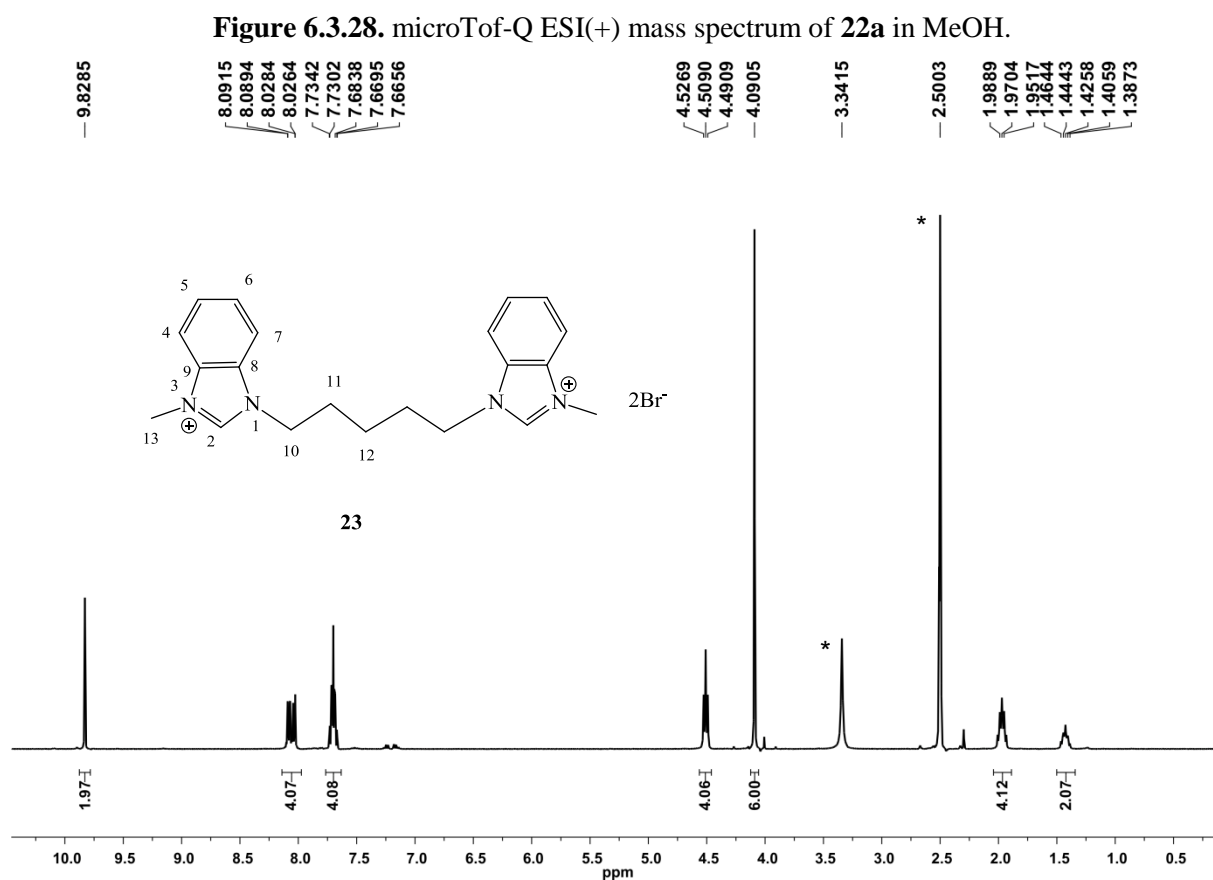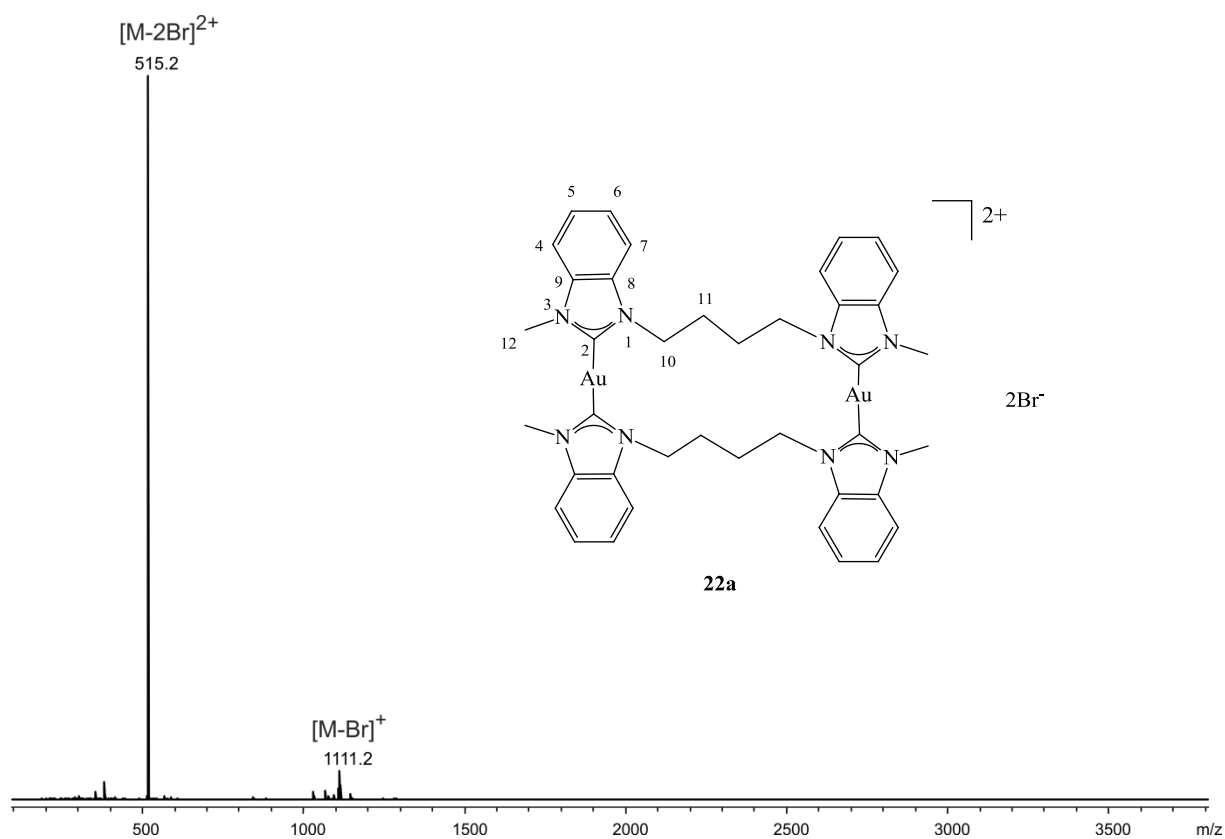
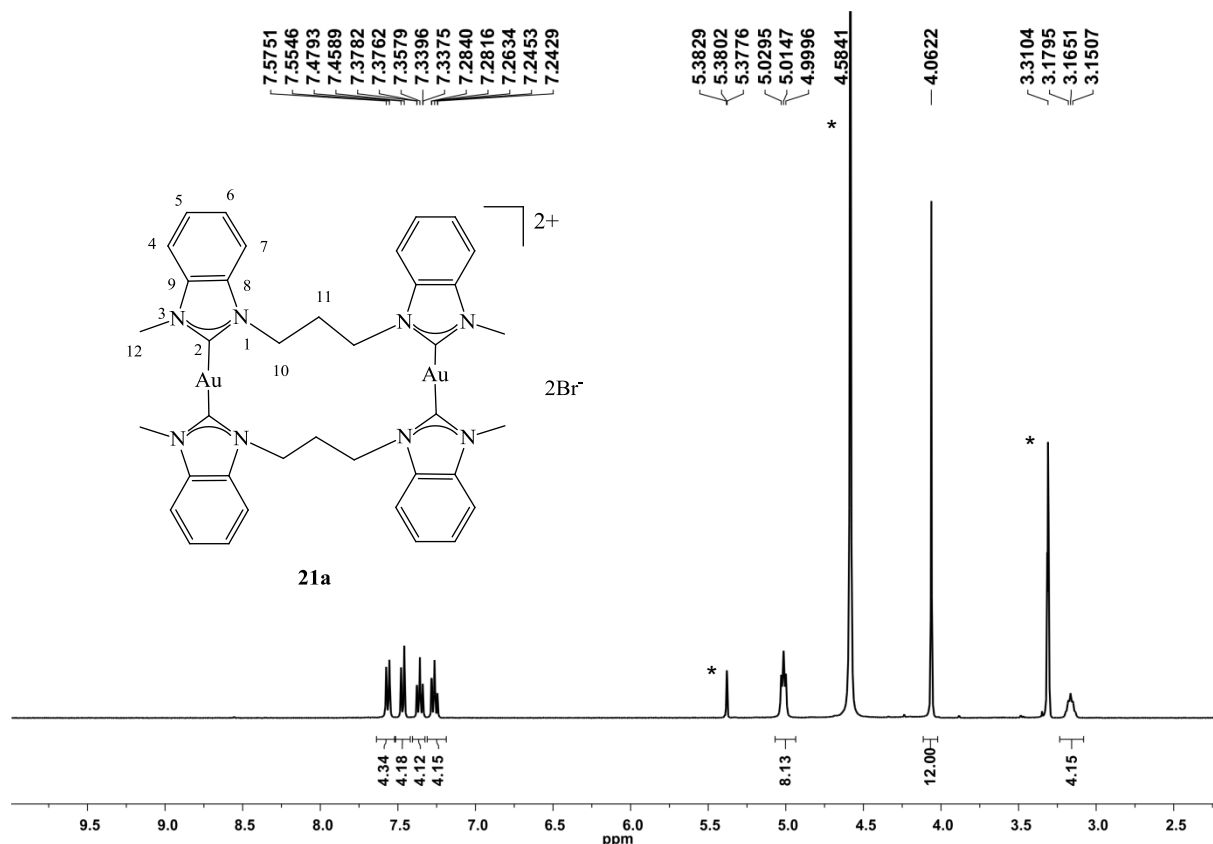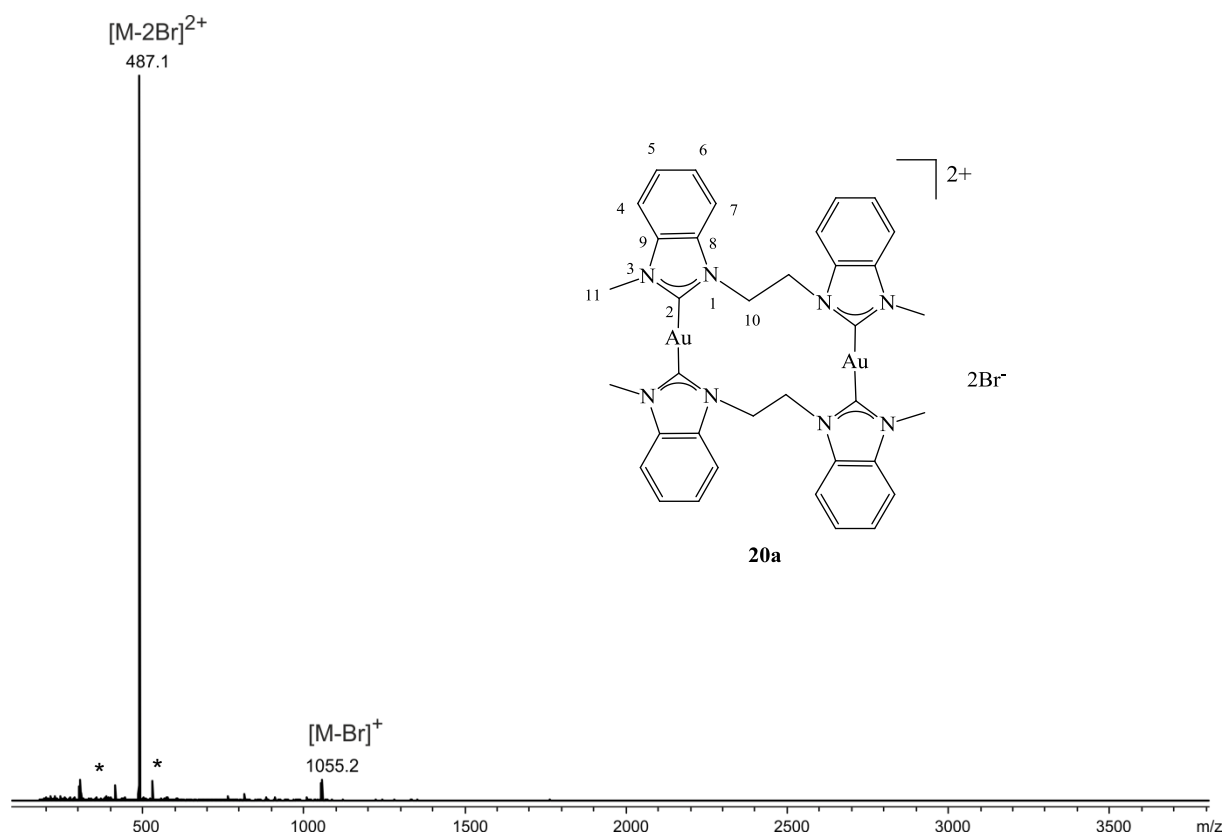**Figure 6.3.30.** ^{13}C NMR (100 MHz, [D6]DMSO, r. t.) spectrum of **23**. *partially deuterated and undeuterated DMSO, respectively.
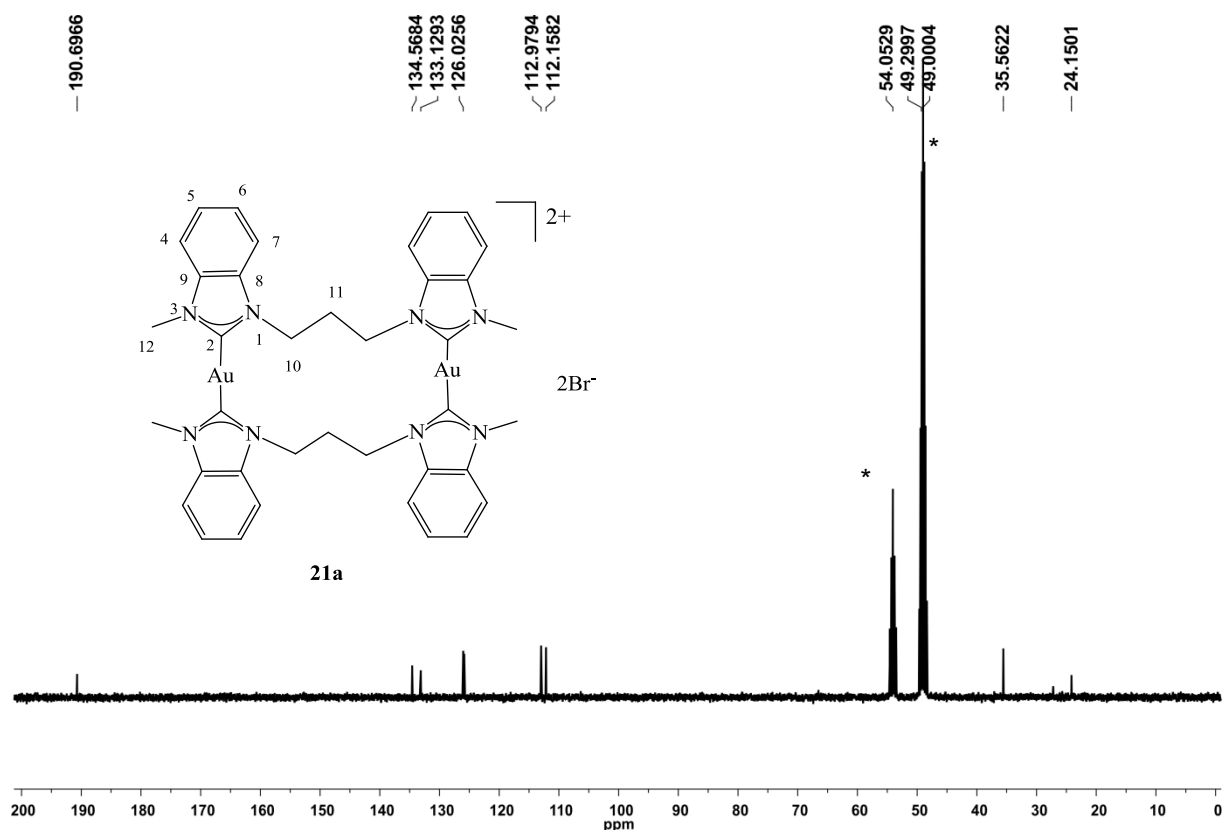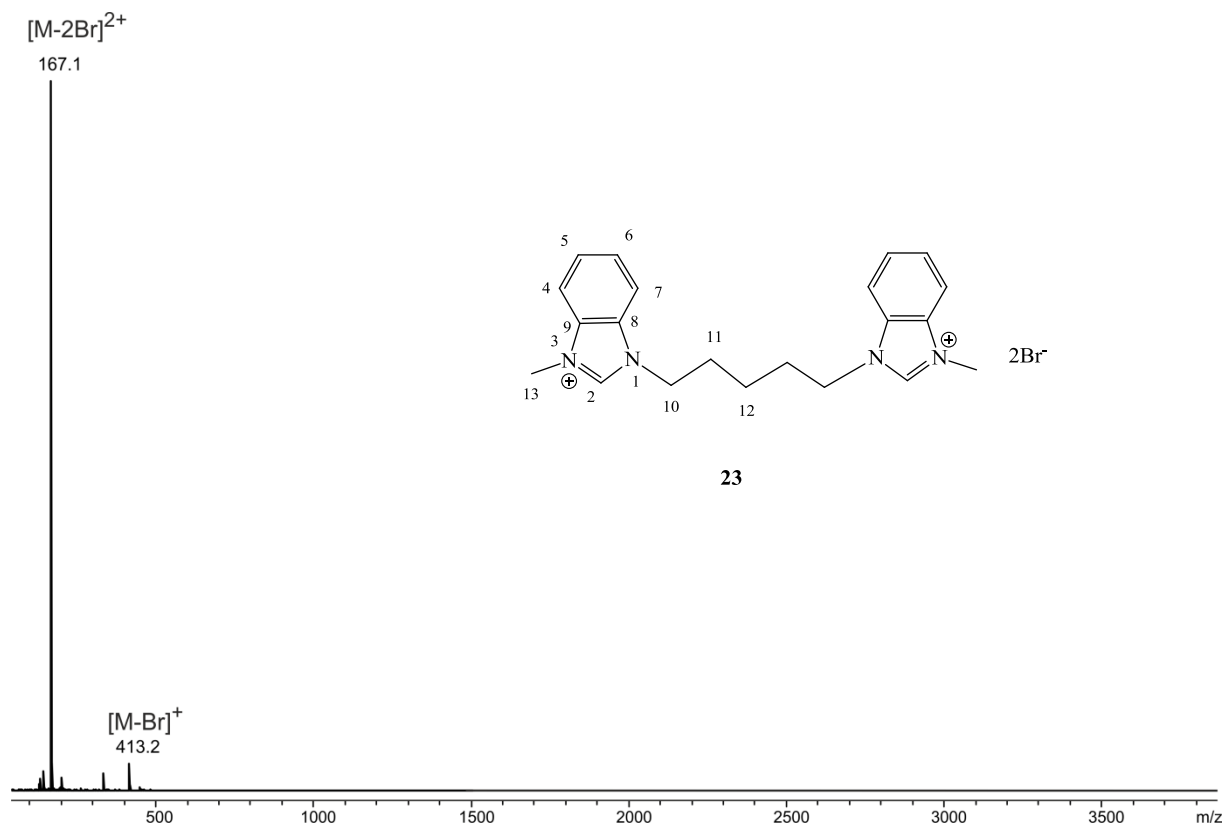

Figure 6.3.31. microTof-Q ESI(+) mass spectrum of **23** in MeOH.
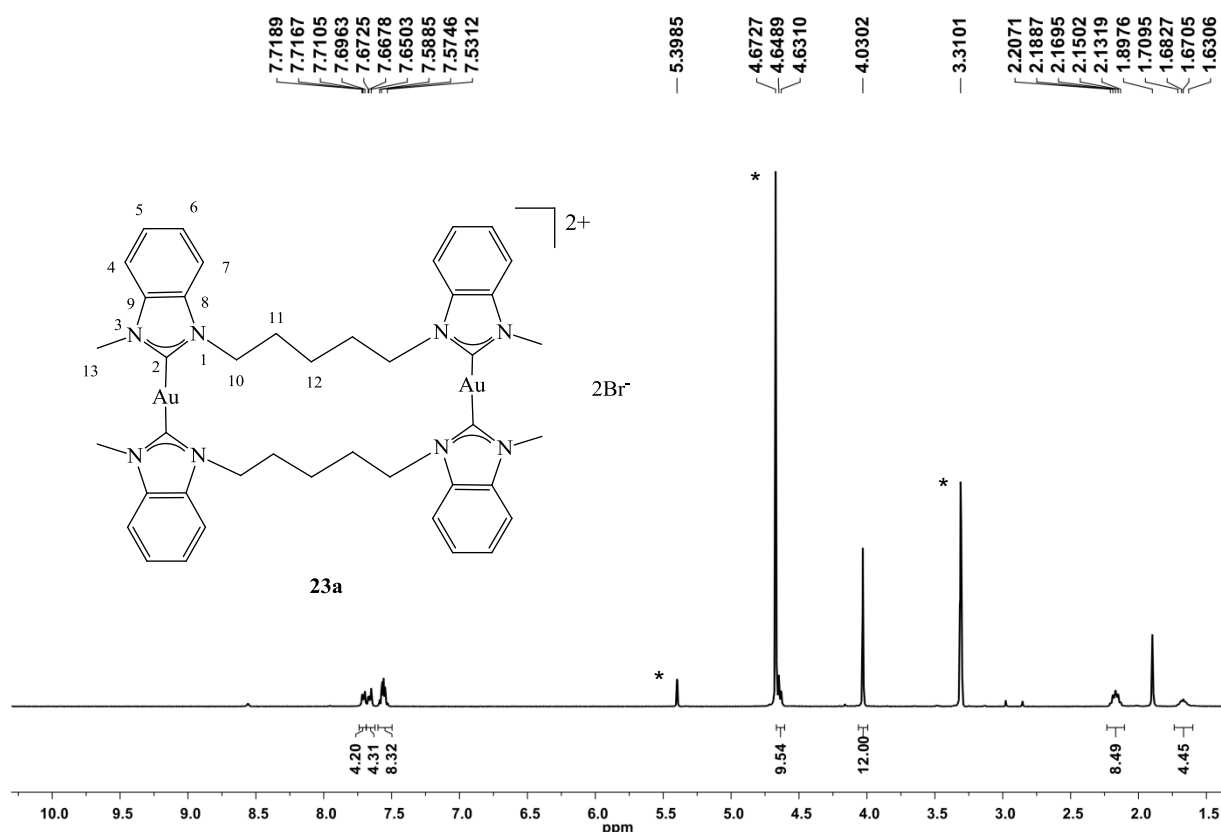
Figure 6.3.32. ^{1}H NMR (400 MHz, CD$_3$OD/CD$_2$Cl$_2$, r. t.) spectrum of **23a**. *partially deuterated and undeuterated MeOH and DCM and water, respectively.

Figure 6.3.33. ^{13}C NMR (75 MHz, CD$_3$OD/CD$_2$Cl$_2$, r. t.) spectrum of **23a**. *partially deuterated and undeuterated MeOH and DCM, respectively.

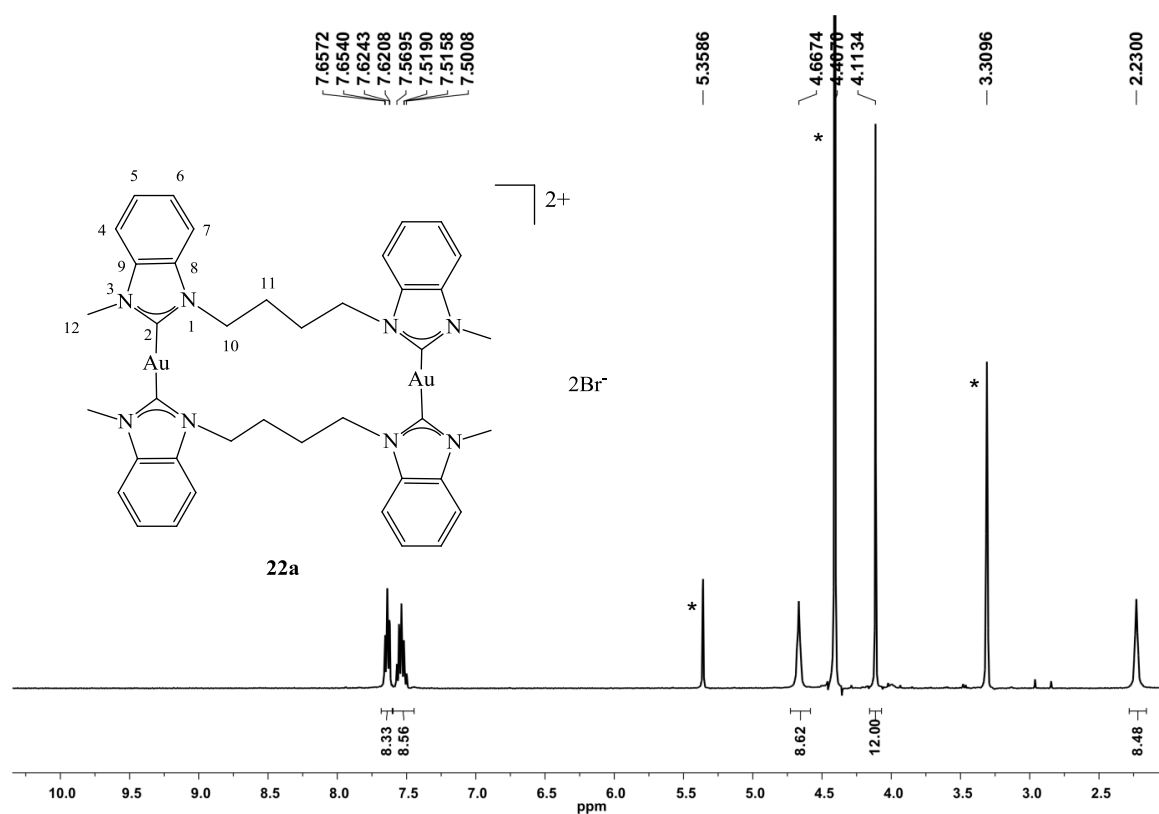**Figure 6.3.34.** microTof-Q ESI(+) mass spectrum of **23a** in MeOH.

Figure 6.3.35. ¹H NMR (400 MHz, CD₃OD/CD₂Cl₂, r. t.) spectrum of **24a**. *partially deuterated and undeuterated MeOH and DCM and water, respectively.
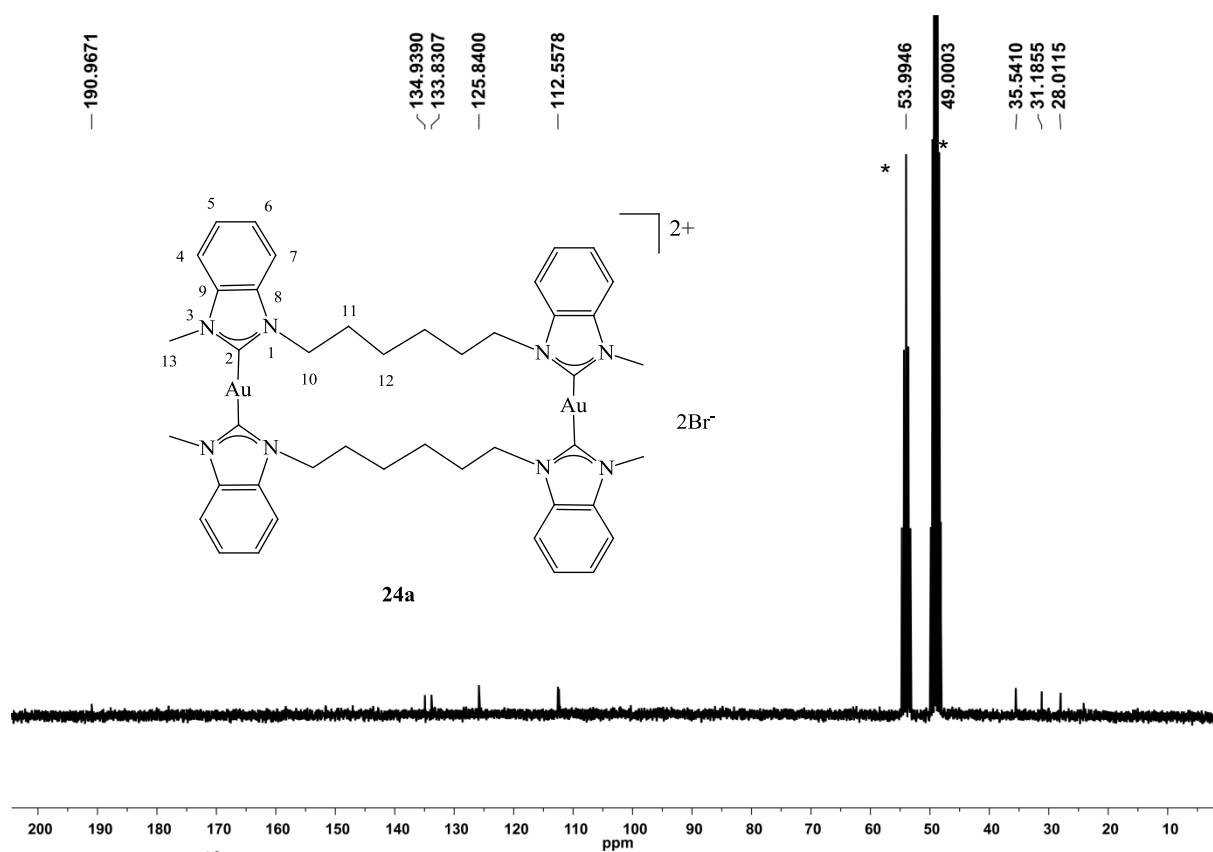
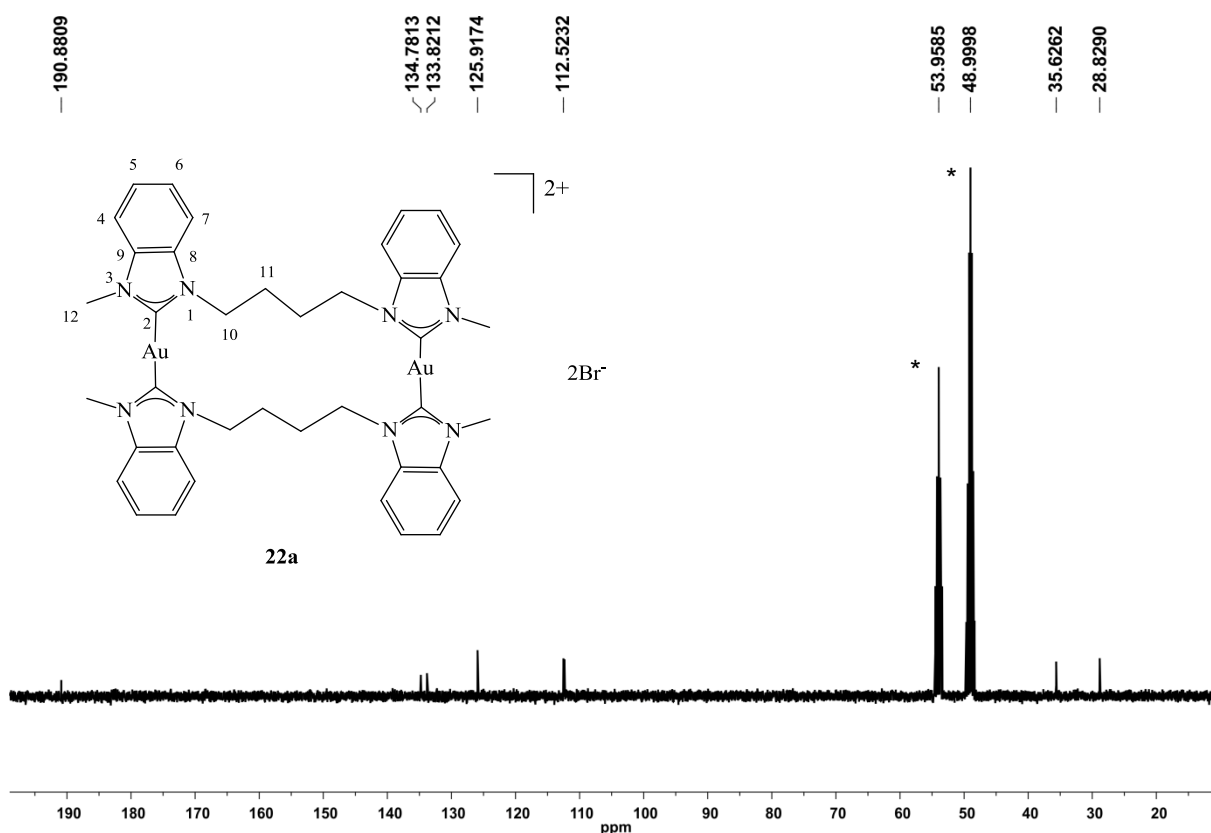**Figure 6.3.36.** ^{13}C NMR (75 MHz, CD$_3$OD/CD$_2$Cl$_2$, r. t.) spectrum of **24a**. *partially deuterated and undeuterated MeOH and DCM, respectively.

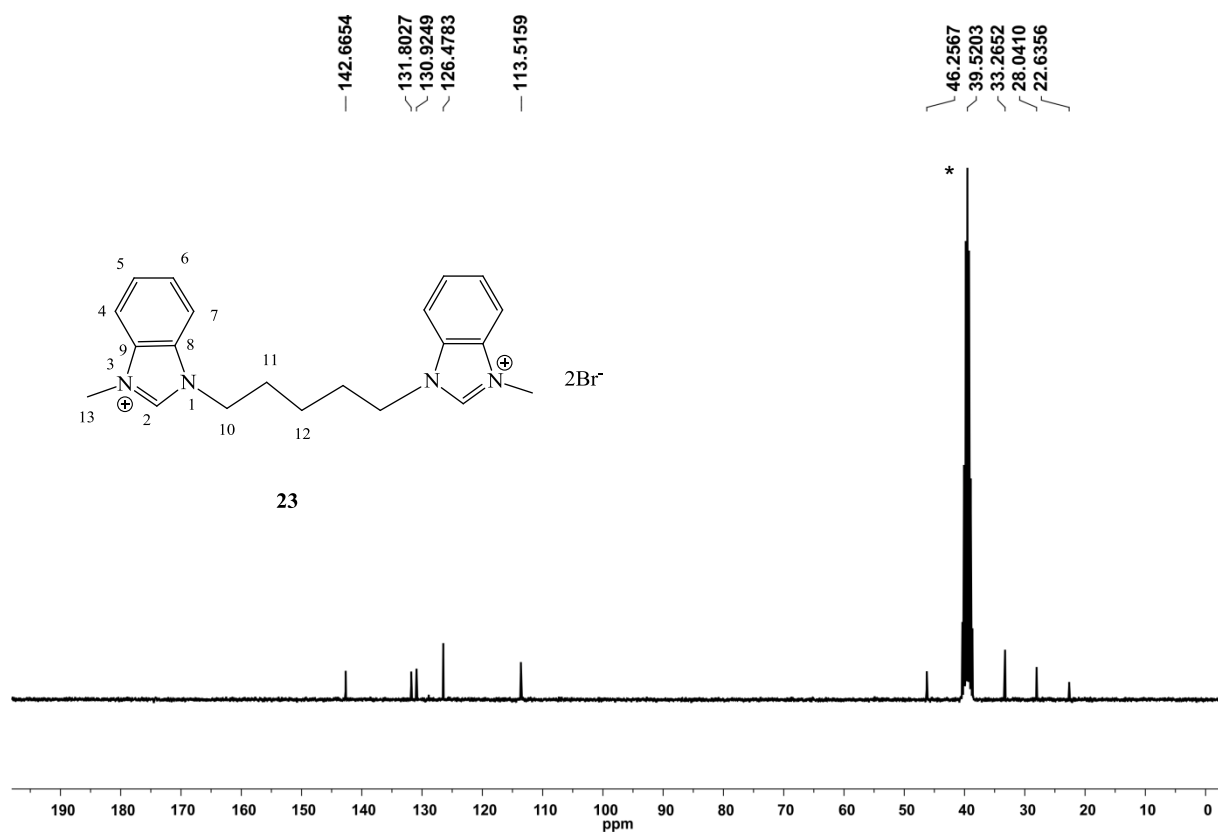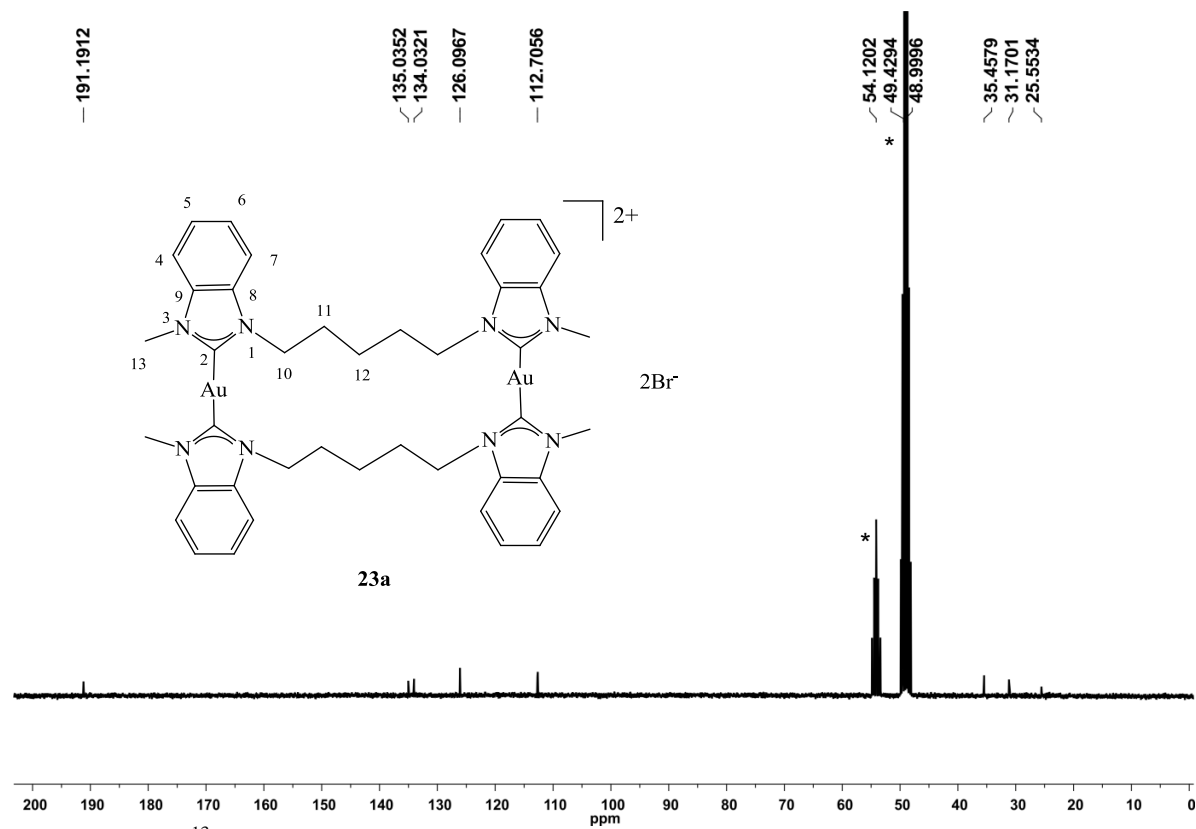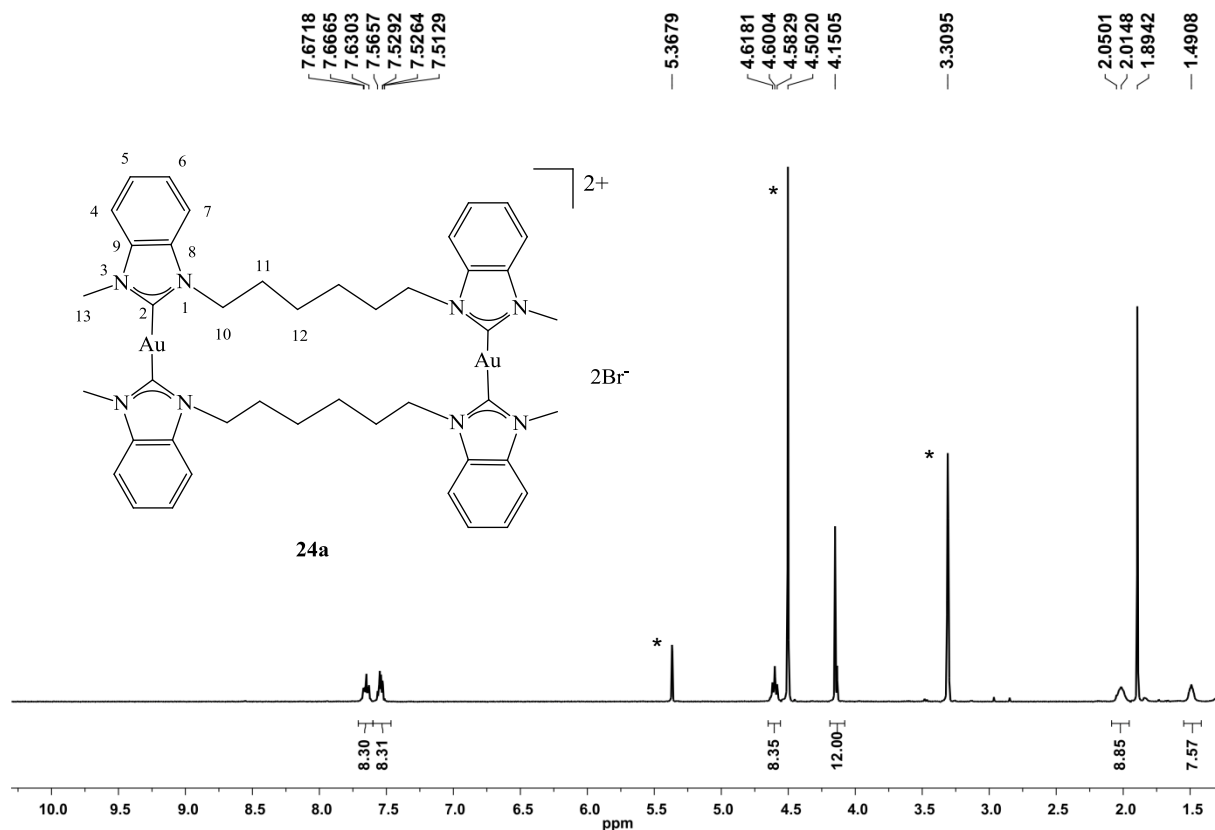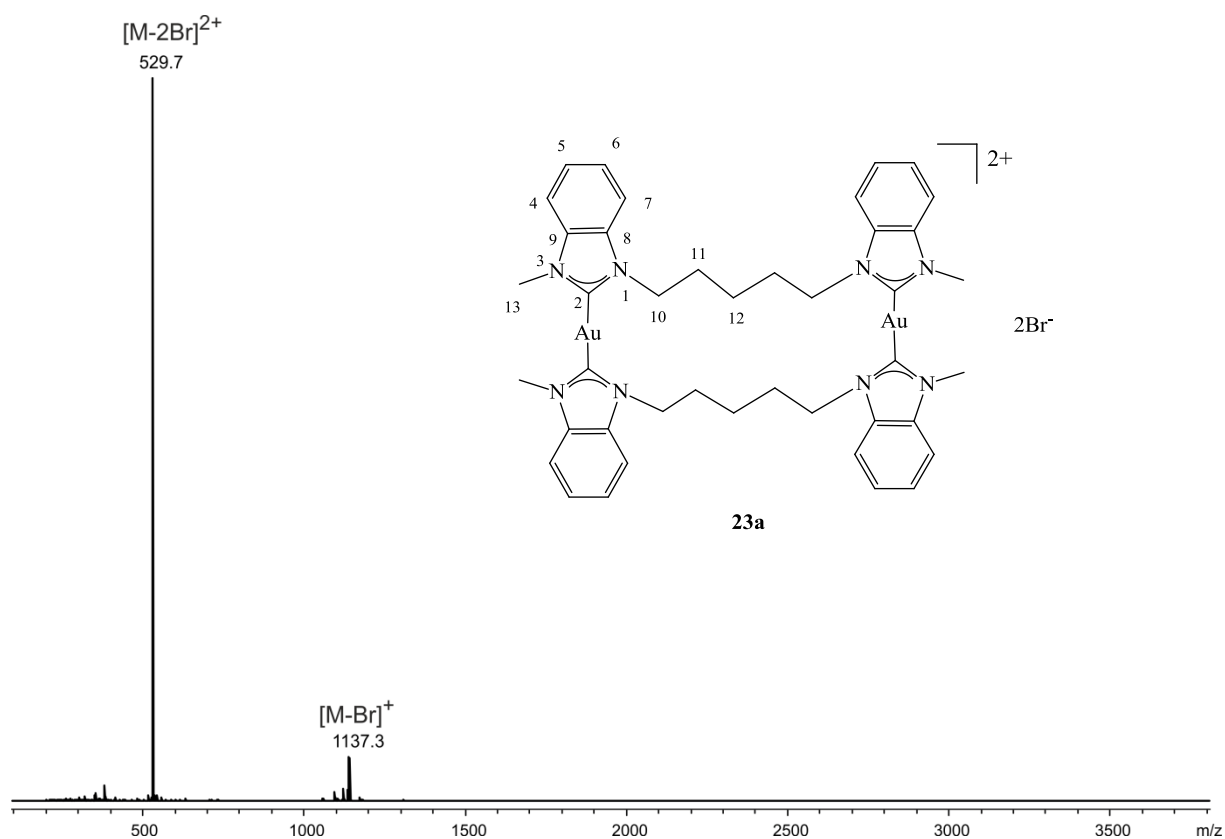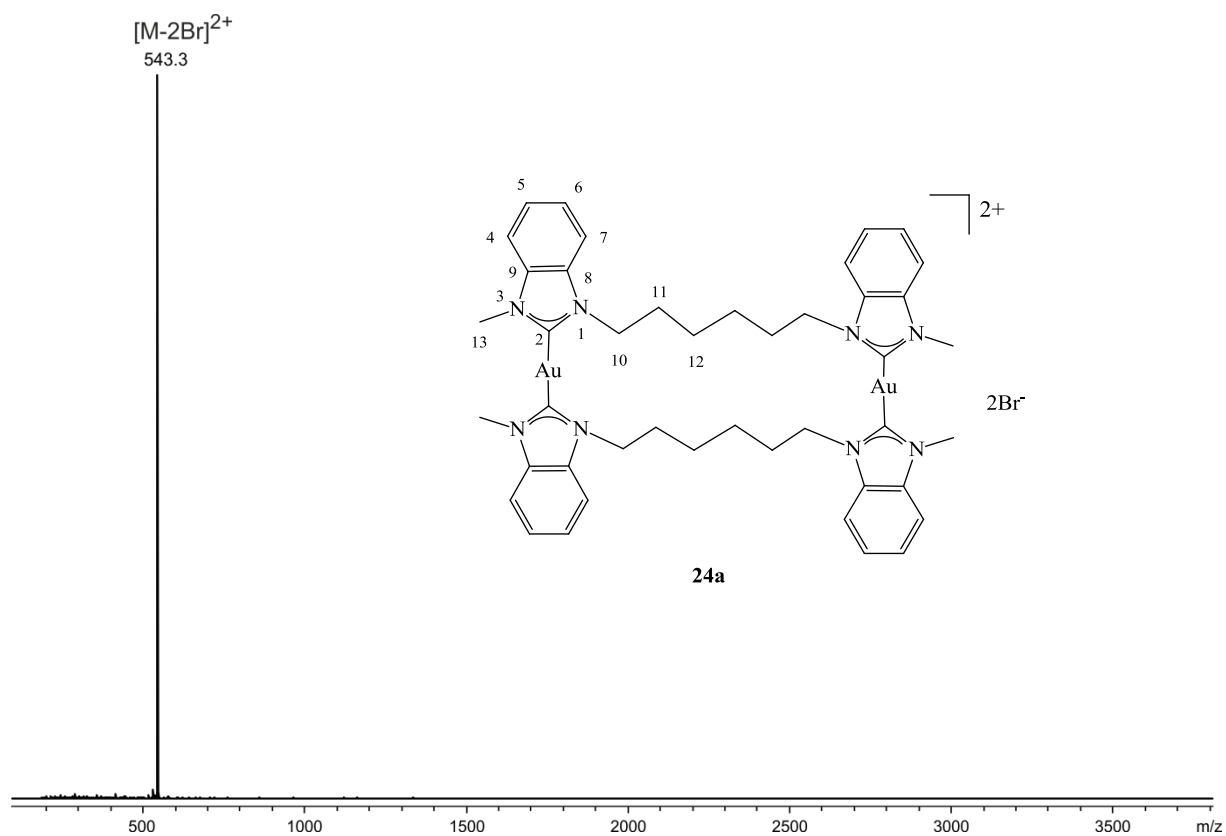**Figure 6.3.37.** microTof-Q ESI(+) mass spectrum of **24a** in MeOH.

6.3.4. Crystallographic Data

Crystal structure determination: Data for the X-ray crystallographic analyses were performed on a Nonius KappaCCD diffractometer (**13a**, **14a**, **15a**, **16a**, **22a**) or a STOE IPDS2T diffractometer (**21a**, **24a**) using graphite monochromated Mo-Kα radiation ($\lambda = 0.71073$ Å). Intensities were measured by fine-slicing φ- and ω-scans and corrected for background, polarization and Lorentz effects. A semi-empirical absorption correction was applied for the data sets following Blessing's method[94]. The structures were solved by direct methods and refined anisotropically by the least squares procedure implemented in the ShelX programme system[95]. The hydrogen atoms were included isotropically using the riding model on the carbon atoms.

Table 6.3.2. Crystallographic Data of **13a** and **14a**.

	13a	**14a**
formula	$C_{38}H_{40}Au_2N_8Br_2 * CH_3OH$	$C_{40}H_{44}Au_2N_8Br_2 * Et_2O$
cryst size (mm^3)	0.28 x 0.07 x 0.06	0.38 x 0.18 x 0.06
cryst syst	monoclinic	monoclinic
space group	C 2/c	C 2/c
a (Å)	26.1417(6)	22.3983(13)
b (Å)	19.0405(6)	12.5583(6)
c (Å)	19.1794(5)	17.8798(10)
α (deg)	90	90
β (deg)	120.9390(14)	120.889(2)
γ (deg)	90	90
V (Å^3)	8188.2(4)	4316.0(4)
Z	8	4
ρ_{calcd} (mg m^3)	1.938	1.946
F_{000}	4560	2440
μ (mm^{-1})	9.151	8.687
$\varTheta$ range (deg)	2.41-27.00	2.65-27.00
reflns collected	26370	13633
R_{int}	0.0659	0.0518
GOF	0.955	1.082
R1	0.0334-0.0474	0.0524-0.0782
wR2	0.0748-0.0786	0.1179-0.1318
largest diff peak (e Å^{-3})	1.058	2.249

Table 6.3.3. Crystallographic Data of **15a** and **21a**.

	15a	21a
formula	$C_{42}H_{48}Au_2N_8Br_2$	$C_{38}H_{40}Au_2N_8Br_2 * CH_3OH$
cryst size (mm^3)	0.41 x 0.11 x 0.10	0.06 x 0.03 x 0.02
cryst syst	triclinic	monoclinic
space group	P-1	C 2/c
a (Å)	9.0687(3)	26.092(3)
b (Å)	9.3648(3)	11.4454(14)
c (Å)	12.6898(3)	18.010(3)
α (deg)	105.1110(18)	90
β (deg)	91.103(2)	128.499(9)
γ (deg)	95.9969(18)	90
V (Å^3)	1033.53(5)	4209.2(11)
Z	1	4
ρ_{calcd} (mg m^3)	1.958	1.951
F_{000}	584	2376
μ (mm^{-1})	9.063	8.905
Θ range (deg)	3.02-28.00	2.84-28.00
reflns collected	14553	21810
R_{int}	0.0682	0.2344
GOF	1.002	0.897
R1	0.0296-0.0348	0.0747-0.1470
wR2	0.0624-0.0639	0.1597-0.1859
largest diff peak (e Å^{-3})	1.324	1.750

Table 6.3.4. Crystallographic Data of **16a** and **22a**.

	16a	22a
formula	$C_{44}H_{52}Au_2N_8Br_2 * 2H_2O$	$C_{40}H_{44}Au_2N_8Br_2$
cryst size (mm^3)	0.40 x 0.08 x 0.04	0.24 x 0.18 x 0.06
cryst syst	triclinic	monoclinic
space group	P-1	C 2/c
a (Å)	8.5985(10)	14.352(3)
b (Å)	10.7275(8)	17.026(2)
c (Å)	13.8999(18)	19.823(3)
α (deg)	73.469(7)	90
β (deg)	86.916(5)	109.315(12)
γ (deg)	66.904(6)	90
V ($Å^3$)	1128.1(2)	4571.2(12)
Z	1	4
ρ_{calcd} (mg m^3)	1.888	1.823
F_{000}	620	2416
μ (mm^{-1})	8.312	8.202
Θ range (deg)	2.81-28.00	2.63-28.00
reflns collected	11719	4923
R_{int}	0.0583	0.1430
GOF	0.992	0.888
R1	0.0481-0.0831	0.0465-0.0640
wR2	0.0995-0.1094	0.1201-0.1238
largest diff peak (e $Å^{-3}$)	2.288	2.33

Table 6.3.5. Crystallographic Data of **24a**.

	24a
formula	$C_{44}H_{52}Au_2N_8Br_2 * 4CH_3OH$
cryst size (mm^3)	0.15 x 0.12 x 0.06
cryst syst	monoclinic
space group	$P2_1/n$
a (Å)	11.0344(6)
b (Å)	16.9454(12)
c (Å)	13.8312(7)
α (deg)	90
β (deg)	105.732(4)
γ (deg)	90
V (Å^3)	2489.3(3)
Z	2
ρ_{calcd} (mg m^3)	1.834
F_{000}	1344
μ (mm^{-1})	7.543
Θ range (deg)	2.85-28.00
reflns collected	10480
R_{int}	0.0598
GOF	0.476
R1	0.0352-0.0766
wR2	0.0807-0.0959
largest diff peak (e Å^{-3})	1.86

6.4 Abbrevations

ACN	acetonitrile
approx.	approximately
br	broad
d	doublet
DCM	dichloromethane
DMF	N,N-dimethylformamide
DMSO	dimethylsulfoxide
ESI	electrospray ionization
et al.	et alia, and others
H,H-COSY	correlated spectroscopy
HMBC	heteronuclear multiple-bond correlation
HMQC	heteronuclear multiple-quantum correltion
HPLC	High-performance liquid chromatography
J	coupling constant
L	ligand
λ_{em}	emission wavelength
λ_{ex}	excitation wavelength
M	metal
m	multiplet
MeOH	methanol
MS	mass spectrometry
NHC	N-heterocyclic carbene
NMR	nuclear magnetic resonance
ORTEP	Oak Ridge Thermal-Ellipsoid Plot
q	quartet
quint	quintet
s	singlet
sept	septet
t	triplet
UV/Vis	ultraviolet-visible light
VT	variable temperature

6.5 References

[1]   I. J. B. Lin, C. S. Vasam, *Can. J. Chem.* **2005**, *83*, 812-825.

[2]   J. C. Y. Lin, R. T. W. Huang, C. S. Lee, A. Bhattacharyya, W. S. Hwang, I. J. B Lin**,** *Chem. Rev.* **2009**, *109*, 3561-3598.

[3]   A. S. K. Hashmi, G. J. Hutchings, *Angew. Chem. Int. Ed.* **2006**, *45*, 7896-7936.

[4]   N. Marion, S. P. Nolan, *Chem. Soc. Rev.* **2008**, *37*, 1776-1782.

[5]   S. P. Nolan, *Acc. Chem. Res.* **2011**, *44*, 91-100.

[6]   *Chem. Soc. Rev.* **2008**, *37*, Issue 9: *Chemistry, Materials and Catalysis of Gold*.

[7]   K. M. Lee, C. K. Lee, I. J. B. Lin, **1997***, 36,* 1850-1852*.

[8]   *Coord. Chem. Rev.* **2009**, *253*, Issue 11-12: *Bioinorganic and Biomedical Chemistry of   Gold*.

[9]   F. Mohr, (Ed.) *Gold Chemistry. Applications and Future Directions in the Life   Sciences*; Wiley-VCH, Weinheim, **2009**.

[10]   P. J. Barnard, S. J. Berners-Price, *Coord. Chem. Rev.* **2007**, *251*, 1889-1902.

[11]   K. M. Hindi, M. J. Panzner, C. A. Tessier, C. L. Cannon, W. J. Youngs, *Chem.   Rev.* **2009**, *109*, 3859-3884.

[12]   H. M. J. Wang, I. J. B. Lin, *Organometallics* **1998**, *17*, 972-975.

[13]   H. M. J. Wang, C. Y. L. Chen, I. J. B Lin, *Organometallics* **1999**, *18*, 1216-1223.

[14]   F. Bonati, A. Burini, B. R. Pietroni, B. Bovio, *J. Organomet. Chem.* **1989**, *375*, 147-160.

[15]   H. G. Raubenheimer, L. Lindeque, S. Cronje, *J. Organomet. Chem.* **1996**, *511*, 177-184.

[16]   H. G. Raubenheimer, P. J. Olivier, L. Lindeque, M. Desmet, J. Hrusak, G. J. Kruger, *J. Organomet. Chem.* **1997**, *544*, 91-100.

[17]   U. E. I. Horvath, G. Bentivoglio, M. Hummel, H. Schottenberger, K. Wurst, M. J. Nell, C. E. J. van Rensburg, S. Cronje, H. G. Raubenheimer, *New. J. Chem.* **2008**, *32*, 533-539.

[18]   M. V. Baker, P. J. Barnard, S. J. Berners-Price, S. K. Brayshaw, J. L. Hickey, B. W. Skelton, A. H. White, *Dalton Trans.* **2006**, 3708-3715.

[19]   J. L. Hickey, R. A. Ruhayel, P. J. Barnard, M. V. Baker, S. J. Berners-Price, A. Filipovska, *J. Am. Chem. Soc.* **2008**, *130*, 12570-12571.

[20]   M. K. Samantaray, K. Pang, M. M. Shaikh, P. Ghosh, *Inorg. Chem.* **2008**, *47*, 4153-4165.

[21]   P. C. Kunz, C. Wetzel, S. Kögel, M. U. Kassack, B. Spingler, *Dalton Trans.* **2011**, *40*, 35-37.

[22]   C. Hemmert, A. Fabié, A. Fabre, F. Benoit-Vical, H. Gornitzka, *Eur. J. Med. Chem.* **2013**, *60*, 64-75.

[23]   J.-W. Wang, Q.-S. Li, F.-B. Xu, H. B. Song, Z.-Z. Zhang, *Eur. J. Org. Chem.* **2006**, 1310-1316.

[24]   J. Gil-Rubio, V. Cámara, D. Bautista, J. Vicente, *Inorg. Chem.* **2013**, *52*, 4071-4083.

[25]   R. Fränkel, J. Kniczek, W. Ponikwar, H. Nöth, K. Polborn, W. P. Fehlhammer, *Inorg. Chim. Acta* **2001**, *312*, 23-39.

[26]   G. Papini, G. Bandoli, A. Dolmella, G. Gioia Lobbia, M. Pellei, C. Santini, *Inorg. Chem. Comm.* **2008**, *11*, 1128-1131.

[27]   P. J. Barnard, M. V. Baker, S. J. Berners-Price, B. W. Skelton, A. H. White, *Dalton Trans.* **2004**, 1038-1047.

[28]   P. J. Barnard, L. E. Wedlock, M. V. Baker, S. J. Berners-Price, D. A. Joyce, B. W. Skelton, J. H. Steer, *Angew. Chem. Int. Ed.* **2006**, *45*, 5966-5970.

[29]   L. E. Wedlock, J. B. Aitken, S. J. Berners-Price, P. J. Barnard, *Dalton Trans.* **2013**, *42*, 1259-1266.

[30]   J. W. Wang, H.-B. Song, Q.-S. Li, F.-B. Xu, Z.-Z. Zhang, *Inorg. Chim. Acta* **2005**, *358*, 3653-3658.

[31]   A. Liu, X. Zhang, W. Chen, H. Qiu, *Inorg. Chem. Comm.* **2008**, *11*, 1128-1131.

[32]   F. J.-B. dit Dominique, H. Gornitzka, A. Sournia-Saquet, C. Hemmert, *Dalton Trans.* **2009**, 340-352.

[33]   J. Cure, R. Poteau, I. C. Gerber, H. Gornitzka, C. Hemmert, *Organometallics* **2012**, *31*, 619-626.

[34]   C. Carcedo, J. C. Knight, S. J. A. Pope, I. A. Fallis, A. Dervisi, *Organometallics* **2011**, *30*, 2553-2562.

[35] M. Baron, C. Tubaro, A. Biffis, M. Basato, C. Graiff, A. Poater, L. Cavallo, N. Armaroli, G. Accorsi, *Inorg. Chem.* **2012**, *51*, 1778-1784.

[36] C. Tubaro, M. Baron, M. Costante, M. Basato, A. Biffis, A. Gennaro, A. A. Isse, C. Graiff, G. Accorsi, *Dalton Trans.* **2013**, *42*, 10952-10963.

[37] A. Biffis, M. Cipani, C. Tubaro, M. Basato, M. Costante, E. Bressan, A. Venzo, C. Graiff, *New J. Chem.* **2013**, *37*, 4176-4184.

[38] V. Gierz, C. Maichle-Mössmer, D. Kunz, *Organometallics* **2012**, *31*, 739-747.

[39] V. Gierz, A. Seyboldt, C. Maichle-Mössmer, K. W. Törnroos, M. T. Speidel, B. Speiser, K. Eichele, D. Kunz, *Organometallics* **2012**, *31*, 7893-7901.

[40] A. Poethig, T. Strassner, *Organometallics* **2012**, *31*, 3431-3434.

[41] F. E. Hahn, C. Radloff, T. Pape, A. Hepp, *Chem. Eur. J.* **2008**, *14*, 10900-10904.

[42] A. Rit, T. Pape, F. E. Hahn, *Organometallics* **2011**, *30*, 6393-6401.

[43] C. Schulte to Brinke, T. Pape, F. E. Hahn, *Dalton Trans.* **2013**, *42*, 7330-7337.

[44] Y.-F. Han, G.-X. Jin, F. E. Hahn, *J. Am. Chem. Soc.* **2013**, *135*, 9263-9266.

[45] M. Z. Ghdhayeb, R. A. Haque, S. Budagumpi, *Journal of Organometallic Chemistry* **2014**, *757*, 42-50.

[46] I. Özdemir N. Temelli, S. Günal, S. Demir, *Molecules* **2010**, *15*, 2203-2210.

[47] X. Hu, I. Castro Rodriguez, K. Olsen, K. Meyer, *Organometallics* **2004**, *23*, 755-764.

[48] Y. Zhou, W. Chen, *Organometallics* **2007**, *26*, 2742-2746.

[49] A. Biffis, G. Gioia Lobbia, G. Papini, M. Pellei, C. Santini, E. Scattolin, C. Tubaro, *J. Organomet. Chem.* **2008**, *693*, 3760-3766.

[50] A. Rib, T. Pape, F. E. Hahn, *J. Am. Chem. Soc.* **2010**, *132*, 4572-4573.

[51] H. Schmidbaur, A. Schier, *Chem. Soc. Rev.* **2008**, *37*, 1931-1951.

[52] H. Schmidbaur, A. Schier, *Chem. Soc. Rev.* **2012**, *41*, 370-412.

[53] H. Schmidbaur, W. Graf, G. Müller, *Angew. Chem. Int. Ed. Engl.* **1988**, *27*, 417-419.

[54]   R. Narayanaswamy, M. A. Young, E. Parkhurst, M. Ouellette, M. E. Kerr, D. M. Ho, R. C. Elder, A. E. Bruce, M. R. M. Bruce, *Inorg. Chem.* **1993**, *32*, 2506-2517.

[55]   A. Deák, T. Megyes, G. Tárkányi, P. Király, L. Biczók, G. Pálinkás, P. J. Stang, *J. Am. Chem. Soc.* **2006**, *128*, 12668-12670.

[56]   A. Vogler, H. Kunkely, *Coord. Chem. Rev.* **2001**, *219-221*, 489-507.

[57]   V. W.-W. Yam, E. C.-C. Cheng, *Top. Curr. Chem.* **2007**, *281*, 269-309.

[58]   V. W.-W. Yam, E. C.-C. Cheng, *Chem. Soc. Rev.* **2008**, *37*, 1806-1813.

[59]   X. He, V. W.-W. Yam, *Coord. Chem. Rev.* **2011**, *255*, 2111-2123.

[60]   J. C. Lima, L. Rodríguez, *Chem. Soc. Rev.* **2011**, *40*, 5442-5456.

[61]   L. Rodríguez, M. Ferrer, R. Crehuet, J. Anglada, J. C. Lima, *Inorg. Chem.* **2012**, *51*, 7636-7641.

[62]   A. Vogler, H. Kunkely, *Coord. Chem. Rev*. **2001**, *219–221*, 489–507.

[63]   E. R. T. Tiekink, J.-G. Kang, *Coord. Chem. Rev.* **2009**, *253*, 1627–1648.

[64]   M. Ferrer, A. Gutiérrez, L. Rodríguez,O. Rossell, J. C. Lima, M. Font-Bardia, X. Solans, *Eur. J. Inorg. Chem.* **2008**, 2899–2909.

[65]   W.-F. Fu, K.-C. Chan, K.-K. Cheung, C.-M. Che, *Chem.–Eur. J.* **2001**, *7*, 4656–4664.

[66]   W.-F. Fu, K.-C. Chan, V. M. Miskowski, C.-M. Che, *Angew. Chem., Int. Ed.* **1999**, *38*, 2783–2785.

[67]   H.-R. C. Jaw, M. M. Savas, R. D. Rogers and W. R. Mason, *Inorg. Chem.* **1989**, *28*, 1028–1037.

[68]   H.-X. Zhang, C.-M. Che, *Chem.–Eur. J.* **2001**, *7*, 4887–4893.

[69]   K. H. Leung, D. L. Phillips, M.-C. Tse, C.-M. Che, V. M. Miskowski, *J. Am. Chem. Soc*. **1999**, *121*, 4799–4803.

[70]   D. Rios, D. M. Pham, J. C. Fettinger, M. M. Olmstead, A. L. Balch, Inorg. Chem. **2008**, *47*, 3442-3451.

[71]   M. Saitoh, A. L. Balch, J. Yuasa, T. Kawai, *Inorg. Chem.* **2010**, *49*, 7129-7134.

[72]   C. Müller, *Diploma Thesis*, Rheinische Friedrich-Wilhelms-Universität Bonn, **2010**.

[73]   S. Kobialka, *Diploma Thesis*, Rheinische Friedrich-Wilhelms-Universität Bonn, **2011**.

[74]   Q.-X. Liu, X.-Q. Yang, X.-J. Zhao, S.-S. Ge, S.-W. Liu, Y. Zang, H.-b. Song, J.-H. Guo, X.-G. Wang, *CrystEngComm* **2010**, *12,* 2245-2255.

[75]   K. Okuyama, J. Sugiyama, R. Nagahata, M. Asai, M. Ueda, K. Takeuchi, *J. Mol. Catal. A: Chem.* **2003**, *203*, 21-27.

[76]   K. Ito, N. Nishina, H. Ohno, *Electrochim. Acta* **2000**, *45*, 1295-1298.

[77]   A. A. D. Tulloch, A. A. Danopoulos, S. Winston, S. Kleinhenz, G. Eastham, *J. Chem. Soc., Dalton Trans.* **2000**, 4499.

[78]   J. C. Garrison, R. S. Simons, J. M. Talley, C. Wesdemiotis, C. A. Tessier, W.J. Youngs, *Organometallics* **2001**, *20*, 1276.

[79]   C. K. Lee, K. M. Lee, I. J. B. Lin; *Organometallics* **2002**, *21*, 10-12.

[80]   P. H. M. Budzelaar, 'gNMR version 5.1', **1995**.

[81]   K. M. Lee, H. M. J. Wang, I. J. B. Lin, *Dalton Trans.* **2002**, 2852-2856.

[82]   L. Ray, M. M. Shaikh, P. Ghosh, *Inorg. Chem.* **2008**, *47*, 230.

[83]   J. C. Garrison, W. J. Young, *Chem. Rev.* **2005**, *105*, 3978-4008.

[84]   M. M. Díaz-Requejo, P. J. Perez, *Organomet. Chem.* **2005**, *690*, 5441-5450.

[85]   P. L. Arnold, *Heteroat. Chem.* **2002**, *13*, 534-539.

[86]   D. Wang, *Acta Cryst.* **2006**, *E62*, m1565-m1566.

[87]   R. Kishore, S. K. Das, *Cryst. Growth Des.* **2012**, *12*, *3684-3699*.

[88]   X.-M. Wu, Q.-X. Liu, X.-G. Wang, H.-B. Song, Z.-Y. Zheng, *Acta Cryst.* **2007**, *E64*, o4263.

[89]   Q.-X. Liu, M.-C. Shi, Z.-Q. Wang, S.-W. Liu, S.-S- Ge, Y. Zang, X.-G- Wang, J.-H. Guo, *Polyhedron* **2010**, *29*, 2121-2126.

[90]   Z. Shi, R. P. Thummel, *J. Org. Chem.* **1995**, *60*, (18), 5935-5945.

[91]   S. Riederer, P. Gigler, M. Högerl, E. Herdtweck, B. Bechlars, W. Herrmann, F. Kühn, *Organometallics* **2010**, *29*, *5681-5692*.

[92]   J. Berding, M. Lutz, A. Spek, E. Bouwman, *Organometallics* **2009**, *28*, *1845-1854*.

[93]   K. Iwamoto, H. Kimura, M. Oike, M. Sato, *Org. Biomol. Chem.* **2008**, *6*, *912-915*.

[94]   R. H. Blessing, *Acta Cryst. A* **1995**, 51, 33.

[95]   G. M. Sheldrick, SHELXS97 and SHELXL97, University of Göttingen, Germany, **1997**.

7. Publications

• "Direct experimental evidence for an enamine radical cation in SOMO catalysis"
    R. Beel, S. Kobialka, M. L. Schmidt, M. Engeser, *Chem. Comm.* **2011**, *47*, 3293-3295

This work will be published (in extracts) in:

•   "Synthesis, Spectroscopy and Crystallography of dinuclear Gold(I) NHC Macrocycles".
        submitted at Inorganic Chemistry